UNIVERSITÀ DEGLI STUDI DI MILANO
DOTTORATO DI RICERCA IN SCIENZE DELLA TERRA
*Curricula in Georesources*
*Ciclo: XXXV*

DIPARTIMENTO DI SCIENZE DELLA TERRA

TESI DI DOTTORATO DI RICERCA

# GEOARCHAEOLOGICAL AND PALAEOENVIRONMENTAL RECONSTRUCTION OF THE HOLOCENE CLIMATE-ENVIRONMENTAL-HUMAN NEXUS IN THE KURDISTAN REGION OF IRAQ

GEO/04

DOTTORANDO
LUCA FORTI

TUTOR Prof. Andrea Zerboni
CO-TUTOR Dott.ssa Eleonora Regattieri (CNR-IGG)

COORDINATORE DEL DOTTORATO
Prof. Maria Iole Spalla

AA 2021/2022

## Acknowledgements

# Chapter 1

## Introduction

Earth's landscapes are generally modelled by the interplay between endogenous and exogenous processes that produces various landforms in different geomorphological, geological, and climatic contexts (Burbank & Pinter, 1999; Burbank & Anderson, 2011). During the Quaternary, especially in the arid and semi-arid regions of the Northern hemisphere, the intensity of surface and sub-surface processes was strongly influenced by climate factors that affected the availability of water resources (Gutiérrez, 2005; Nicholson, 2011; Kirby & Whipple, 2012; Zerboni et al., 2020). Moreover, in tectonically dynamic regions the intensity of major processes shaping the landscape is often controlled by the combination between Pleistocene to Holocene rainfall fluctuations and tectonic deformations, namely: uplift, faulting and folding (Hüneburg et al., 2019; Zerboni et al., 2020, Forti et al., 2021). Consequently, folding, stretching, shearing, and faulting influenced the distribution and the formation of physiographic units, exerting a major control over the evolution of landscapes; this is particularly evident considering the evolution of hydrographic networks (Bishop, 2007; Burbank & Anderson, 2011). The interplay between regional tectonic dynamicity and climate changes is particularly evident in the arid regions of Western Asia. In fact, the footprint of Quaternary environmental and climate changes is dramatically evident in the present-day landscapes of Southwestern Asia, Levant, and the Arabian Peninsula (Hasan et al., 2019; Forti et al., 2021). Such arid and semiarid regions have been the scenario for many milestones in human evolution like the earliest onset of agriculture, the formation of the first complex societies and the emergence of ancient urban centers (Watkins, 2010; Van de Mieroop, 2015; Arranz-Otaegui et al., 2016; Palmisano et al., 2021). In the same region, throughout the Early to Middle Holocene, the progressive transition from mobile hunter-gathering groups to the emergence of sedentary farmers and herders' societies also promoted an intensification of the human contribution in shaping landscapes. The emerging of permanent settlements and the onset of the so-called "Neolithic Revolution" involved a socio-economic and technological transformations that influenced the different responses and adaptation to climate changes, landscape modifications, and variations of the availability of natural resources (Cole, 1961; Watkins, 2010; Simmons, 2011). The economy of the first urban entities was based on agriculture and livestock herding, with cultivation of cereals and legume (Kamlah & Riehl, 2020) and exploitation of sheep, goats, and cattle (Hammer & Arbucke, 2017). This social transformation and shift of land use occurred in different landscape-climate frameworks from the Levant to Southwestern of Asia; in all contexts, such processes encompassed an intense land exploitation due to agricultural and grazing activities, introduction of sophisticated systems for water harvesting, and expansion of

the urban settlements, with the development of complex social hierarchy with the emergency of the state (Lawrence et al., 2021). The birth of urbanization marked the pristine anthropogenic signature on the management of the natural resource and adaptation to the landscape with the construction of monumental architecture such as the wide and complex canal systems employed to feed crop fields and urban centre, public palaces and temples and others (Lawrence et al., 2021 and references therein). Present-day landscapes still have such anthropogenic landforms/markers. In the region the most remarkable evidence of anthropogenic landforms are anthropogenic mounds or tells (Rosen, 1986). They rise several metres above the surrounding plains and are composed of multiple accumulation of archaeological layers, building layers and wastes, which grew up through time due to stationary occupation of the site and subsequent phases of in-situ buildings decay (Rosen, 1986; Wilkinson, 2003). Thus, Western Asia landscapes appear to be a palimpsest resulting from the interplay between natural and anthropogenic processes. To better understand and reconstruct the timing and steps of such a palimpsest landscape evolution and climate changes a geoarchaeological approach is required to explain the human adaptive strategies to climate-environmental changes (Nicoll & Zerboni, 2020). In this context, geoarchaeology offers many tools useful in interpreting the archaeological record in order to identify the time-space and dynamics of depositional, erosional, and post-depositional processes and disentangling climatic and human impacts on the landscape (Cremaschi et al., 2014; Mariani et al., 2020).

## 1.2 State of art

The geoarchaeological investigation as a tool to reconstruct the evolution of landscape, quantify the impact of Quaternary climate changes on the mobile hunter-gathers groups and on the first sedentary archaeological communities is widely applied in Anatolia, Southwestern of Asia, Levant, North and Central Africa and in the Arabia Peninsula. For instance, scholars have traced evidence of the mobility of the hunter-gathers group from archaeological deposits, reconstructed settlement dynamics related to past landscape and environment, extrapolated environmental-climate data from archaeobotanical and palynological analysis and other proxy useful to highlight the relationship between climate and environment changes and human evolution (Nicoll, 2012; Cremaschi et al.,2014; Langgut et al.,2014; Forti et al.,2022). Besides that, paleoclimatic data extrapolated from natural archives, such as speleothem and lake sequences, are the main proxies that help correlating the trajectory of human communities with the Late Quaternary climate fluctuations (Cremaschi & Zerboni, 2011; Wilkinson et al., 2014; Clarke et al., 2016). In this framework, several geoarchaeological surveys and investigations were carried out in different environmental and climatic settings, such as in the Central Sahara of SW Libya, where paleoenvironmental, paleoclimatic and archaeological data allowed

reconstructing the major societal response to the Early-Middle Holocene climate-environment changes (e.g., Cremaschi & Zerboni, 2011; Cremaschi et al., 2014). Likewise in the Eastern Sahara, the geoarchaeological approach was applied to characterize the evolution of different hydrological basins with the elaboration of paleoenvironmental data useful to interpret the different phases of human occupation and social transformations occurred in the Holocene Humid Phase of North Africa (e.g., Kropelin 2005, Gallinaro 2008, Nicoll, 2012). Similarly in the Levant, a geoarchaeological analysis based on a multidisciplinary data derived from sedimentological and stratigraphic analysis of alluvial sequences, palynological reconstruction and from isotopic analysis on snail shell allowed to interpret the human exploitation of the Negev Desert (Rosen 2007, Langgut et al.,2014). The cross correlation of such data revealed an intrigued organization of the human cultural system related to farmer system in the northern of Negev and a southern arid pastoral community (Rosen 2011) with a different subsistence strategy acted in responses to Middle Holocene climate fluctuations (Clarke et al., 2016). The main paleoclimatic datasets used to interpret such fluctuations were speleothems of Soreq, Jeita cave (Bar-Matthews & Ayalon, 2003; Verheyden et al., 2008), cores from the Dead Sea (Migowski et al., 2006) and those from the southeastern corner of Mediterranean Sea (core site SL112; Hamman et al., 2008). In the Arabian Peninsula, such as in Oman and Saudi Arabia, geoarchaeology has been used to reconstruct the relationship between the Early Holocene human occupation and climate fluctuation related to Indian monsoon system. Especially, in Jebel Qara (Southern Oman) paleoclimate data derived from speleothems revealed the response of local hunter-gathers archaeological communities during the transition from arid phases of Late Pleistocene to Early Holocene humid period (Cremaschi et al.,2015). In the NW of Saudi Arabia, the Holocene humid period derived from sedimentary and microfaunal assemblage of sabkha in the Tayma oasis highlight a progressive drought around 8500 cal BP that affected the Neolithic communities and subsequent late Chalcolitic to early Bronze Age communities (Engel et al.,2012). Whereas in the southern of Saudi Arabia, Crassard et al., (2013) revealed that the several Middle Palaeolithic to Neolithic occupations along the Mundafan paleolake within the Rub' al-Khali were connected with period of climate ameliorate period. These highlight that during drought periods the human groups were not able to survive within the Mundafan area. In the eastern Saudi Arabia, the reconstruction of the Holocene relative sea-level in the Gulf allowed to highlight an occupation of Dosariyah settlement during the Neolithic coincided with the mid-Holocene marine transgression to facilitate marine exchange activities (Parker et al., 2020)

In Southwestern of Asia, especially in Syria and Iraqi Mesopotamia, geoarchaeology tools were applied in different context to interpret the role played by Early Holocene climate changes in promoting the development of the first urban entities and the wide arrays of social transformation and

adaptation tuned by such process. In the desert of Western Syria, along the Orontes Valley and the Middle Euphrates Valley, regional paleoclimatic data from Lakes of Mirabad and Zeribad revealed a wetter Early Holocene phase that corresponded to the onset of agriculture, followed by a progressive Middle Holocene climate deterioration (Wilkinson et al., 2012; Clarke et al., 2016). Geoarchaeological data highlight that during the arid period several archaeological communities displayed the increase of settlements expansion and a marked demographic growth (Wilkinson et al.,2014; Palmisano et al.,2021), supported by local adaptation toward herding activities. These factors allowed to interpret the adaptation of past human communities to climate changes with a progressive increase in human sedentarism in this area (Wilkinson et al., 2012; Wilkinson et al., 2014). In Southern Mesopotamia, the main geoarchaeological record preserved evidence of a major relationship between the Early to Middle Holocene transgression of Persian Gulf and the onset of Sumerian civilization. In fact, the Sumerian civilization arise in environmental settings characterized by the evolution of the Euphrates and Tigris alluvial plain ant its interplay with a seaward coastal-deltaic system, where marshes and swamp were exploited for cultivation. Geomorphological field evidence, analysis on the distribution of archaeological sites and geoarchaeological investigation on specific sites emphasize the extraordinary ability of Sumerian civilization in the management of water resources with a very deep knowledge of the environment and processes that affected the area. This is also demonstrated by the settlement strategy on elevated natural points ("turtleback") such as river levees, bars or crevasse splay to be protected from floods (Pournelle 2012, Forti et al.,2022).

These are only few of the many evidence on the complicate human/climate/environment relationship disclosed by geoarchaeological investigation. Many other examples are available for a variety of geographic, environmental, and cultural contexts of the world. What is evident for this brief review is the potentiality of a multidisciplinary approach that join the geomorphological investigation aimed at reconstructing how climate changes tuned the dynamic of surface processes and the geological interpretation of archaeological site formation and distribution to reconstruct the scenario of the interplay between climate changes and human adaptations.

## 1.3 General goals

This research project envisages a geoarchaeological approach to Holocene paleoclimatic reconstruction, including the identification of the response of natural environments and archaeological communities to climate changes in the Kurdistan Region of Iraq. This is the first attempt to accomplish a holistic geoarchaeological investigation in this region, critical for human dynamic. A major emphasis will be devoted to several main phases of the Late Quaternary, as the termination of the Last Glacial Maximum (ca 21 ka BP), the beginning of the Holocene and the

transition between the Northgrippian (ca 8.2 ka BP) and Meghalayan stages (ca 4.2 ka BP). The aim of the project is to obtain paleoenvironmental data from different natural and anthropogenic archives from two key areas: the territories between (i) the Navkur, Faideh and Nineveh plains and (ii) the Erbil plain. The project aims to compare climatic and environmental changes to human occupation of the region since the Lateglacial phase (from the Pre-Pottery Neolithic to the historical period), and eventually propose hypothesis to explain the trajectory of settlements distribution, land use, and subsistence strategies implemented by Mesopotamian archaeological communities in response to climate and landscape changes. The aims of the project will be pursued by considering various tools of Earth Sciences: analysis in remote sensing and GIS of satellite imagery; geomorphological survey; sedimentological, geochemical, micropaleontological, pollen and geochronological analyses of natural and anthropogenic sequences. Beside the geomorphological reconstruction of ancient hydrology and landforms, considered archives for proxy data will be lake sediments, speleothems, and anthropogenic sequences (open-air and cave archaeological sites). The project wants to reconstruct the environmental evolution and the human response in the Kurdistan Region of Iraq because the latter played a major role in the development of subsistence strategies such as the extensive and intensive agriculture and – later – specialized pastoralism. Moreover, the project will include predictive tools for archaeological research to identify the main ongoing erosional processes that acted on the archaeological sites and suggest strategies for its study and preservation.

## 1.4 Study areas

The study area is in the Kurdistan Region of Iraq (KRI). Therein, the main physiographic elements are the northern mountain belt of the Zagros Mt. and the flat areas belonging to Northern Mesopotamia Plain. The main hydrographic network is related to the watersheds of the Tigris River and its two major tributaries: the Great Zab and the Lesser Zab Rivers. The region is subdivided in two macro-areas, namely the northwestern and central sectors of the KRI. The northwestern KRI (NWKRI) covers 12,000 $km^2$ inside the governorates of Dohuk, Nineveh, and Erbil; while the central KRI (CKRI) covers 12,000 $km^2$ encompassing the Governorates of Erbil, Niniveh, Kirkuk, and Sulaymaniyah (Figure 1). Detailed geomorphological features of the two areas are discussed in Chapters 3 and 4 respectively. In the NWKRI the climate of the lowlands is semi-arid to temperate-warm climate with an average annual rainfall around 380 mm/yr and temperatures ranging from −0.6 to 37.3°C (Wilkinson, 2003); while in the along the foothills, the climate is classified as Mediterranean, with precipitation up to 1000 mm/yr and a long-wet season (November– April) (Eklund & Seaquist, 2015; Al-Zuhairi et al., 2016). In the CKRI, the climate is principally semi-arid,

continental, sub-tropical type with an average annual rainfall of 428 mm/yr. and temperatures ranging from 7.8 °C to 34.2 °C (Rivas-Martinez, 2004; Yacoub et al., 2012).

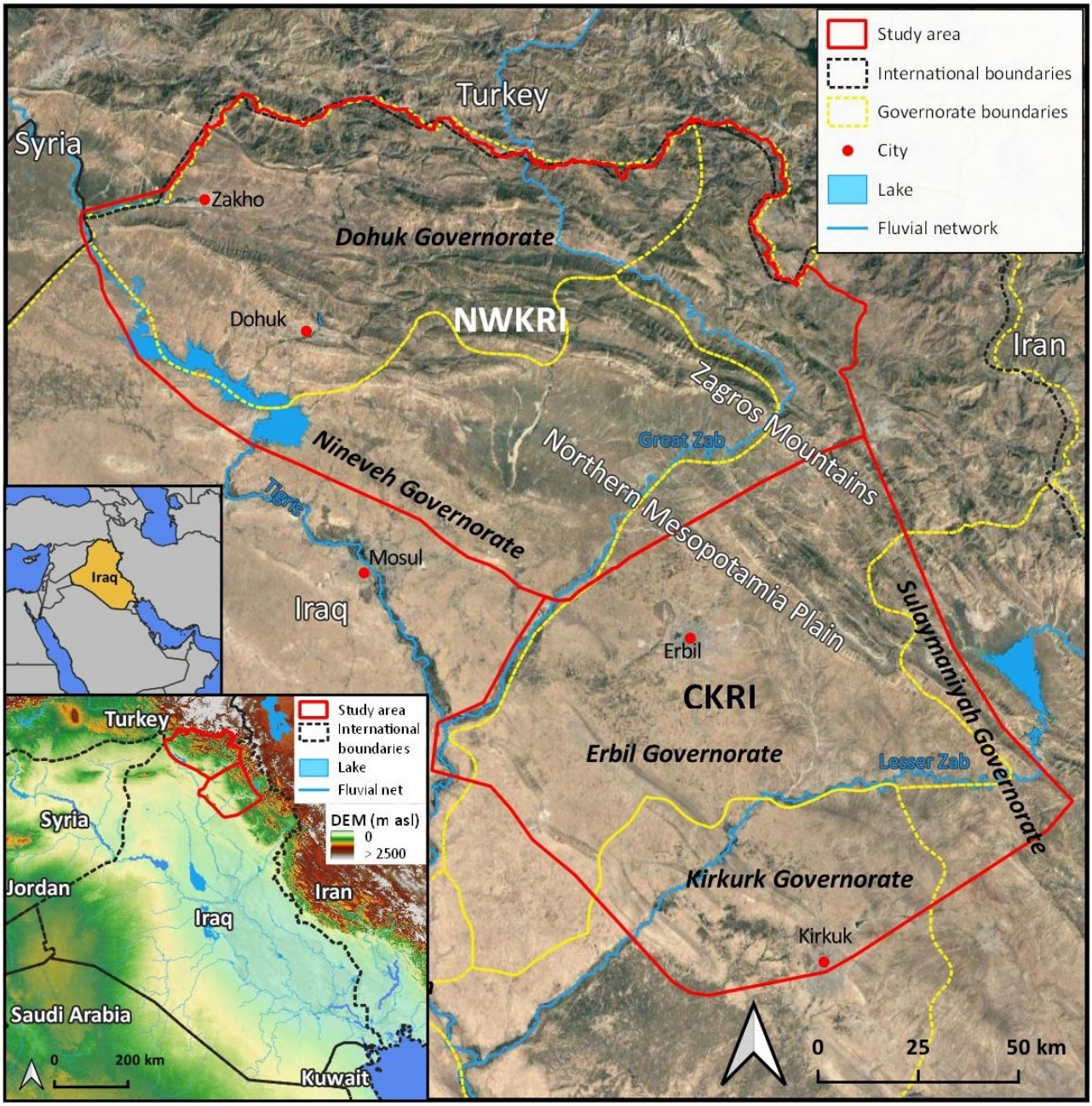


**Figure 1.** Physiographic map of the study areas

From the geological point of view, the KRI is part of the Zagros-Fold Thrust Belt (ZFTB), resulting from the continental collision between the Arabian and Eurasia plates that started in the Early Miocene and still actively progressing today (Csontos et al., 2012; Mouthereau et al., 2012; Fouad, 2015). The Zagros Mt. deformation has propagated over the NE margin of the Arabian Plate toward the Mesopotamian Foreland Basin and the Persian Gulf (Blanc et al., 2003; Vergés et al., 2011; Csontos et al., 2012). In the KRI, tectonic deformation along the ZFTB is organized into four different

zones from the inner part of the orogeny (Imbricated and High Fold zones) to its foreland (Foothills zone and Mesopotamian Foreland Basin) (Berberian, 1995; Frizon de Lamotte et al., 2011; Jassim & Goff, 2006; Fouad, 2015). The deformation is expressed by formation of a series of anticline folds coupled with thrusts along the Mountain Front Flexure and in the FHZ; while the HFZ displays both fault-related and buckle folds (Zebari et al., 2020). These are the main structural features within the regional landscape that exposed Upper Triassic/Lower Cretaceous to Pliocene units. The anticlinal ridges consist of reefal limestone, dolomitic limestone with bedded marls and shales of Upper Triassic-Upper Cretaceous ages with several outcrops of Ordovician sandstones and Carboniferous-Permian limestones and shale. In the southern sector sequences of limestone, dolostone and sandstone from the Upper Paleocene to the Lower Miocene are exposed. Middle to Late Miocene mudstones and sandstones with Plio-Pleistocene conglomerates form the substrate of lowlands. Fluvial, floodplain, alluvial fan, colluvial and anthropogenic deposits characterize the Quaternary sequences at the hillslope of anticlines and in the low relief areas (Fouad, 2014; Jassim & Goff, 2006) (Figure 2). The KRI and adjoining regions have been inhabited since at least the Middle Palaeolithic (Braidwood & Howe, 1960; Conati Barbaro et al., 2019), as confirmed by various occurrences such as the archaeological site of Shanidar Cave, where nine Neanderthals were buried (Solecki, 1971). Since the late Upper Pleistocene, hunter-gatherer communities began to intensively exploit plants, especially wild cereals, and legumes (Conati Barbaro et al., 2019). However, the agricultural revolution and its economic and social changes appear in the Neolithic (Wilkinson et al., 2014), when major sites (here in shape of tells or mounds) show a complex architecture and an economy based on agriculture and herding during both the pre-ceramic and ancient ceramic Neolithic (Matthews et al., 2016, 2019). Since the Bronze Age, the study region was intensively occupied, with a dense network of permanent settlements that developed into large tells that remained active through the Islamic era, and a landscape that was intensely modified. The two areas of interest are investigated by two Italian Archaeological Missions that operated in the NWKRI and in in CKRI. The Land of Nineveh Archaeological Project (LoNAP; P.I.: Daniele Morandi Bonacossi; http://www.terradininive.com/land-of-niniveh/?lang=en ) headed by the University of Udine in collaboration with the Universities of Milan, Venice and Rome investigates the NWKRI with a multidisciplinary territorial research project that investigates the onset of the earliest urban centers and state formation during the Late Chalcolithic and Early Bronze age, the impact of empires of the Iron Ages and later periods on landscape and settlement patterns (Morandi Bonacossi & Iamoni, 2015; Morandi Bonacossi et al., 2018). The MAIPE Archaeological Project of the University of Milan (P.I.: Luca Peyronel; https://orienteantico.unimi.it/it/)[2] investigates since 2013 the Erbil Plain in the CKRI. The MAIPE team surveyed and investigated the two multi-period mounds of Tell Helawa and

Aliawa that allow to reconstruct a long occupational sequence spanning from the prehistoric period to the Islamic Age in the Erbil Plain (Peyronel et al., 2019). The Erbil Plain is densely settled and human-modified landscape with hundreds of archaeological sites, including tells, identified by means of extensive survey coverage carried out by the EPAS Expedition of the University of Harvard (P.I.: Jason Ur) over the last decade (Ur et al., 2013; Ur et al., 2021). Targeted ongoing excavations at different sites are also providing a reliable chronological scheme for the reconstruction of human occupation and landscape exploitation through time.

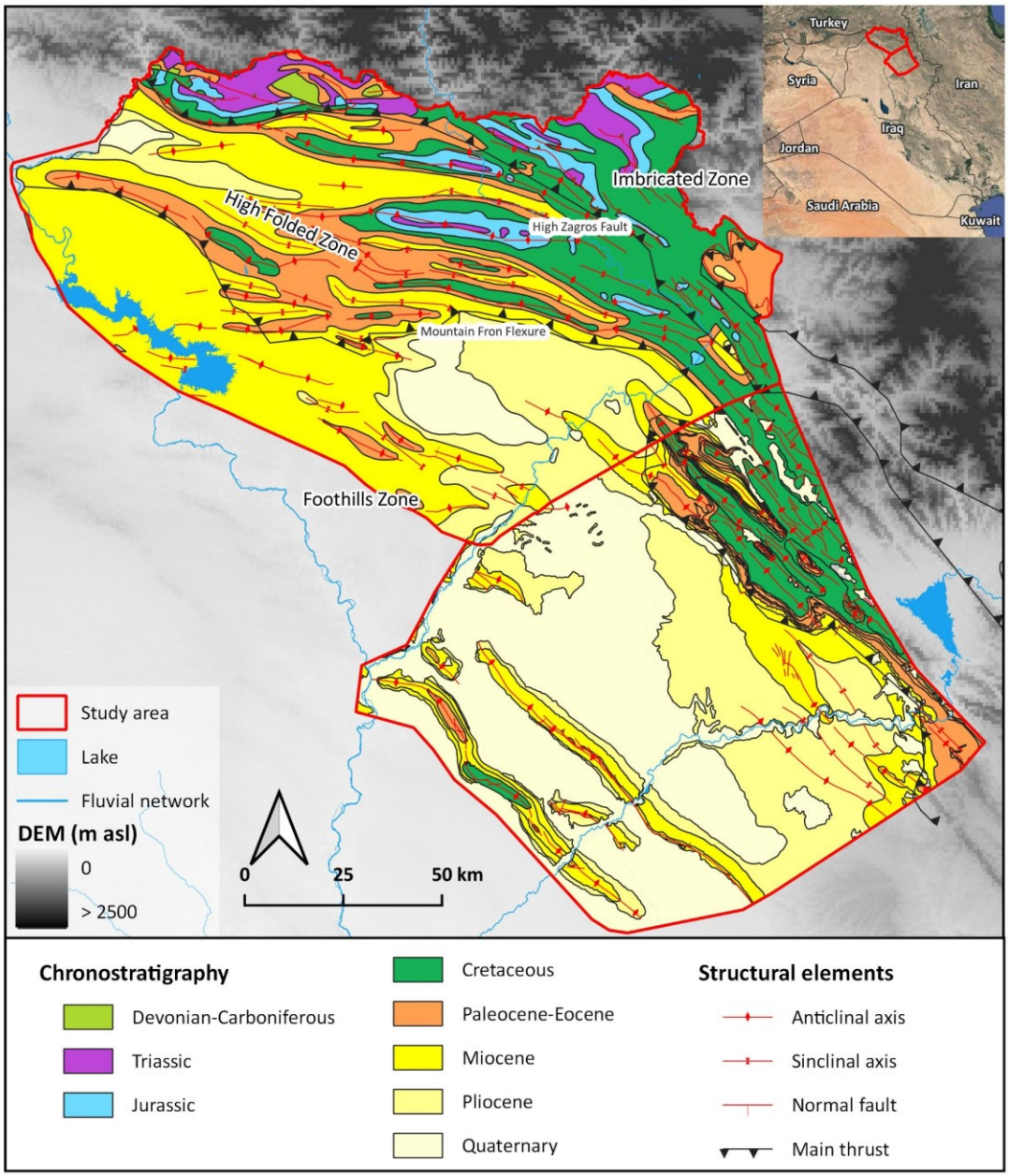


**Figure 2.** Schematic structural elements and chronostratigraphic units in the study areas

## 1.5 Materials and methods

### 1.5.1 Multiscale geomorphological mapping

Geomorphological and geoarchaeological mapping of the two areas was performed to better define the actual landscape and interpret— the landforms from both remote sensing images and field observations, according to the approach proposed by several authors for mapping arid and semi-arid regions (Perego et al., 2011; Azzoni et al., 2017; Hüneburg et al., 2019; Zerboni et al., 2015, 2020; Costanzo et al., 2021). Different datasets were retrieved and analysed through remote sensing; all data has been reprojected to WGS 84 - UTM Zone 38N reference system within QGIS 3.16 and 3.20 software (QGIS Development Team, 2021). Recently acquired high resolution satellite imagery (2013-2021) (Landsat, Sentinel 2A/2B, Esri World Imagery, Bing Virtual Earth and GoogleEarth™ satellite images) was analysed and visualized through "QuickMapServices" plugin (NextGis, 2021). Furthermore, declassified CORONA intelligence satellite imagery, downloaded from CAST Atlas of the University of Arkansas (https://cast.uark.edu/research/corona.php) (USGS, 1968), collected between 1967-1968 and British Royal Air Force (RAF) aerial imagery captured in 1919 (archivied at Archaeological Institute at University College of London UCL) were utilised to recognize variations of landforms through historical time scales (Forti et al., 2022b). An AW3D30 Digital Surface Model (DSM) with 1° horizontal resolution (~30 m at the equator) available on the Japan Aerospace Exploration Agency (JAXA, 2020). The current high-resolution satellite imagery permits the identification of various landforms and archaeological sites, but with the actual urban expansion that has taken place over the past 50 years in the SW areas of Asia, several forms are hidden or destroyed. Thus, the Corona and RAF imagery captured before the urbanisation of several areas allow us to detect the pristine landforms and reconstruct the evolution of landscape. Contour lines derived from this model were used for landform interpretation as well as hillshade and slope models. An elevation-dependent colour scale was applied to the Digital Elevation Model (DEM), imported in QGIS and superimposed over a hillshade, in order to observe specific landforms (river terraces, water and wind gaps and alluvial fans). The channel network was extracted from the DEM using SAGA software. Results were reliable in the mountainous area, while the automatically rendered model of the alluvial plain was manually corrected using satellite and field data. Other than topographical and satellite visual information, the Arbeel-Mahabad. Al-Mosul, Zakho, Kani Rash, Kirkuk and Sulaimanyia quadrangles (1:250,000 sheets) of the Series of Geological Map of Iraq helped define the bedrock geology and delineate linear structural features and occasionally supported the recognition and interpretation of landform features and trends. Several field surveys (carried out in October-November 2019, 2021, 2022) confirmed and validated the geomorphological elements detected

during the desktop study. The field survey included the Zagros Mountains, the low relief fluvial plains, and foothills. High-resolution geomorphological mapping of the archaeological sites was performed by MAIPE team member (E. Ginoli) using an UAV DJI Phantom 4 with a flight at 30 m above the sites and several nadiral photos taken to obtain a detailed and updated topography of the two sites. The photos were taken to achieve a 60% overlap, in regular parallel movements to reduce data loss. The images are at a 72-dpi resolution with 12000 pixels. Afterwards, L. Forti imported and processed the oblique aerial photos into Agisoft Metashape Professional (Version 1.5.5, 2022) with the standard workflow that includes photo alignment, built of dense cloud and mesh to produce a 3D model of the two sites with the extrapolation of Digital Surface Model (DSM). Consequently, from the elaboration of DSM a RUSLE empirical model was developed to estimate long to term average annual soil loss and to map erosion hazard on the archaeological site. RUSLE's elaboration requires five different factors describing the environmental settings of the region of interest and is based on the equation (1):

$$A=R\times K\times LS\times C\times P \qquad (1)$$

where R is the rainfall erosivity, K the soil erodibility, LS is the slope-length topographic factor, C and P represents the land cover and land management variables respectively, and A is the resulting average annual erosion rate measured in tonnes/hectare/year. Several methods have been developed in the last decades to calculate the five RUSLE factors (Ghosal et al., 2020).

### 1.5.2 Reconstruction of Late Quaternary palaeohydrological changes

The reconstruction of palaeohydrological changes in the study area for the Late Quaternary were performed both on the sediment lacustrine deposits of Faide section located on the right bank of Mosul Lake and on speleothems sampled in two caves along the foothills of Zagros in the NWKRI (LoNAP 541 and Āşkaft-ê Haşārok) (Figure 3). Geochemical, sedimentological and palynological analysis performed on lacustrine deposits of Faide (S2) recorded the continuous terrestrial environmental change during the Late Pleistocene to Early Holocene in the Northern Mesopotamia Plain. Analysis on oxygen and carbon isotopic composition revealed information about past amount of rainfall and evaporation rate of the ancient lake. The ratios of nitrogen and carbon isotopes on organic matter inform on the source of organic matter, past productivity, and changes in nutrient supply of the lake. These data correlate with palynological analysis allowed us to reconstruct the past landscape and plant cover along the present-day left bank of the Mosul Lake (Figure 4). Unfortunately, in this thesis the Faide section has not been considered due to some problems with radiometric dating. Instead, stable isotope analysis and U/Th dating performed on speleothems are used to reconstruct the palaeoclimate of the region during the Early-Middle Holocene. The analysis

on stalagmite and flowstone permits to define several environmental proxies retrieved from oxygen and carbon stable isotopes such as the amount of rainfall, the climate-palaeovegetation signals, the variation of meteoric water and its isotopic signature and measurement of palaeotemperature variations. The speleothem LoNAP514 is a flowstone 86 mm thick and composed of compact columnar calcite. Samples for $\delta^{13}C$ and $\delta^{18}O$ were drilled at a mean resolution of 0.3 mm and analysed using a Precision AP2003 continuous-flow isotope-ratio mass spectrometer at the School of Geography, Earth and Atmospheric Sciences at the University of Melbourne (UoM) using the method reported in (Bajo et al., 2020). Mean analytical uncertainties are 0.07‰ and 0.05‰ for δ18O and δ13C, respectively. U-Th dating was performed at the School of Geography, Earth and Atmospheric Sciences (UoM) on 17 calcite prisms of ~100 mg, employing a multi-collector inductively coupled plasma mass spectrometer (MC-ICP-MS; Nu-Instruments Plasma) and the method presented in Hellstrom (2003). The age-depth model has been obtained by Monte Carlo modelling and stratigraphic constrains following Hellstrom (2006).

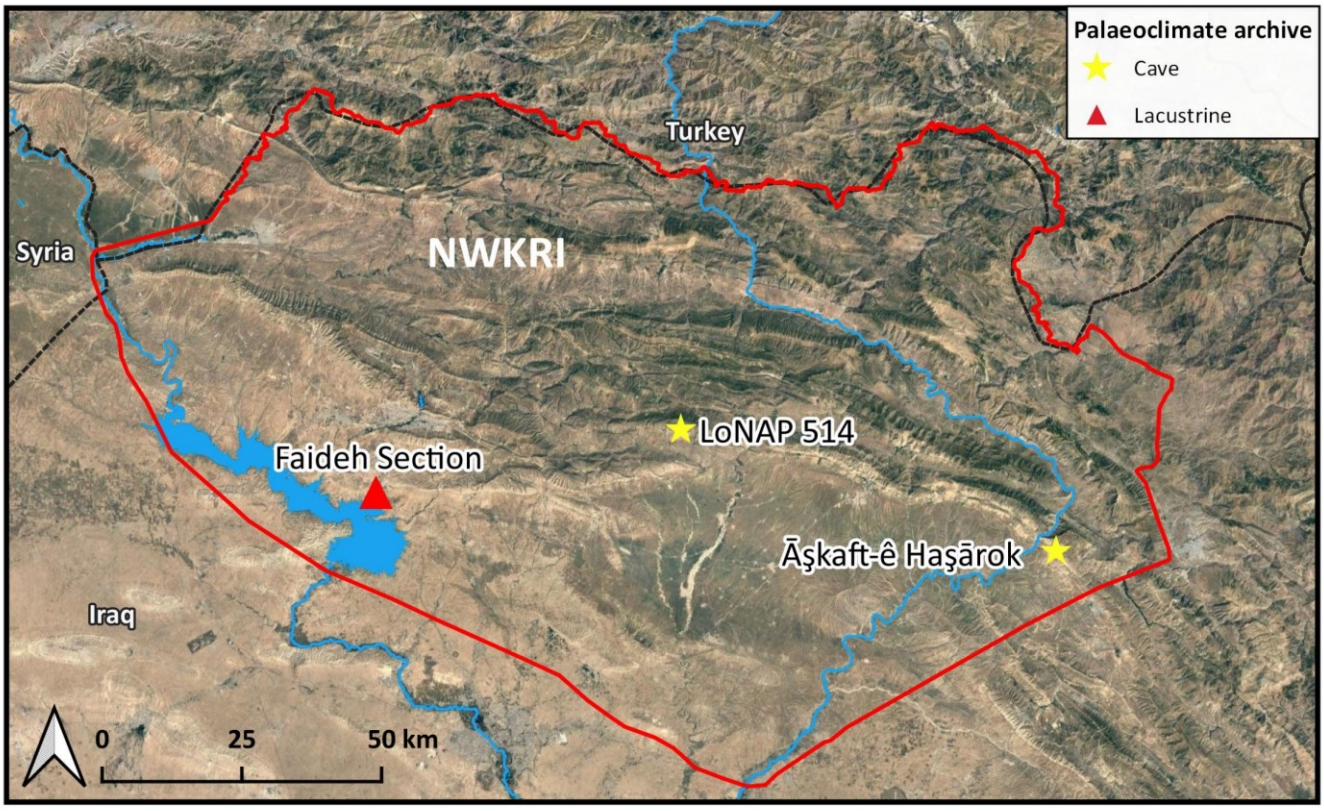


**Figure 3.** The palaeoclimate archives in the NWKRI

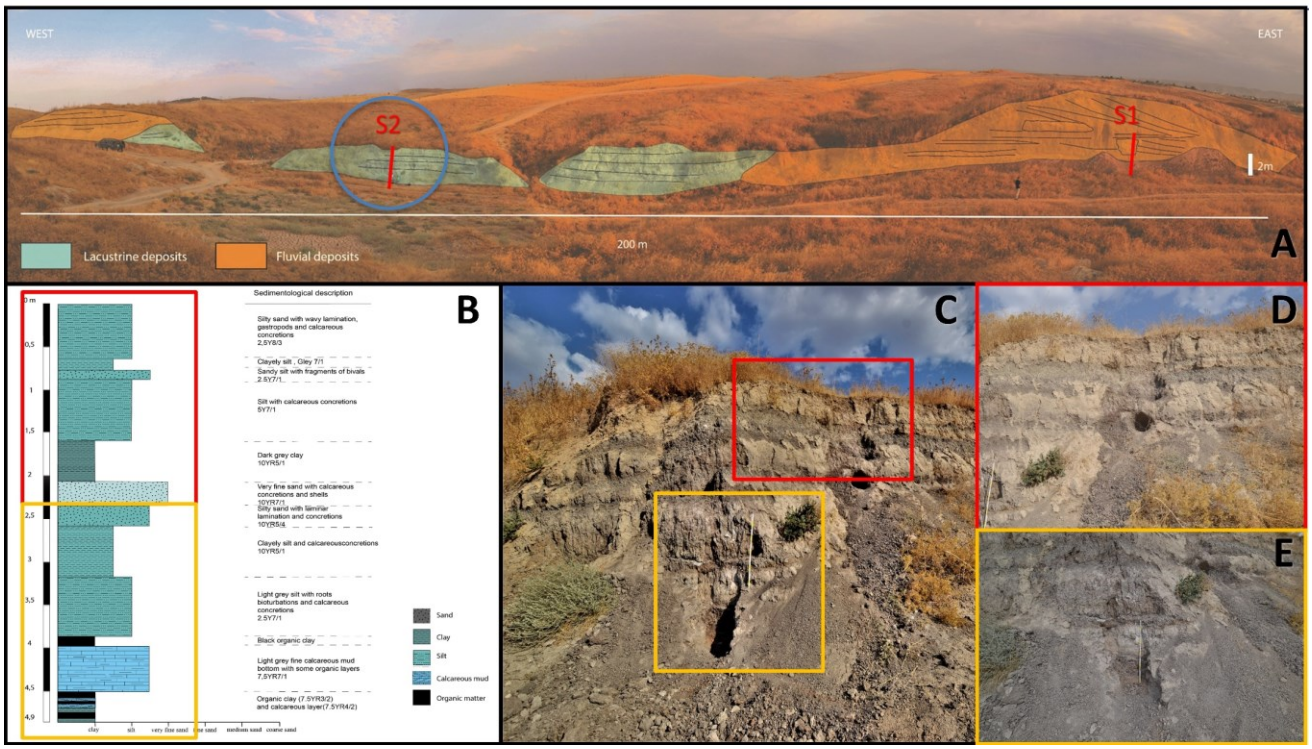


**Figure 4.** A) The section of Faide where fluvial (S1) and lacustrine (S2) profiles were analyzed. B) Stratigraphic log of the S2 lacustrine deposits. C-D-E) Details of the top and bottom S2 profile.

### 1.5.3 Analysis on archaeological deposit

Analyses on the archaeological sediments were carried out to understand how the archaeological site was formed, its phases of use and later abandonment. In this case, post-depositional geological and pedological processes were analysed both in the field and in the laboratory. Samples for sedimentological analyses were collected, labelled, and processed with reference to the Stratigraphic Units (SU) identified during the archaeological excavation of the trenches. Physical sedimentological characterization of sediments was carried out at the Earth Sciences Department of the University of Milan. Characterization of sediments included the following analyses: grain-size distributions were performed after removing organics by hydrogen peroxide (130 vol) pre-treatment; sediments were wet sieved (diameter 1.0–0.63 mm), then the fine fraction (<0.63 mm) was determined by hydrometer based on Stokes' law (Gale and Hoare, 1991). For the micromorphological investigations undisturbed blocks were collected from clean sections and thin sections were manufactured by Massimo Sbrana – Servizi per la Geologia laboratory (Piombino, Italy) following the procedure described by Murphy (1986). The finished thin section product is a 55x95mm slice mounted on a glass support. The thin sections were studied employing an optical petrographic microscope (Olympus BX41) mounting a digital camera (Olympus E420) for image acquisition. Observation was carried out at various magnifications (20x, 40x, 100x, 400x) under plane polarised light (PPL) and cross-polarized light

(XPL). The description of the thin sections followed the terminology suggested by Stoops (2021), and their interpretation was aided by the coloured atlases and concepts summarised in Nicosia & Stoops (2017), Macphail & Goldberg (2018), and Stoops et al. (2018).

## 1.6 Structure of the thesis

The PhD project was performed through a multi-scalar approach, defined by Butzer (2008) as "scale-switching, from the large to the small and back", and provides links between landscape (remote sensing) and site stratigraphy (micro-analysis), which significantly enhance the interpretative potential of studying human responses and adaptation to climate, landscapes, ecosystems, and natural resources availability changes in different regions of our planet, and eventually identify human influence on them. In this scenario, the second and third chapters introduce the major landscape features of the two abovementioned areas of the KRI. In detail, Chapter 2 is the geomorphological map of the NWKRI that highlights the main landforms, surface processes and factors that affected the evolution of the landscape. Likewise, Chapter 3 report the main geomorphological aspects of the central sector of the Kurdistan Region of Iraq, in which the relationship between tectonics, climate variations and geomorphological processes influenced the local drainage network. Geomorphological maps discussed in Chapters 2 and 3 are reported in the appendix of the thesis. Afterward, the topic of the fourth chapter is related to paleoclimatic data derived from a speleothem sampled at foothills of Zagros Mountains. Paleoclimate data displayed the hydroclimatic fluctuations occurred in the Early Holocene and the comparison with the local archaeological framework highlights an influence of the hydroclimatic changes on the settlement patterns and on the exploitation of water resources. This is the first record for the region providing palaeo-precipitation data describing the Early Holocene and encompassing several major cultural transitions. A special focus on water resources and their management was broached in the Chapter 5, in which the declassified intelligence satellite imagery was used to reconstruct past landforms and surface processes below the Mosul Dam Lake. A detailed geomorphological reconstruction of the pristine pattern of Tigris River reveals a strong control on the present-day aspect of the lake. This manuscript is an example of the ancient landscape reconstruction through remote sensing analysis on historical images to investigate the surface processes and the sudden geomorphological processes changes. Chapters 6 and 7 combines the geoarchaeological analysis applied to archaeological sites-scale. Chapter 6 proposes a fresh approach to the preservation of archaeological sites. The elaboration of an empirical model usually applied to describe soil loss (RUSLE) and derived from UAV imagery estimates the annual soil loess on the slopes of archaeological sites and outlines the natural and human-driven factors that mining the preservation of archaeological record. Chapter 7 examines the different phases of use, abandonment a repurposing

of Assyrian canals with micromorphological and sedimentological analysis on the filling sediments that revealed a shifting in land use related to climate and human dynamics changes. This chapter suggest the potentiality of micromorphology in reconstruct variations in surface processes and ancient shift of land use. Chapter 8 is a reconstruction of the landscape before the large-scale urbanisation of the city of Erbil. A comparison of historical images from 1919 to the present day reveal the great anthropic impact and geomorphological changes of a river landscape and surface processes modified by continuous urbanisation. This chapter highlights the anthropogenic impact on the modification of the landscape by making it more sensitive to hydrological and environmental risks.

## 1.7 References

Al-Zuhairi, M. F., Al-Jumaily, K. J., & Al-Salihi, A. M. (2016). Characteristics of precipitation systems over Iraq observed by TRMM radar. *American Journal of Engineering Research*, *5*(11), 76-81.

Anderson, R. S., & Burbank, D. W. (2011). *Tectonic Geomorphology*. John Wiley & Sons.

Arranz-Otaegui, A., Colledge, S., Zapata, L., Teira-Mayolini, L. C., & Ibáñez, J. J. (2016). Regional diversity on the timing for the initial appearance of cereal cultivation and domestication in southwest Asia. *Proceedings of the National Academy of Sciences*, *113*(49), 14001-14006.

Azzoni, R. S., Zerboni, A., Pelfini, M., Garzonio, C. A., Cioni, R., Meraldi, E., ... & Diolaiuti, G. A. (2017). Geomorphology of Mount Ararat/Ağri Dağı (Ağri Dağı Milli Parki, Eastern Anatolia, Turkey). *Journal of Maps*, *13*(2), 182-190.

Bajo, P., Drysdale, R. N., Woodhead, J. D., Hellstrom, J. C., Hodell, D., Ferretti, P., ... & Fallick, A. E. (2020). Persistent influence of obliquity on ice age terminations since the Middle Pleistocene transition. *Science*, *367*(6483), 1235-1239.

Bar-Matthews, M., & Ayalon, A. (2004). Speleothems as palaeoclimate indicators, a case study from Soreq Cave located in the Eastern Mediterranean Region, Israel. In *Past climate variability through Europe and Africa* (pp. 363-391). Springer, Dordrecht.

Berberian, M. (1995). Master "blind" thrust faults hidden under the Zagros folds: active basement tectonics and surface morphotectonics. *Tectonophysics*, *241*(3-4), 193-224.

Bishop, P. (2007). Long-term landscape evolution: linking tectonics and surface processes. *Earth Surface Processes and Landforms: The Journal of the British Geomorphological Research Group*, *32*(3), 329-365.

Blanc, E. P., Allen, M. B., Inger, S., & Hassani, H. (2003). Structural styles in the Zagros simple folded zone, Iran. *Journal of the Geological Society*, *160*(3), 401-412.

Braidwood, R. J., & Howe, B. (1960). Prehistoric Investigations in Iraqi Kurdistan. *Studies in ancient oriental civilization*, *31*.

Burbank, D. W., & Pinter, N. (1999). Landscape evolution: the interactions of tectonics and surface processes. *Basin Research*, *11*(1), 1-6.

Clarke, J., Brooks, N., Banning, E. B., Bar-Matthews, M., Campbell, S., Clare, L., ... & Zerboni, A. (2016). Climatic changes and social transformations in the Near East and North Africa during the 'long'4th millennium BC: A comparative study of environmental and archaeological evidence. *Quaternary Science Reviews*, *136*, 96-121.

Cole, S. (1961). The neolithic revolution. Paléorient, 10, 2-1984.

Conati Barbaro, C., Moscone, D., Iamoni, M., Morandi Bonacossi, D., & Qasim, H. A. (2019). The prehistory and protohistory of the northwestern region of Iraqi Kurdistan: Preliminary results from the first survey campaigns. *Paléorient. Revue pluridisciplinaire de préhistoire et de protohistoire de l'Asie du Sud-Ouest et de l'Asie centrale*, (45-2), 207-229.

Costanzo, S., Zerboni, A., Cremaschi, M., & Manzo, A. (2021). Geomorphology and (palaeo-) hydrography of the Southern Atbai plain and western Eritrean Highlands (Eastern Sudan/Western Eritrea). *Journal of Maps*, *17*(2), 51-62.

Crassard, R., Petraglia, M. D., Drake, N. A., Breeze, P., Gratuze, B., Alsharekh, A., ... & Schiettecatte, J. (2013). Middle Palaeolithic and Neolithic occupations around Mundafan palaeolake, Saudi Arabia: implications for climate change and human dispersals. PLoS One, 8(7), e69665.

Cremaschi, M., & Zerboni, A. (2010). Human communities in a drying landscape: Holocene climate change and cultural response in the central Sahara. In *Landscapes and Societies* (pp. 67-89). Springer, Dordrecht.

Cremaschi, M., Zerboni, A., Charpentier, V., Crassard, R., Isola, I., Regattieri, E., & Zanchetta, G. (2015). Early Middle Holocene environmental changes and pre-Neolithic human occupations as recorded in the cavities of Jebel Qara (Dhofar, southern Sultanate of Oman). Quaternary International, 382, 264-276.

Cremaschi, M., Zerboni, A., Mercuri, A. M., Olmi, L., Biagetti, S., & Di Lernia, S. (2014). Takarkori rock shelter (SW Libya): an archive of Holocene climate and environmental changes in the central Sahara. *Quaternary Science Reviews*, *101*, 36-60.

Csontos, L., Sasvári, Á., Pocsai, T., & Kósa, L. (2011, May). Structural evolution of the northwestern Zagros, Kurdistan Region, Iraq and alternative models for formation of a curved mountain chain. In *73rd EAGE Conference and Exhibition-Workshops 2011* (pp. cp-239). European Association of Geoscientists & Engineers.

Eklund, L., & Seaquist, J. (2015). Meteorological, agricultural, and socioeconomic drought in the Duhok Governorate, Iraqi Kurdistan. *Natural Hazards*, *76*(1), 421-441.

Engel, M., Brückner, H., Pint, A., Wellbrock, K., Ginau, A., Voss, P., ... & Frenzel, P. (2012). The early Holocene humid period in NW Saudi Arabia–Sediments, microfossils and palaeo-hydrological modelling. Quaternary International, 266, 131-141.

Forti, L., Mariani, G. S., Brandolini, F., Pezzotta, A., & Zerboni, A. (2022b). Declassified intelligence satellite imagery as a tool to reconstruct past landforms and surface processes. The submerged riverscape of the Tigris River below the Mosul Dam Lake, Iraq. *Earth Surface Processes and Landforms*.

Forti, L., Perego, A., Brandolini, F., Mariani, G. S., Zebari, M., Nicoll, K., ... & Zerboni, A. (2021). Geomorphology of the northwestern Kurdistan Region of Iraq: landscapes of the Zagros Mountains drained by the Tigris and Great Zab Rivers. *Journal of Maps*, *17*(2), 225-236.

Forti, L., Romano, L., Celant, A., D'Agostino, F., Di Rita, F., Jotheri, J., ... & Milli, S. (2022). The paleoenvironment and depositional context of the Sumerian site of Abu Tbeirah (Nasiriyah, southern Mesopotamia, Iraq). *Quaternary Research*, 1-19.

Fouad, S. F. (2014). Western Zagros fold–Thrust Belt, part II: The high folded zone. *Iraqi bulletin of geology and mining*, (6), 53-71.

Frizon de Lamotte, D., Raulin, C., Mouchot, N., Wrobel-Daveau, J. C., Blanpied, C., & Ringenbach, J. C. (2011). The southernmost margin of the Tethys realm during the Mesozoic and Cenozoic: Initial geometry and timing of the inversion processes. *Tectonics*, *30*(3).

Gallinaro, M. (2009). Il nomadismo pastorale nel Deserto Occidentale Egiziano durante l'Olocene: il ruolo rivestito dagli Steinplatz nei modelli di occupazione del territorio [Nomadic pastoralism in the Egyptian Western Desert during the Holocene: the role of the Steinplätze in regional settlement patterns], Università di Napoli 'L'Orientale', 2008. *Azania: Archaeological Research in Africa*, *44*(1), 159-160.

Ghosal, K., & Das Bhattacharya, S. (2020). A review of RUSLE model. *Journal of the Indian Society of Remote Sensing*, *48*(4), 689-707.

Gutiérrez, M. (2005). *Climatic geomorphology*, Amsterdam, The Netherlands: Elsevier.

Hamann, Y., Ehrmann, W., Schmiedl, G., Krüger, S., Stuut, J. B., & Kuhnt, T. (2008). Sedimentation processes in the Eastern Mediterranean Sea during the Late Glacial and Holocene revealed by end-member modelling of the terrigenous fraction in marine sediments. *Marine Geology*, *248*(1-2), 97-114.

Hasan, A. A., Hussien, M. L., Fadhil, L. A., Hasan, M. I., & Mosquera, C. D. (2019). Crustal Deformations and Geomorphological Units of Arabian Plate Foreland Region, North and Northeast of Iraq. *Journal of Southwest Jiaotong University*, *54*(5).

Hellstrom, J. (2003). Rapid and accurate U/Th dating using parallel ion-counting multi-collector ICP-MS. *Journal of Analytical Atomic Spectrometry*, *18*(11), 1346-1351.

Hellstrom, J. (2006). U–Th dating of speleothems with high initial 230Th using stratigraphical constraint. *Quaternary Geochronology*, *1*(4), 289-295.

Hüneburg, L., Hoelzmann, P., Knitter, D., Teichert, B., Richter, C., Lüthgens, C., ... & Luciani, M. (2019). Living at the wadi–integrating geomorphology and archaeology at the oasis of Qurayyah (NW Arabia). *Journal of Maps*, *15*(2), 215-226.

Jassim, S. Z., & Goff, J. C. (Eds.). (2006). *Geology of Iraq*. DOLIN, sro, distributed by Geological Society of London.

JAXA (2021) - ALOS Global Digital Surface Model "ALOS World 3D – 30m (AW3D30)" Retrieved August 11, 2021, from https://www.eorc.jaxa.jp/ALOS/en/aw3d30/.

Kamlah, J., & Riehl, S. (2020). Agriculture in the bronze age Levant. *A companion to ancient agriculture*, 193-209.

Kirby, E., & Whipple, K. X. (2012). Expression of active tectonics in erosional landscapes. *Journal of structural geology*, *44*, 54-75.

Kröpelin, S., (2005). The geomorphological and palaeoclimatic framework of prehistoric occupation in the Wadi Bakht area. *Wadi Bakht. Köln, Heinrich Barth Institut, Africa Praehistorica*, *18*, 51-65.

Langgut, D., Neumann, F. H., Stein, M., Wagner, A., Kagan, E. J., Boaretto, E., & Finkelstein, I. (2014). Dead Sea pollen record and history of human activity in the Judean Highlands (Israel) from the Intermediate Bronze into the Iron Ages (~ 2500–500 BCE). *Palynology*, *38*(2), 280-302.

Lawrence, D., Philip, G., & de Gruchy, M. W. (2021). Climate change and early urbanism in Southwest Asia: A review. *Wiley Interdisciplinary Reviews: Climate Change*, *13*(1), e741.

Macphail, R. I., & Goldberg, P. (2018). *Applied soils and micromorphology in archaeology*. Cambridge University Press.

Mariani, G. S., Muntoni, I. M., & Zerboni, A. (2020). The Eneolithic/Bronze Age transition at Tegole di Bovino (Apulia): geoarchaeological evidence of climate change and land-use shift. *Quaternary*, *3*(2), 14

Matthews, R., Matthews, W., Rasheed, K., & Aziz, K. (2016). Current investigations into the early Neolithic of the Zagros foothills of Iraqi Kurdistan. *The Archaeology of the Kurdistan Region of Iraq and Adjacent Regions, edited by K. Kopanias, and J. MacGinnis*, 219-228.

Matthews, R., Matthews, W., Richardson, A., Walsh, S., Iversen, I., Mudd, D., ... & Elliott, S. (2019). The early Neolithic of Iraqi Kurdistan: Current research at bestansur, shahrizor plain. *Paléorient. Revue pluridisciplinaire de préhistoire et de protohistoire de l'Asie du Sud-Ouest et de l'Asie centrale*, (45-2), 13-32.

Migowski, C., Stein, M., Prasad, S., Negendank, J. F., & Agnon, A. (2006). Holocene climate variability and cultural evolution in the Near East from the Dead Sea sedimentary record. *Quaternary Research*, *66*(3), 421-431.

Morandi Bonacossi, D., & Iamoni, M. (2015). Landscape and settlement in the eastern upper Iraqi Tigris and Navkur plains (Northern Kurdistan region, Iraq). The land of Nineveh archaeological project, seasons 2012-2013. *Iraq*, 77(1), 9-40.

Morandi Bonacossi,D., Qasim, H. A., Coppini, C., Gavagnin, K., Girotto, E., Iamoni, M., & Tonghini, C. (2018). The Italian-Kurdish excavations at Gir-e Gomel in the Kurdistan region of Iraq. Preliminary report on the 2017 and 2018 field seasons. *Mesopotamia*, *53*, 67-162.

Mouthereau, F., Lacombe, O., & Vergés, J. (2012). Building the Zagros collisional orogen: timing, strain distribution and the dynamics of Arabia/Eurasia plate convergence. *Tectonophysics*, *532*, 27-60.

Murphy, C. P. (1986). *Thin section preparation of soils and sediments*. AB Academic.

NextGIS (2021) - QuickMapServices. https://nextgis.com/blog/quickmapservices/.

Nicholson, S. E. (2011). Dryland climatology.

Nicoll, K. (2012). Geoarchaeological perspectives on Holocene climate change as a civilizing factor in the Egyptian Sahara. *Landscape, Climate and Ancient Civilizations. American Geophysical Union, Washington, DC*, 157-162.

Nicoll, K., & Zerboni, A. (2020). Is the past key to the present? Observations of cultural continuity and resilience reconstructed from geoarchaeological records. *Quaternary International*, *545*, 119-127.

Nicosia, C., & Stoops, G. (Eds.). (2017). *Archaeological soil and sediment micromorphology*. John Wiley & Sons.

Palmisano, A., Lawrence, D., de Gruchy, M. W., Bevan, A., & Shennan, S. (2021). Holocene regional population dynamics and climatic trends in the Near East: A first comparison using archaeo-demographic proxies. *Quaternary Science Reviews*, *252*, 106739.

Parker, A. G., Morley, M. W., Armitage, S. J., Engel, M., Parton, A., Preston, G. W., ... & Drechsler, P. (2020). Palaeoenvironmental and sea level changes during the Holocene in eastern Saudi Arabia and their implications for Neolithic populations. Quaternary Science Reviews, 249, 106618.

Perego, A., Zerboni, A., & Cremaschi, M. (2011). Geomorphological Map of the messak settafet and mellet (central Sahara, SW Libya). *Journal of Maps*, *7*(1), 464-475.

Peyronel, L., Minniti, C., Moscone, D., Naime, Y., Oselini, V., Perego, R., & Vacca, A. (2019). The Italian Archaeological Expedition in the Erbil Plain, Kurdistan Region of Iraq: Preliminary Report on the 2016-2018 Excavations at Helawa.

Pournelle, J. R. (2013). Physical geography. In *The Sumerian World* (pp. 37-56). Routledge.

QGIS Development Team (2021) - QGIS Geographic Information System. Open-Source Geospatial Foundation Project.

Rivas-Martínez, S. (2004). Global bioclimatics. *Clasificaciòn Bioclimàtica de la tierra*.

Rosen, A. M. (1986). *Cities of clay: the geoarcheology of tells*. University of Chicago Press.

Rosen, A. M. (2007). *Civilizing climate: social responses to climate change in the ancient Near East*. Rowman Altamira.

Rosen, S. A. (2011). *An investigation into early desert pastoralism: excavations at the Camel Site, Negev* (Vol. 69). ISD LLC.

Simmons, A. H. (2011). The Neolithic revolution in the Near East: transforming the human landscape. University of Arizona Press.

Solecki, R. S. (1971). Shanidar, the first flower people. Knopf.

Stoops, G. (2021). *Guidelines for analysis and description of soil and regolith thin sections* (Vol. 184). John Wiley & Sons.

Ur, J., Babakr, N., Palermo, R., Creamer, P., Soroush, M., Ramand, S., & Nováček, K. (2021). The Erbil Plain Archaeological Survey: Preliminary Results, 2012–2020. *Iraq*, *83*, 205-243

Ur, J., De Jong, L., Giraud, J., Osborne, J. F., & MacGinnis, J. (2013). Ancient Cities and Landscapes in the Kurdistan Region of Iraq: The Erbil Plain Archaeological Survey 2012 Season1. *Iraq*, *75*, 89-117.

USGS (1968) - Declassified Corona Imaging data. Data retrvied on 16 august, 2020, from https://corona.cast.uark.edu.

Van de Mieroop, M. (2015). *A history of the ancient Near East, ca. 3000-323 BC*. John Wiley & Sons.

Vergés, J., Saura, E., Casciello, E., Fernandez, M., Villaseñor, A., Jimenez-Munt, I., & García-Castellanos, D. (2011). Crustal-scale cross-sections across the NW Zagros belt: implications for the Arabian margin reconstruction. *Geological Magazine*, *148*(5-6), 739-761.

Verheyden, S., Nader, F. H., Cheng, H. J., Edwards, L. R., & Swennen, R. (2008). Paleoclimate reconstruction in the Levant region from the geochemistry of a Holocene stalagmite from the Jeita cave, Lebanon. *Quaternary Research*, *70*(3), 368-381.

Watkins, T. (2010). New light on Neolithic revolution in south-west Asia. *Antiquity*, *84*(325), 621-634.

Wilkinson, T. J. (2003). *Archaeological landscapes of the Near East*. University of Arizona Press.

Wilkinson, T. J., Galiatsatos, N., Lawrence, D., Ricci, A., Dunford, R., & Philip, G. (2012). Late Chalcolithic and Early Bronze Age landscapes of settlement and mobility in the Middle Euphrates: a reassessment. *Levant*, *44*(2), 139-185.

Wilkinson, T. J., Philip, G., Bradbury, J., Dunford, R., Donoghue, D., Galiatsatos, N., ... & Smith, S. L. (2014). Contextualizing early urbanization: Settlement cores, early states and agro-pastoral strategies in the Fertile Crescent during the fourth and third millennia BC. *Journal of World Prehistory*, *27*(1), 43-109.

Yacoub, S. Y., Othman, A. A., & Kadhim, T. H. (2012). Geomorphology of the low folded zone. *Iraqi Bulletin of Geology and Mining*, (5), 7-37.

Zebari, M., Balling, P., Grützner, C., Navabpour, P., Witte, J., & Ustaszewski, K. (2020). Structural style of the NW Zagros Mountains and the role of basement thrusting for its Mountain Front Flexure, Kurdistan Region of Iraq. *Journal of Structural Geology*, *141*, 104206.

Zerboni, A., Perego, A., & Cremaschi, M. (2015). Geomorphological map of the Tadrart Acacus massif and the Erg Uan kasa (Libyan Central Sahara). *Journal of Maps*, *11*(5), 772-787.

Zerboni, A., Perego, A., Mariani, G. S., Brandolini, F., Al Kindi, M., Regattieri, E., ... & Cremaschi, M. (2020). Geomorphology of the Jebel Qara and coastal plain of Salalah (Dhofar, southern Sultanate of Oman). *Journal of Maps*, *16*(2), 187-1

# Chapter 2

# Geomorphology of the northwestern Kurdistan Region of Iraq: landscapes of the Zagros Mountains drained by the Tigris and Great Zab Rivers

## 2.1 Introduction

The interplay between endogenous and exogenous processes produces various landscapes on Earth (Burbank & Pinter, 1999; Burbank & Anderson, 2011). In tectonically active regions like the Kurdistan Region of Iraq (KRI), vertical and lateral movements of faults and surface processes influenced the distribution and formation of landforms. Folding, stretching, shearing, and faulting of rocks exert major control over the evolution of the region's hydrographic networks (Oberlander, 1965, 1985; Bishop, 2007; Nicoll, 2010; Burbank & Anderson, 2011; Kirby & Whipple, 2012; Hasan et al., 2019). In arid and semi-arid regions, where climatic factors appear to be dominant, local water availability affects the intensity of surface and sub-surface processes. This is ultimately related to present-day climatic settings and Quaternary rainfall variations (Goudie, 2013). By contrast, in tectonically dynamic regions like the KRI, the evolution of surface processes is often controlled by the interplay between climate changes and tectonic influence, namely uplift, faulting and folding (Hüneburg et al., 2019; Zerboni et al., 2020). The KRI is a semi-arid, arid to Mediterranean climate region where the interaction between thrust and fold processes, climate, and rate of weathering erosion- depositional processes is dramatically evident in the present-day landscape (Jassim & Goff, 2006; Fouad, 2015; Alwan et al., 2019). At the same time, the role of fluvial dynamics, slope, karst, and anthropogenic processes significantly impacted the developing mountain and lowland physiography. The KRI has been the scene for many milestones in human evolution: among others, the 'Out of Africa' dispersion of Homo, the earliest onset of agriculture, the creation of the first complex societies and the emergence of ancient urban centers (Van de Mieroop, 2015). Understanding the timing and steps of landscape evolution of the KRI is thus vital for explaining the adaptive strategies of its ancient human dwellers (Pomeroy et al., 2017). The interpretation of such a palimpsest landscape where geologic processes and climatic fluctuations have interacted for a long time requires a detailed geomorphological investigation. Therefore, we developed a geomorphological map (Main Map) of the KRI in order to (i) map the distribution of fundamental geomorphological features, (ii) recognize the different contribution of both endogenous and

*Forti, L., Perego, A., Brandolini, F., Mariani, G. S., Zebari, M., Nicoll, K., ... & Zerboni, A. (2021). Geomorphology of the northwestern Kurdistan Region of Iraq: landscapes of the Zagros Mountains drained by the Tigris and Great Zab Rivers. Journal of Maps, 17(2), 225-236. https://doi.org/10.1080/17445647.2021.1906339*

exogenous processes on shaping landforms in order to (iii) correlate them with human subsistence strategies adopted during the Late Quaternary in response to climate fluctuations and environment changes. This work illustrates the geomorphology of the northern KRI, a landscape that includes the Zagros Mountains and the drainage basins of the Tigris and Great Zab Rivers, as the first map contribution toward a further regional interpretation (Appendix I).

## 2.2 The study area: geographic, geological, climatic, and archaeological background

The study area covers 12,000 $km^2$ in the northwestern KRI inside the governorates of Dohuk, Nineveh, and Erbil. The main topographic elements are: (i) the mountain belt of Zagros in the North that merges with its southern foreland expressed as (ii) several wide plains bordered by the Tigris River in the Southwest and the Great Zab River in the East. In the whole area, fluvial patterns are influenced by the tectonic activity related to the propagation of the Zagros structures: some rivers flow from WNW–ESE to N–S (Gomel Su, Nahr al-Kazir and Great Zab Rivers), others from N–S to W (Khabur River and its tributaries). Regional, long-term climatic data are scanty; the only reliable data series comes from the meteorological station in the city of Mosul, also known as ancient Nineveh, and located 20 km towards South outside the Main Map. The available models suggest a semi-arid to temperate-warm climate for the lowlands, with an average annual rainfall around 380 mm and temperatures ranging from −0.6 to 37.3°C with wide variations due to orographic effects and mountain air circulation patterns (Wilkinson & Tucker, 1995; Wilkinson, 2003). Winters are moderate to cold, while summers are dry and hot to extremely hot. Roughly, 90% of the annual rainfall occurs in the winter months between December and March. In the mountainous foothills, the climate is classified as the Mediterranean, with precipitation up to 1000 mm/yr. and a long-wet season (November– April) (Eklund & Seaquist, 2015; Al-Zuhairi et al., 2016). Most rivers and tributaries are active during the rainy period (Othman & Gloaguen, 2013) and ephemeral or inactive in the dry season. The Tigris, Great Zab, Nahr al-Khazir and Khabur are perennially active rivers. The KRI region is part of the Zagros-Fold Thrust Belt (ZFTB), resulting from the continental collision between the Arabian and Eurasia plates that started in the Early Miocene and still actively progressing today (Dewey et al., 1973; Csontos et al., 2012; Mouthereau et al., 2012; Fouad, 2015). The Zagros deformation has propagated over the NE margin of the Arabian Plate toward the Mesopotamian Foreland Basin and the Persian Gulf (Blanc et al., 2003; Vergés et al., 2011; Csontos et al., 2012). In the KRI, tectonic deformation along the ZFTB is organized into four different zones from the inner part of the orogeny (Imbricated and High Fold zones) to its foreland (Foothills zone and Mesopotamian Foreland Basin) (Berberian, 1995; Jassim & Goff, 2006; Frizon de Lamotte et al.,

2011; Fouad, 2015). The deformation is expressed by formation of a series of anticline folds that comprise the main structural pattern within the regional landscape. Some scholars suggest that a strike-slip fault with dextral shear shifted the orientation of anticline relief and related synclinal valleys with different uplift and exhumation rates (Reilinger et al., 2006; Csontos et al., 2012). Anticlines are W–E trending in the Dohuk area, while in the eastern and southern sector of the mountain belt, the orientation of anticlines changes into NW–SE. The folded and deformed sedimentary succession exposed in the area includes Upper Triassic/Lower Cretaceous to Pliocene units. Within the Imbricated and the High Folded zone, the anticlinal ridges mainly consist of reefal limestone, dolomitic limestone with bedded marls and shales of Upper Triassic-Upper Cretaceous ages. At the border with Turkey, there are outcrops of Ordovician sandstones and Carboniferous-Permian limestones and shale; while to the North and East of the Dohuk City, the Eocene carbonates form the ridges of anticlines (Sissakian, 2014; Zebari et al., 2019). Along the Foothill Zone, sequences of limestone, dolostone and sandstone from the Upper Paleocene to the Lower Miocene are exposed. Middle to Late Miocene mudstones and sandstones form the substrate of lowlands. Finally, Plio-Pleistocene conglomerates outcrop close to the Great Zab River and Mosul Dam Lake (Al-Dabbagh & Al-Naqib, 1991; Fouad, 2014; Sissakian, 2014). Fluvial, floodplain, alluvial fan, colluvial and anthropogenic deposits characterize the Quaternary sequences in the hillslope of anticlines and in the low relief areas (Jassim & Goff, 2006; Fouad, 2014). The anticlines within the foothills are widely spaced and the synclines between them create swales and plains filled by various Quaternary sediments, including alluvial fans and floodplain deposits. As a consequence of recent tectonic activity, fluvial terraces and part of the alluvial plain are tilted following the deformation pattern of the main orogen (Figure1). The KRI and adjoining regions have been inhabited since at least the Middle Palaeolithic (Morandi Bonacossi, 2017), as confirmed by various occurrences such as the archaeological site of Shanidar Cave, where nine Neanderthals were buried (Solecki, 1971). Since the late Upper Pleistocene, hunter-gatherer communities began to intensively exploit plants, especially wild cereals, and legumes (Conati Barbaro et al., 2016, 2019). However, the agricultural revolution and its economic and social changes appear in the Neolithic (Watkins et al., 1989; Bader,1993; Kozlowski, 1998, 2002), when the major sites (here called tells or mounds) show a complex architecture and an economy based on agriculture and herding during both the pre-ceramic and ancient ceramic Neolithic (Braidwood, 1983; Matthews et al., 2016, 2019). Since the Bronze Age, the study region was intensively occupied, with a dense network of permanent settlements that developed into large tells that remained active through the Islamic era, and a landscape that was intensely modified.

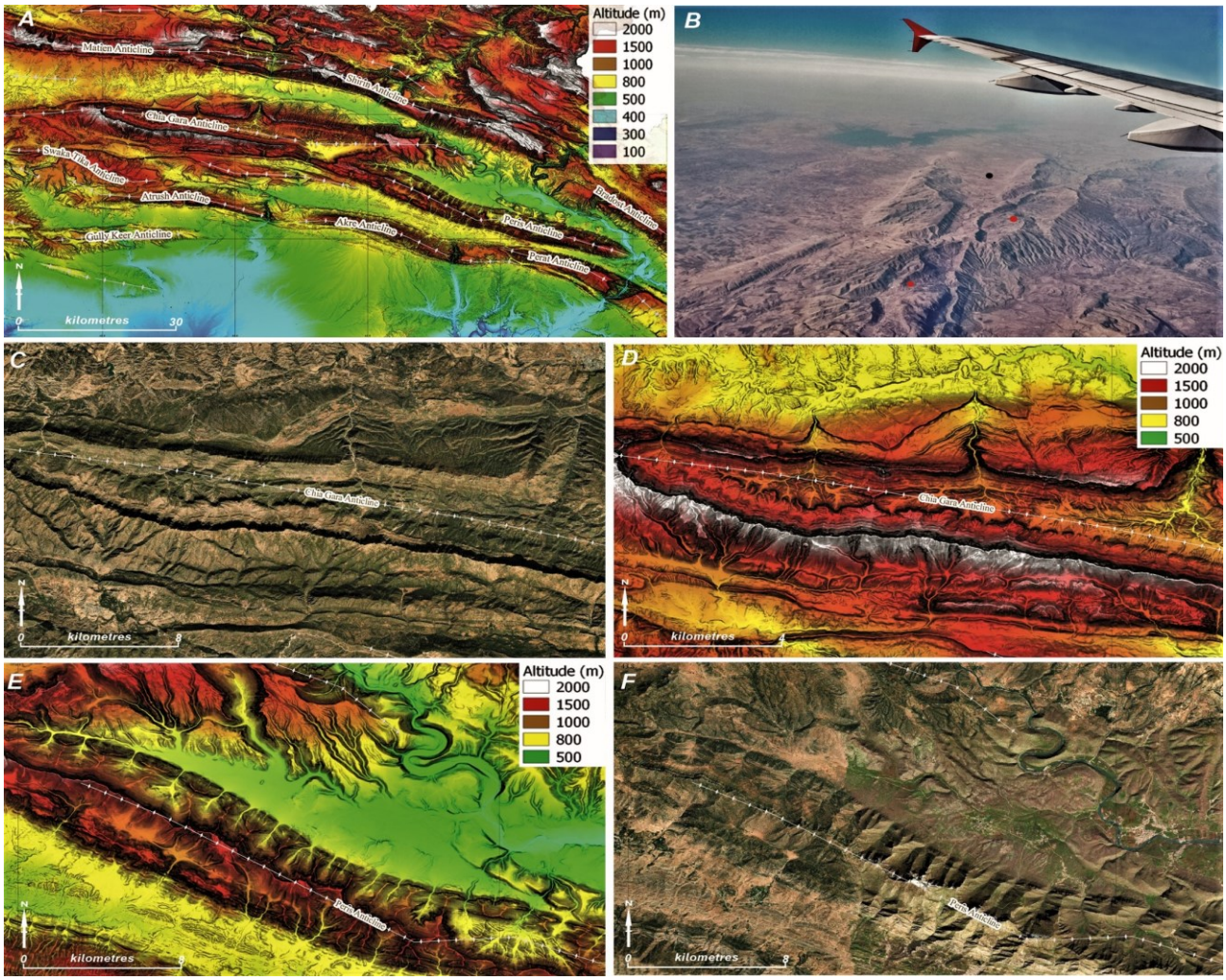


**Figure 1.** (A) DEM illustrating the distribution of anticlines and synclines in the eastern part of study area. (B) Oblique aerial picture showing the general geomorphological aspects of the Zagros Mountains with erosional anticline valleys (red dots) and syncline valleys (black dots); in the background, the Mosul Dam Lake. (C and D) Hogback hillslope of Chia Gara Anticline as Esri World Imagery and DEM. (E and F) Cuestas hillslopes of Peris Anticline as DEM and in Esri World Imagery.

## 2.3 Methods

Mapping of the area was performed on data interpreted from both remote sensing images and field observations, according to the approach proposed by several authors for mapping arid and semi-arid regions (Perego et al., 2011; Azzoni et al., 2017; Hüneburg et al., 2019; Zerboni et al., 2015, 2020). Costanzo et al., 2021) Data analysis from remote sensing was derived from several available datasets. Recent (11 August 2019) multispectral images (visible and infrared) with up to 10-metre spatial resolution from ESA Copernicus Satellite 2A (tiles T38SLF, T38SLG, T38SMF, T38SMG, T38SKF and T38SKG, source: https://scihub.copernicus.eu/) (Copernicus, 2019) were composed in false colours (visible + near infrared). Images were then projected to UTM Zone 38 reference system and used as the background for remote observations in QGIS software. An AW3D30 Digital Surface

Model (DSM) with 1° horizontal resolution (~30 m at the equator) available on the Japan Aerospace Exploration Agency (JAXA, 2020) platform was reprojected to UTM Zone 38 with 30-metre spatial resolution. Contour lines at 100 and 250 m derived from this model were used for landform interpretation as well as hillshade and slope models. An elevation-dependent colour scale was applied to the Digital Elevation Model (DEM), imported in QGIS, and superimposed over a hillshade, in order toobserve specific landforms (river terraces, water and wind gaps and alluvial fans). The channel network was extracted from the DEM using SAGA software. Results were reliable in the mountainous area, while the automatically rendered model of the alluvial plain was manually corrected using satellite and field data. Other than topographical and satellite visual information, the Arbeel-Mahabad. Al-Mosul, Zakho and Kani Rash quadrangles (1:250,000 sheets) of the Series of Geological Map of Iraq helped define the bedrock geology and delineate linear structural features and occasionally supported the recognition and interpretation of landform features and trends. High-resolution (0.5–1 m) natural colour satellite images provided from Esri World Imagery (Esri, 2020) and visualised in QGIS were used to identify and validate detail and small-scale landforms. Declassified Corona Images were also used to observe the fluvial pattern of the part of the Tigris River below the Mosul Dam Lake before its construction (USGS, 1968). Several field surveys confirmed and validated the geomorphological elements detected during the desktop study. The field survey included the Zagros Mountains, the low relief fluvial plains, and foothills, and the area of the Mosul Dam Lake, which was investigated for Late Quaternary sedimentary sequences. Some features recognized in the field were discussed in the following parts, but not included in the Main Map due to the scale of representation. Such elements include small scale karst landforms, anthropogenic features, and gorges.

## 2.4 Main geomorphological features

### 2.4.1 Structural landforms

Most landforms in the study area are directly or indirectly related to the effect of on-going convergence: the formation and orientation of mountain ridges and valleys are direct surface expressions of tectonic folding, as well as the evolution of other landforms (see following sections). Since the Messinian, intense uplift affected the relief of the KRI area (Zebari et al., 2019); progressive development of the numerous anticlines (Al-Obaidi & Al-Moadhen, 2015) that are oriented E–W to the west of the Greater Zab River (namely the Tsawoq, Matien, Be'khair, Ber Bahr, Al Qosh, Gully Keer, Dahkan, Zainiyat, Geri Baran, Duhok, Atrush, Swaka Tika, Ravan, Chia Gara, Shirin, Peris, Akre and Perat Anticlines), and NW–SE to the east of the Greater Zab River and in the south lowland (the Kand, Shaikhan, Maqloub, Barda Rash, Bashiqa, Ain Al Safra, Bradost, Sarta Anticlines). In the

western sector of the study area, between Dohuk and Zacko, the Gera Ban and Be'khair anticlines show little different change in direction due to an en-echelon system faults, that were active during the Quaternary (2020). Rock weathering (mainly karstic dissolution) and linear erosion affected anticlines in subsequent phases, shaping specific landforms according to the different dipping of strata (Figure 2A). Along monocline slopes, cuestas develop in forelimbs and along the gently dipping strata, while hogbacks are in the inner limbs marked by steeply dipping strata (Sissakian, 2014; Hasan et al., 2019) (Figure 2B). In the Main Map, these features were not differentiated mostly because the different exposure of satellite images hamper their immediate attribution to one of the previous categories. However, several forelimbs and toe of anticlines showed very evident slope triangular shape mapped as flatiron areas (Figure 2C).

### 2.4.2 Hillslope landforms

The slopes of monoclines are influenced by processes controlled by gravitational forces. The presence and relevance of mass movements is documented in thearea by Sissakian et al. (2016), most of them at a scale not compatible with the one of the Main Map. The largest slope landforms are represented by deepseated gravitational slope deformations (DSGSD,sensu Dramis & Sorriso-Valvo, 1994) usually several hundred meters high. Their occurrence is occasional, but widespread over the whole study area, mostly in relation to the southern slopes of the anticlines. DSGSDs, as those along the Dohuk, Swaka Tika. Al Qosh and Bradost anticlines, are controlled by the structural orientation of strata in the dip-slope direction. The age of Al Qosh landslide is estimated about 3000 years (Sissakian et al., 2016). The presence of faulting and dipping strata is usually a main control on the formation of DSGSDs on sedimentary bedrock, influencing their occurrence and geomorphological development (Mariani & Zerboni, 2020). A gentle slope is present at the junction between anticline foothills and alluvial plains; it consists of a belt of pediment or peneplain composed of fine to coarse alluvial sediments derived from the dismantling of upland rocks. When these pediments development along unconfined valleys they are affected by sheet erosion and exploited for cultivation. The fine grained and unconsolidated conglomerates slopes and footslope are characterized by intense gully erosion by overland flow, resulting in a badlands landscape (Figure 3). In the proximity of the Akre city, Plio-Pleistocene conglomerates bajada spread out at footslope of Perat anticline. Near the Great Zab River, conglomerates are dissected by several rills and gullies; in some locations, they are tilted by neotectonic (Sissakian et al., 2014) (Figure 3). In the western part of the area and at the northern border with Turkey, the low gradient hillsides of silty clay to arenaceous limestone and the Quaternary unconsolidated bedrock outcrops are dissected by strong gullies erosion, due to unconcentrated overland flow to sculpt a badland landscape (Figure 3).

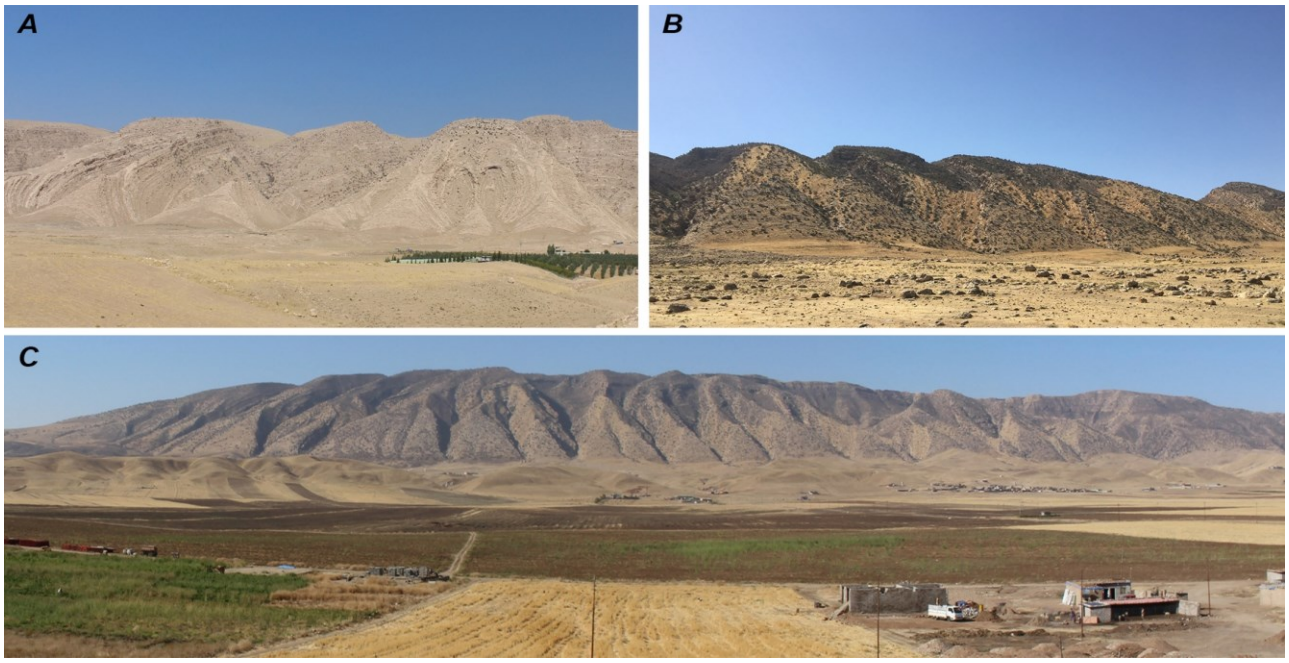


**Figure 2.** (A) A slope of an anticline near the Atrush Valley. Notice the combined result of erosion and karst weathering on deformed rock strata. (B) Detail of a flatiron along the slope of an anticline. (C) Panoramic view on northern slope of the Jebel Maqlub Anticline.

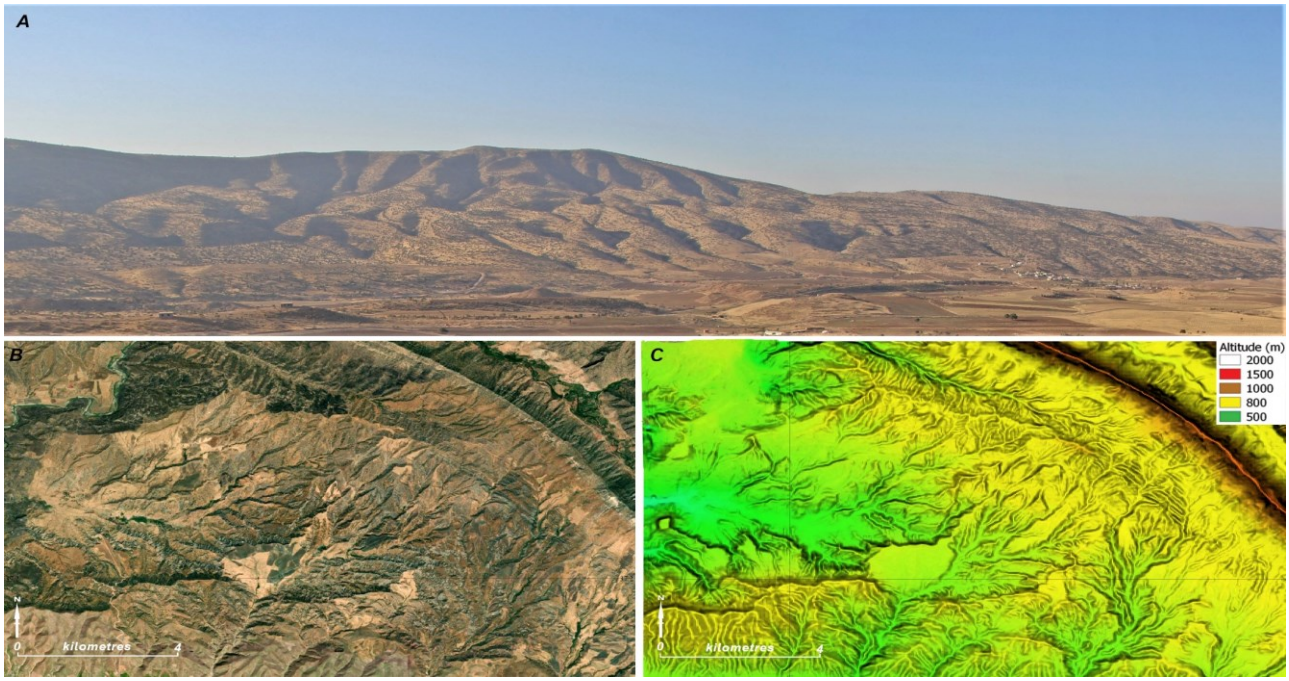


**Figure 3.** (A) A pediment along the Atrush Valley; the anticline is dissected by gully erosion. (B and C) Badland landscape of Zacko town in Esri World imagery and DEM.

### 2.4.3 Karst landforms

Karst related processes are very active in the study area, especially well expressed in the mountains, where the combination of tectonic deformation, uplift and climate-related processes produced epikarst and ipokarst landforms (Fouad, 2014; Sissakian et al., 2015). The most evident karstic

landforms formed by the combination of prolonged deep and surface dissolution, fluvial erosion, vertical uplift and a further lithological constraint due to limestone resistance to erosion (Zerboni et al., 2020). The interaction of these processes produces a complex system of incised deep gorges, canyons and gullies erosion on monocline limestone slopes and some large polje-like depressions that open towards the main drainage systems (Stevanović et al., 2009). Small to medium-scale visible epikarst landforms are evident in the field. Karst pavements, walls with grikes and clint, and solutional flutes (rillenkarren) are evident along the flanks of the Atrush and Chi Gara anticline ridges. Many caves and rock shelters open along the slopes of the Zagros Mountains and at the head of valleys; in the study area, underground networks were not systematically explored, but like elsewhere in the KRI, speleogenesis resulted from hypogenic and epigenic processes (Laumanns et al., 2008). The local caves and rock shelters preserve important archives of human and climate changes during the late Quaternary (Flohr et al., 2017; Conati Barbaro et al., 2019). Springs, also exploited by humans for agricultural purposes since the Bronze Age (Morandi Bonacossi, 2018), are further evidence of the underground karst system in the KRI. The spring discharge is influenced by rainfall regime, size of catchment area, and aquifer residence time, seasonal or intermittent activity; only a few springs are perennial (Figure 4).

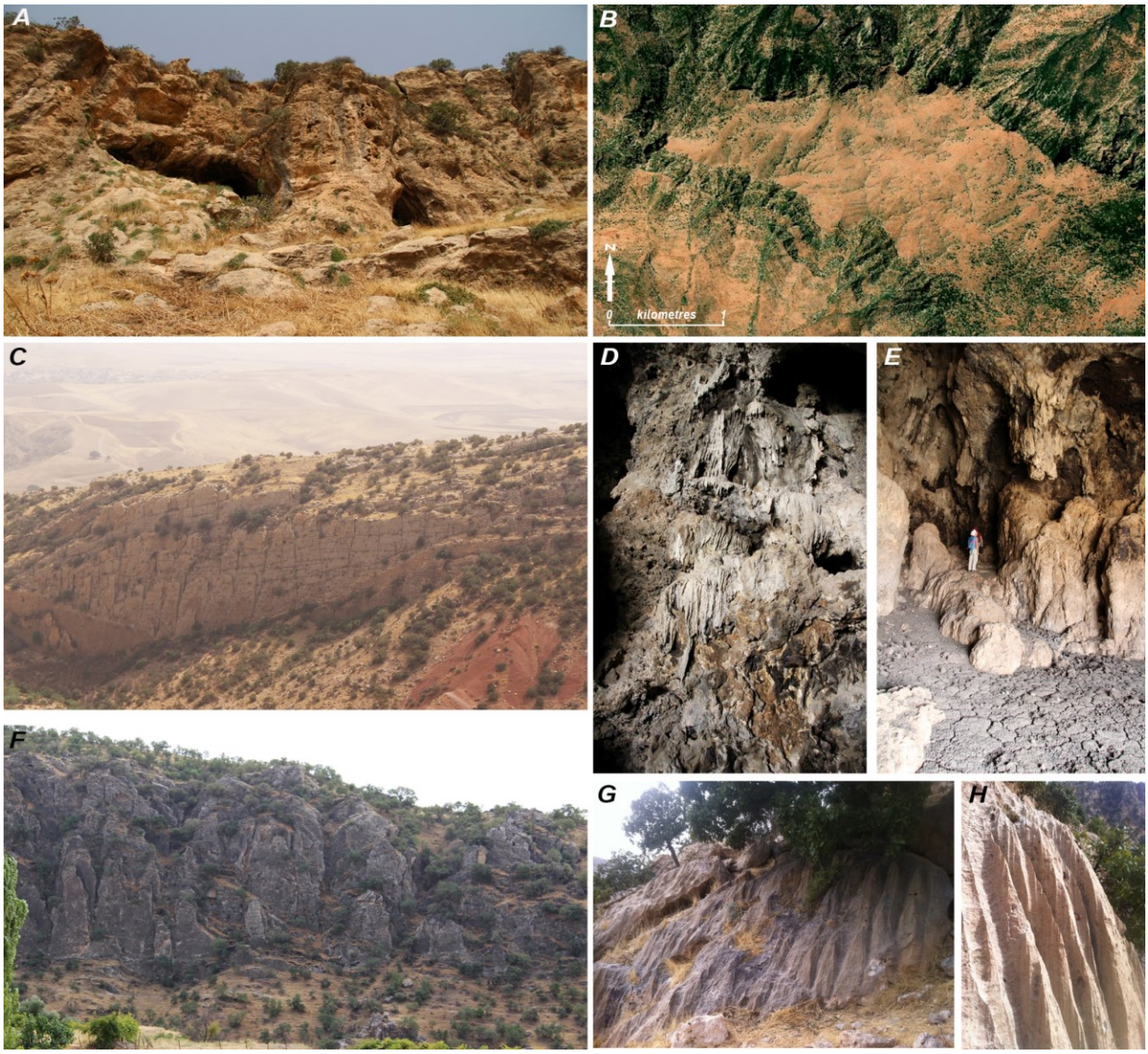


**Figure 4.** Examples of karst landforms. (A) Caves entrance (or rockshelters) along the hillslopes of the Atrush Anticline. (B) Limestone pavement on the Chia Gara Anticline (Esri World Imagery). (C) Karst dissolution along vertical fractures of a limestone wall. (D and E) Speleothems inside caves. (F) Karst pinnacles in the central Zagros Mountains. (G and H) Rillenkarren on bare limestone.

### 2.4.4 Fluvial landforms

The Tigris River and its tributaries Khabur, Rubar Dohuk, Khosur, Nahr-al-Khazir and the Great Zab are the main water network of the northern KRI. In the mountains, rivers follow a NW–SE trending pattern according to the regional structural setting, while fluvial patterns inside the plain are almost all N–S oriented except for the Khabur River, which displays a N–S to W trend. The Tigris River has a high degree of sinuosity and a regularly meandering course in most of the area, where it incises sandstones, marls and evaporites. The Khabur River has a linear to meandering pattern in the mountain area, which changes into irregular meandering channels in the lowlands. The Great Zab River is braided before it reaches Dereluk plain, where its pattern becomes a linear to irregularly

meandering after cutting through the Perat Anticline, and as its course traverses Plio-Pleistocene conglomerates, it develops anastomosing-irregular meandering channels. The growth of anticlines, the presence of different lithotypes and climate changes drove the evolution of these drainage systems into a major river network of asymmetrical and symmetrical branch tributaries. Water gap and wind gap gorges form actual to ancient routes allowing the Great Zab, Khabur, Nahr-al-Khazir, Rubar el Atrush and Rubar Dohuk rivers to flow from the Zagros valleys to alluvial plains Several water and wind gaps cut the Akre, Perat, Atrush, and Dohuk anticlines. Some of the major water gaps are the deep gorges of the Greater Zab, Kabur and Nahr-al-Khazir Rivers, where canyons reach 300 m deep; many other small canyons exist in the area of Dohuk (Fouad, 2014; Al-Obaidi & Al-Moadhen, 2015; Zebari et al., 2019). Here, the distribution of wind and water gaps reflects the response of the fluvial network to ongoing uplift (Burbank & Pinter, 1999; Burbank & Anderson, 2011). Along syncline valleys, the main rivers have several perpendicular tributaries and flow along symmetric valleys, whose shape are controlled by tectonics. Along the Khabur, Great Zab and Nahr-al-Khazir Rivers some tributaries show a braided pattern with coarse to medium size bars; others follow instead a mature meandering pattern with several changes in sinuosity. Different fluvial patterns depend on both bedrock lithologies and flow regime; on conglomerate, rivers display a braided pattern, whereas they meander while traversing fine clastic sediments. Abandoned and occasional deeply incised meanders are evident along the Great Zab and Nahr-al-Khazir catchments (Figure 5). The lowlands are covered by floodplains; the largest one belongs to the Nahr-al-Khazir and Gomel Nardush fluvial system; it consists of coarse gravels overlaid by fine sand, silt and clay deposits and interlayered pebble lenses with erosional surfaces (channel facies) (Sissakian et al., 2014). Along the Tigris, Great Zab, Khabur and Nahr-al-Khazir Rivers fluvial terraces are present at different elevations; they incise fluvial gravel and conglomerates of former alluvial fans, and some are tectonically displaced. The Great Zab River has at least 3/4 levels of fluvial terrace cut into Plio-Pleistocene and Holocene conglomerates and fine to medium sand bodies (Al-Dabbagh & Al- Naqib, 1991; Sissakian et al., 2014, 2015). On the Main Map, four different terrace levels are represented and labelled T1, T2, T3 and T4, progressively upper and older. The younger terrace levels (T1, T2 and T3) are composed by fine-grained sand with basal lenses of conglomerates cupped by silty-clay sediments. The T4 terrace consists of conglomerates with interlayered lenses of fine to coarse sand. Runoff discharge from the mountains accreted several alluvial fans along the anticline foothills, which connect the steep mountainsides to the plain below. The largest is located near the Al-Qosh and Dohuk municipalities; Plio-Pleistocene alluvial fans are also evident along the Akre-Great Zab transect. In this area, alluvial fans are composed by conglomerates deeply incised by ephemeral streams; they are also strongly

tilted by Quaternary tectonic activity (Figure 6). In the 1980s, a large dam was built along the course of Tigris River (upstream of Mosul) creating an artificial lake basin and submerging ca. 350 km2 of the region around the Tigris canyon, including hundreds of archaeological sites (Sconzo & Simi, 2020). Observations of declassified Corona aerial photographs helped identify the course of the Tigris River before the construction of the dam. It meandered inside deep gorges with scroll and point bars along convex banks; four levels of fluvial terraces can be spotted along its submerged course Such terraces recorded the lateral migration E to W of the river, and a progressive transition from a continuous meandering to a braided pattern (Al-Dabbagh & Al-Naqib, 1991).

### 2.4.5 Anthropogenic landforms

Anthropogenic landforms – created by artificial processes – are present and testify to the long-lasting human exploitation of the KRI. The most important cultural features are tells and artificial canals. Tells are raised mounds, very common in the archaeological landscape of the Near East, marking the location of ancient settlements and formed by the accumulation of anthropogenic sediments after several millennia of activity (Miller Rosen, 1986). Tell mounds are truncated cones with sloping sides, up to a few tens of metres high. They are common in the floodplains (Dohuk, Gomel Su plains) and along valleys (Atrush Valley) and are generally distributed along active streams or palaeochannels where they often offer an elevated position exploited by modern villages. Canals are anthropogenic landforms typical of this part of Mesopotamia and were built by the Assyrians from 900 to 600 BC. The better-preserved system of canals, still evident in the field and from high-resolution satellite imagery were built by king Sennacherib (Ur, 2005; Morandi Bonacossi, 2018). Artificial canals were excavated in the geological bedrock, roughly following contour lines. Their intended function was to collect water from springs and streams at the foothills of the Zagros Mountains and convey it to the lowlands and Nineveh, the capital of the kingdom, for irrigation purposes (Figure 7).

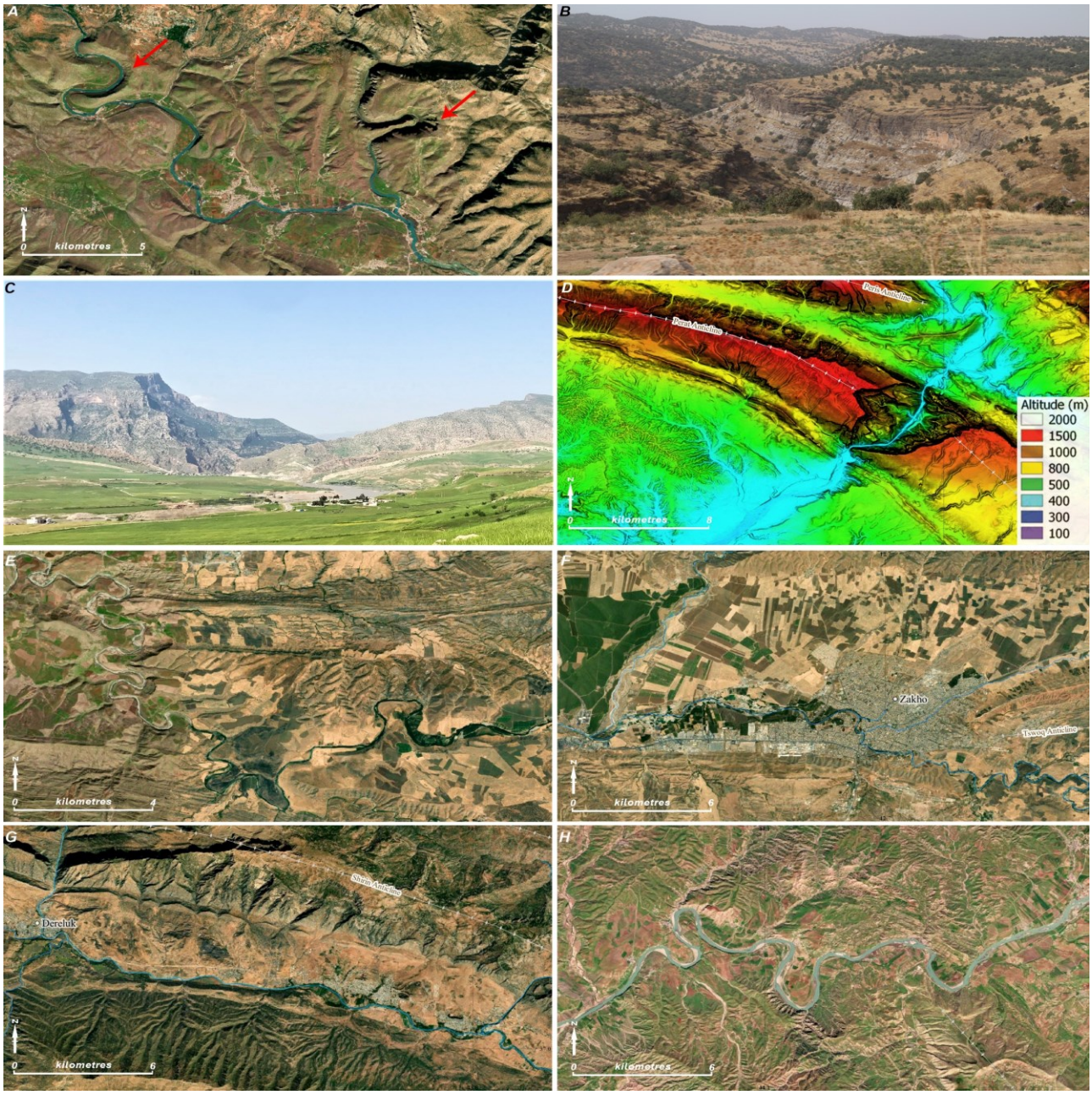


**Figure 5**. Examples of fluvial landforms. (A) Esri World image of the Great Zab and one of its left tributaries; arrows indicate deeply incised meanders. (B) Field pictures of a gorge valley near the Atrush village. (C) Panoramic view of a Great Zab water gap in the Perat Anticline. (D) DEM of the Great Zab water gap in proximity of the Perat Anticline (eastern sector of the study area). (E) Esri World image showing the meandering to tortuous channel pattern of the Khabur River, south of Zacko town. (F) Esri satellite image showing the low sinuous channel pattern of the Khabur River in proximity of Zacko town. (G and H) Esri World image illustrating changes of channel pattern along the course of the Great Zab River; from upstream to downstream, it shifts from low sinuous (G) to meandering channel (H).

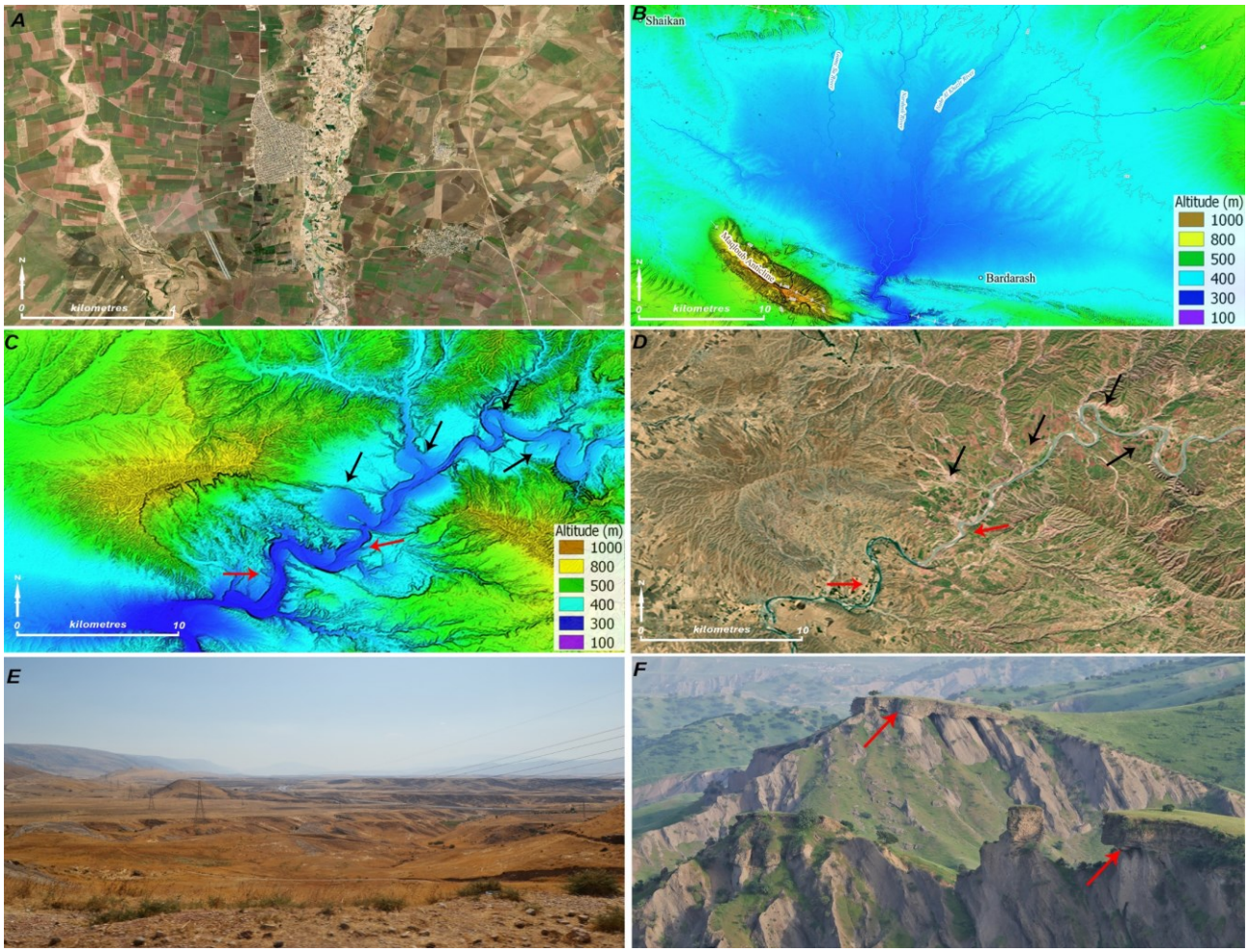


**Figure 6**. (A) Esri World image of the Nardush–Gomel Su alluvial plain; notice the belt of anastomosing channels of the Nardush River. (B) The DEM of the same area of (A) reveals the dendritic pattern of the drainage system. (C and D) DEM and Esri World image of the Great Zab River illustrating the meandering to sinuous straight channel belt; abandoned meanders (black arrows) and the effects of erosion forming an anticline valley (red arrows) are evident in the DEM. (E) General view SE of the Akre village showing several levels of terraces. (F) Field picture of tilted alluvial terraces (red arrows) (modified from Zebari et al., 2020).

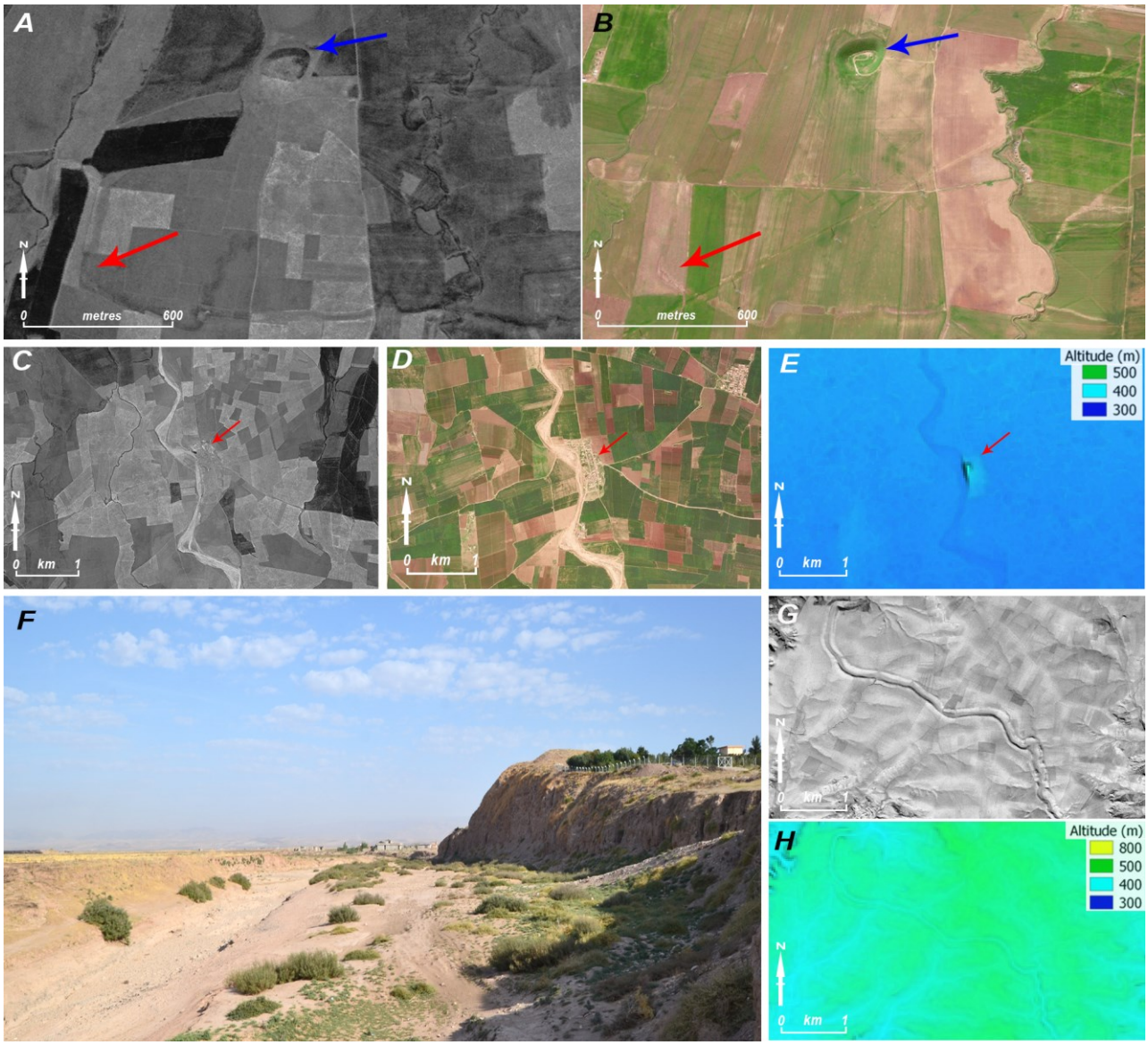


**Figure 7**. (A and B) Declassified Corona image (acquisition 16 August 1968) and Esri World image illustrating the Nardush alluvial plain; such images are helpful to identify anthropogenic landscape features as in the case of Tell Mubarak (blue arrow) and Khinis canal (red arrow). (C–E) Corona image, Esri World image and DEM showing Tell Gomel (ancient Gaugamela), along the Gomel Su River. (F) Field picture of Tell Gomel illustrating the destructive effects of fluvial erosion along the hillside of the tell. (G and H) Declassified Corona image and DEM of a well-preserved part of the Bandwai Assyrian canal, which can be interpreted in context with the natural hydrographic network.

## 2.5 Conclusions

Geomorphological analysis and mapping of the North Kurdistan Region of Iraq offers important insights about the active tectonic and climatic processes that affected landforms and fluvial development during the Neogene–Quaternary. Different physiographic units in this complex landscape reflect the uplift and exhumation rate of the anticlinal ridges and syncline troughs. In fact, the presence of tilted alluvial fans and fluvial terraces or the development of water and wind gaps are

clearly related to geomorphological processes triggered by tectonic. The analysis of further data on tectonic control over the evolution of the fluvial pattern of the Tigris River is ongoing, but preliminary data suggest that the same lithological and structural factors influenced the meandering pattern of the river north of the Mosul Lake Dam and the dynamic of the lake itself. Also, the evolution of the area is influenced by climate variations, especially after the Last Glacial Maximum, when the succession of dry and wet periods influenced erosion and karst processes. Finally, Late Quaternary human activities become progressively more impacting on the natural landscape: from the one hand, humans built monumental canals that are quite evident in the field and altered the local hydrography. On the other hand, a more intense and widespread modification of the landscape occurred when land use strategies shifted towards pastoralism, thus becoming progressively more impactful with the development of more complex societies (Zerboni & Nicoll, 2019). In conclusion, our geomorphological mapping of the northern KRI suggests that the interaction between endogenous and exogenous processes led to a complicate landscape. Since the late Cenozoic surface processes were modulated by lithological and structural factors, and climatic fluctuation and, more recently, by human agency.

## 2.6 References

Al-Dabbagh, T. H., & Al-Naqib, S. Q. (1991). Tigris River terrace mapping in northern Iraq and the geotechnical properties of the youngest stage near Dao Al-Qamar village. *Geological Society, London, Engineering Geology Special Publications*, *7*(1), 603-609.

Alwan, I. A., Karim, H. H., & Aziz, N. A. (2019, May). Agro-climatic zones (ACZ) using climate satellite data in Iraq Republic. In *IOP conference series: Materials Science and Engineering* (Vol. 518, No. 2, p. 022034). IOP Publishing.

Al-Zuhairi, M. F., Al-Jumaily, K. J., & Al-Salihi, A. M. (2016). Characteristics of precipitation systems over Iraq observed by TRMM radar. *American Journal of Engineering Research*, *5*(11), 76-81.

Azzoni, R. S., Zerboni, A., Pelfini, M., Garzonio, C. A., Cioni, R., Meraldi, E., ... & Diolaiuti, G. A. (2017). Geomorphology of Mount Ararat/Ağri Dağı (Ağri Dağı Milli Parki, Eastern Anatolia, Turkey). *Journal of Maps*, *13*(2), 182-190.

Berberian, M. (1995). Master "blind" thrust faults hidden under the Zagros folds: active basement tectonics and surface morphotectonics. *Tectonophysics*, *241*(3-4), 193-224.

Bishop, P. (2007). Long-term landscape evolution: linking tectonics and surface processes. *Earth Surface Processes and Landforms: The Journal of the British Geomorphological Research Group*, *32*(3), 329-365.

Blanc, E. P., Allen, M. B., Inger, S., & Hassani, H. (2003). Structural styles in the Zagros simple folded zone, Iran. *Journal of the Geological Society*, *160*(3), 401-412.

Burbank, D. W., & Anderson, R. S. (2011). Tectonic geomorphology. John Wiley and Sons.

Burbank, D. W., & Pinter, N. (1999). Landscape evolution: the interactions of tectonics and surface processes. *Basin Research*, 11(1), 1-6.

Conati Barbaro, C., Moscone, D., Iamoni, M., Morandi Bonacossi, D., & Qasim, H. A. (2019). The prehistory and protohistory of the northwestern region of Iraqi Kurdistan: Preliminary results from the first survey campaigns. *Paléorient. Revue pluridisciplinaire de préhistoire et de protohistoire de l'Asie du Sud-Ouest et de l'Asie centrale*, (45-2), 207-229.

Conati Barbaro, C., Zerboni, A., Moscone, D., Cremaschi, M., Iamoni, M., Savioli, A., & Bonacossi, D. M. (2016). The prehistory of the land of nineveh. *Antiq. Proj. Gall.*, *90*, 1-3.

Csontos, L., Sasvári, Á., Pocsai, T., & Kósa, L. (2011, May). Structural evolution of the northwestern Zagros, Kurdistan Region, Iraq and alternative models for formation of a curved mountain chain. In *73rd EAGE Conference and Exhibition-Workshops 2011* (pp. cp-239). European Association of Geoscientists & Engineers.

Copernicus (2019). Sentinel-2A satellite imaging data. Retrieved from https://earth.esa.int/web/sentinel/technical-guides/sentinel-2-msi/level-2a/algorithm (accessed 11/08/2020), processed by ESA.

Dewey, J.F., Pitman, W.C., Ryan, W.B.F. & Bonnin, J. (1973) Plate tectonics and the evolution of the Alpine System. *Geol. Soc. Am. Bull*., 84, 3137^3180.

Dramis, F., & Sorriso-Valvo, M. (1994). Deep-seated gravitational slope deformations, related landslides, and tectonics. *Engineering Geology*, *38*(3-4), 231-243.

Eklund, L., & Seaquist, J. (2015). Meteorological, agricultural, and socioeconomic drought in the Duhok Governorate, Iraqi Kurdistan. *Natural Hazards*, *76*(1), 421-441.

ESRI (2020) "World Imagery [basemap]. "World Imagery". July 22, 2020. http://www.arcgis.com/home/item.html?id=10df2279f9684e4a9f6a7f08febac2a9 (accessed 11/08/2020).

Flohr, P., Fleitmann, D., Zorita, E., Sadekov, A., Cheng, H., Bosomworth, M., ... & Matthews, R. (2017). Late Holocene droughts in the Fertile Crescent recorded in a speleothem from northern Iraq. *Geophysical Research Letters*, *44*(3), 1528-1536.

Ford, D., & Williams, P. (2007). Karst Hydrogeology and Geomorphology, John Willey, and Sons Ltd. *Chicester, UK*.

Fouad, S. F. (2014). Western Zagros fold–Thrust Belt, part II: The high folded zone. *Iraqi bulletin of geology and mining*, (6), 53-71.

Fouad, S. F. (2015). Tectonic map of Iraq, scale 1: 1000 000, 2012. *Iraqi Bulletin of Geology and Mining*, *11*(1), 1-7.

Frizon de Lamotte, D., Raulin, C., Mouchot, N., Wrobel-Daveau, J. C., Blanpied, C., & Ringenbach, J. C. (2011). The southernmost margin of the Tethys realm during the Mesozoic and Cenozoic: Initial geometry and timing of the inversion processes. *Tectonics*, *30*(3).

Goudie, A. S. (2013). *Arid and semi-arid geomorphology*. Cambridge university press.

Hasan, A. A., Hussien, M. L., Fadhil, L. A., Hasan, M. I., & Mosquera, C. D. (2019). Crustal Deformations and Geomorphological Units of Arabian Plate Foreland Region, North and Northeast of Iraq. *Journal of Southwest Jiaotong University*, *54*(5).

Hüneburg, L., Hoelzmann, P., Knitter, D., Teichert, B., Richter, C., Lüthgens, C., ... & Luciani, M. (2019). Living at the wadi–integrating geomorphology and archaeology at the oasis of Qurayyah (NW Arabia). *Journal of Maps*, *15*(2), 215-226.

Jassim, S. Z., & Goff, J. C. (Eds.). (2006). *Geology of Iraq*. DOLIN, sro, distributed by Geological Society of London.

Kirby, E., & Whipple, K. X. (2012). Expression of active tectonics in erosional landscapes. *Journal of structural geology*, *44*, 54-75.

JAXA (2020). ALOS Global Digital Surface Model "ALOS World 3D - 30m (AW3D30)" Retrieved from: https://www.eorc.jaxa.jp/ALOS/en/aw3d30/ (accesed 11/08/2020).

Laumanns, M., Rasch, A., & Audra, P. (2008). *Karst and Caves of Iraq:(including the Results of a 2007 Kurdish-German Speleological Project and an Overview on Hypogenic Sulphidic Speleogenesis)*. Speläoclub.

Matthews, R., Matthews, W., Richardson, A., Walsh, S., Iversen, I., Mudd, D., ... & Elliott, S. (2019). The early Neolithic of Iraqi kurdistan: Current research at bestansur, shahrizor plain. *Paléorient. Revue pluridisciplinaire de préhistoire et de protohistoire de l'Asie du Sud-Ouest et de l'Asie centrale*, (45-2), 13-32.

Matthews, R., Matthews, W., Rasheed, K., & Aziz, K. (2016). Current investigations into the early Neolithic of the Zagros foothills of Iraqi Kurdistan. *The Archaeology of the Kurdistan Region of Iraq and Adjacent Regions, edited by K. Kopanias, and J. MacGinnis*, 219-228.

Morandi Bonacossi, D. (2017). Italian Research in the Nineveh Region between Archaeological Investigation and Cultural Heritage Protection and Management. In: Petit, L.P., Morandi Bonacossi D., (Eds.), Nineveh, the Great City. Symbol of Beauty and Power. Papers on Archaeology of the Leiden Museum of Antiquities (PALMA) 13, Sidestone Press, Leiden, 98-103.

Morandi Bonacossi, D. (2018). Water for Nineveh. The Nineveh Irrigation System in the regional context of the 'Assyrian Triangle': A first geoarchaeological assessment. *Studia Chaburensia*, *7*, 77-115.

Mouthereau, F., Lacombe, O., & Vergés, J. (2012). Building the Zagros collisional orogen: timing, strain distribution and the dynamics of Arabia/Eurasia plate convergence. *Tectonophysics*, *532*, 27-60.

Mustafa R. S. Al-Obaidi & Ahmed A. H. Al-Moadhen (2015). Thrust Fault Tectonics In The Duhok Region (High Folded Zone, N Iraq). *International Journal of Civil Engineering and Technology*, 6(10), pp. 132-146.

Nicoll, K. (2010). Landscape development within a young collision zone: implications for post-Tethyan evolution of the Upper Tigris River system in southeastern Turkey. *International Geology Review*, *52*(4-6), 404-422.

Oberlander, T. M. (1965). The Zagros streams: a new interpretation of transverse drainage in an orogenic zone. *Syracuse Geographical Series*, *1*.

Oberlander, T. M., & Morisawa, M. (1985). Origin of drainage transverse to structures in orogens. In *Tectonic geomorphology* (Vol. 15, pp. 155-182). Allen and Unwin Boston.

Othman, A. A., & Gloaguen, R. (2013). River courses affected by landslides and implications for hazard assessment: A high resolution remote sensing case study in NE Iraq–W Iran. *Remote sensing*, *5*(3), 1024-1044.

Perego, A., Zerboni, A., & Cremaschi, M. (2011). Geomorphological Map of the Messak Settafet and Mellet (central Sahara, SW Libya). *Journal of Maps*, *7*(1), 464-475.

Pomeroy, E., MirazónLahr, M., Crivellaro, F., Farr, L., Reynolds, T., Hunt, C.O. & Barker, G. 2017. Newly discovered Neanderthal remains from Shanidar Cave, Iraqi Kurdistan, and their attribution to Shanidar 5. Journal of Human Evolution 111: 102–18.

Reilinger, R., McClusky, S., Vernant, P., Lawrence, S., Ergintav, S., Cakmak, R., ... & Karam, G. (2006). GPS constraints on continental deformation in the Africa-Arabia-Eurasia continental collision zone and implications for the dynamics of plate interactions. *Journal of Geophysical Research: Solid Earth*, *111*(B5).

Sconzo, P., & Simi, F. (2020). Settlement dynamics on the banks of the upper Tigris, Iraq: The Mosul dam reservoir survey (1980). *Journal of Open Archaeology Data*, *8*.

Sissakian, V. K., & Fouad, S. F. (2014). Geological Map of Sulaimaniyah Quadrangle, scale 1: 250 000. *Iraq Geological Survey Publications, Baghdad, Iraq*.

Sissakian, V. K. (2013). Geomorphology and morphometry of the Greater Zab River Basin, north of Iraq. *Iraqi Bulletin of Geology and Mining*, *9*(3), 21-49.

Sissakian, V. K., Kadhim, T. H., & Jab'bar, M. F. A. (2014). Geomorphology of the high folded zone. *Iraqi Bulletin of Geology and Mining*, (6), 7-51.

Sissakian, V. K. (2014). Geological Map of Arbeel and Mahabad Quadrangles Sheets NJ-38- 14 and NJ-38-15, Scale 1 V 250:000. *Geological Survey Publications, Baghdad, Iraq*

Sissakian, V.K., Al-Ansari, N. & Knutsson, S. (2015). Karst Forms in Iraq. *Journal of Earth Sciences and Geotechnical Engineering*, 5, 4, 1 – 26.

Sissakian, V., Jabbo, B., Al-Ansari, N., & Knutsson, S. (2016). Age estimation of alqosh main landslide, north Iraq using exposure Dating method. *Journal of Earth Sciences and Geotechnical Engineering*, *6*(3), 163-176.

Sissakian, V. K., Al-Ansari, N., & Abdullah, L. H. (2020). Neotectonic activity using geomorphological features in the Iraqi Kurdistan region. *Geotechnical and Geological Engineering*, *38*(5), 4889-4904.

Solecki, R. S. (1971). Shanidar, the first flower people. Knopf.

Stevanović, Z., Iurkiewicz, A., & Maran, A. (2009). New insights into karst and caves of Northwestern Zagros (Northern Iraq). *Acta carsologica*, 38(1).

Ur, J. (2005). Sennacherib's northern Assyrian canals: new insights from satellite imagery and aerial photography. *Iraq*, *67*(1), 317-345.

USGS (1968). Declassified Corona Imaging data. Retrieved from https://corona.cast.uark.edu (accessed 11/08/2020).

Van de Mieroop, M. (2015). *A history of the ancient Near East, ca. 3000-323 BC*. John Wiley & Sons.

Vergés, J., Saura, E., Casciello, E., Fernandez, M., Villaseñor, A., Jimenez-Munt, I., & García-Castellanos, D. (2011). Crustal-scale cross-sections across the NW Zagros belt: implications for the Arabian margin reconstruction. *Geological Magazine*, *148*(5-6), 739-761.

Wilkinson, T. J. (2003). *Archaeological landscapes of the Near East*. University of Arizona Press.

Wilkinson, T. J., and Tucker, D. J. (1995). Settlement development in the North Jazira, Iraq: A study of the archaeological landscape. Aris and Phillips; Department of Antiquities and Heritage.

Zebari, M., Grützner, C., Navabpour, P., & Ustaszewski, K. (2019). Relative timing of uplift along the Zagros Mountain Front Flexure (Kurdistan Region of Iraq): Constrained by geomorphic indices and landscape evolution modeling. *Solid Earth*, *10*(3), 663-682.

Zebari, M., Preusser, F., Grützner, C., Navabpour, P., & Ustaszewski, K. (2021). Late Pleistocene-Holocene Slip Rates in the Northwestern Zagros Mountains (Kurdistan Region of Iraq) Derived from Luminescence Dating of River Terraces and Structural Modeling. *Tectonics*, *40*(8).

Zerboni, A., Perego, A., & Cremaschi, M. (2015). Geomorphological map of the Tadrart Acacus massif and the Erg Uan kasa (Libyan Central Sahara). *Journal of Maps*, *11*(5), 772-787.

Zerboni, A., Perego, A., Mariani, G. S., Brandolini, F., Al Kindi, M., Regattieri, E., ... & Cremaschi, M. (2020). Geomorphology of the Jebel Qara and coastal plain of Salalah (Dhofar, southern Sultanate of Oman). *Journal of Maps*, *16*(2), 187-1

# Chapter 3

# Geomorphology of the Central Kurdistan Region of Iraq: landscapes of the Erbil Plain between the Great Zab and Little Zab Rivers

## 3.1 Introduction

The evolution, structure, and deformation of Earth's lithosphere play a huge influence on a variety of landforms of present-day landscapes (Burbank and Anderson, 2012). Among the many types of lithosphere dynamics, compressive tectonics can exhibit specific landforms (Owen, 2013). In fact, along collisional mountain belt, compressive dynamic exerts a deep control over the evolution of hydrographic networks and related fluvial landforms; in such contexts the trajectories of evolution of rivers result in different patterns depending on the structural settings of each region (Fryirs and Brierley, 2013; Trost et al., 2020). For instance, the Central Kurdistan Region of Iraq (CKRI) represents a typical example of landscapes controlled by the compressive tectonic of the Zagros fold and thrust belt (ZFTB; Viltres et al., 2022) and shows a complex channel network (Forti et al., 2021; Forti et al., 2022). Its orientations and development are mainly related to the shortening of the ZFTB, evidencing that tectonic deformation acted as the main force on present and past geomorphic processes (Burbank and Anderson, 2012; Hugget, 2016). Moreover, river behavior is used as a control system to understand the deformations produced by lateral and frontal folds growth, usually associated with thrust activity (Jackson et al., 1998; Holbrook and Schumm, 1999; Ramsey et al., 2008; Bretis et al., 2011). In arid and semi-arid regions, water plays a key role in shaping the landscape and thanks to the poor plant cover their setting are evident in the field as much as from remote Earth observation (e.g., Costanzo et al.,2021; Perego et al., 2011). In such setting, fluvial landforms, and processes, as channel network, river dynamics and characteristics (e.g., fluvial incision, basin drainage, and river avulsions), can be investigated to detect and quantify tectonic activity and subsurface structures (Obaid and Allen, 2017; Zebari et al., 2021). The combination of field and remote observation can also help in identifying the contribution of Quaternary climate fluctuations and how they affected the distribution and the amount of precipitation in the area. The latter, concurrently with the development of active tectonics, had a strong impact on alteration, erosion, transport, and deposition processes. The interplay between climate oscillations and tectonic forces is expressed in the present-day landscapes that characterize the CKRI (Jassim and Goff, 2006;

*Forti, L., Pezzotta, A., Zebari M. & Zerboni A. (2023) Geomorphology of the Central Kurdistan Region of Iraq: landscapes of the Erbil Plain between the Great Zab and Little Zab Rivers. Journal of Maps.* https://doi.org/10.1080/17445647.2022.2164527

Fouad, 2015; Zerboni et al., 2020; Forti et al., 2021). In this work we focus on the geomorphological analysis of the CKRI through the development of a regional geomorphological map (Main Map) ùaimed at reconstructing the Quaternary evolution of landforms and describing the influence on them of regional tectonic, which is likely the major factor controlling landscape evolution in the region, and climatic factors. We also report on active and inactive surface geomorphological processes and how they are controlled by endogenous and exogenous triggers, highlighting the role of compressive tectonic in shaping the hydrographic network. Moreover, we carefully consider the interplay between natural geomorphic processes and human activities because the region has been widely exploited by human communities since the Early Holocene, leaving their footprints over natural landforms (Appendix II).

## 3.2 Geographic, geological, and climatic backgrounds

The study area covers 12000 km2 within the CKRI encompassing the Governorates of Erbil, Niniveh, Kirkuk, and Sulaymaniyah. The main rivers are the Great Zab River (GZ) and the Little Zab River (LZ) that belong to into the Tigris River watershed. The high mountains within the ZFTB make the northeaster boundary of the Main Map, also these high mountains represent the principal orographic elements that characterize the landscape, reaching 2200 m asl. The mountain range is oriented NW-SE, and it is characterized by deep and incised canyons interspersed by with small plains. The connection between mountains and the flat area is transitional, through a foothills belt that reaches a maximum height of 1100 m asl. The flat areas, with minimum altitudes around 170 m asl along the main floor river valleys, are characterized by a fluvial network influenced by the ZFTB tectonic history and flowing alternatively in NW-SE and NE-SW directions. The Erbil Plain and the southern Kirkuk plain are the main alluvial areas. The ZFTB is a S-verging thrust and fold belt that is part of the Alpine-Himalayan orogenic system and comprises the KRI (Jassim and Goff, 2006; Forti et al., 2021). The ZFTB resulted from the convergence between Arabian and Eurasian plates, caused by the Neo-Thetys Ocean subduction starting in Early Cretaceous, and subsequent continental collision from the Late Cretaceous to the Miocene-Pliocene (Vergés et al., 2011; Zebari et al., 2019, 2020). The deformation propagated SW-ward on the NE passive margin of the Arabian Platform toward the Zagros Foreland Basin. The deformation is represented by the interplay between basement structures and fault-related folding of the sedimentary cover in which the lithological composition influenced the deformation style (Bretis et al., 2011; Vergés et al., 2011; Zebari et al., 2020). The NW portion of the ZFTB can be divided into different morphotectonic zones, oriented NW-SE and separated by main faults. The study area is comprised between the High Folded Zone (HFZ), towards NE, and the

Foothill Zone (FHZ), towards SW, separated by the Mountain Front Flexure (Jassim and Goff, 2006; Zebari et al., 2019, 2020). The Mountain Front Flexure is the main topographical and structural element that separates the HFZ, characterized by closely spaced (5-10 km wavelength) high anticlines, and the FHZ, showing widely spaced (up to 60 km wavelength) low anticlines and shallow synclines. The anticlines are frequently coupled with thrusts along the Mountain Front Flexure and in the FHZ; while the HFZ displays both fault-related and buckle folds (Zebari et al., 2020). The bedrock, composed by different sedimentary rocks, shows a rejuvenation in rock age from NE toward SW. Mesozoic-Paleogene sequence mainly consists of carbonates, while Neogene-Quaternary succession tends to be mainly siliciclastic (Sissakian and Al-Jibouri, 2012, 2014; Sissakian and Fouad, 2012). Quaternary deposits essentially consist of different continental terrigenous sediments covering small basins and infilling synclinal valleys especially in the FHZ (Sissakian and Al-Jibouri, 2012, 2014; Zebari et al., 2021). The climate of the study area is principally semi-arid, continental, sub-tropical type with an average annual rainfall of 428 mm and temperatures ranging from 7.8 ° C to 34.2 ° C (Rivas-Martinez, 2004; Yacoub et al., 2012; Sissakian et al., 2014). Finally, the regions have been settled by human communities since the prehistory and local natural resources continuously exploited that have been investigated by several research projects (e.g., Ur et al.,2021; Peyronel et al.,2019). Human exploitation of the CKRI left a variety of anthropogenic landforms still evident in the field, such as the ancient citadels of Erbil and Kirkuk, the many tells dispersed along the Erbil Plain, and canal systems (Forti et al., 2021).

## 3.3 Methods

Geomorphological mapping of semi-arid and arid regions can be performed through a consolidated methodology that combines Earth observation techniques and field works (Perego et al., 2011; Zerboni et al., 2015, 2020; Azzoni et al., 2017, 2022; Hüneburg et al., 2019; Costanzo et al., 2021; Forti et al., 2021), and has been applied to the study area. Different datasets were retrieved and analysed through remote sensing; all data has been reprojected to WGS 84 - UTM Zone 38N reference system within QGIS 3.16 and 3.20 software (QGIS Development Team, 2021). Recent high resolution satellite imagery (2013-2021) was analysed and visualized through “QuickMapServices” plugin (NextGis, 2021). Furthermore, declassified CORONA intelligence satellite imagery (USGS, 1968), collected between 1967-1968 was utilised to recognize variations of landforms through historical time scales (Forti et al., 2022). Simultaneously, two digital terrain models (DTM) were used to valuate and observe landforms: (i) Digital Surface Model (DSM) AW3D30 with horizontal resolution of 1 arcsecond (circa 30 m at the equator; JAXA, 2021); (ii) Digital Elevation Model (DEM) MERIT, with horizontal resolution of 3 arcseconds (circa 90 m at the equator; Yamazaki et

al., 2017). These digital models were reprojected with a spatial resolution of 30 m for DSM AW3D30 and of 90 m for DEM MERIT. Contour lines at 5, 10 and 100 m were extracted from digital terrain models and used for the landform interpretations, respectively, at 5 and 10m for alluvial plain and detailed scale landforms, and at 100 m for highlands and general scale morphologies. In addition, elevation-dependent colour scale, hillshade and slope models were derived from the DTMs through GRASS 7.8.3 and 7.8.5 (GRASS Development Team, 2020); these products were imported in QGIS and superimposed to observe different landforms (like river terraces, alluvial fans, wind, and water gaps) and to make comparisons with satellite imagery (Forti et al., 2021). The Quadrangles of the Series of geological Map of Iraq (1:250,000) of Arbeel-Mahabad, Al-Mosul, Kirkuk and Sulaimanyia, compared with Geological Map of Iraq (1:1,000,000) have been digitalized and analysed to identify bedrock chronology, lithologies, and structural elements (Maàla, 2008; Sissakian and Fouad, 2012, 2014; Sissakian, 2013) helpful in landscape reconstruction. The channel network was derived from Natural Earth (naturalearthdata.com), partially modified through comparison with satellite imagery and channel network extracted with GRASS. Field surveys validated geomorphological landforms and elements recognised through remote sensing analysis.

The channel network was also derived from DEM MERIT (Yamazaki et al., 2017) through GRASS software, and was processed to obtain a Strahler's hierarchical classification vector layer (Strahler, 1958). Analyses between channel segments and structural elements (faults and folds, mapped on the basis of Quadrangles of the Series of geological Map of Iraq) were illustrated through rose diagrams, extracted with the "Line Direction Histogram" QGIS plugin (version 3.1.1; Tveite, 2015). Analyses of channel network orientations considered both the totality of drainage segments and subdivided in each Strahler order. Histograms support comparison between the orientation of the channel network and major structural linear elements and allow validating hypothesis to explain the preferred orientation changes of channels according to the hierarchical order (e.g., Castiglioni, 1991; Kober et al., 2015; Obaid and Allen, 2017, 2019).

## 3.4 Main geomorphological features

### 3.4.1 Structural landforms

The development of mountain ridges and valley troughs and their orientations and morphologies are surface expression of the structures in the ZFTB orogen and pre-existing basement configuration (Obaid and Allen, 2017, 2019; Zebari et al., 2019, 2020). In this area, ridges generally correspond to anticline culminations, whereas valleys are the core of synclines (Figure 1A); in some cases, wine glass features are present and expose older geological successions at the fold core, such as along the Qara Chough Anticline (Figures 1A-5D). The study area includes the HFZ and FHZ that display

different shortening rates and structural orientations (Jassim and Goff, 2006; Fouad, 2015; Zebari et al., 2019, 2020). Anticlines in the HFZ (from NW to SE are Korak, Hareer, Pelewan, Kamosk, Mirawa, Shak Rook, Khalikan, Saafen, Permam, Bana Bawi and Maila anticlines; see Table 1 for comparisons between Iraqi and Kurdish nomenclature given the literature) are mainly oriented NW-SE to the east of the GZ and oriented nearly E-W to the west of the FZ. These anticlines are separated by narrow and deep synclinal valleys (Figures 1A-1B). Lateral extension and linkage between adjacent anticlines are influenced by NE-SW trending transversal basement faults, flat thrusts, and normal faults along the Mesozoic strata (Zebari et al., 2020; Csontos et al., 2022). These anticlines consist of Mesozoic-Paleogenic carbonates at the core and less competent Paleogene-Neogene terrigenous formations along the limbs and show a broad box geometry (Sissakian and Al-Jibouri, 2014; Zebari et al., 2019, 2021; Forti et al., 2021). Instead, anticlines in the FHZ (from NW to SE are Kewee Shirnella, Taq Taq, Cham Chamal, Erbil, Dameer Dagh East and West, Guwair, Bai Hassan, Northern and Southern Qara Chough, Qara Botak 1 and 2, and the ones associated with Kirkuk Thrust, as the Khormala Dome; see Table 1 for comparisons between Iraqi and Kurdish nomenclature given the literature) show NW-SE orientations (Figure 1C). Compared to the ones from the HFZ, they are more spaced and display lower elevations; this is due to relatively lower deformation intensity in the HFZ in which only less competent lithological compositions of foreland basin are exposed, often characterized by Miocene-Pliocene marls, claystones, sandstones and conglomerates that are more erodible than the Mesozoic-Paleogenic carbonates exposed the HFZ. In the FHZ, only the Qara Chough anticline show higher elevation thanks to its resistant limestone core, that is a former Mesozoic graben subsequently deformed in folding after the Cretaceous (Fouad, 2015; Sissakian et al., 2018). Furthermore, anticlines in the FHZ show major changes in the orientation of fold axis, corresponding to an en-echelon system, caused by differential uplift of each anticline. In this area, the anticlines are mostly fault related (Bretis et al., 2011). Wide synclines (Taqultu and Khal Khalan) are hanging synclines, filled by Quaternary fluvial, slope, and polygenetic sediments up to 1000 m thickness (Sissakian, 2013; Sissakian and Fouad, 2014; Obaid and Allen, 2017, 2019; Zebari et al., 2020, 2021). Along their slopes and limbs, folds often show monocline motives, including cuestas and hogbacks slope reliefs. In the Main Map, cuestas and hogbacks are not differentiated because the exposure of satellite images prevents their certain attribution to one of the two categories. Yet, flatirons belts were mapped to evidence forelimbs and toe of anticlines that show slope triangular shapes (Forti et al., 2021) (Figure 1D). The Shaqlawa Syncline valley, located in the southern edge of the Saafen and Shak Rook anticline and influenced by a thrust fault (Sissakian et al., 2021), is an

example of inverted relief; in fact, erosion was more efficient along the soft sandstone Paleocene-Eocene core than along the Cretaceous carbonate limbs (Figure 1E).

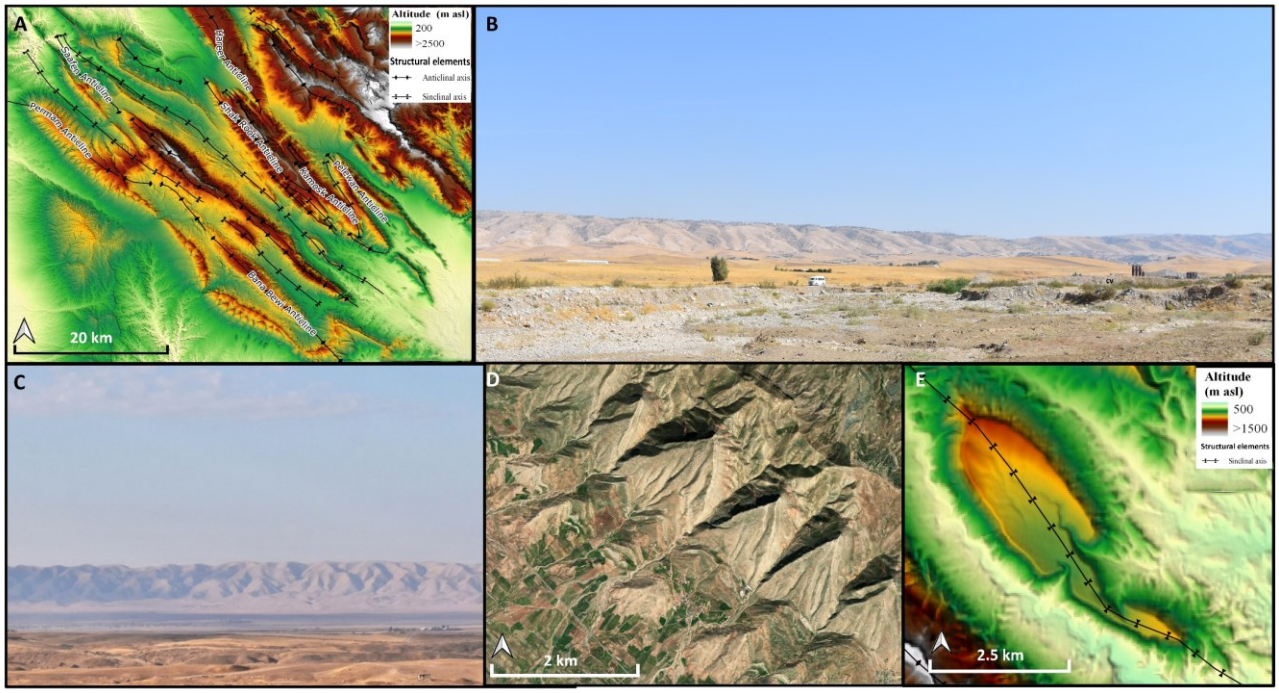


**Figure 1.** A) DEM illustrating the orientation of the main anticlines and synclines in HFZ. (B) Western slope of the Permam Anticline. (C) Eastern limb of the Qara Choug Anticline crossed by several streams. (D) Esri satellite imagery showing the southern edge of the Bana Bewi Anticline marked by flatirons. (E) DEM of the syncline ridge valley located in the southern edge of the Saafen and Shak Rook Anticlines, resulting after differential erosion of sandstone (core) and limestone (forelimbs) strata.

### 3.4.2 Hillslope and gravitative landforms

Apart of being cut into flatirons, the hillslope of anticlines in the HFZ and FHZ are affected by different processes related to gravity, seasonal climate variability, bedrock type, weathering amount, erosional and transport capacities (Sissakian et al., 2020; Forti et al., 2021). Sissakian et al. (2020) report that several localities along the LZ are affected by hillslope gravitative processes (e.g., landslide, mudflow and rockfalls) that influenced the river dynamics. Most of landslides are small and not suitable to be represented at the scale of the Main Map. A few large landslides are included in the Main Map, and they are located along the slopes of Hareer and Maila anticlines and on the ridges at the left bank of GZ (Figure 2A). Monocline slopes E and SE of Erbil and N of Kirkuk consists of terrigenous lithologies and are widely dissected by rills and gullies networks, resulting in a badland landscape (Figure2B). The connection between erosional slopes and plains is characterized by a gently pediment incised by seasonal rills and gullies networks and today exploited for cultivation (Figures 2C-D).

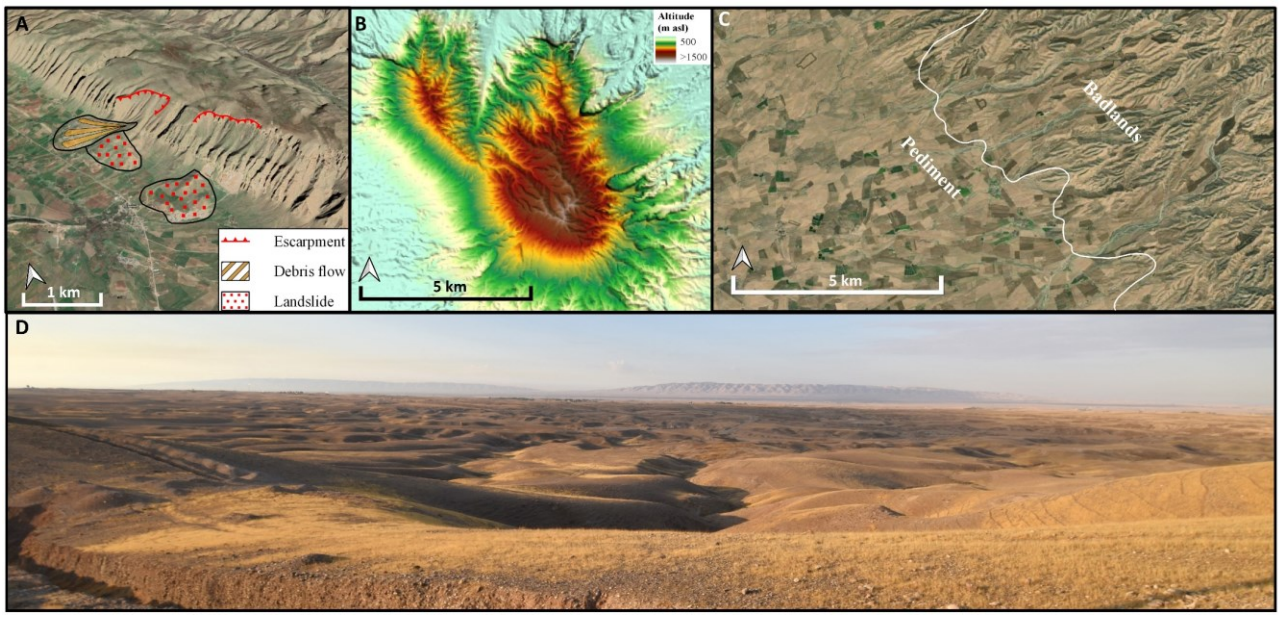


**Figure. 2**. (A) Slope instability along the southern flank of the Hareer Anticline (sketch on GoogleEarth™ 3D imagery, 2x vertical exaggeration). (B) Badlands landscape north of Kirkuk extrapolated from DEM. (C) A pediment gently connected to the badland landscape north of Kirkuk (the white line indicated the boundary) (Esri World Imagery). (D) Western hillslope of the Khormala Anticline with a gently sloping pediment deep incised by gullies. In the background the Qara Chough anticline.

### 3.4.3 Karst landforms

Limestone ridges are affected by dissolution processes resulting into a karst landscape including epikarst and ipokarst landforms (Figure3A). Major caves are not known in the study area, but several caves and rock shelters open in nearby areas of the Zagros, resulting from hypogenic and epigenic processes (Laumanns et al., 2008; Forti et al., 2021). On top of the ridges, limestone pavements are evident with small to medium scale epikarst features (Figure 3B). Moreover, several deeply incised gorges and canyons are likely the result of interplay between geological setting, fluvial and karst processes; among the others, gorges cut the Saafen, Bana Bewi, Pelewan, Hareer, and Permam anticlines (Figure 3C). Several dolines are located at the top of anticlines of Permam and Bana Bewi (Figure 3D).

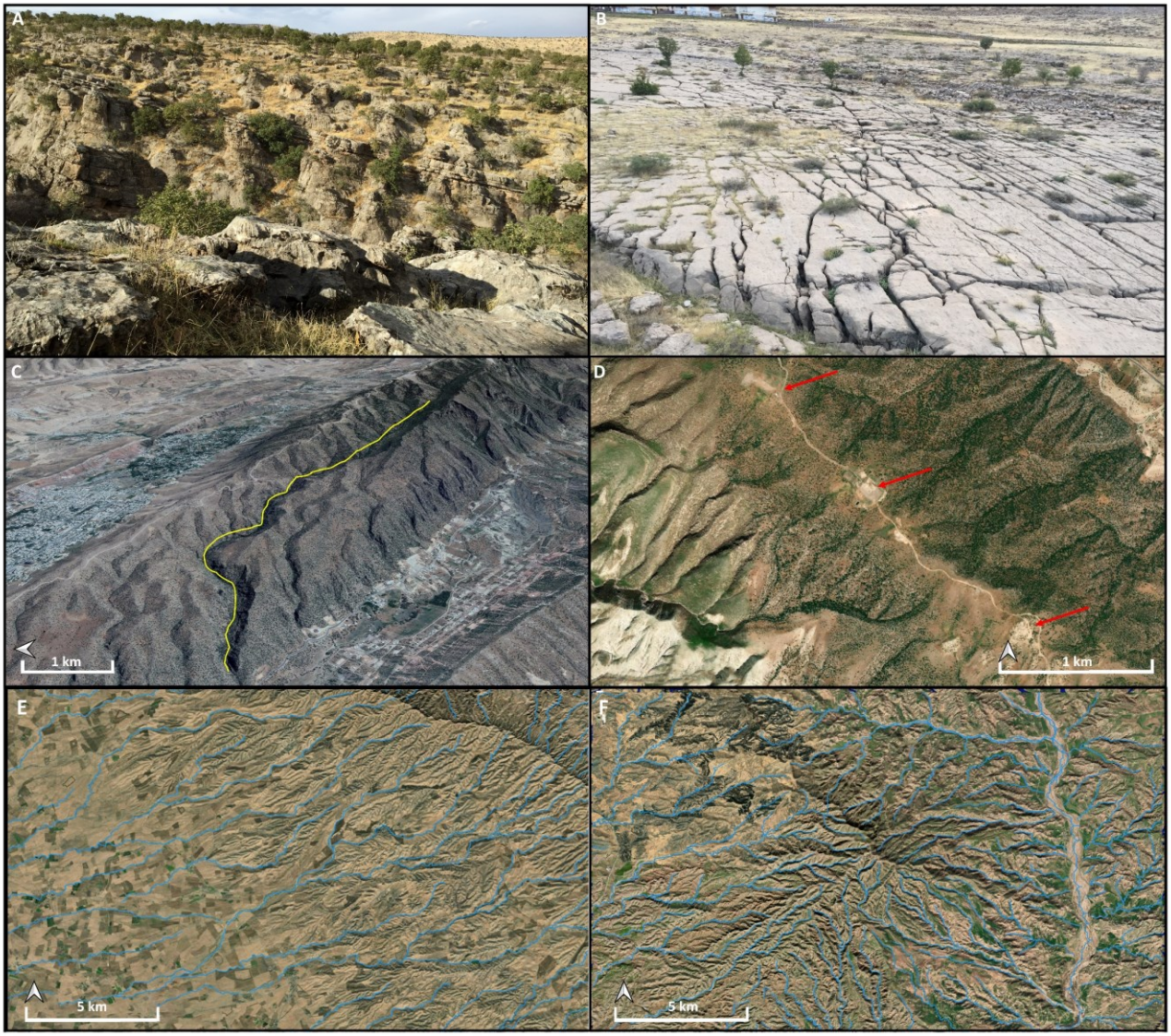


**Figure 3.** (A) Limestone landscape with epikarst landforms. (B) Slope anticline of Karak anticline characterized by limestone pavement (C) Stephead valley (red line) in the northern sector of the Saafen Anticline resulted by the interaction between karst and fluvial processes (Google Earth™ 3D imagery, 2x vertical exaggeration). (D) Dolines at the top of the Bana Bewi anticline (red arrows). Different types of drainage pattern driven by the geological and structural setting of the study area: (E) dendritic and (D) radial settings.

### 3.4.4 Fluvial landforms

The fluvial landscape of the CKRI is modelled along the catchments of the GZ and LZ rivers. Therein, the direction and plan geometry of fluvial networks is related to (i) the orientation of anticline and syncline systems and regional faults, (ii) slope gradient, (iii) lithology of the bedrock, (iv) and landslides (Fryirs and Brierley, 2013; Tooth et al., 2014; Obaid and Allen, 2017, 2019; Sissakian et al., 2020; Zebari et al., 2021). Such factors influenced the evolution of a differentiated fluvial pattern. In fact, in the mountainous area of HFZ the network is dendritic, with a NW-SE preferential orientation that follows the direction of syncline valleys; on the contrary, in the FHZ streams have a NE-SW to NW-SE direction and display a dendritic to radial drainage setting (Figures 3E-F).

Considering the two major rivers, the GZ follows a NE-SW orientation, locally shifting WSW-ENE in the proximity of the Guwair anticline. In the area between the upstream to its connection with the Tigris River, the GZ River has a single thread with a low sinuosity degree of meandering and irregular meanders pattern. Before merging into the Tigris River, the course of the GZ River shifts to an anabranching channel planform with up to 3 seasonal channels (Figures 4A-B). The LZ River follows a general ENE-WSW trend with a change toward NE-SW sectors 15 km before the Altun Kupri town. In its upstream sector, located between the HFZ and NE of FHZ, different lithotypes and landslides oversee the fluvial dynamic of the LZ River (Figure 4C). Between the Goptapa village and the Taq Taq anticline, the LZ River crosses conglomerates and sandstones displaying a single tortuous to irregular meandering thread pattern. From the Taq Taq anticline to Altun Kupri the course of the LZ becomes straight, displaying a channel with a low sinuosity and irregular meandering pattern. The final reach of the LZ River –in the FHZ – shows a low sinuosity with irregular meanders close to the Kirkuk anticline with a progressive increase in the degree and type of sinuosity before the Qara Botak anticline (Figures 4D-4E). This is triggered by the decrease in the slope gradient and growth of anticlines. Sissakian et al. (2020) suggest that the pattern of different portions of the extant shape of LZ are influenced by the activation of landslides (Taq Taq, Bul-Qamish and Saralu landslides) which modify the meandering and the general plan geometry of LZ. Today, water gap gorges are the main waterways connecting the HFZ highland with FHZ lowland (Figure 5A). The main water gap gorges are 500 m to 50 m deep and developed into the Hareer, Saafen, Khalikan and Bana Bewi anticlines in the HFZ. Several wind gaps dry valley cut the southern sector of the Bana Bewi anticline (Figure 5B). Along the LZ watercourse from upstream to downstream, several water gap gorges developed into the anticlines of Maila, Taq Taq, Chamchamal, Kirkuk Structure, Bai Hassan and Qara Botak. The slopes of HFZ ridges are carved by streams forming series of wineglass landforms and by deep V-shaped valleys, resulting into deep gorges. Unconsolidated materials characterized the valley floor of these gorges in which at termination we notice the presence of debris flow and alluvial fans, the oldest are covered by a thick calcrete, locally dissected by linear erosion (Sissakian et al., 2015) (Figure 5C). Anticlines' slopes in the LFZ are dissected by streams that build outlet of the valleys several coalescing alluvial fans forming a bajada feature (Figure 5D).

Lowlands are characterized by wide floodplains located in the surrounding Erbil and Kirkuk. Floodplains mainly consist of reddish silty-clay deposits interbedded with coarser layers and it is dissected into four orders of fluvial terraces; the main river courses display a gravel-dominated to silty bed. The younger terraces (T1, T2 and T3) formed in the Late Quaternary and are composed by pebble and cobble in a sandy matrix with interlayered medium to coarse sand, while the oldest terrace

(T4) consists of Plio-Pleistocene conglomerates (Dokan Fms. in the upperstream portion of the LZ) (Figure 5E) (Sissakian and Fouad, 2015). In the NW sector of the study area, some of the GZ fluvial terraces are tilted by Quaternary neotectonics (Zebari et al., 2021).

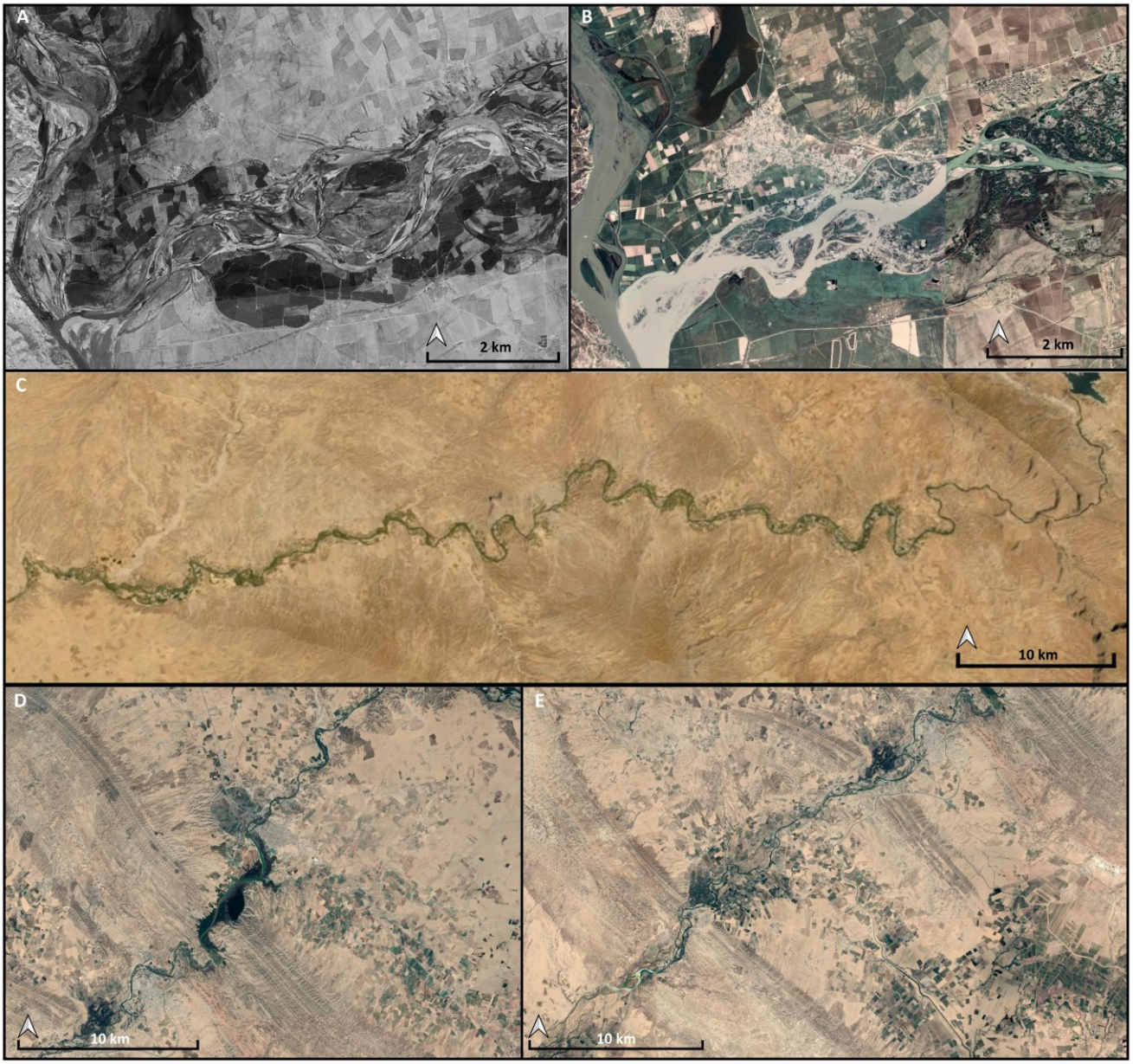


**Figure 4.** The anabranching planform of the GZ River before its conjunction with the Tigris River from (A) declassified Corona Imagery (Aug.1968) and (B) Google Earth™ satellite imagery (captured in Jan. 2019). (AC) Upstream reach of the LS River that flows with a E-W trend and displays a decrease in meanders sinuosity (Esri Satellite). (D) Downstream reach of LZ before in the NE of Kirkuk city, where the river switch toward NE-SW (Google Earth™ satellite imagery). (E) Downstream reach of LZ in the NE of Kirkuk city, with development of floodplain (Google Earth™ satellite imagery).

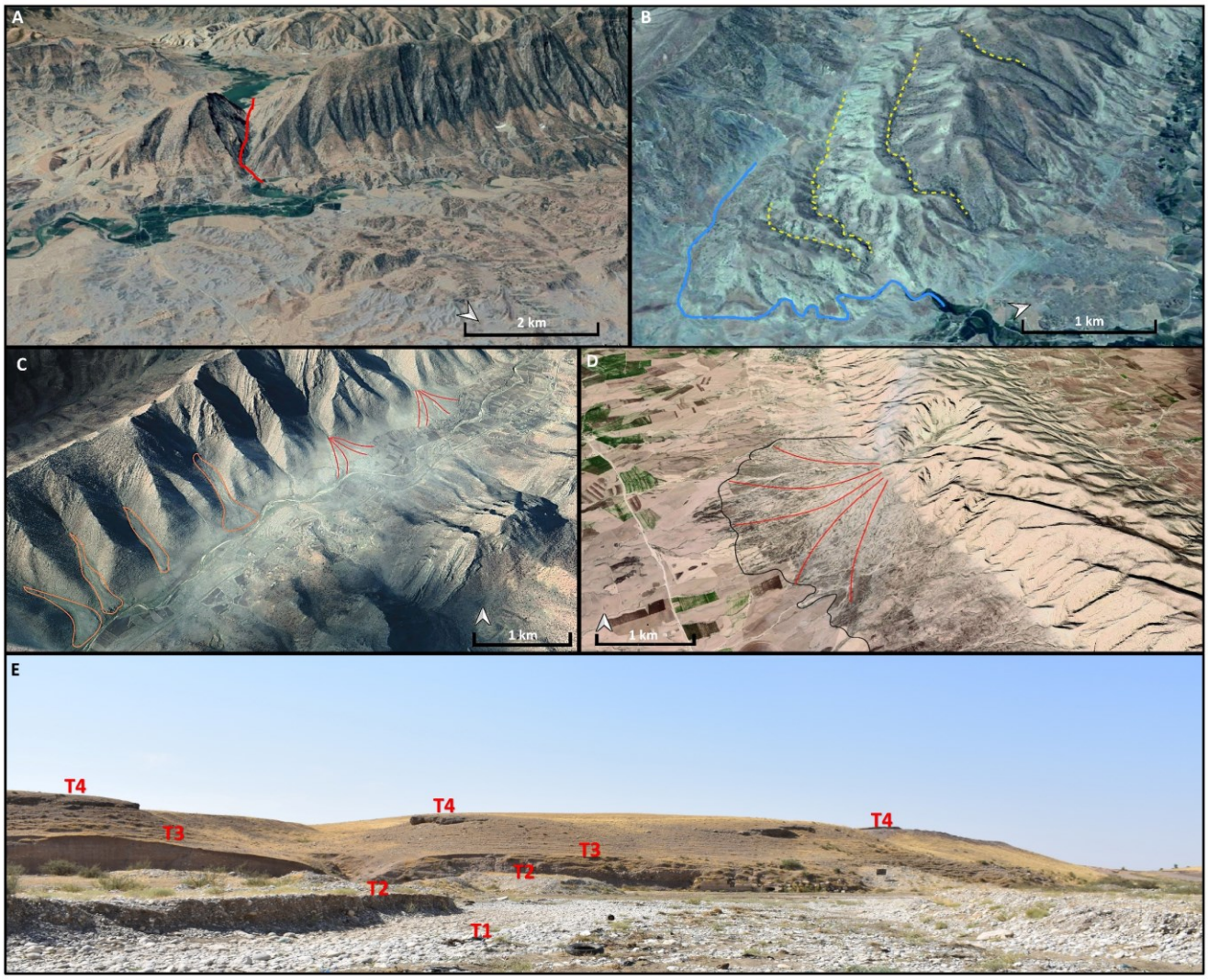


**Figure 5.** Water gap in SE sector of Saafen anticline (elaborated from Google EarthTM D imagery, 2x vertical exaggeration). (B) Southern edge of the Bana Bewi Anticline showing four wind gaps (yellow dotted lines) and the active river course (blue line) (elaborated from Google EarthTM D imagery, 2x vertical exaggeration). (C) Google EarthTM 3D imagery (3x vertical exaggeration) of the eastern limb of the Pelewan anticline dissected by several V-shape valleys (wineglass landform) with debris flow fans (orange polygons) and outlet alluvial fans (red lines). (D) Alluvial fan (red lines) and bajada envelope (black line) along the western limb of the Qara Chough anticline (elaborated on Google EarthTM 3D imagery, 2x vertical exaggeration). (E Terraced banks of the Chai Basturah River, NE of Erbil; the order of terraces is reported.

### 3.4.5 Anthropogenic landforms

Since the Early and Middle Holocene, the natural landscape of the CKRI has been strongly affected by human activities, including cultivation, herding, and water management in the region. Consequently, several anthropogenic landforms are the result of an intense land exploitation that started in the prehistory and recently exacerbated by exponential growth of urban centres (Figures 6A-B). In the Late Holocene, the progressively increasing demand for primary resources (such as water) and enhanced aridity promoted the introduction of extensive implements for water

management; for instance, the underground qanat (Kahreeze) system (Figure 6C) for water harvesting from the alluvial fans was introduced several centuries ago (Shoroush et al., 2020). Moreover, several dams, water reservoirs, and artificial canals were recently built to support intensive cultivation. Modern facilities for water management are located mostly in the proximity of Erbil and Kirkuk, notably along the GZ and LZ Rivers and at the foothills of anticline ridges. A large artificial canal excavated S of Kirkuk connects the LZ with the southern Adhaim and Diyala plains. Dams and related water reservoirs are in the sector N of Kirkuk and SE of the Bana Bewi anticline.

Several archaeological mounds arise from the surrounding flat areas; they are tell sites and were formed by the accumulation of human sediments after millennia of occupation (Miller Rosen, 1986; Wilkinson, 2003) (Figure 6D). Such anthropogenic landforms testify for the long-term exploitation of CKRI. Tells are common in the floodplain S of Erbil (Peyronel et al., 2019; Ur et al., 2021), and they are generally located along active/ephemeral meandering streams or palaeochannels.

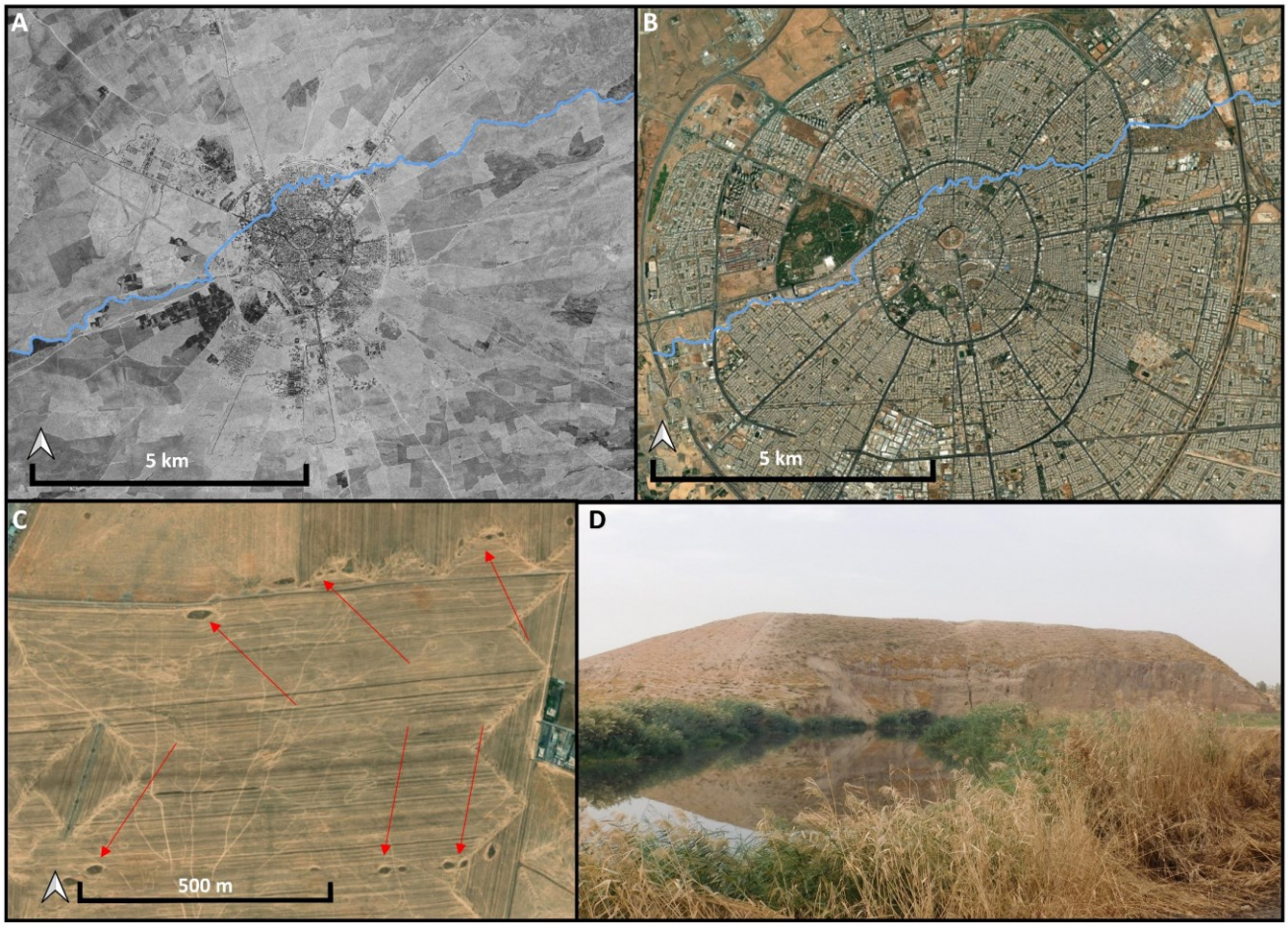


**Figure 6.** Anthropogenic landforms in the study area. Comparison between (A) 1968 Declassified Corona and (B) Esri World view imagery (captured in Nov. 2020) that show the intense urban expansion of Erbil; the blue line indicates a former fluvial channel recently forced underground with consequence hydrographic network modification. (C) Qanat alignment in the proximity of Erbil (red arrows) (Bing Virtual Earth). (D) Archaeological mound (tell) in the Erbil Plain (Tell Awena).

## 3.5 Hydro-morphometric analysis: tectonic influence on channel network organization

The effects of differential uplift, linked to Neogene-recent tectonic activity, can be recognized also through the analyses of different fluvial patterns and river variation. In fact, in tectonically dynamic areas rivers tend to set up their directions based on structural elements (e.g., Kober et al., 2015; Obaid and Allen, 2017, 2019; Trost et al., 2020; Siravo et al., 2021; Woolderink et al., 2021). Our analyses of fluvial network (summarized in Figure 7) illustrates that the rose diagram of the 1st order of stream segments has a NE-SW preferential orientation, perpendicular to the trend of structural elements (anticlines and faults). This reflects the tendency of the minimum hierarchical tracts to set along the direction of maximum slope gradient. The 2nd order of stream segments shows a preferential trend directed NE-SW, but there is a significant NW-SE and E-W component. In this case, directional variability is ruled out by the interplay between: (i) the NE-SW preferential trend is influenced by direction of maximum slope gradient, (ii) the NW-SE alignment corresponds to the trend of folds and faults, (iii) E-W trend is determined principally by hydrographic networks developed in the reliefs NE of the Erbil Plain. The 3rd and 4th orders of stream segments show a NW-SE preferential orientation, responding to a major structural control; these segments run parallel to faults and synclinal valleys axis. They are responsible of the accretion of floodplains along synclinal valleys. Rose diagram of the 5th order of stream segments shows a NE-SW preferential orientation, but in this hierarchical class only includes some segments of the GZ and LZ Rivers. The latter align along basement strike-slip faults that dislocate tectonic blocks (Jassim and Goff, 2006). The 6th order of stream segments (corresponding to the Tigris River and last part of GZ River) show a NE-SW preferential trend followed by a N-S orientation. The NE-SW direction is influenced by basement strike-slip faults, while NNW-SSE trend is also related to an inferred strike-slip fault located along the Tigris River course (Jassim and Goff, 2006; Fouad, 2015) (Figure 7)

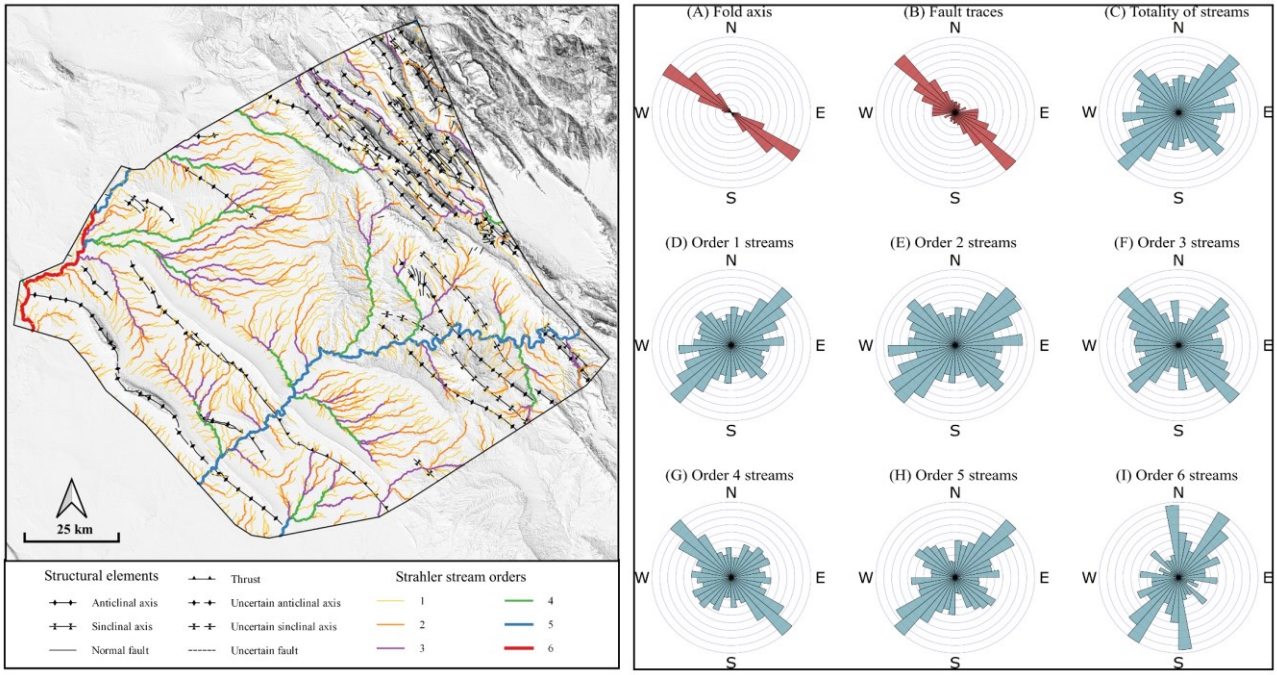


**Figure 7.** Grayscale Dem of the study area with the different structural and Strahler's stream orders Rose Diagram histograms. Rose diagrams are based on number of analyzed elements and on weight of length. The histograms show that structures (references for geological features see Methods) have a general NW-SE orientation, with a principal concentration for the fold axis, while fault traces have a broader distribution. Channel network's histograms are more complex. The histogram of all fluvial courses' marks three preferential orientations (in order, NE-SW, NW-SE, E-W). The rose diagrams of lower hierarchical Strahler's classes (order 1 and 2) show a NE-SW preferential orientation, perpendicular respect to structural elements trend. Order 3 and 4 stream segments have a NW-SE preferential orientation, parallel to structural elements direction. Histogram of order 5 waterways shows a NE-SW trend, while order 6 channels show a NE-SW preferential trend followed by an NNW-SSE orientation.

## 3.6 Conclusion

Geomorphological mapping of the CKRI permitted to recognize different geomorphological units resulting from the many processes that shaped the landscape at the regional scale during the Late Cenozoic. Our investigation highlights the major influence of tectonic and climatic variations in modelling landforms. Compressive tectonic and Quaternary neotectonic led to the organization of the landscape into subsequent ridges and valleys corresponding to anticlines and synclines respectively; this also influenced the evolution of the channels network. Quaternary climate oscillations impacted on the variations in flow rate, amount of solid load and consequently on fluvial landforms. In the last millennia, anthropic impact has grown, which determined modifications of natural landscape and creation of anthropogenic landforms. The exploitation of natural resources has determined the transformation and continuous shaping of the territory, which have increased in parallel with the development of complex societies. In this scenario, overlapping of endogenous and exogenous factors has determined the formation of a palimpsest landscape, in which active and fossil stratified elements and processes can be recognized. Finally, geomorphological mapping of long-time settled landscapes

– as the CKRI is – offers important tools for urban planning as much as a plethora of information to reconstruct past human adaptations, subsistence strategies, and early human overprints on pristine geomorphic systems.

| | Iraqi anticlines-synclines nomenclature | Kurdish anticlines-synclines nomenclature |
|---|---|---|
| High Folded Zone (HFZ) | Korak | Kurak |
| | Hareer | Harir |
| | Pelewan | Pelewan |
| | Kamosk | Kamosk |
| | Mirawa | Mirawa |
| | Shak Rook | Shakrok |
| | Shaqlawa | Seqlawa |
| | Khalikan | Khalakan |
| | Saafen | Safeen |
| | Permam | Pirmam |
| | Bana Bawi | Bina Bawi |
| | Maila | Maila |
| Foothill Zone (FHZ) | Kewee Shirnella | Kewee Shirnella |
| | Taq Taq | Taq Taq |
| | Cham Chamal | Chemchemal |
| | Erbil | Erbil |
| | Dameer Dagh | Demir Dagh |
| | Khormala Dome | Khurmala Dome |
| | Guwair | Guwair |
| | Bai Hassan | Bai-Hasan |
| | Qara Chough | Qara Chug |
| | Qara Botak | Qara Botak |
| | Kirkuk | Kirkuk |
| | Taqultu | Taqultu |
| | Khal Kalan | Khalakan |

**Table 1.** Nomenclature of the anticlines and synclines in the study area transliterated from the Arabic and Kurdish. Arabic names are from Maàla (2008), Sissakian (2013), Sissakian and Fouad (2014). Kurdish names are from Shamaran petroleum (2011), Kurdistan Oil Resources (2013) and Koshnaw et alii (2020).

## 3.7. References

Azzoni, R. S., Bollati, I. M., Pelfini, M., Sarıkaya, M. A., & Zerboni, A. (2022). Geomorphology of a recently deglaciated high mountain area in Eastern Anatolia (Turkey). *Journal of Maps*, 1-10.

Azzoni, R. S., Zerboni, A., Pelfini, M., Garzonio, C. A., Cioni, R., Meraldi, E., ... & Diolaiuti, G. A. (2017). Geomorphology of Mount Ararat/Ağri Dağı (Ağri Dağı Milli Parki, Eastern Anatolia, Turkey). *Journal of Maps*, *13*(2), 182-190.

Bretis, B., Bartl, N., & Grasemann, B. (2011). Lateral fold growth and linkage in the Zagros fold and thrust belt (Kurdistan, NE Iraq). *Basin Research*, *23*(6), 615-630.

Burbank, D. W., & Anderson, R. S. (2011). Tectonic geomorphology. John Wiley and Sons.

Castiglioni, G.B., (1991). Geomorfologia. Seconda edizione. UTET, Torino, 436 p.

Costanzo, S., Zerboni, A., Cremaschi, M., & Manzo, A. (2021). Geomorphology and (palaeo-) hydrography of the Southern Atbai plain and western Eritrean Highlands (Eastern Sudan/Western Eritrea). *Journal of Maps*, *17*(2), 51-62.

Csontos, L., Forián-Szabó, M., Pocsai, T., Magyari, Á., & Soós, B. (2022). Fold formation in Kurdish Zagros (N Iraq). *Marine and Petroleum Geology*, *146*, 105914.

Flohr, P., Fleitmann, D., Zorita, E., Sadekov, A., Cheng, H., Bosomworth, M., ... & Matthews, R. (2017). Late Holocene droughts in the Fertile Crescent recorded in a speleothem from northern Iraq. *Geophysical Research Letters*, *44*(3), 1528-1536.

Forti, L., Mariani, G. S., Brandolini, F., Pezzotta, A., & Zerboni, A. (2022). Declassified intelligence satellite imagery as a tool to reconstruct past landforms and surface processes. The submerged riverscape of the Tigris River below the Mosul Dam Lake, Iraq. *Earth Surface Processes and Landforms*.

Forti, L., Perego, A., Brandolini, F., Mariani, G. S., Zebari, M., Nicoll, K., ... & Zerboni, A. (2021). Geomorphology of the northwestern Kurdistan Region of Iraq: landscapes of the Zagros Mountains drained by the Tigris and Great Zab Rivers. *Journal of Maps*, *17*(2), 225-236.

Fouad, S. F. (2015). Tectonic map of Iraq, scale 1: 1000 000, 2012. *Iraqi Bulletin of Geology and Mining*, *11*(1), 1-7.

Fryirs, K. A., & Brierley, G. J. (2012). *Geomorphic analysis of river systems: an approach to reading the landscape*. John Wiley & Sons.

GRASS Development Team, (2020). Geographic Resources Analysis Support System (GRASS) Software, Version 7.8. Open-Source Geospatial Foundation, https://grass.osgeo.org.

Holbrook, J., & Schumm, S. A. (1999). Geomorphic and sedimentary response of rivers to tectonic deformation: a brief review and critique of a tool for recognizing subtle epeirogenic deformation in modern and ancient settings. *Tectonophysics*, *305*(1-3), 287-306.

Huggett, R. (2016). *Fundamentals of geomorphology*. Routledge.

Hüneburg, L., Hoelzmann, P., Knitter, D., Teichert, B., Richter, C., Lüthgens, C., ... & Luciani, M. (2019). Living at the wadi–integrating geomorphology and archaeology at the oasis of Qurayyah (NW Arabia). *Journal of Maps*, *15*(2), 215-226.

Jackson, J., van Dissen, R., & Berryman, K. (1998). Tilting of active folds and faults in the Manawatu region, New Zealand: evidence from surface drainage patterns. *New Zealand Journal of Geology and Geophysics*, *41*(4), 377-385.

Jassim, S. Z., & Goff, J. C. (Eds.). (2006). *Geology of Iraq*. DOLIN, sro, distributed by Geological Society of London.

JAXA (2021). ALOS Global Digital Surface Model "ALOS World 3D – 30m (AW3D30)" Retrieved August 11, 2021, from https://www.eorc.jaxa.jp/ALOS/en/aw3d30/.

Kober, F., Zeilinger, G., Hippe, K., Marc, O., Lendzioch, T., Grischott, R., ... & Zola, R. (2015). Tectonic and lithological controls on denudation rates in the central Bolivian Andes. *Tectonophysics*, *657*, 230-244.

Koshnaw, R. I., Stockli, D. F., Horton, B. K., Teixell, A., Barber, D. E., & Kendall, J. J. (2020). Late Miocene deformation kinematics along the NW Zagros fold-thrust belt, Kurdistan region of Iraq: Constraints from apatite (U-Th)/He thermochronometry and balanced cross sections. *Tectonics*, *39*(12), e2019TC005865.

Kurdistan Oil Resources (2013). Discoveries and Development. Wildcat International FZ-LLC, The Oil & Gas Year, Kurdistan Region of Iraq. http://archive.gov.krd/mnr/mnr.krg.org/images/pdfs/Discoveries_and_development_TOGY_2013_1.pdf

Laumanns, M., Rasch, A., & Audra, P. (2008). Karst and Caves of Iraq:(including the Results of a 2007 Kurdish-German Speleological Project and an Overview on Hypogenic Sulphidic Speleogenesis). Speläoclub.

Maàla, K.A., (2008). Geological Map of Sulaimaniya Quadrangle Sheet NI-38-3, Scale 1: 250.000, 1st Edition. Iraq Geological Survey, Baghdad, Iraq.

Rosen, A. M. (1986). *Cities of clay: the geoarcheology of tells*. University of Chicago Press.

NextGIS (2021). QuickMapServices. https://nextgis.com/blog/quickmapservices/.

Obaid, A. K., & Allen, M. B. (2017). Landscape maturity, fold growth sequence and structural style in the Kirkuk Embayment of the Zagros, northern Iraq. *Tectonophysics*, *717*, 27-40.

Obaid, A. K., & Allen, M. B. (2019). Landscape expressions of tectonics in the Zagros fold-and-thrust belt. *Tectonophysics*, *766*, 20-30.

Owen, L.A., (2013). Tectonic geomorphology. In: J.F. Shroder (Ed.), Treatise on Geomorphology, Academic Press.

Perego, A., Zerboni, A., & Cremaschi, M. (2011). Geomorphological Map of the messak settafet and mellet (central Sahara, SW Libya). Journal of Maps, 7(1), 464-475.

Peyronel, L., Minniti, C., Moscone, D., Naime, Y., Oselini, V., Perego, R., & Vacca, A. (2019). The Italian Archaeological Expedition in the Erbil Plain, Kurdistan Region of Iraq: Preliminary Report on the 2016-2018 Excavations at Helawa.

QGIS Development Team (2021). QGIS Geographic Information System. Open Source Geospatial Foundation Project.

Ramsey, L. A., Walker, R. T., & Jackson, J. (2008). Fold evolution and drainage development in the Zagros mountains of Fars province, SE Iran. *Basin Research*, *20*(1), 23-48.

Rivas-Martínez, S. (2004). Global bioclimatics. *Clasificaciòn Bioclimàtica de la tierra*. Worldwide Bioclimatic Classification System. Phytosociological Research Center, Spain, http://www.global-bioclimatics.org

Shamaran petroleum (2011). Kurdistan Oil & Gas Activity. November 2011. http://www.iraqoilforum.com/wp-content/uploads/2011/11/Kurdistan-Oil-Gas-Activity-Map-Nov-2011.pdf.

Siravo, G., Molin, P., Sembroni, A., Fellin, M. G., & Faccenna, C. (2021). Tectonically driven drainage reorganization in the Eastern Cordillera, Colombia. *Geomorphology*, *389*, 107847.

Sissakian, V. K., & Al-Jibouri, B. S. (2012). Stratigraphy of the low folded zone. *Iraqi Bulletin of Geology and Mining*, (5), 63-132.

Sissakian, V. K., & Al-Jiburi, B. M. (2014). Stratigraphy of the high folded zone. *Iraqi Bulletin of Geology and Mining*, *6*, 73-16.

Sissakian, V. K., & Fouad, S. F. (2012). Geological Map of Sulaimaniyah Quadrangle, scale 1: 250 000. Iraq Geological Survey Publications, Baghdad, Iraq.

Sissakian, V. K., & Fouad, S. F. (2014). Geological Map of Sulaimaniyah Quadrangle, scale 1: 250 000. *Iraq Geological Survey Publications, Baghdad, Iraq*.

Sissakian, V.K., (2013). Geological Map of Kirkuk Quadrangle Sheet NI-38-2, Scale 1: 250.000, 2nd Edition. *Iraq Geological Survey, Baghdad, Iraq.*

Sissakian, V. K., Al-Ansari, N., & Abdulahad, A. D. (2020). Indicating the Possibility of Activation of Large and Old Landslides and Risk Estimation Using Remote Sensing and Field Data, Examples from the Iraqi Kurdistan Region, Iraq. *Geotectonics*, *54*(2), 240-255.

Sissakian, V., Al-Mousawi, H., Al-Ansari, N., & Knutsson, S. (2015). Old alluvial fan relics in North and Northeast Iraq. *Journal of Earth Sciences and Geotechnical Engineering*, *5*(2), 45-62.

Sissakian, V. K., Ghafur, A. A., Abdulhaq, H. A., & Omer, H. O. (2021). Shakrook Anticline, a Very Complicated Structural Form, North Iraq, Kurdistan Region. *The Iraqi Geological Journal*, 162-177.

Sissakian, V. K., Kadhim, T. H., & Jab'bar, M. F. A. (2014). Geomorphology of the high folded zone. Iraqi Bulletin of Geology and Mining, (6), 7-51.

Sissakian, V. K., Othman, A. A., & Shihab, A. T. (2018). Factors Controlling the Development of Wine-Glass Forms in the Mountains of the Kurdistan Region, Iraq. *ARO-The Scientific Journal of Koya University*, *6*(2), 39-48.

Solecki, R. S. (1971). Shanidar, the first flower people. Knopf.

Soroush, M., Mehrtash, A., Khazraee, E., & Ur, J. A. (2020). Deep learning in archaeological remote sensing: Automated qanat detection in the kurdistan region of Iraq. *Remote Sensing*, *12*(3), 500.

Strahler, A. N. (1958). Dimensional analysis applied to fluvially eroded landforms. *Geological Society of America Bulletin*, *69*(3), 279-300.

Tooth, S., McCarthy, T., Rodnight, H., Keen-Zebert, A., Rowberry, M., & Brandt, D. (2014). Late Holocene development of a major fluvial discontinuity in floodplain wetlands of the Blood River, eastern South Africa. *Geomorphology*, *205*, 128-141.

Trost, G., Robl, J., Hergarten, S., & Neubauer, F. (2020). The destiny of orogen-parallel streams in the Eastern Alps: The Salzach–Enns drainage system. *Earth Surface Dynamics*, *8*(1), 69-85.

Tveite, H. (2015). The QGIS line direction histogram plugin. [WWW Document]. URL. http://arken.umb.no/~havatv/gis/qgisplugins/LineDirectionHistogram/.

Ur, J., Babakr, N., Palermo, R., Creamer, P., Soroush, M., Ramand, S., & Nováček, K. (2021). The Erbil Plain Archaeological Survey: Preliminary Results, 2012–2020. *Iraq*, *83*, 205-243.

USGS (1968). Declassified Corona Imaging data. Retrieved from https://corona.cast.uark.edu (accessed 11/08/2020).

Van de Mieroop, M. (2015). A history of the ancient Near East, ca. 3000-323 BC. John Wiley & Sons.

Vergés, J., Saura, E., Casciello, E., Fernandez, M., Villaseñor, A., Jimenez-Munt, I., & García-Castellanos, D. (2011). Crustal-scale cross-sections across the NW Zagros belt: implications for the Arabian margin reconstruction. Geological Magazine, 148(5-6), 739-761.

Viltres, R., Jónsson, S., Alothman, A. O., Liu, S., Leroy, S., Masson, F., ... & Reilinger, R. (2022). Present-day motion of the Arabian plate.

Wilkinson, T. J. (2003). *Archaeological landscapes of the Near East*. University of Arizona Press.

Woolderink, H. A. G., Cohen, K. M., Kasse, C., Kleinhans, M. G., & Van Balen, R. T. (2021). Patterns in river channel sinuosity of the Meuse, Roer and Rhine rivers in the Lower Rhine Embayment rift-system, are they tectonically forced? *Geomorphology*, *375*, 107550.

Yacoub, S. Y., Othman, A. A., & Kadhim, T. H. (2012). Geomorphology of the low folded zone. *Iraqi Bulletin of Geology and Mining*, (5), 7-37.

Yamazaki, D., Ikeshima, D., Tawatari, R., Yamaguchi, T., O'Loughlin, F., Neal, J. C., ... & Bates, P. D. (2017). A high-accuracy map of global terrain elevations. *Geophysical Research Letters*, *44*(11), 5844-5853.

Zebari, M., Balling, P., Grützner, C., Navabpour, P., Witte, J., & Ustaszewski, K. (2020). Structural style of the NW Zagros Mountains and the role of basement thrusting for its Mountain Front Flexure, Kurdistan Region of Iraq. *Journal of Structural Geology*, *141*, 104206.

Zebari, M., Grützner, C., Navabpour, P., & Ustaszewski, K. (2019). Relative timing of uplift along the Zagros Mountain Front Flexure (Kurdistan Region of Iraq): Constrained by geomorphic indices and landscape evolution modeling. *Solid Earth*, *10*(3), 663-682.

Zebari, M., Preusser, F., Grützner, C., Navabpour, P., & Ustaszewski, K. (2021). Late Pleistocene-Holocene Slip Rates in the Northwestern Zagros Mountains (Kurdistan Region of Iraq) Derived from Luminescence Dating of River Terraces and Structural Modeling. *Tectonics*, *40*(8).

Zerboni, A., Perego, A., & Cremaschi, M. (2015). Geomorphological map of the Tadrart Acacus massif and the Erg Uan kasa (Libyan Central Sahara). *Journal of Maps*, *11*(5), 772-787.

Zerboni, A., Perego, A., Mariani, G. S., Brandolini, F., Al Kindi, M., Regattieri, E., ... & Cremaschi, M. (2020). Geomorphology of the Jebel Qara and coastal plain of Salalah (Dhofar, southern Sultanate of Oman). *Journal of Maps*, *16*(2), 187-1

# Chapter 4

# Neolithic hydroclimatic change and water resources exploitation in the Fertile Crescent

## 4.1 Introduction

During the first half of the Holocene (11.6-7 ka, 9600-5000 BCE), human communities across SW Asia developed new strategies for living as sedentary farmers and herders following millennia of a mobile hunter-gathering existence (Childe, 1936, Watkins 2010). This so-called "Neolithic Revolution" was a progressive and spatially nuanced process that involved fundamental social, economic, and technological transformations, resulting in the aggregation of people into permanent settlements (Matthews et al.2019), the progressive domestication of animal and plant species (Zeder & Hesse 2000; Riehl et al., 2013), and dramatic population growth (Palmisano et al., 2021). Such innovations reorganized human-environment and social interactions, ultimately leading to the rise of complex societies (Rindos, 2013; Roberts et al., 2018). Detailed records of climate variability and its underlying mechanisms from these nascent regions are crucial to fully understand the environmental context of the Neolithic transition. In particular, such records can shed light on the potential nexus between climatic and environmental change on the one hand, and local cultural trajectories, demographic trends, and the dispersal of farming practices on the other. The first part of the Holocene was also punctuated by multidecadal- to centennial-scale rapid climate changes (also called RCCs) of hemispheric-to-global scale which are characterized by a high degree of temporal and spatial variability, and by complex and non-stationary patterns of regional climate teleconnections (Mayewski et al., 2004). Two major centennial-scale intervals of abrupt climate change have been recognized globally around 9.3 ka and 8.2 ka (e.g., Alley et al., 1997; Fleitmann et al., 2008;) with the latter being the most prominent and widespread (e.g., Cheng et al., 2009; Nicolussi & Schlüchter 2012). These events were triggered by drainage of freshwater from the last remnants of the Laurentide ice sheet to the North Atlantic and caused short-term weakening of the North Atlantic overturning circulation (AMOC), with downstream effects on oceanic and atmospheric conditions (Clarke et al., 2004; Yu et al., 2010). Given their pervasive influence and their significance at the scale of humans and ecosystems, their expression in SW Asia has long been investigated to identify potential links with Neolithic phases of socio-economic transformations (e.g., Weninger et al., 2006; Flohr et al.,

*Regattieri, E., Forti, L., Drysdale, R. N., Mannella, G., Hellstrom, J. C., Conati Barbaro, C., ... & Zerboni, A. (2023). Neolithic hydroclimatic change and water resources exploitation in the Fertile Crescent. Scientific Reports, 13(1), 45.* https://doi.org/10.1038/s41598-022-27166-y

2016). Yet, contrasting evidence exists regarding the local impacts of these events, with some studies suggesting they were associated with droughts – especially at 8.2 ka (Weninger et al.,2006)– whilst others pointing to a muted or even wetter climate, sometimes within longer intervals of particularly unstable conditions (Rohling & Pälike, 2005; Rohling et al., 2019). Even more debated is the influence of such climatic events on Neolithic populations and their adaptive response, with some scholars identifying major cultural outbreaks at the time, and others suggest more complex scenarios of resilience and cultural adaptation (Weninger et al.,2006; Flohr et al., 2016). Geochemical records from cave chemical deposits (speleothems) are ideally suited for comparison with contextually robust evidence from modern archaeological and historical studies because they preserve multiple environmentally sensitive properties that can be attributed to regional and extra-regional climatic forcing (Carolin et al., 2019; Regattieri et al., 2019a; Nicholson et al., 2021). Speleothems can also be precisely dated by the U-Th disequilibrium method, providing an independent time frame by which to interrogate the triggers and propagation mechanisms of change (e.g., Corrick et al., 2020). Here, we present a multi-decadal hydroclimatic reconstruction spanning the 11.0 to 7.6 ka period (9000 to 5600 yr. BCE) obtained from a speleothem from the Zagros Mountains piedmont zone of Iraqi Kurdistan, located in the core region of the Fertile Crescent (FC). Current research along the Zagros high steppe and foothills indicates the region was a key zone in the Neolithic transition (Matthews et al., 2019). Ancient DNA evidence suggests that the area experienced an independent trajectory from hunter gathering to cultivation of cereal crops and animal husbandry (Riehl et al., 2013; Zader & Hesse 2000; Daly et al., 2018), while archaeological research indicates that it hosted some of the earliest, large, and permanent settlements (Matthews et al., 2019), and some of the earliest evidence for pottery production (Iizuka & Terry, 2021). The speleothem record presented here encompasses the local cultural entities of the Early Neolithic (Pre-Pottery Neolithic or PPN 11.6–9.0 ka / 9600–7000 yr BC), Late Neolithic (Pottery Neolithic or PN 9–7.3 ka / 7000–5300 yr BC), and the Early Chalcolithic (7.3–6.5 ka, 5300–4500 yr BCE) (Matthews et al., 2019; Nieuwenhuyse & Akkermans, 2019). Throughout these periods, local communities underwent profound transformations in material cultures and subsistence strategies, as well as marked changes in settlement patterns (Matthews et al., 2019; Nieuwenhuyse & Akkermans, 2019). The speleothem records multi-centennial changes in regional moisture availability, reaching their maximum amplitude between 9.5 and 8.0 ka (7500–6000 BCE). A comparison with regional and extra-regional records reveals that the North Atlantic-triggered 9.3 and 8.2 ka events had only a limited impact on the local climate, and that hydrologic variability in the northern FC was mostly affected by changes in the intensity of the Siberian High (SH). The SH, the dominant semi-permanent anticyclone that occurs during winter-early spring and controls temperature and precipitation in large parts of Asia (Cohen et al., 2001; Gong & Ho, 2002),

triggered changes in the amount and style of precipitation, and modulated the length of the wet season in the northern FC. By exploring the temporal relationship with the major cultural transitions apparent from the local archaeological record, we found that hydroclimatic fluctuations are coeval with major changes in settlement's pattern and re-organization of the strategies for the exploitation of water resource. This evidence suggests a link between hydroclimatic variability, social organization, and human exploitation of the environment in the Neolithic and at the Neolithic-Chalcolithic transition.

## 4.2 Site settings

The speleothem studied here was collected during survey activities within the "Land of Ninive Archaeological Project" (LoNAP, see Aknowledgement), from a shallow, unnamed cave corresponding to GPS way point 514 of the survey (Figure 1). Therefore, the specimen is named LoNAP514 hereinafter. The cavity, located in the northern Kurdistan Region of Iraq, is opened at ~940 m a.s.l. on the Paleogene limestone in the SW foothills of the Zagros Mountains, fronting the alluvial plains formed by the Tigris River and its tributaries (Forti et al., 2021) (Figure 1, and Supplementary Information text 1). Total annual precipitation at the cave site, based on 0.5° grid cell re-analysis data, averages ~600 mm (1901-2016) (Mohammadzadeh et al., 2020) and is higher than in the southern semi-arid part of the country due to local orographic effects. About 98% of the precipitation occurs between November and May (Schneider et al., 2018). There is an overall influence of westerly circulation, with most of the precipitation events associated to storm tracks originating in the eastern Mediterranean, especially at the Cyprus low, and following an eastward route. A significant amount of precipitation is also related to strong convective instability associated with low-level water vapor supply (Evans et al.,2004). In wet transition months (ON and MAM), southeasterly winds also supply vapor from the Persian Gulf, and the Arabian and Red Seas, increasing convection and contributing significantly to total annual precipitation (Trigo et al., 2010; Al-Nassar et al., 2020; Mohammadzadeh et al., 2020). These low-level, southern humidity fluxes are almost suppressed in dry years (Trigo et al., 2010). The Black and Caspian Seas contribute little to precipitation in the region (Evans et al., 2004). On multidecadal timescales, low correlation (>10%) is observed between the inter-annual variability of FC precipitation and the index of the North Atlantic Oscillation (Evans et al., 2004), implying that latitudinal shifts and/or changes in the strength of westerly winds do not directly affect precipitation variability in the study area.

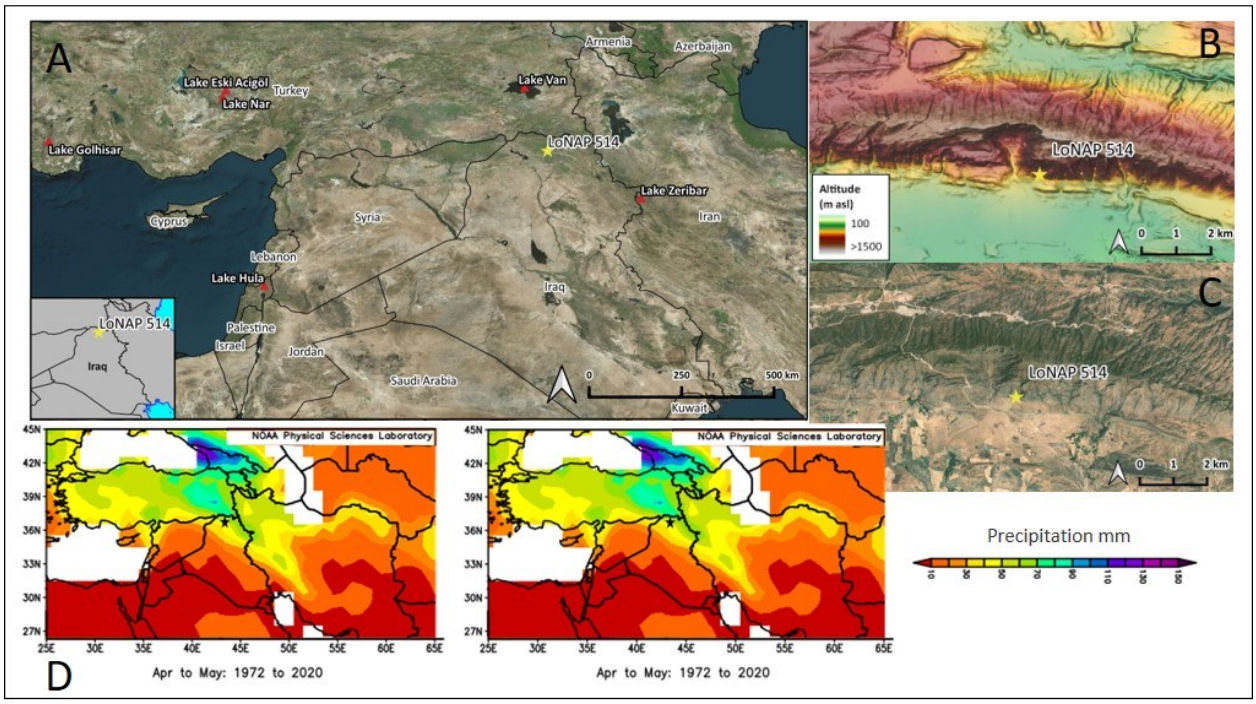


**Figure 1**. (A) The area of the Fertile Crescent indicating the location of the study site (LoNAP 514) and the main regional paleoclimatic archives discussed in the text (elaborated with QGIS 3.16.7 plugin https://nextgis.com/blog/quickmapservices/); (B-C) Digital elevation model (DEM) and satellite imagery of the northern Kurdistan region of Iraq indicating the position of cave LoNAP 514 (yellow star) (DEM free downloaded from https://www.eorc.jaxa.jp/ALOS/en/aw3d30/ and elaborated with QGIS 3.16.7; satellite imagery elaborated with QGIS 3.16.7 plugin https://nextgis.com/blog/quickmapservices/) ; (D) Maps of mean monthly precipitation in winter and spring (downloaded from https://psl.noaa.gov/), the black star is the LoNAP514 site.

## 4.3 Methods

Subsamples for δ13C and δ18O were drilled at a mean resolution of 0.3 mm and analysed using a Precision AP2003 continuous-flow isotope-ratio mass spectrometer at the School of Geography, Earth, and Atmospheric Sciences at the University of Melbourne (UoM) using the method reported in (Hellstrom 2003). Mean analytical uncertainties are 0.07‰ and 0.05‰ for δ18O and δ13C, respectively. U-Th dating was performed at the School of Geography, Earth and Atmospheric Sciences (UoM) on 17 calcite prisms of ~100 mg, employing a multi-collector inductively coupled plasma mass spectrometer (MC-ICP-MS; Nu-Instruments Plasma) and the method presented in (Hellstrom, 2006). The age-depth model (Supplementary Information, Figure S2) has been obtained by Monte Carlo modelling and stratigraphic constrains following (Hellstrom, 2006). Systematic survey work has been carried out within the framework of the LoNAP project, by applying 'extensive methodology', that is via analysis of modern as well as older satellite images followed by direct ground-truthing through direct field walking, details can be found in refs (Conati Barbaro et al., 2019; Iamoni, 2018).

## 4.4 Results and hydroclimatic significance of the record

LoNAP514 was sampled from a flowstone. It is 86 mm thick and composed of compact columnar calcite (Figure S1). The age-depth model (Figure S2) is based on 15 U/Th ages (Table S1) and covers the 11.0±0.3 to 6.6±0.2 ka time span; the mean age uncertainty is 140 yr. Ages are given in thousands of years (ka) with respect to the year of measurement (2020) and reported in BCE when discussed along with the archaeological information. The speleothem stable carbon and oxygen isotope composition ($\delta^{13}C$ and $\delta^{18}O$, Table S2) time series have a decadal resolution. They are significantly positively correlated (r=0.69) and show very similar centennial to multi-centennial patterns (Figure 2 and Supplementary Information text 2). This indicates a common first-order driver for their coupled variability over these time scales. Assuming quasi-isotopic equilibrium calcite precipitation (Supplementary Information, text 3) and given minimal early-mid Holocene temperature changes inside the cave, the LoNAP514 $\delta^{18}O$ is a proxy for drip-water $\delta^{18}O$, which reflects local meteoric precipitation $\delta^{18}O$ ($\delta^{18}Op$). $\delta^{18}Op$ results from changes in moisture source location and isotopic composition, condensation temperature and seasonality (Baker et al., 2019) (Supplementary information text-4 and Figure S3). Here, we interpret centennial-scale variations in the δ18O as primarily recording rainfall fluctuations, with lower/higher $\delta^{18}O$ ratios occurring during wetter/drier periods respectively (Supplementary information text-4). This interpretation is consistent with speleothem $\delta^{18}O$ records from central to eastern Mediterranean, the Middle East, and the Arabian Peninsula (e.g., Burns et al., 2001; Al-Manmi et al., 2019). For LoNAP514, it is also supported by the positive covariance with the δ13C time series. In fact, the range of $\delta^{13}C$ values (-9.80‰ to -4.81‰) is indicative of a prevalent input of organic, $^{13}C$-depleted $CO_2$ from the overlying soil, and is typical of a predominantly C3 vegetation, which was likely present in the cave catchment over the period of LoNAP514 deposition (Supplementary Information text-5). In these settings, $\delta^{13}C$ variations arise from fluctuating soil biological activity, in turn related to temperature and precipitation (Fohlmeister et al., 2020), with the latter likely predominating for LoNAP514 due to relatively stable Holocene temperatures. Higher rainfall amounts (lower $\delta^{18}Op$) foster soil metabolism and vegetation development, leading to lower $\delta^{13}C$. Under drier conditions (higher $\delta^{18}Op$), the biogenic $CO_2$ supply is reduced, causing higher $\delta^{13}C$. The hydrological sensitivity of both $\delta^{18}O$ and $\delta^{13}C$ is further increased during drier periods by evaporation at the topsoil, in the epikarst, and degassing at the site of stalagmite deposition. These processes cause preferential loss of lighter C and O isotopes, leading to stronger covariation and increased isotope ratios in speleothem calcite (Flohr et al., 2017). This is particularly apparent in our record between 9.0 and 8.4 ka and between 7.6 and 7.0 ka, where the isotope series show highest values and the lowest difference between

normalized values (Figure 2). The largest discrepancy between the two series is observed between 10.8 and 9.4 ka, corresponding to the most negative and least variable $\delta^{18}O$ values. This interval is near-synchronous with depleted $\delta^{18}O$ values observed in the planktonic foraminifera (*Globigerinoides ruber*) record from marine cores LC21 and SL21 from the central Aegean Sea (Figure S5), which reflect the inflow of fresh (isotopically depleted) surface waters from the Nile River due to an enhanced African monsoon recharging the upper Nile catchment (Marino et al.,2009). Such freshwater influx corresponds to a calculated decrease of ~1.3‰ in local surface seawater $\delta^{18}O$ (Marino et al.,2009). Given that the Eastern Mediterranean is one of the main sources of precipitation for our study area (Evans et al., 2004; Mohammadzadeh et al., 2020), this depletion was likely transmitted to our oxygen record via the source effect (Supplementary information, text 4). The latter likely buffered centennial-scale variability due to the rainfall amount effect over this interval and might result in an internal variability (or absence of it) that is not linked to the amount of precipitation. A prevailing influence of the source effect over our oxygen record in some particular intervals can be also inferred by the comparison between with the record of Fe/Ca from core MS27PT located at the Nile mouth (Revel et al., 2010), that represent a direct proxy for fluvial terrigenous input related to increased monsoonal rain over the upper Nile catchment (Figure S5). Enhanced Nile input is indeed apparent before 9.4 ka, and centennial-scale terrigenous peaks correspond to negative spikes in the $\delta^{18}O$ record (e.g., at 8.4 ka, 8.1 ka, Figure S5), but have no strict correspondence in the carbon record (Figure S5). Therefore, we consider the $\delta^{13}C$ as a more robust and direct proxy for moisture changes at the cave site. The regional significance of the LoNAP514 $\delta^{13}C$ hydroclimatic record is attested by a comparison with lacustrine carbonate $\delta^{18}O$ changes from the FC and Anatolia (Stiller & Hutchinson, 1980; Dean et al., 2015) (Figure 3). Eastern Mediterranean/Anatolian lacustrine $\delta^{18}O$ is mostly driven by the precipitation/evaporation ratio and, similarly to speleothems, lower/higher $\delta^{18}O$ ratios usually indicate higher/lower precipitation (Roberts et al., 2008). Within the combined uncertainties, and accounting for diverse time-resolution, a very similar multi-centennial pattern is apparent, especially within the 10.0–8.0 ka interval (Figure 3). Between 9.7±0.2 and 9.0±0.1 ka, all records coherently express wetter conditions. This is followed by an abrupt reduction of precipitation between 9.0 and 8.5±0.1 ka, and by a wetter interval between 8.5 and 8.0±0.2 ka (Figure 3). The high temporal resolution of the LoNAP514 $\delta^{13}C$ also reveals superimposed, lower-amplitude, centennial-scale moisture fluctuations. Reduced precipitation occurred between 9.3±0.2 ka and 9.1±0.1 ka, at 8.9±0.1 ka, between 8.1±0.2 ka and 7.9±0.2 ka, and at 7.1±0.2 ka. Considering the associated age uncertainties, the first and the third of these events are consistent, in terms of both duration and timing, with the 9.3 and 8.2 ka climatic anomalies described above. However, they are not particularly prominent (Figure 3). This suggests that the downstream atmospheric changes related to these RCCs

had only a limited impact on local precipitation, and that there are other drivers for the observed climatic variability.

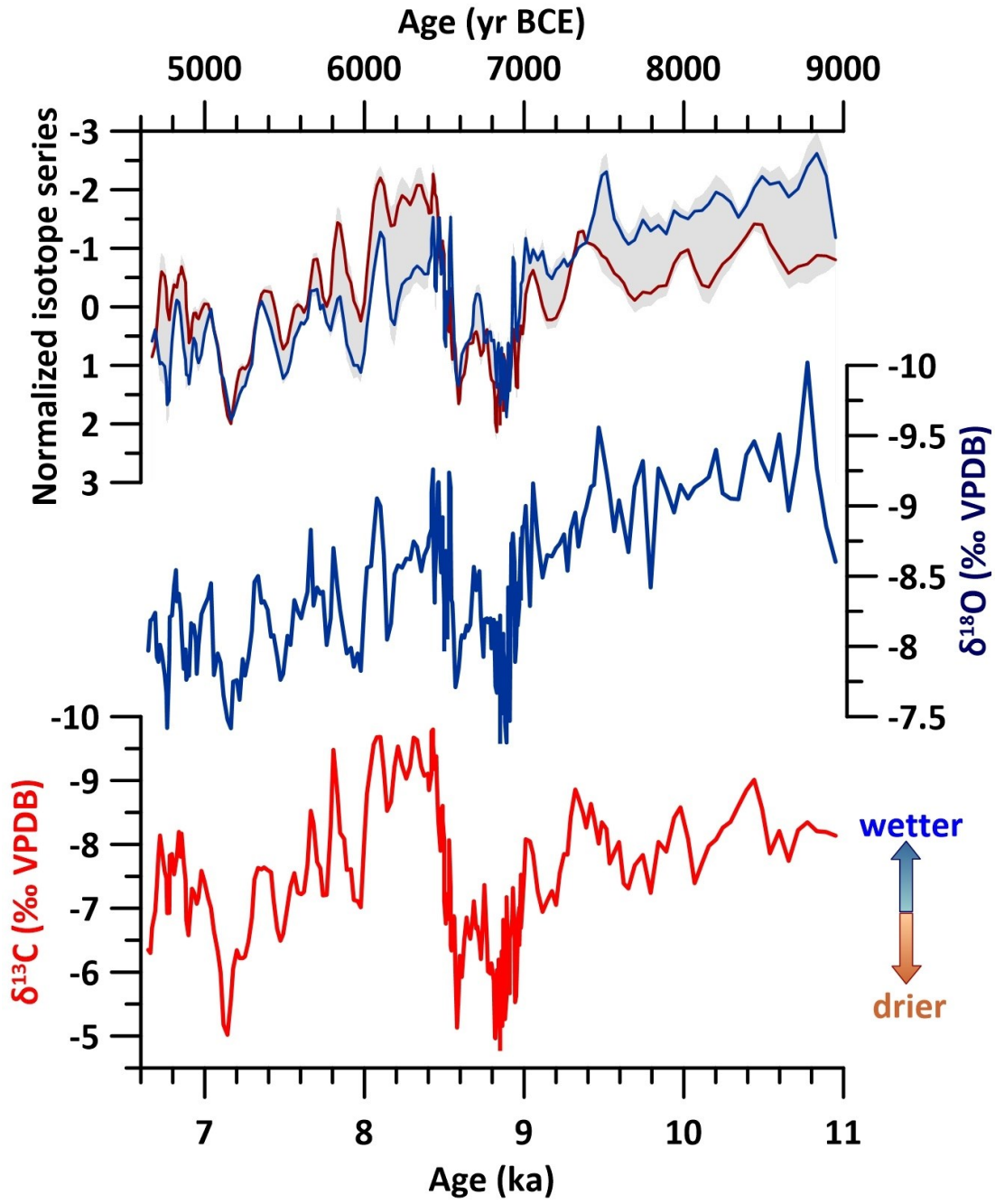


**Figure 2**. Stable carbon ($\delta^{13}C$, red) and oxygen ($\delta^{18}O$, blue) isotope series for flowstone LoNAP514; top: 3 points-smoothed and normalized isotope time series (SOM text), the grey band represents the standard deviation between the normalized series (see Supplementary Information).

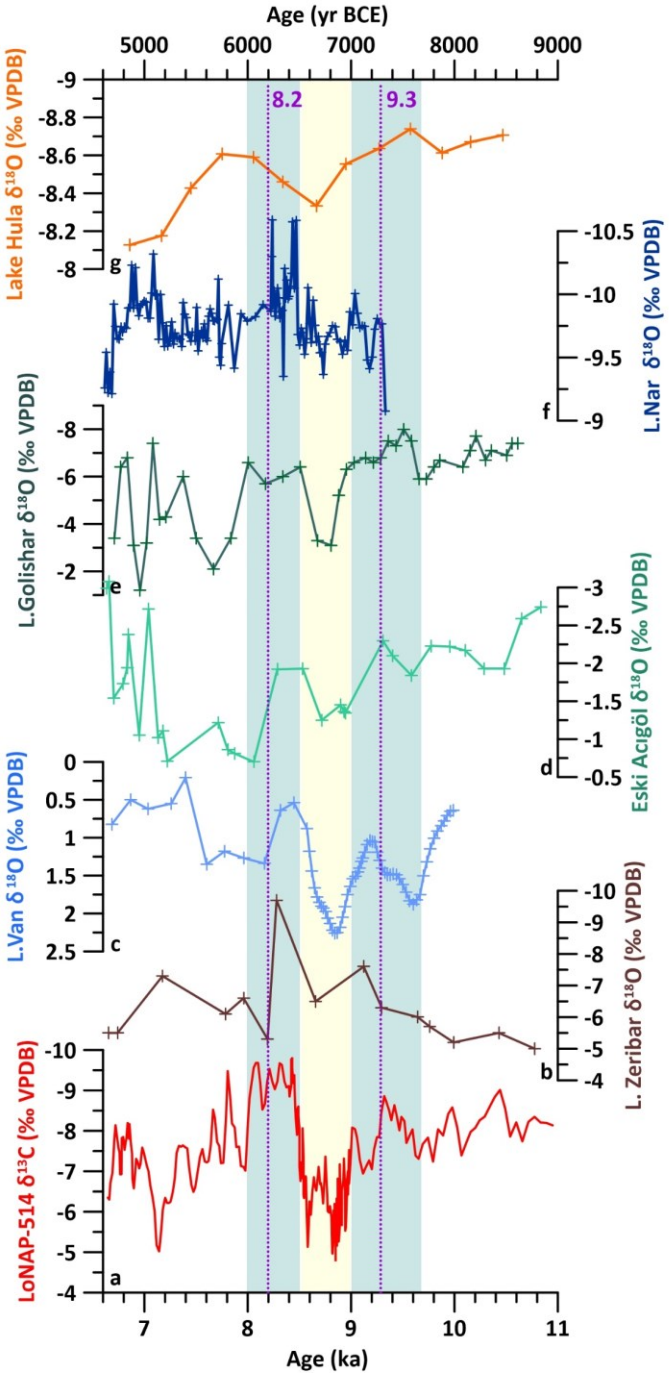


**Figure 3**. Regional comparison among a) LoNAP514 $\delta^{13}C$ (this study) and $\delta^{18}O$ records from b) Lake Zeribar (Dean et al., 2015), c) Lake Van (Mayewski et al., 1994), d) Lake Eski Acigöl (Roberts et al.,2008), e) Lake Golishar ( Mayewski et al., 1997), f) Nar Gölü (Saaroni et al.,1996), g) Lake Hula (Wastwood et al.,2007). Blue/yellow shaded areas highlight the common main wetter/drier intervals; dotted lines indicate the 9.3 and 8.2 ka events.

## 4.5 Teleconnections and mechanisms of hydroclimate variability

Despite differences in the long-term (millennial) trends, the LoNAP514 precipitation record closely mimics centennial-scale fluctuations in the non-sea-salt potassium (nssK+) record from the Greenland GISP2 ice core (Mayewsky et al., 1994), with higher precipitation at the cave site

corresponding to increases in nssK+ content (Figure 4). Such increases have been correlated to enhanced dust transport from Asia, related to an intensified Siberian High (SH) in winter/spring (Mayewsky et al., 1994). This implies a strong teleconnection between centennial-scale fluctuations in the intensity of the SH and precipitation in the northern FC during the early to mid-Holocene. Noteworthy, the similarity is more expressed between ca. 10 and 8 ka, where the SH is at its strongest (Figure 4). Currently, seasonal, and inter-annual rainfall variability in the FC is explained mostly by changes in the intensity, frequency, and orientation of eastern Mediterranean storm tracks and by changes in the supply of water vapor from southern sources (Evans et al., 2004). Thus, to understand the mechanisms modulating precipitation patterns in our record, we need to consider the influence of the SH on both Mediterranean and southern synoptic conditions. Current observations and modelling show that a strengthening of the SH increases the frequency and intensity of cold northerly air outbreaks that are channelled through gaps in the mountain ranges along the north-eastern Mediterranean borderlands (Saaroni et al., 1996). These northerly fluxes deliver cold/dry air masses to the warm/moist Aegean Sea sector, promoting intense evaporation and creating or intensifying local cyclogenesis. This causes extreme precipitation events in the Levant, exceptional snowfall around the Aegean region, and flash floods in the Middle East (Saaroni et al.,1996). Cluster analyses of eastern Mediterranean cyclones also shows that the intensification of the SH influences storm-track trajectories. In particular, a blocking configuration over central Asia and eastern Europe favours a direct eastward route toward southern Anatolia and the northern FC, instead of the usual north-eastward trajectories to the north of the Black Sea (Labban et al., 2021). Looking at the paleo-record, the centennial to multi-centennial influence of the SH-induced cold outbreaks on Eastern Mediterranean conditions can be demonstrated by the consistent timing between increases in the GISP nsK+ content and sea-surface temperature (SST) cooling events in the Aegean Sea (Marino et al., 2009; Rohling et al., 2019). Specifically, changes in the abundance of the cold-water dinocyst *Spiniferites elongatus* from core SL21 have been used to identify relative winter SST changes through the early to middle Holocene in the central Aegean (Marino et al., 2009). The LoNAP514 precipitation record shows strong similarities with the S. elongatus record, with colder winter conditions in the Aegean corresponding to higher precipitation (Figure 4). Rohling et al., (2019) modelled the effect of northerly outbreaks in the Aegean on the local hydroclimatic cycle and found that their increased frequency and intensity cause strong evaporation in the eastern Aegean, enhancing the atmospheric moisture content over the sea. When these moist air masses subsequently make landfall and are cooled and/or uplifted, their relative humidity increases and precipitation may develop, leading to cooler and wetter conditions over the Levant. Despite our site being located further away from the Mediterranean coast than the Levant, the similarity with the Aegean record

suggests that a critical component for the increase in precipitation in the northern FC during intervals of enhanced SH is the effect of cold northerly outbreaks in promoting eastern Mediterranean evaporation and cyclogenesis. In particular, an intensified cyclonic circulation increases the advection of moist air towards the north/northeast, whereas the westward expansion of the SH causes a southward shift in storm tracks (Labban et al., 2021, see also sketch on Figure 5). These combined effects likely increased the amount of winter precipitation in the northern FC during early Holocene intervals of intensified SH, especially between 9.7 and 9.0 ka and between 8.5 and 8.0 ka. Regarding the influence of the SH on southerly vapor supply and synoptic conditions, it has been found that the increase of SH strength is one of the dynamic factors generating Active Red Sea Troughs (ARST) Krichak et al., 2021). ARST originates from the Sudan Low, which is a part of the large-scale subtropical/equatorial low-pressure thermal system known as the intertropical convergence zone (ITCZ). ARST development results from the interaction between a lower-tropospheric inflow of warm, moist air of tropical origin extending northward from the southern Red Sea toward the eastern Mediterranean and the Middle East, and a mid-tropospheric southward inflow of cold and dry air from Eurasian mid-latitudes (Krichak et al., 2021). Such conditions are associated with unstable stratification and a high concentration of vapor sourced from the Persian Gulf/Arabian Sea reaching the FC. This favours the development of highly energetic mesoscale convective systems, which can produce intense precipitation and flooding, especially at the fringe of high-relief regions, such as along the SW Zagros flanks (De Vries et al., 2013). Regional climate models simulate convective precipitation maxima in transitional months, especially in April-May, when enough energy is present to trigger local convection, but before the summer season, when high pressure related to the descending branch of the Hadley Cell begins to dominate the area (Evans et al., 2004). The position of the Hadley Cell is directly related to the seasonal movement of the ITCZ, that also determines the onset, duration, and termination of the Indian summer monsoon (ISM) (Gadgil, 2003). In the last 150 years, the date of ISM onset has varied between May 11 (1918) and June 18 (1972) (Zhou et al.,2019). ISM onset is modulated by large-scale forcing, such as the land-sea thermal contrast between the Eurasian landmass and the Indian Ocean. A delayed onset is usually associated with colder spring conditions over the Tibetan Plateau and negative SST anomalies in the tropical and subtropical oceans during the season prior to the monsoon onset (i.e., March–May) (Gao et al., 2014; Senan et al., 2016). Winter-spring temperatures over central and East Asia are negatively correlated with the strength of the SH (Gong & Ho, 2002; Riaz et al., 2018), and a relationship have been found between a stronger SH and negative SST anomalies in the Indian Ocean (Hasanean et al., 2013). Furthermore, at present, the intensity of the SH and the strength of the Hadley circulation exhibit a significant negative correlation both for their inter-annual variability and for their secular trend (Hasanean et al., 2013).

Therefore, we propose that, across the 9.7–9.0 and the 8.5–8.0 ka intervals, the strengthening of the SH was responsible for increased evaporation and advection from southerly source, and for increased convective instability related to the formation of a more frequent/stronger ARST (see sketch on Figure 5). At the same time, a stronger SH also caused a delayed onset of the ISM due to negative temperature anomalies that persisted longer in spring over the Eurasian land masses and in the sub-tropical oceans. The two combined effects boosted the occurrence of convective precipitation, and allowed their development to persist well within May, causing a net increase in spring precipitation over the FC. After 8.0 yr. BP, the Northern Hemisphere ice sheets were reduced and the SH weakened (Mayewski et al., 2004), leading to reduced convective instability across the Middle East, and to warmer spring conditions across Eurasia, preventing the delayed onset of the ISM, reducing the length of the wet season in the FC and also leading to a divergence between the long-term trends of the SH and of precipitation at our site (Figure. 4).

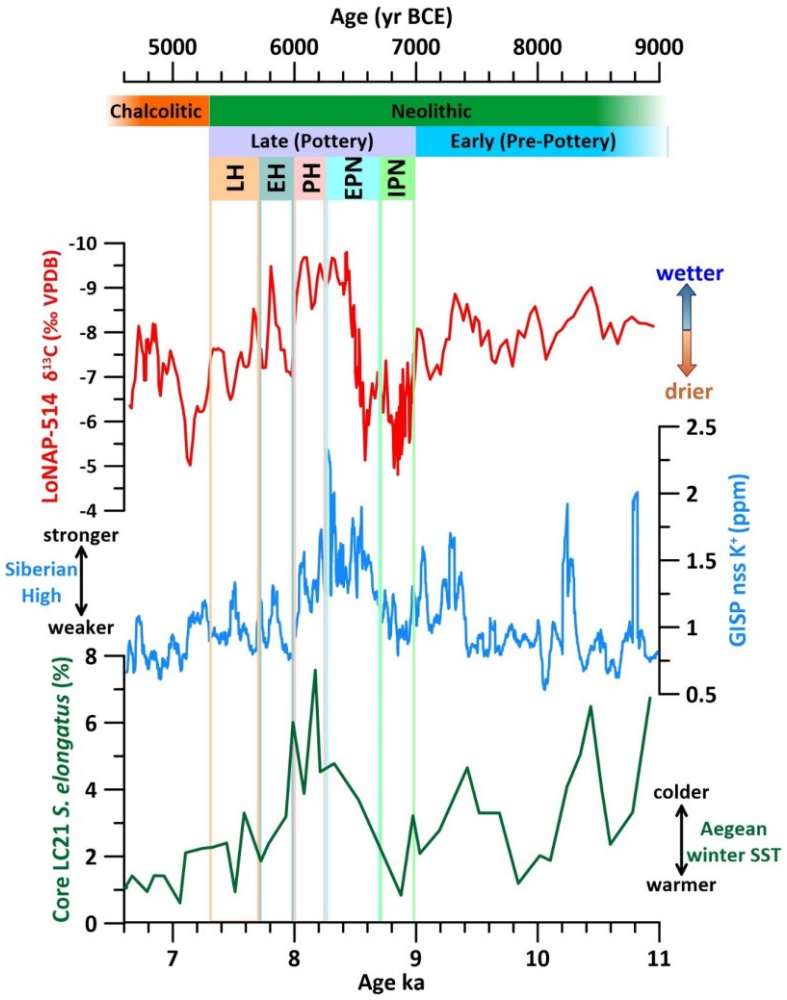


**Figure 4**. From bottom: Percentage of cold dynocist *Spiniferites elongatus* from the Aegean core SL2 (Wick et al., 2003) 15 points-smoothed nssK+ from Greenland ice core GISP2 (Krichak et al.,2012); $\delta^{13}C$ (this study); Major cultural phases identified in the northern FC (Matthews et al., 2019) (IPN: Initial Pottery Neolithic; EPN: Early Pottery Neolithic; PH: Pre-Halaf; EH: Early Halaf; LH: Late Halaf).

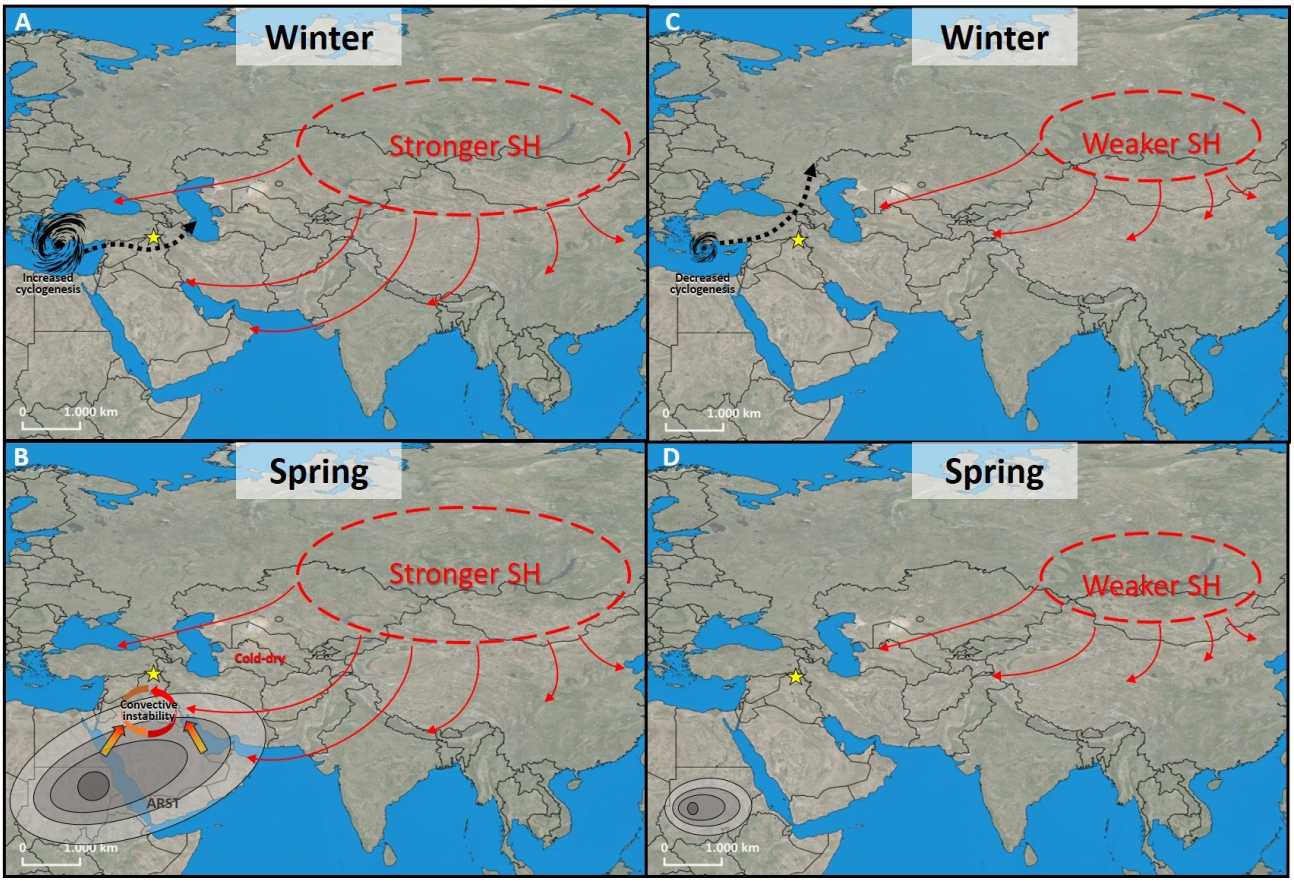


**Figure 5**: Sketch of the proposed mechanisms influencing precipitation in Northern Iraq. For stronger (A-B) and weaker (C-D) Siberian High on winter (A-C) and spring (B-D) conditions. The star is the LoNAP514 cave site. Red arrows represent the influx of cold-dry air from the SH; The black dotted arrows in panels A-C represent the trajectories of the Eastern Mediterranean storm tracks; the thick red-yellow arrows in panel B represent the low-tropospheric southerly influx of warm and moist air. ARST=Active Red Sea Trough (contracted to Sudan Low in panel; See text for explanation). All maps are elaborated with QGIS 3.16.7 plugin https://nextgis.com/blog/quickmapservices/. From bottom: Percentage of cold dynocist *Spiniferites elongatus* from the Aegean core SL21 15 points-smoothed nssK+ from Greenland ice core GISP2 ; $\delta^{13}C$ (this study); Major cultural phases identified in the northern FC (IPN: Initial Pottery Neolithic; EPN: Early Pottery Neolithic; PH: Pre-Halaf; EH: Early Halaf; LH: Late Halaf).

## 4.6 Archaeological implications and final highlight

In the last decade, a wealth of data from surveys and excavations in the northern FC have deepened the knowledge on regional Neolithic and early Chalcolithic cultural traits and settlement patterns (i.e., size, distribution, and duration of occupation), and of their interrelationships with landscape and environmental resources (Iamoni, 2018; Conati Barbaro et al., 2019; Matthews et al., 2019). Updated summaries of the latest regional evidence anchored to a comprehensive radiocarbon-dated framework are now available (Matthews et al., 2019; Nieuwenhuyse & Akkermans, 2019) providing a detailed regional archaeological background that allow a robust comparison with the hydroclimatic variability revealed by the LoNAP514 record. Furthermore, systematic archaeological survey has been

performed by the LoNAP project (see acknowledgement) specifically in the cave region (i.e., the Zagros foothills and the Tigris River tributaries; Figure 6), leading to the identification of a number of sites, that were attributed to the different cultural phases within the PN mostly through analyses of pottery types. The LoNAP survey data for the PPN are instead scarce, mostly because PPN sites are challenging to locate, either because they can be covered by later levels at tell sites or because their conservation is hampered by natural or anthropogenic erosion. Thus, they are not discussed here. Thanks to this new evidence, inferences can be made regarding relationships between settlements and the key factor for their survival by way of water resources, whose availability is linked to precipitation patterns. During the latest stage of the Early (Pre-Pottery) Neolithic (PPN), populations in the northern FC took full advantage of a rich environment, pursuing a flexible mix of subsistence strategies. These included hunting and foraging of wild game and plants, as well as herding a small number of species, especially goats (Zeder & Hesse, 2000), and cultivating a range of pulse and cereal crops in fields on the surrounding plains (Matthews et al., 2019). Regionally, sites are widespread in both the plains and the foothills; they are usually small (less than 1 ha) and often appear to be only seasonally occupied (Matthews et al., 2019). Over this period, the LoNAP514 record shows relatively wet conditions (Figure 6) that would have allowed the first forms of rain-fed and/or décrue cultivation during the rainy season (Lancellotti et al., 2019). At regional scale, the initial phase of the Pottery Neolithic (IPN, 9.0–8.7 ka; 7000–6700 BCE) (Rohling et al., 2019 and references therein) witnessed a contraction of the inhabited sites, with most of the settlements located in the upper part of the valleys, and above of the present-day 220 mm isohyet. All these sites fall close to major and perennial watercourses (Iamoni, 2018). This contraction corresponds precisely to the marked reduction in precipitation apparent from the LoNAP514 record (Figure 4), suggesting that climatic factors hampered the expansion of settlements in the IPN and influenced their location. The early Pottery Neolithic (EPN, 8.7–8.3 ka, 6700 to 6250 BCE) (Nieuwenhuyse & Akkermans, 2019) saw the full uptake of pottery techniques. During the EPN, settlements were remarkably short-lived and had a highly mobile nature, and the number of settlements increased, thus suggesting a noticeable demographic growth (Nieuwenhuyse & Akkermans, 2019). A gradual spread from the upper part of the valleys to more down valley locations is apparent. Specifically in the study area, survey data shows that the EPN is marked by the first systematic exploitation of the lowlands along main streams (Figure 6A). Sites still appear to cluster around watercourses, either permanent or seasonally active, whereas no EPN sites have been found on the semi-arid steppe separating them. In particular, a detailed analysis of settlement distribution shows that they were located mostly within 100–200 m of a watercourse (Iamoni, 2018). Over this period, the LoNAP514 record shows the transition from drier conditions (up to 8.5 ka, 6500 BCE) towards a marked increase in precipitation characterized,

according to our interpretation, by a longer rainy season with a potential increase in extreme convective events. This scenario fits well with the regional archaeological evidence (Iizuka, & Terry, 2021; Palmisano et al., 2021): in the initial phase of the EPN, the adoption of more durable pottery containers likely facilitated the collection of surpluses over longer times, giving a net advantage under drier conditions and allowing the inferred demographic rise. Subsequently, wetter climate conditions supported the growth and the new spreading of human groups (Palmisano et al., 2021) to locations that were abandoned during the IPN, and along (now) seasonal streams, that at the time were likely active for most of the year. However, due to the increased frequency of extreme precipitation events, sites were located at a certain distance from the rivers, preventing the risk of settlement flooding but close enough to exploit inundated land for seasonal cultivation (Iamoni, 2018). The period between 8.3 and 7.3 ka corresponds to the Pre-Halaf (PH; 6250–6000 BCE) and (Early to Later) Halaf cultural phases (EH, 6000–5700 BCE; LH 5700–5300, Figure 4) (Nieuwenhuyse & Akkermans, 2019). During the PH at regional scale, site distribution still resembled that of the preceding EPN, with small sites (1-2 ha) concentrated along rivers and streams (Nieuwenhuyse & Akkermans, 2019). Further, the LoNAP514 record does not highlight significant changes leading up to 8.0 ka. Subsequently, with the onset of the Halaf phase at 6000 BCE (i.e., from 8 ka) regional synthesis shows settlements expansion, and dispersion of some communities into the steppe. This pattern is evident also from survey data in the study region, with Halaf settlements' distribution suggesting the progressive colonization of inter-river areas (Figure 6B). This colonization is part of a multifaceted package of economic, technological, and cultural innovations and adaptations (e.g., full adoption of administrative systems and an intensified reliance on secondary products) that profoundly transformed the Late Neolithic societies and increased their complexity (Nieuwenhuyse & Akkermans, 2019). Throughout the EH, people appear to move around the landscape dynamically, founding new settlements, relocating to others, and abandoning them easily (Nieuwenhuyse & Akkermans, 2019; Cohen et al.,2001). Furthermore, these communities also adopted flexible subsistence strategies relying on a combination of agriculture and herding a range of domesticated plants and animals, but also on hunting and foraging of wild species. Likely, this residential and subsistence flexibility made the best of challenging environments, such as those of the semi-arid steppe (Nieuwenhuyse & Akkermans, 2019). The subsequent LH witnessed a surge in the number of sites, and their continuous spreading into regions far from water resources. Settlement size and internal complexity appear to increase towards the end of the Halaf phase, with the largest sites (up to at least 10 ha) located near perennial water courses (Nieuwenhuyse & Akkermans, 2019; Iamoni,2018). However, recent interpretations that take account of the dynamism of frequent relocation apparent for the northern FC suggest that the Halafian "mega-site" can be better explained

as a small-scale settlement shifting over favourable spots in the local landscape across several generations (Nieuwenhuyse & Akkermans, 2019). According to our record, the EH and LH phases occurred in the context of the change in precipitation amount and style towards more arid climatic conditions between 8.0 and 7.7 ka (6000 to 5700 BCE), and in the subsequent highly variable period up to 7.3 ka (5300 BCE), respectively (Figure 4). This coincidence suggests that many of the transformations observed in the archaeological record across this period may have been expedited by climatic stress but were mostly triggered by technological and cultural innovations. A dynamic response to changing background climatic conditions is even more apparent in the subsequent Early Chalcolithic phase, from ca 5300 BCE (ca 7.3 ka): in this time span, villages evolved towards increased complexity; the same applies to their social organization. Furthermore, in the whole FC, the total number of sites appears to increase markedly during the Early Chalcolithic (Palmisano et al., 2019). Interestingly, the shift from the late Neolithic to the Chalcolithic, marked in our record by a quite drastic precipitation reduction (Figure 4), appears also characterized by a change in the use of water resources, with many sites located close to perennial springs and rivers in the Zagros Mountain piedmont zone. This regional trend is confirmed by local survey data, that also highlight the increase in settlement number in the Chalcolithic and a change in the strategy of exploitation of permanent water resources (Figure 6C). This suggests that the climatic deterioration fostered the use of previously poorly exploited resources well before the onset of irrigated cultivation in the Bronze Age. In summary, the integration of high-resolution climate records with robust, contextualised archaeological data is a crucial strategy for better understanding both the climatic variability itself and its potential societal consequences (Izdebski et al., 2016). Our inference regarding the influence of the SH on precipitation amount and seasonality in the FC brings clarity to a rich collection of climate proxy records in the region that indicate significant variability but lack a clear temporal coherency with - or a univocal expression of - the major Early Holocene RCCs (the 9.3 and the 8.2 ka events). In fact, our record does not support a direct influence of Early Holocene RCCs on the process of Neolithization and its cultural dispersal. Although it is still debated whether Neolithic cultural changes were forced directly by climatic variability, we show robust chronological agreement between changes in precipitation pattern and the alternation of local cultural phases, suggesting that hydroclimate variability influenced the way in which Neolithic population exploited the surrounding environment. This is particularly significant in terms of settlement strategies and use of water resources. In this view, climate variability, leading to increased stress or amelioration of background environmental conditions, appears to accelerate and force existing cultural and subsistence dynamics, which were however not directly attributed to the climatic change itself (Roberts et al., 2018; Lancelotti et al., 2019). Climate variability thus acts as a stimulus that continuously interacted with

technological and cultural adaptations of complex societies (Rosen & Rivera-Collazo, 2012), fostering the evolution of new and multifaceted adaptive strategies that progressively increased the resilience of ancient populations and modified the way they interacted with their environment.

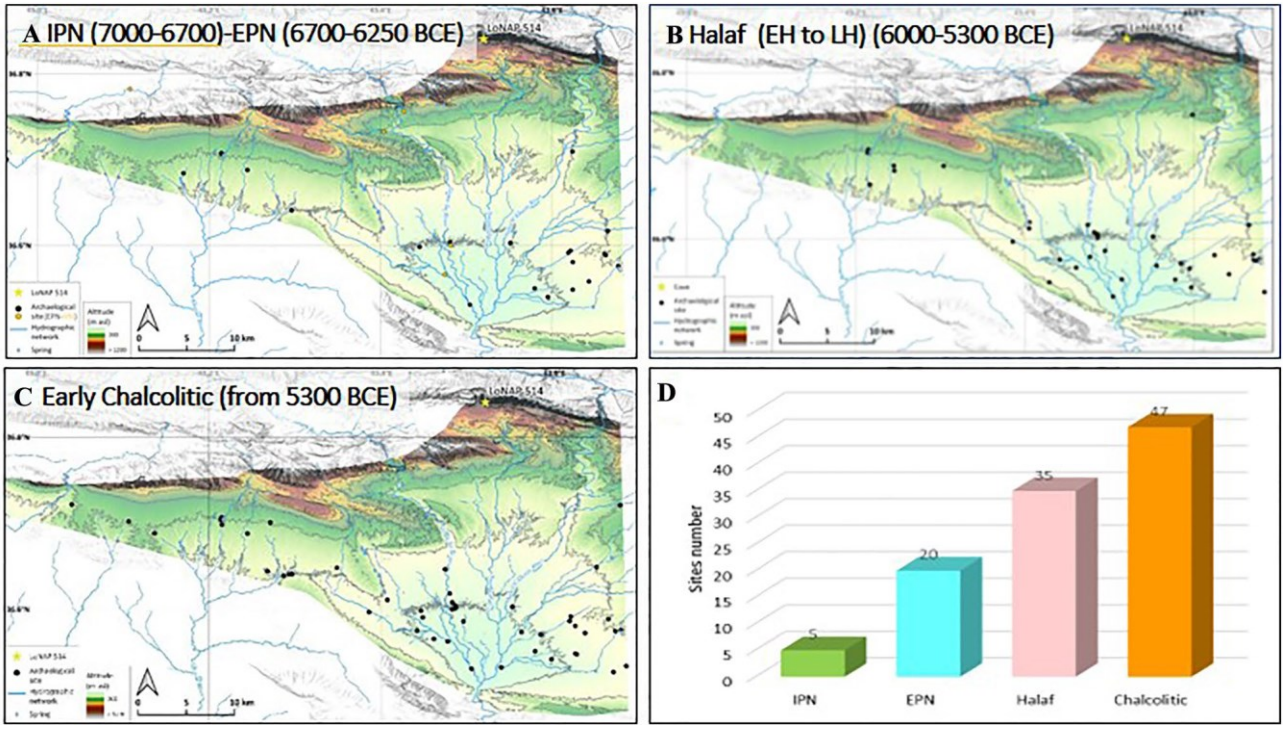


**Figure 6.** A-C) Maps illustrating the distribution of archaeological sites identified by LoNAP survey and their relationship with water resources. The different panels cover the different cultural phases discussed in the text. (Basemaps are derived from DEM free downloaded from https://www.eorc.jaxa.jp/ALOS/en/aw3d30/ and elaborated with QGIS 3.16.7). D) graph showing the number of sites for the different periods.

## 4.7 Supplementary material

### 4.7.1 Geological and geomorphological background

Specimen LoNAP514 was retrieved at ~15 m from the entrance of a shallow cave (36°50'24.87"N 43°31'2.95"E) located in the part of the Zagros Mountains traversing the governorate of Dohuk, in the northern Kurdistan Region of Iraq. The region is part of the Zagros-Fold Thrust Belt (ZFTB) formed by continental collision - active since the Early Miocene - between the Arabian and Eurasia plates (Dewey et al., 1973; Dercourt et al., 1986; Csontos et al., 2012; Mouthereau et al., 2012; Fouad, 2015). Deformation of the Zagros Mountains has propagated over the NE margin of the Arabian Plate towards the Mesopotamian Foreland Basin and the Persian Gulf (Blanc et al., 2003; Vergés et al., 2011; Csontos et al., 2012). In the study area, the ZFTB is organized into four different zones, moving from the inner part of the orogeny (Imbricated and High Fold zones) to its foreland (Foothills zone

and Mesopotamian Foreland Basin) (Berberian, 1995; Jassim and Goff, 2006; Frizon de Lamotte et al., 2011; Fouad, 2015). The deformation created a series of anticline folds that represent the main structural features of the local landscape (Forti et al., 2021). In the Dohuk area, anticlines are W–E trending, while in the eastern and southern sector of the mountain belt they are NW–SE oriented. Geological strata folded and deformed in this section of the ZFTB include Upper Triassic/Lower Cretaceous to Pliocene units. Lithologically, the local bedrock includes Ordovician sandstones and Carboniferous-Permian limestones and shale, Upper Triassic to Upper Cretaceous reef limestone and dolomitic limestone with interbedded marls and shales, Eocene limestone (Sissakian, 2014; Zebari et al., 2019), Upper Paleocene to Lower Miocene limestone, dolostone and sandstone, and Plio-Pleistocene conglomerates. From the geomorphological point of view, the anticlines are widely spaced, and the synclines create swales and plains filled by various Quaternary sediments, including alluvial fans and floodplain deposits, which are occasionally deformed by recent tectonic activity. Tectonic uplift and exhumation rate of the anticlinal ridges and syncline troughs promoted the formation of different physiographic units, resulting in a complex landscape (Forti et al., 2021). The large plain opening at the foothills of the anticlines is crossed by the Tigris River and its many left-bank tributaries, whose watersheds extend along the Zagros Mountains. Today, most of the streams show seasonal-to-ephemeral activity, and only the Tigris and its major tributaries are permanent. In the rainy season, the discharge of streams increases and flooding along the plains is common.

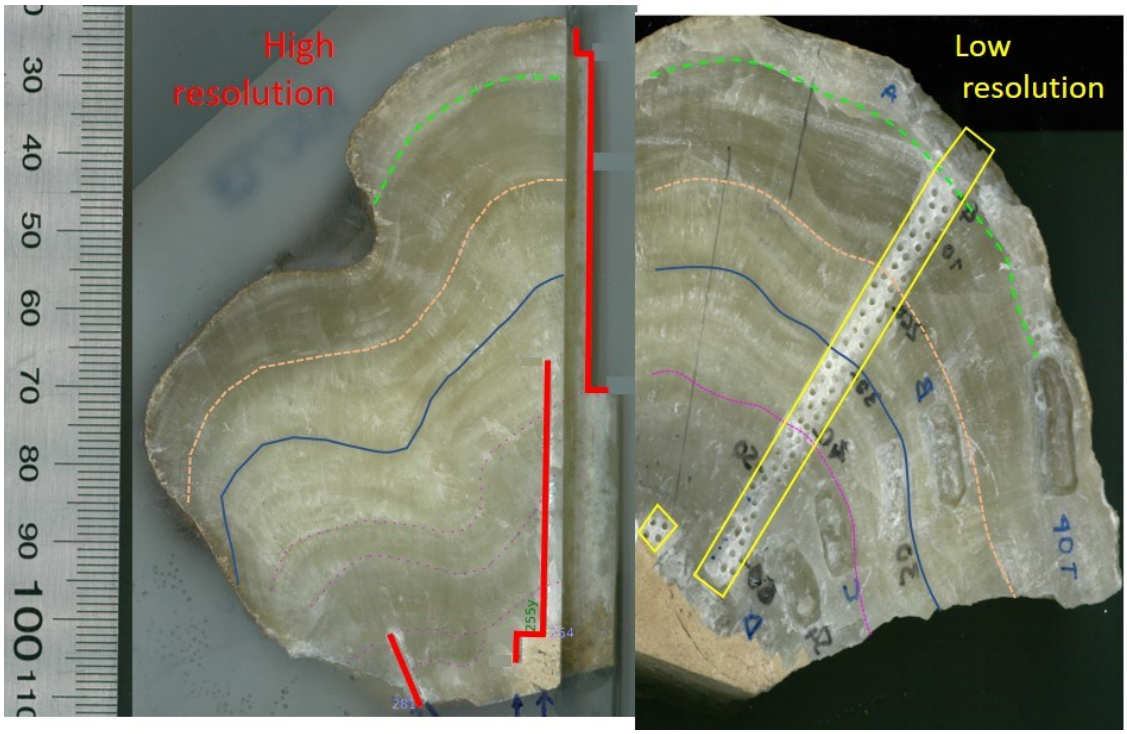


**Figure S1**. The sampled pieces of flowstone KR713 reporting the stable isotope sampling tracks (low in yellow and high resolution in red). The low-resolution sampling was done manually with a 1 mm drill-bit. The high-resolution sampling was performed with a milling machine with an average resolution of 0.3 mm. Samples for dating were cut

from the step resulting from the high-resolution sampling. Coloured thin lines represent identified laminations used to match the high- and low-resolution isotope series.

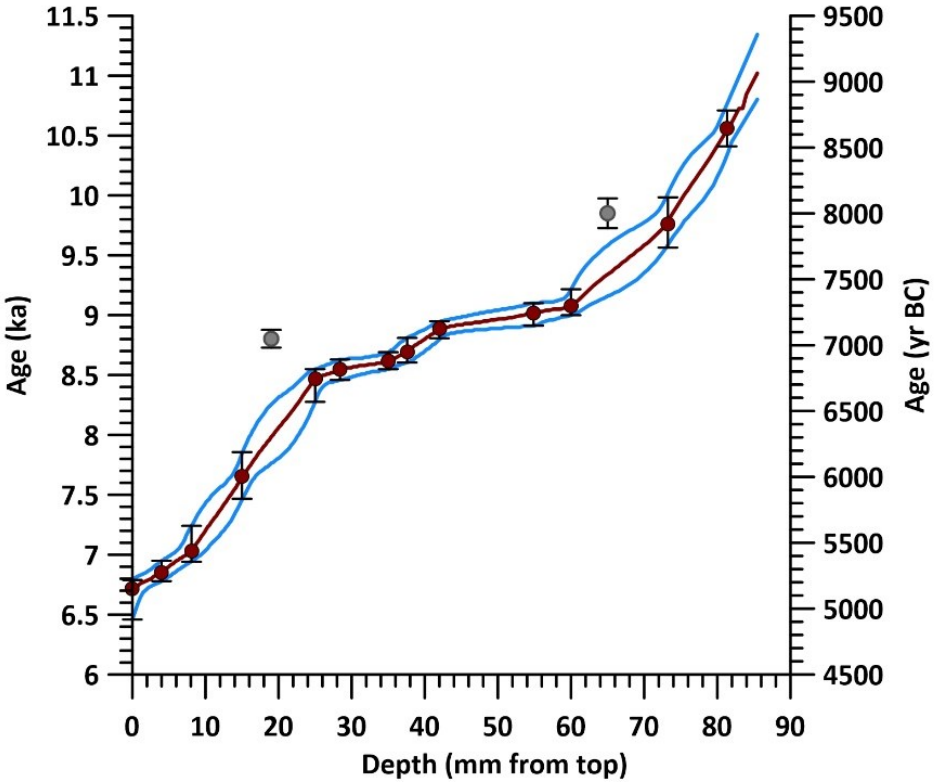


**Figure S2**. Age-depth model for flowstone KR713, in grey ages rejected as outliers, The Age depth model was constructed following Drysdale et al., 2005 and Hellstrom et al., 2006.

| Sample | $^{238}U$ (ppb) | Depth (mm) | $^{230}Th/^{238}U$ | $^{234}U/^{238}U$ | Age unc (ka) | 2se (ka) | $^{232}Th/^{238}U$ | $^{230}Th/^{232}Th$ | **Age (ka)** | **2se (ka)** |
|---|---|---|---|---|---|---|---|---|---|---|
| K713-A | 246 | 0 | 0.0627 | 1.0483 | 6.722 | 0.046 | 0.000035 | 1769.6 | **6.72** | **0.046** |
| KR713 4 | 258 | 4.00 | 0.0641 | 1.0482 | 6.878 | 0.068 | 0.000134 | 478.6 | **6.86** | **0.071** |
| K713-top | 238 | 8.10 | 0.0657 | 1.0503 | 7.040 | 0.046 | 0.000039 | 1684.9 | **7.03** | **0.046** |
| K713-F | 224 | 15 | 0.0716 | 1.0562 | 7.646 | 0.081 | 0.000036 | 1973.3 | **7.64** | **0.081** |
| K713-G | 238 | 25 | 0.0799 | 1.0625 | 8.518 | 0.073 | 0.000266 | 300.0 | **8.48** | **0.084** |
| KR713 B | 240 | 28.40 | 0.0807 | 1.0647 | 8.584 | 0.114 | 0.000272 | 296.9 | **8.54** | **0.123** |
| KR713 35 | 236 | 35.00 | 0.0811 | 1.0646 | 8.634 | 0.077 | 0.000128 | 635.9 | **8.61** | **0.081** |
| KR713 30 | 255 | 37.59 | 0.0819 | 1.0671 | 8.704 | 0.111 | 0.000083 | 982.8 | **8.69** | **0.113** |
| KR713 42 | 244 | 42.00 | 0.0839 | 1.0685 | 8.910 | 0.056 | 0.000143 | 588.2 | **8.89** | **0.061** |
| KR713 C | 254 | 54.87 | 0.0859 | 1.0742 | 9.079 | 0.119 | 0.000302 | 284.2 | **9.03** | **0.126** |
| K713-H | 263 | 60 | 0.0857 | 1.0731 | 9.066 | 0.084 | 0.000021 | 4172.7 | **9.06** | **0.083** |
| KR713 S4 | 182 | 73.24 | 0.0935 | 1.0869 | 9.800 | 0.158 | 0.000121 | 772.4 | **9.78** | **0.159** |
| K713-D | 177 | 81.34 | 0.1008 | 1.0900 | 10.568 | 0.069 | 0.000145 | 696.0 | **10.55** | **0.072** |
| KR713 19* | 207 | 19.00 | 0.0826 | 1.0611 | 8.830 | 0.069 | 0.000178 | 463.5 | **8.80** | **0.074** |
| KR713 65* | 171 | 65.00 | 0.0949 | 1.0900 | 9.921 | 0.103 | 0.000461 | 205.7 | **9.85** | **0.124** |

**Table S1**. Corrected (in bold) and uncorrected U/Th ages for KR713 flowstone. The activity ratios have been standardized to the HU-1 secular equilibrium standard. Ages were calculated using decay constants of 9.195 ×10−6 ($^{230}$Th) and 2.835 × $10^{-6}$ ($^{234}$U) and corrected with an initial activity ratios of detrital thorium ($^{230}$Th/$^{232}$Th)$_i$ of 1.5 ± 1.5. Depths are mm from top. Ages with asterisk were rejected as outliers.

### 4.7.2 Statistical comparison of $\delta^{13}C$ and $\delta^{18}O$ isotope ratios

To quantify similarities between the two-isotope series, we apply the procedure previously described by Regattieri et al. (2014). We first smoothed the two-isotope series using a 3-points moving average. Then we normalize each series (by using their mean and standard deviation as normalization parameters) to produce a correspondent time series of anomalies (i.e., deviations from a zero-mean expressed in standard deviation units, Figure S3). The standard deviation between the two normalized series was then calculated and plotted as a grey shadow, together with the two individual anomaly series, in Figure 2 of the main text.

### 4.7.3 Equilibrium deposition

For flowstone LoNAP514, the assumption of quasi-isotope equilibrium deposition was tested by two different lines of reasoning. First, microstratigraphic observations of thin section reveal that the dominant fabric is compact columnar calcite (Frisia, 2015). In sparitic speleothem, columnar fabric and its subtypes are associated with relatively constant drip discharge and low calcite supersaturation state and are commonly associated with quasi-equilibrium deposition (Frisia and Borsato, 2010; Frisia, 2015). Second, from LoNAP514, two different stable isotope series were retrieved (low and high spatial resolution). These followed two different sampling tracks located in different portions of the same flowstone (Figure S1). The extremely good coherency between the two series, both in term of absolute isotope values and in term of variability along the depth scale (Figure S3) testify the absence of significant kinetic fractionation, which would have resulted in different isotope patterns. Indeed, when deposition occurs close to equilibrium, almost constant values of $\delta^{18}O$ and $\delta^{13}C$ along a single growth layer are observed (Hendy, 1971). The small discrepancies between the two series may indicate minor kinetic effects (that are always apparent in speleothems, Daëron et al., 2019) and/or the influence of slightly different growth rates for the two lobes of the flowstone from which the series were retrieved, but these differences are small compared to the overall range of values.

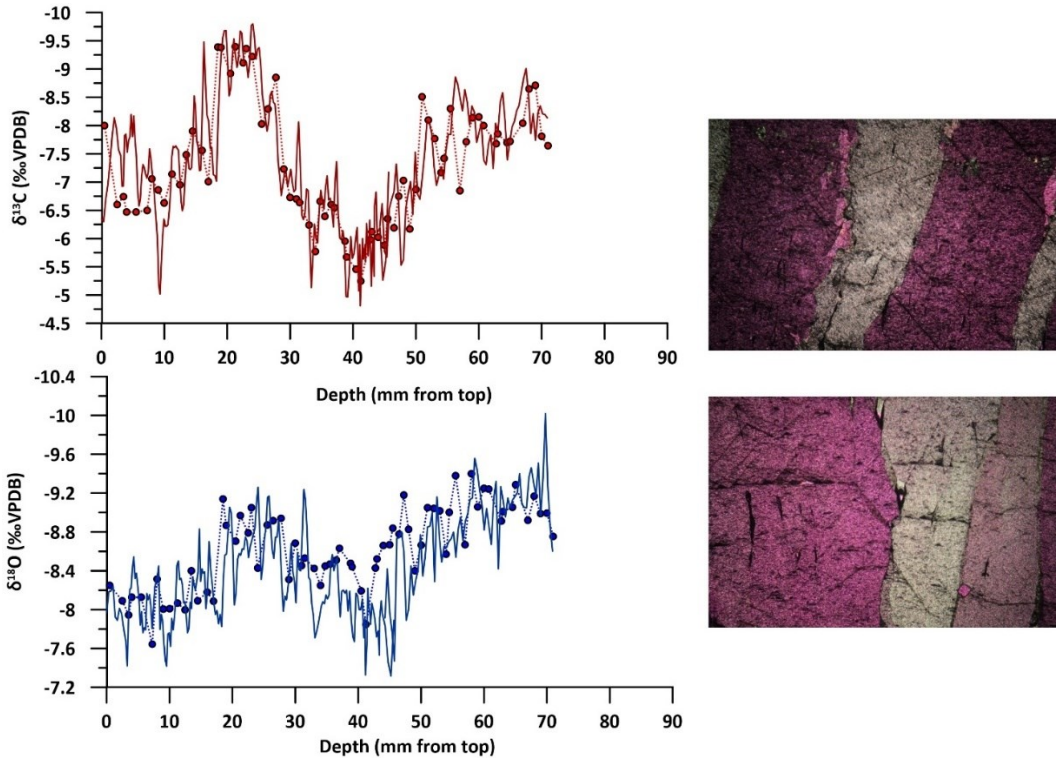


**Figure S3**. Left panel: Low (dotted) vs. high (solid) resolution stable isotope time series for flowstone LoNAP514 plotted versus depth. Right panel: Thin section microphotographs showing compact columnar calcite (cross polarized nicols, base of the photo 5.2 mm).

### 4.7.4 Palaeoclimatic interpretation of LoNAP514 $\delta^{18}O$

Assuming quasi-isotopic equilibrium calcite precipitation, the speleothem $\delta^{18}O$ is a proxy for drip-water $\delta^{18}O$, which reflects local meteoric precipitation $\delta^{18}O$ ($\delta^{18}O_p$) and eventually further solution modification occurring in the soil and in the epikarst (mostly evaporation) (e.g., Baker et al. 2019). Presently, at the annual scale, northern FC $\delta^{18}Op$ is strongly influenced by both the condensation temperature (with a 0.79‰ increase for 1°C of increasing temperature) and the amount effect (with a depletion of 2.3‰ for 100 mm of increase in precipitation) (Figure S4).

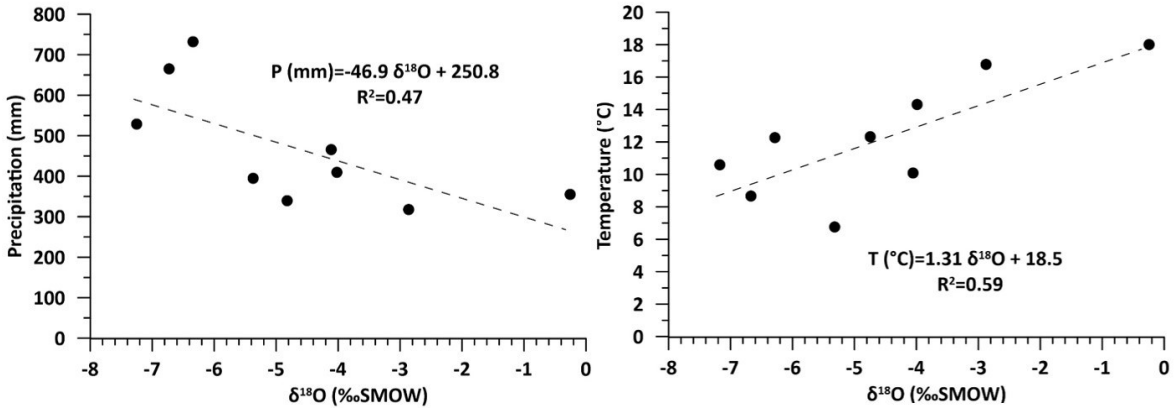


**Figure S4.** Correlation between precipitation $\delta^{18}O$ and precipitation amount (left) and temperature (right) in west Iran-East Iraq; re-drafted from Mohammadzedeh et al., 2020

This means that both temperature changes and precipitation fluctuations influence, in an opposite fashion, the $\delta^{18}$Op. The effect of these gradients on the forming speleothem calcite can be difficult to disentangle. However, despite condensation temperature changes can be important when the seasonal or annual scale is considered, at the time scale considered here (i.e., centennial to multicentennial) the effect of changes in the amount of rainfall appear to be dominant on the final speleothem $\delta^{18}$O, as testified by the strong covariance with the $\delta^{13}$C record (see also main text and SI text 5).

At the time scale considered here, another important factor affecting the speleothem $\delta^{18}$O is the effect of changes in the isotopic composition of the moisture source. The Eastern Mediterranean is the main source of precipitation for the Northern FC, and its surface water $\delta^{18}$O ($\delta^{18}O_{sw}$) is known to be influenced by changes in freshwater discharge (i.e., $^{18}$O depleted) by the Nile River, related to changes in monsoonal activity recharging the upper Nile catchment. Holocene changes in EMed $\delta^{18}$Osw are recorded -at low-resolution- by the $\delta^{18}$O record of planktonic foraminifera *G. ruber* in cores LC21 (Marino et al., 2009; Figure S5). Despite some mismatch between the age models (related to the higher uncertainty of the marine record) the comparison with the LoNAP514 $\delta^{18}$O record shows the highest similarities when the standard deviation between the two speleothem isotope series is higher (Figure S5). A more detailed view on the influence of the source effect on the LoNAP $\delta^{18}$O can be obtained by the comparison with the record of Fe/Ca from core MS27PT, recovered directly at the Nile mouth (Revel et al., 2010). Here, changes in Fe/Ca are considered a proxy for changes in terrigenous input from the Nile, with increases in the Fe/Ca ratio related to increased fluvial discharge (Figure S5). For this comparison is apparent that some of the centennial-scale negative spikes observed in the oxygen record have a close analogue in the detrital record, indicating the influence of short-time freshwater pulses on the isotopic composition of precipitation reaching the FC.

Overall, the comparison with the E Mediterranean record shows that the speleothem $\delta^{18}$O is, at various time scales, influenced by changes in the isotopic composition of the source of precipitation, that may be unrelated to precipitation variability in the cave area. Considering that this "source effect" does not influence the speleothem $\delta^{13}$C record, the latter can be considered a more robust proxy for hydroclimatic change in the cave area.

### 4.7.5 Holocene vegetation in the cave area and influence on the $\delta^{13}$C composition of LoNAP514

Today, the vegetation cover in the cave area is sparse and mostly represented by seasonal wild grasses. However, this is unlikely to represent a direct analogue for the Early to Mid-Holocene vegetation due to long-lasting human land-use for agriculture and pastoralism, which deeply altered the natural vegetation and caused impoverishment and erosion of the soil cover (e.g., Roberts et al., 2002; 2011). Most of the Zagros Mountains area is covered by 'Kurdo-Zagrosian steppe-forest', which is

composed of three major vegetation types, depending on the altitudinal belt. In the mid-altitudes (1800-1200 m a.s.l.), deciduous oak woodland occurs, dominated by the xerophilous Quercus brantii that has expanded in the region since the Mid-Holocene (Djamali et al., 2010; Roberts, 2002). In the lower altitude belt (1200-750 m a.s.l.), to which the cave catchment belongs, the dominant vegetation is represented by Pistacia-Amygdalus scrubland. In the lower (below 750 m a.s.l), drier altitudes, the Irano-Turanian Artemisia steppes in the east (central Iran) and the Mesopotamian lowland savannas in the west, represents the most common vegetation (Zohary, 1973). Other species typical of the medium altitude vegetation are *Pyrus syriaca, Crataegus aronia, Cerasus microcarpa, Acer monspessulanum, L. subsp. cinerascens, Amygdalus scoparia* (Browicz and Zielinski, 1982). All these species belong to the C3 vegetation type. Soil $\delta^{13}C$ at C3 vegetation sites is expected to be in the range -26‰ to -20‰ (Rudzka et al., 2011; Cerling et al., 1991). Assuming a simplified system working near isotopic equilibrium at each stage, it is possible to obtain a raw estimation of the δ13C of speleothem calcite in equilibrium with a labile soil carbon pool by adding ~10‰ to the value of soil $CO_2$ (Rudzka et al., 2011). This produces a range of -16‰ to -10‰ for the calcite. The range of $\delta^{13}C$ values observed for LoNAP514 is slightly lower (~-5 to -10‰). This difference could be related to an incomplete equilibration between soil $CO_2$ and the dissolved inorganic carbon (DIC), resulting in a more pronounced contribution of 13C-enriched $CO_2$ from bedrock dissolution (Bajo et al., 2017; Rudzka et al., 2011; Hendy et al., 1971). However, due to the thin bedrock above the cave where LoNAP514 was retrieved, this effect is likely negligible for our sample. Lowering of drip rates, increased cave ventilation, and water evaporation in the soil and in the epikarst - all capable of promoting preferential degassing of $^{12}CO_2$ - can also result in enriched $\delta^{13}C$ values. Of these, the latter yields strong covariation with the $\delta^{18}O$ (because also $^{16}O$ would be preferentially evaporated) but does not imply significant kinetic fractionation during calcite precipitation (as the other effects do). Because equilibrium conditions appear to be maintained throughout the deposition of LoNAP514 owing to its consistent fabric, we therefore consider evaporation in the soil and in the epikarst as the main factor causing the enriched $^{13}C$ composition of LoNAP514 (see also the main text). Furthermore, it is noteworthy that all the above-mentioned effects shift the isotopic signal in the same direction, driving the speleothem $\delta^{13}C$ toward less negative ratios when the climate is drier. This further supports the use of LoNAP514 $\delta^{13}C$ ratios as the most reliable hydroclimatic proxy.

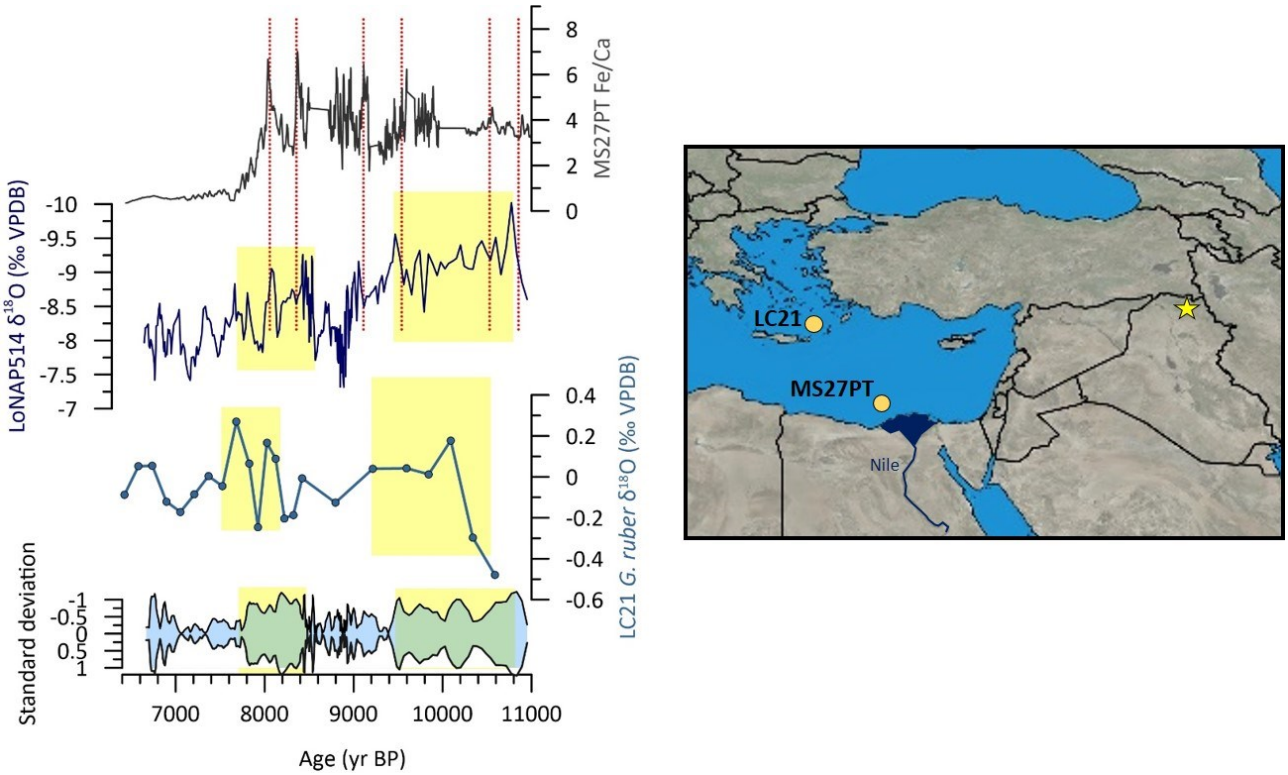


**Figure S5.** Left panel, from bottom: standard deviation between normalized $\delta^{18}O$ and $\delta^{13}C$ record for LoNAP514; $\delta^{18}O$ record of planktic foraminifera Globigerinoides ruber in core LC21 (Marino et al., 2009); LoNAP514 $\delta^{18}O$ record (this study); Fe/Ca ratio from core MS27PT (Revel et al., 2010). Yellow rectangles mark the intervals where the standard deviation between the speleothem isotope series is higher (corresponding to stronger similarities between the speleothem and the planktic $\delta^{18}O$ series); red dotted lines highlight negative spikes in the speleothem $\delta^{18}O$ and correspondent peaks in terrigenous input from the Nile. Right panel: location of cores LC21 and MS27PT, the star is the LoNAP514 cave site. Map elaborated with QGIS 3.16.7 plugin https://nextgis.com/blog/quickmapservices/.

## 4.8 References

Alley, R. B., Mayewski, P. A., Sowers, T., Stuiver, M., Taylor, K. C., & Clark, P. U. (1997). Holocene climatic instability: A large event 8000–8400 years ago. Geology, 25(6), 482-486.

Al-Manmi, D. A. M. A., Ismaeel, S. B., & Altaweel, M. (2019). Reconstruction of palaeoclimate in Shalaii Cave, SE of Sangaw, Kurdistan Province of Iraq. Palaeogeography, Palaeoclimatology, Palaeoecology, 524, 262-272.4

Al-Nassar, A. R., Pelegrí, J. L., Sangrà, P., Alarcon, M., & Jansa, A. (2020). Cut-off low systems over Iraq: Contribution to annual precipitation and synoptic analysis of extreme events. International Journal of Climatology, 40(2), 908-926.

Bajo, P., Borsato, A., Drysdale, R., Hua, Q., Frisia, S., Zanchetta, G., ... & Woodhead, J. (2017). Stalagmite carbon isotopes and dead carbon proportion (DCP) in a near-closed-system situation: An interplay between sulphuric and carbonic acid dissolution. Geochimica et Cosmochimica Acta, 210, 208-227.

Bajo, P., Drysdale, R. N., Woodhead, J. D., Hellstrom, J. C., Hodell, D., Ferretti, P., ... & Fallick, A. E. (2020). Persistent influence of obliquity on ice age terminations since the Middle Pleistocene transition. Science, 367(6483), 1235-1239.

Baker, A., Hartmann, A., Duan, W., Hankin, S., Comas-Bru, L., Cuthbert, M. O., ... & Werner, M. (2019). Global analysis reveals climatic controls on the oxygen isotope composition of cave drip water. Nature communications, 10(1), 1-7.

Baker, A., Hartmann, A., Duan, W., Hankin, S., Comas-Bru, L., Cuthbert, M. O., ... & Werner, M. (2019). Global analysis reveals climatic controls on the oxygen isotope composition of cave drip water. Nature communications, 10(1), 1-7.

Berberian, M. (1995). Master “blind” thrust faults hidden under the Zagros folds: active basement tectonics and surface morphotectonics. Tectonophysics, 241(3-4), 193-224.

Blanc, E. P., Allen, M. B., Inger, S., & Hassani, H. (2003). Structural styles in the Zagros simple folded zone, Iran. Journal of the Geological Society, 160(3), 401-412.

Browicz, K. (1982). Chorology of trees and shrubs in South-West Asia and adjacent regions. Vol. 1. Chorology of trees and shrubs in South-West Asia and adjacent regions. Vol. 1.

Burns, S. J., Fleitmann, D., Matter, A., Neff, U., & Mangini, A. (2001). Speleothem evidence from Oman for continental pluvial events during interglacial periods. Geology, 29(7), 623-626.

Carolin, S. A., Walker, R. T., Day, C. C., Ersek, V., Sloan, R. A., Dee, M. W., ... & Henderson, G. M. (2019). Precise timing of abrupt increase in dust activity in the Middle East coincident with 4.2 ka social change. Proceedings of the National Academy of Sciences, 116(1), 67-72.

Cerling, T. E., Solomon, D. K., Quade, J. A. Y., & Bowman, J. R. (1991). On the isotopic composition of carbon in soil carbon dioxide. Geochimica et Cosmochimica Acta, 55(11), 3403-3405.

Cheng, H., Fleitmann, D., Edwards, R. L., Wang, X., Cruz, F. W., Auler, A. S., ... & Matter, A. (2009). Timing and structure of the 8.2 kyr BP event inferred from δ18O records of stalagmites from China, Oman, and Brazil. Geology, 37(11), 1007-1010.

Childe, V. G. (1936). Man makes himself London. Watts and Company.

Clarke, G. K., Leverington, D. W., Teller, J. T., & Dyke, A. S. (2004). Paleohydraulics of the last outburst flood from glacial Lake Agassiz and the 8200BP cold event. Quaternary Science Reviews, 23(3-4), 389-407.

Cohen, J. L., & Saito, K. (2003). Eurasian snow cover, more skillful in predicting US winter climate than the NAO/AO? Geophysical research letters, 30(23).

Conati Barbaro, C., Moscone, D., Iamoni, M., Morandi Bonacossi, D., & Qasim, H. A. (2019). The prehistory and protohistory of the northwestern region of Iraqi Kurdistan: Preliminary results from the first survey campaigns. Paléorient. Revue pluridisciplinaire de préhistoire et de protohistoire de l'Asie du Sud-Ouest et de l'Asie centrale, (45-2), 207-229.

Corrick, E. C., Drysdale, R. N., Hellstrom, J. C., Capron, E., Rasmussen, S. O., Zhang, X., ... & Wolff, E. (2020). Synchronous timing of abrupt climate changes during the last glacial period. Science, 369(6506), 963-969.

Csontos, L., Sasvári, Á., Pocsai, T., & Kósa, L. (2011, May). Structural evolution of the northwestern Zagros, Kurdistan Region, Iraq and alternative models for formation of a curved mountain chain. In 73rd EAGE Conference and Exhibition-Workshops 2011 (pp. cp-239). European Association of Geoscientists & Engineers.

Daëron, M., Drysdale, R. N., Peral, M., Huyghe, D., Blamart, D., Coplen, T. B., ... & Zanchetta, G. (2019). Most Earth-surface calcites precipitate out of isotopic equilibrium. Nature communications, 10(1), 1-7.

Daly, K. G., Maisano Delser, P., Mullin, V. E., Scheu, A., Mattiangeli, V., Teasdale, M. D., ... & Bradley, D. G. (2018). Ancient goat genomes reveal mosaic domestication in the Fertile Crescent. Science, 361(6397), 85-88.

de Vries, A. J., Tyrlis, E., Edry, D., Krichak, S. O., Steil, B., & Lelieveld, J. (2013). Extreme precipitation events in the Middle East: dynamics of the Active Red Sea Trough. Journal of Geophysical Research: Atmospheres, 118(13), 7087-7108.

Dean, J. R., Jones, M. D., Leng, M. J., Noble, S. R., Metcalfe, S. E., Sloane, H. J., ... & Roberts, C. N. (2015). Eastern Mediterranean hydroclimate over the late glacial and Holocene, reconstructed from the sediments of Nar lake, central Turkey, using stable isotopes and carbonate mineralogy. Quaternary Science Reviews, 124, 162-174.

Dercourt, J., Zonenshain, L. P., Ricou, L. E., Kazmin, V. G., Le Pichon, X., Knipper, A. L., ... & Biju-Duval, B. (1986). Geological evolution of the Tethys belt from the Atlantic to the Pamirs since the Lias. Tectonophysics, 123(1-4), 241-315.

Dewey, J. F., Pitman, W. C., Ryan, W. B. F., Bonnin, J. (1973). Plate tectonics and the evolution of the alpine system. Geological Society of America Bulletin, 84(10), 3137– 3180.

Djamali, M., Akhani, H., Andrieu-Ponel, V., Braconnot, P., Brewer, S., de Beaulieu, J. L., ... & Stevens, L. (2010). Indian Summer Monsoon variations could have affected the early-Holocene woodland expansion in the Near East. The Holocene, 20(5), 813-820.

Drysdale, R. N., Zanchetta, G., Hellstrom, J. C., Fallick, A. E., & Zhao, J. X. (2005). Stalagmite evidence for the onset of the Last Interglacial in southern Europe at 129±1 ka. Geophysical Research Letters, 32(24).

Eastwood, W. J., Leng, M. J., Roberts, N., & Davis, B. (2007). Holocene climate change in the eastern Mediterranean region: a comparison of stable isotope and pollen data from Lake Gölhisar, southwest Turkey. Journal of Quaternary Science: Published for the Quaternary

Evans, J. P., Smith, R. B., & Oglesby, R. J. (2004). Middle East climate simulation and dominant precipitation processes. International Journal of Climatology: A Journal of the Royal Meteorological Society, 24(13), 1671-1694.

Fleitmann, D., Burns, S. J., Pekala, M., Mangini, A., Al-Subbary, A., Al-Aowah, M., ... & Matter, A. (2011). Holocene and Pleistocene pluvial periods in Yemen, southern Arabia. Quaternary Science Reviews, 30(7-8), 783-787.

Fleitmann, D., Mudelsee, M., Burns, S. J., Bradley, R. S., Kramers, J., & Matter, A. (2008). Evidence for a widespread climatic anomaly at around 9.2 ka before present. Paleoceanography, 23(1).

Flohr, P., Fleitmann, D., Matthews, R., Matthews, W., & Black, S. (2016). Evidence of resilience to past climate change in Southwest Asia: Early farming communities and the 9.2 and 8.2 ka events. Quaternary Science Reviews, 136, 23-39.

Flohr, P., Fleitmann, D., Zorita, E., Sadekov, A., Cheng, H., Bosomworth, M., ... & Matthews, R. (2017). Late Holocene droughts in the Fertile Crescent recorded in a speleothem from northern Iraq. Geophysical Research Letters, 44(3), 1528-1536

Fohlmeister, J., Voarintsoa, N. R. G., Lechleitner, F. A., Boyd, M., Brandtstätter, S., Jacobson, M. J., & Oster, J. L. (2020). Main controls on the stable carbon isotope composition of speleothems. Geochimica et Cosmochimica Acta, 279, 67-87.

Forti, L., Perego, A., Brandolini, F., Mariani, G. S., Zebari, M., Nicoll, K., ... & Zerboni, A. (2021). Geomorphology of the northwestern Kurdistan Region of Iraq: landscapes of the Zagros Mountains drained by the Tigris and Great Zab Rivers. Journal of Maps, 17(2), 225-236.

Fouad, S. F. (2014). Western Zagros fold–Thrust Belt, part II: The high folded zone. Iraqi bulletin of geology and mining, (6), 53-71.

Frisia, S. (2014). Microstratigraphic logging of calcite fabrics in speleothems as tool for palaeoclimate studies.

Frisia, S., & Borsato, A. (2010). Karst. Developments in sedimentology, 61, 269-318.

Frizon de Lamotte, D., Raulin, C., Mouchot, N., Wrobel-Daveau, J. C., Blanpied, C., & Ringenbach, J. C. (2011). The southernmost margin of the Tethys realm during the Mesozoic and Cenozoic: Initial geometry and timing of the inversion processes. Tectonics, 30(3).

Gadgil, S. (2003). The Indian monsoon and its variability. Annual Review of Earth and Planetary Sciences, 31(1), 429-467

Gao, T., Han, J., Gao, L., & Yan, W. (2014). Impacts of the North India Ocean SST on the extremely cold winters of 2011 and 2012 in the region of Da Hinggan Mountains and its western areas in China. Theoretical and applied climatology, 117(3), 693-705.

Gong, D. Y., & Ho, C. H. (2002). The Siberian High and climate change over middle to high latitude Asia. Theoretical and applied climatology, 72(1), 1-9.

Hasanean, H. M., Almazroui, M., Jones, P. D., & Alamoudi, A. A. (2013). Siberian high variability and its teleconnections with tropical circulations and surface air temperature over Saudi Arabia. Climate dynamics, 41(7), 2003-2018.

Hellstrom, J. (2003). Rapid and accurate U/Th dating using parallel ion-counting multi-collector ICP-MS. Journal of Analytical Atomic Spectrometry, 18(11), 1346-1351.

Hellstrom, J. (2006). U–Th dating of speleothems with high initial 230Th using stratigraphical constraint. Quaternary Geochronology, 1(4), 289-295.

Hendy, C. H. (1971). The calculation of the effects of different modes of formation on the isotopic composition of speleothems and their applicability as palaeoclimatic indicators. Geochimica et Cosmochimica Acta, 35, 801-824.

Iamoni, M. (2018). A vital resource in Prehistory: Water and settlement during the Pottery Neolithic and Chalcolithic periods. A preliminary analysis of the Eastern Upper Tigris basin area. Water for Assyria, 7-24.

Iizuka, F., & Terry, K. (2022). Old World Ceramic Origins and Behavioral Contexts from the Late Pleistocene to Mid-Holocene: Unresolved and New Problems. Quaternary International, 608, 1-7.

Izdebski, A., Pickett, J., Roberts, N., & Waliszewski, T. (2016). The environmental, archaeological and historical evidence for regional climatic changes and their societal impacts in the Eastern Mediterranean in Late Antiquity. Quaternary Science Reviews, 136, 189-208.

Jassim, S. Z., & Goff, J. C. (Eds.). (2006). Geology of Iraq. DOLIN, sro, distributed by Geological Society of London.

Krichak, S. O., Breitgand, J. S., & Feldstein, S. B. (2012). A conceptual model for the identification of active Red Sea trough synoptic events over the southeastern Mediterranean. Journal of Applied Meteorology and Climatology, 51(5), 962-971.

Labban, A. H., Mashat, A. W. S., & Awad, A. M. (2021). The variability of the Siberian high ridge over the Middle East. International Journal of Climatology, 41(1), 104-130.

Lancelotti, C., Biagetti, S., Zerboni, A., Usai, D., & Madella, M. (2019). The archaeology and ethnoarchaeology of rain-fed cultivation in arid and hyper-arid North Africa. antiquity, 93(370), 1026-1039.

Marino, G., Rohling, E. J., Sangiorgi, F., Hayes, A., Casford, J. L., Lotter, A. F., ... & Brinkhuis, H. (2009). Early and middle Holocene in the Aegean Sea: interplay between high and low latitude climate variability. Quaternary Science Reviews, 28(27-28), 3246-3262.

Matthews, R., Matthews, W., Richardson, A., Walsh, S., Iversen, I., Mudd, D., ... & Elliott, S. (2019). The early Neolithic of Iraqi kurdistan: Current research at bestansur, shahrizor plain. Paléorient.

Revue pluridisciplinaire de préhistoire et de protohistoire de l'Asie du Sud-Ouest et de l'Asie centrale, (45-2), 13-32.

Mayewski, P. A., Meeker, L. D., Whitlow, S. L., Twickler, M. S., Morrison, M. C., Bloomfield, P., ... & Wumkes, W. (1994). Changes in atmospheric circulation and ocean ice cover over the North Atlantic during the last 41,000 years. Science, 263(5154), 1747-1751.

Mayewski, P. A., Rohling, E. E., Stager, J. C., Karlén, W., Maasch, K. A., Meeker, L. D., ... & Steig, E. J. (2004). Holocene climate variability. Quaternary research, 62(3), 243-255.

Mohammadzadeh, H., Eskandari Mayvan, J., & Heydarizad, M. (2020). The effects of moisture sources and local parameters on the 18O and 2H contents of precipitation in the west of Iran and the east of Iraq. Tellus B: Chemical and Physical Meteorology, 72(1), 1-15.

Mouthereau, F., Lacombe, O., & Vergés, J. (2012). Building the Zagros collisional orogen: timing, strain distribution and the dynamics of Arabia/Eurasia plate convergence. Tectonophysics, 532, 27-60.

Nicholson, S. L., Jacobson, M. J., Hosfield, R., & Fleitmann, D. (2021). The stalagmite record of Southern Arabia: climatic extremes, human evolution, and societal development. Frontiers in Earth Science, 1169.

Nicolussi, K., & Schlüchter, C. (2012). The 8.2 ka event—Calendar-dated glacier response in the Alps. Geology, 40(9), 819-822.

Nieuwenhuyse, O. P., & Akkermans, P. M. M. G. (2019). Transforming the upper Mesopotamian landscape in the late Neolithic. Concluding the Neolithic: The Near East in the Second Half of the Seventh Millennium BCE, 1, 101.

Palmisano, A., Lawrence, D., de Gruchy, M. W., Bevan, A., & Shennan, S. (2021). Holocene regional population dynamics and climatic trends in the Near East: A first comparison using archaeo-demographic proxies. Quaternary Science Reviews, 252, 106739.

Pollock, S. (2013). Defining a Halaf tradition: the construction and use of space. Interpreting the Late Neolithic of Upper Mesopotamia, 171-82.

Regattieri, E., Zanchetta, G., Drysdale, R. N., Isola, I., Hellstrom, J. C., & Dallai, L. (2014). Lateglacial to holocene trace element record (Ba, Mg, Sr) from corchia cave (Apuan Alps, central Italy): paleoenvironmental implications. Journal of quaternary Science, 29(4), 381-392.

Regattieri, E., Zanchetta, G., Isola, I., Bajo, P., Perchiazzi, N., Drysdale, R. N., ... & Wagner, B. (2018). A MIS 9/MIS 8 speleothem record of hydrological variability from Macedonia (FYROM). Global and planetary change, 162, 39-52.4

Regattieri, E., Zanchetta, G., Isola, I., Zanella, E., Drysdale, R. N., Hellstrom, J. C., ... & Magrì, F. (2019). Holocene Critical Zone dynamics in an Alpine catchment inferred from a speleothem multiproxy record: disentangling climate and human influences. Scientific reports, 9(1), 1-9.

Revel, M., Ducassou, E., Grousset, F. E., Bernasconi, S. M., Migeon, S., Révillon, S., ... & Bosch, D. (2010). 100,000 Years of African monsoon variability recorded in sediments of the Nile margin. Quaternary Science Reviews, 29(11-12), 1342-1362.

Riaz, S. M. F., Iqbal, M. J., & Baig, M. J. (2018). Influence of Siberian High on temperature variability over northern areas of South Asia. Meteorology and Atmospheric Physics, 130(4), 441-457.

Riehl, S., Zeidi, M., & Conard, N. J. (2013). Emergence of agriculture in the foothills of the Zagros Mountains of Iran. science, 341(6141), 65-67.

Rindos, D. (2013). The origins of agriculture: an evolutionary perspective. Academic Press.

Roberts, N., Eastwood, W. J., Kuzucuoğlu, C., Fiorentino, G., & Caracuta, V. (2011). Climatic, vegetation and cultural change in the eastern Mediterranean during the mid-Holocene environmental transition. The Holocene, 21(1), 147-162.

Roberts, N., Jones, M. D., Benkaddour, A., Eastwood, W. J., Filippi, M. L., Frogley, M. R., ... & Zanchetta, G. (2008). Stable isotope records of Late Quaternary climate and hydrology from Mediterranean lakes: the ISOMED synthesis. Quaternary Science Reviews, 27(25-26), 2426-2441.

Roberts, N., Reed, J. M., Leng, M. J., Kuzucuoğlu, C., Fontugne, M., Bertaux, J., ... & Karabiyikoğlu, M. (2001). The tempo of Holocene climatic change in the eastern Mediterranean region: new high-resolution crater-lake sediment data from central Turkey. The Holocene, 11(6), 721-736.

Roberts, N., Woodbridge, J., Bevan, A., Palmisano, A., Shennan, S., & Asouti, E. (2018). Human responses and non-responses to climatic variations during the last Glacial-Interglacial transition in the eastern Mediterranean. Quaternary Science Reviews, 184, 47-67.

Rohling, E. J., & Pälike, H. (2005). Centennial-scale climate cooling with a sudden cold event around 8,200 years ago. nature, 434(7036), 975-979.

Rohling, E. J., Marino, G., Grant, K. M., Mayewski, P. A., & Weninger, B. (2019). A model for archaeologically relevant Holocene climate impacts in the Aegean-Levantine region (easternmost Mediterranean). Quaternary Science Reviews, 208, 38-53.

Rosen, A. M., & Rivera-Collazo, I. (2012). Climate change, adaptive cycles, and the persistence of foraging economies during the late Pleistocene/Holocene transition in the Levant. Proceedings of the National Academy of Sciences, 109(10), 3640-3645.

Rudzka, D., McDermott, F., Baldini, L. M., Fleitmann, D., Moreno, A., & Stoll, H. (2011). The coupled δ13C-radiocarbon systematics of three Late Glacial/early Holocene speleothems; insights into soil and cave processes at climatic transitions. Geochimica et Cosmochimica Acta, 75(15), 4321-4339.

Saaroni, H., Bitan, A., Alpert, P., & Ziv, B. (1996). Continental polar outbreaks into the Levant and eastern Mediterranean. International Journal of Climatology, 16(10), 1175-1191.

Schneider, U., Becker, A., Finger, P., Meyer-Christoffer, A., & Ziese, M. (2018). GPCC Full Data Monthly Version 2018.0 at 0.25: Monthly Land-Surface Precipitation from Rain-Gauges built on GTS-based and Historic Data, Global Precipitation Climatology Centre. Global Precipitation Climatology Centre (GPCC) at Deutscher Wetterdienst.

Senan, R., Orsolini, Y. J., Weisheimer, A., Vitart, F., Balsamo, G., Stockdale, T. N., ... & Basang, D. (2016). Impact of springtime Himalayan–Tibetan Plateau snowpack on the onset of the Indian summer monsoon in coupled seasonal forecasts. Climate Dynamics, 47(9), 2709-2725.

Stiller, M., & Hutchinson, G. E. (1980). The Waters of Merom: a study of Lake Huleh VI, Stable isotope composition of carbonates of a 54 m core: paleoclimatic and paleotrophic implications, Fundamental and Applied Limnology, 89(3), 275-302.

Trigo, R. M., Gouveia, C. M., & Barriopedro, D. (2010). The intense 2007–2009 drought in the Fertile Crescent: Impacts and associated atmospheric circulation. Agricultural and forest meteorology, 150(9), 1245-1257.4

Vaks, A., Bar-Matthews, M., Matthews, A., Ayalon, A., & Frumkin, A. (2010). Middle-Late Quaternary paleoclimate of northern margins of the Saharan-Arabian Desert: reconstruction from speleothems of Negev Desert, Israel. Quaternary Science Reviews, 29(19-20), 2647-2662.

Vergés, J., Saura, E., Casciello, E., Fernandez, M., Villaseñor, A., Jimenez-Munt, I., & García-Castellanos, D. (2011). Crustal-scale cross-sections across the NW Zagros belt: implications for the Arabian margin reconstruction. Geological Magazine, 148(5-6), 739-761.

Watkins, T. (2010). New light on Neolithic revolution in south-west Asia. Antiquity, 84(325), 621-634.

Weninger, B., Alram-Stern, E., Bauer, E., Clare, L., Danzeglocke, U., Jöris, O., ... & van Andel, T. (2006). Climate forcing due to the 8200 cal yr BP event observed at Early Neolithic sites in the eastern Mediterranean. Quaternary Research, 66(3), 401-420.

Wick, L., Lemcke, G., & Sturm, M. (2003). Evidence of Lateglacial and Holocene climatic change and human impact in eastern Anatolia: high-resolution pollen, charcoal, isotopic and geochemical records from the laminated sediments of Lake Van, Turkey. The holocene, 13(5), 665-675.

Yu, S. Y., Colman, S. M., Lowell, T. V., Milne, G. A., Fisher, T. G., Breckenridge, A., ... & Teller, J. T. (2010). Freshwater outburst from Lake Superior as a trigger for the cold event 9300 years ago. Science, 328(5983), 1262-1266.

Zebari, M., Grützner, C., Navabpour, P., & Ustaszewski, K. (2019). Relative timing of uplift along the Zagros Mountain Front Flexure (Kurdistan Region of Iraq): Constrained by geomorphic indices and landscape evolution modeling. Solid Earth, 10(3), 663-682.

Zeder, M. A., & Hesse, B. (2000). The initial domestication of goats (Capra hircus) in the Zagros mountains 10,000 years ago. Science, 287(5461), 2254-2257.

Zhou, Z. Q., Xie, S. P., & Zhang, R. (2019). Variability and predictability of Indian rainfall during the monsoon onset month of June. Geophysical Research Letters, 46(24), 14782-14788.

Zohary, M. (1973). Geobotanical foundations of the Middle East. Fischer.

# Chapter 5

# Declassified intelligence satellite imagery as a tool to reconstruct past landforms and surface processes: The submerged riverscape of the Tigris River below the Mosul Dam Lake, Iraq

## 5.1 Introduction

Rivers are among the most dynamic environments in terms of landscape change and impact on human communities (Dollar, 2004; Charlton, 2007; Thorndycraft et al., 2008; Buffington and Montgomery, 2013). Their evolution depends on numerous factors, ranging from tectonics and climate to human intervention, often difficult to recognise as separate triggers and in many cases deeply modified by recent human agency (Brown et al., 2017; Tarolli et al., 2019). Remote sensing and field investigations on water courses and their surrounding landscapes can help in the reconstruction of the processes underlying fluvial evolution. This is especially true for arid regions, where the poor plant cover allows very precise and detailed observations even from remote (Perego et al., 2011). Moreover, in such contexts the effects of lithological and structural constraints are more immediate to be identified (Zerboni et al., 2020), greatly helping the formulation of more effective models. Among the great rivers of the planet, the Tigris and the Euphrates are very important for the natural and human history of Mesopotamia, in the past as well as today. Their courses, from Turkey to the Gulf, is controlled for the most part by the structural evolution of the region, a quite active area of converging plates (Al-Saigh, 2008; Al-Dabbagh and Al-Naqib, 2009; Fouad et al., 2012; Sissakian et al.,2020). The Tigris River flows for 1800 km from the Taurus mountains in Turkey through the border with Iraq and then into the Gulf. Almost 56% of its basin lies in Iraq, with 6 major tributaries and secondary rivers draining most of the runoff from the Iraqi mountainside of the southern Zagros. The Tigris River is less meandering than the Euphrates, and along many of its branches, especially after the Iraq-Turkey border, its course is strongly influenced by the geodynamic setting of the Arabian-Eurasian plate convergence. In modern times, the course of the Tigris River has been constrained in multiple places by human action through the construction of dams, which greatly modified the local landscape and flooded several villages and archaeological sites (ESCWA, 2013; Sconzo and Simi, 2020; Titolo, 2021). At the same time, new artificial basins show non-homogenous

*Forti, L., Mariani, G. S., Brandolini, F., Pezzotta, A., & Zerboni, A. (2022). Declassified intelligence satellite imagery as a tool to reconstruct past landforms and surface processes. The submerged riverscape of the Tigris River below the Mosul Dam Lake, Iraq. Earth Surface Processes and Landforms.* 47(10), 2483-2499. https://doi.org/10.1002/esp.5389

aspects, which probably follow previous natural constraints, ultimately related to the settings of the ancient course of the Tigris River. In the contexts of artificial lakes, despite the arid climate and the low plant cover allowing a very good visibility of ground features, it is hard to map landforms and interpret the factors triggering the evolution of fluvial landforms since a relevant portion of the landscape is submerged and invisible to field observation. To overcome this issue, in the present work we combine geological and geomorphological data with the observations of declassified satellite images collected before the construction of the Mosul Lake Dam (MLD), thus representative of the pristine local riverscape. Such multi-temporal mapping approach (Zerboni et al., 2020) aims to: (i) reconstruct the ancient course of the Tigris River upstream of Mosul, (ii) describe its seasonal dynamics before the construction of the dam, and (iii) correlate the current dynamic of the lake to lithological and structural factors that in the past may have controlled the development of the river. The use of a multidisciplinary approach permitted to reconstruct the submerged riverscape of the Tigris River, showing the underlying causes that shaped fluvial dynamics as much as the current lake and helping in the reconstruction of past geomorphic processes. Finally, we highlight the relevance of declassified intelligence satellite imagery as a tool to interpret the dynamic of past geomorphic processes and landforms today influenced/altered/obscured by human agency.

## 5.2. The study area

### 5.2.1. Geological and climatic background

The study area covers 1250 km2 of the north-western Kurdistan Region of Iraq (KRI) in the governorates of Dohuk and Nineveh (Figure 1). The landscape is the result of the interplay between geological-structural, geomorphological, and climate-driven processes (Forti et al., 2021), and subsequently the construction of Dam and its infilling in the ’80ies (Adamo and Al-Ansari, 2016).

The area is in the Low Folded Zone, within the Outer Platform of the Arabian Plate part of the Zagros-Fold Thrust Belt (ZFTB; Fouad, 2007). This structure is the result of the collision between the Arabian and Eurasian continental plates that started in the Early Miocene and is still actively progressing today (Dercourt et al., 1986; Fouad et al., 2012; Mouthereau et al., 2012; Csontos et al., 2012). Low-elevation mountains and lowlands characterise the area. Their distribution is controlled by the presence of anticline ridges, mainly oriented W-E (Ain Zala, Zainiyat, Butma, Ravan, Dohuk, Dakhan, Masra and Kand anticline) (Figure.1; Figure 2A-B) and NW-SE (Mashura Dag, Sufiya and Baikhair) (Fouad et al., 2012; Abdulnaby, 2019) and by the NW-SE development of the Dohuk Fault System (sensu Al-Dabbagh and Al-Naqib, 2009; Al-Saigh, 2008, 2012) with the main alignment of the Sasa-Bekhair Fault (Fouad et al., 2012; Sissakian et al., 2018). The anticline ridges are mainly composed by Paleocene to Lower Miocene limestone and dolostone, whereby in the Mosul Lake area

the anticline is characterized by the Miocene to Mio-Pliocene Fatha, Injana and Mukdadiyah Formations, alternating marl and gypsum with sandstone and limestone (Sissakian & Fouad, 2012) (Figure1; Figure 2D). Plio-Pleistocene conglomerates outcrop along the northern banks of Mosul Lake and in the proximity of the dam (Figure 2C) (Al-Dabbagh and Al-Naqib, 1991; Sissakian and Al-Jibouri, 2012). Quaternary deposits are mainly located along the hillslopes of anticlines and in the lowland areas of the syncline troughs. They include fluvial, floodplain, alluvial fan, colluvial, and anthropogenic deposits (Jassim and Goff, 2006; Sissakian and Al-Jibouri, 2012, Forti et al., 2021). Quaternary deposits are composed by conglomerates with fine to coarse sand, with levels of silt and clay recognized at different locations of the area, especially on the fluvial terraces above the banks of the Tigris River (Al-Dabbagh & Al-Naqib, 1991). Such deposits are eroded and reworked by the action of the fluvial network draining from NE into the Mosul Lake to the SW.

Climatic data for the study area derive from a meteorological station placed in the cities of Mosul and Dohuk and were elaborated for climate models by Awchi and Kalyana (2017) and Sulaiman (2016). Models suggest that the Mosul Lake is located between two climatic zones of the climate classification proposed by Köppen & Geiger (1936). The first zone is the Mediterranean or Dry Summer Subtropical (Csa), while the second one is Subtropical Steppe (Bsh) (Salman et al., 2019; Malinowski, 2002). The Csa climatic zone in this area is characterized by extremely to moderately cold wet winters and moderately hot arid summers. Precipitations occur during the winter and spring seasons from November to April with an estimated mean rainfall at Dohuk station of 570 mm and seasonal temperature variations from 8.8°C to 34 °C (Malinowski, 2002; Sulaiman, 2016; Awchi & Kalyana, 2017). The Bsh climate zone has moderately cold winters and hot to extremely hot dry summers. Long-term climate data extrapolated from the Mosul meteorological station (Awchi & Kalyana, 2017) show that most rainfall occurs during the winter season and the annual mean rainfall from 1937 to 2010 is 378 mm. Annual mean temperature is 21°C with extremely hot summers with mean temperatures of around 40°C. Most rivers in the region are ephemeral, active during the rainy season (Othman & Gloaguen, 2013) and inactive in the dry season; only the Tigris River and a few of its tributaries are perennial. Several climate models showed a strong increase of drought events in recent times. From the 1980ies to 1990ies the area surrounding the Mosul Lake suffered several periods of drought. At the beginning of the 1990ies and especially in the last decades of the 20th century, severe droughts are recorded (Awchi and Kalyana, 2017; Alwan et al., 2019; Al-Khafaji & Al-Ameri, 2021). In addition to climate change, the dam's water supply has been threatened by ongoing conflicts in the area over the past four decades (Hasan et al., 2019).

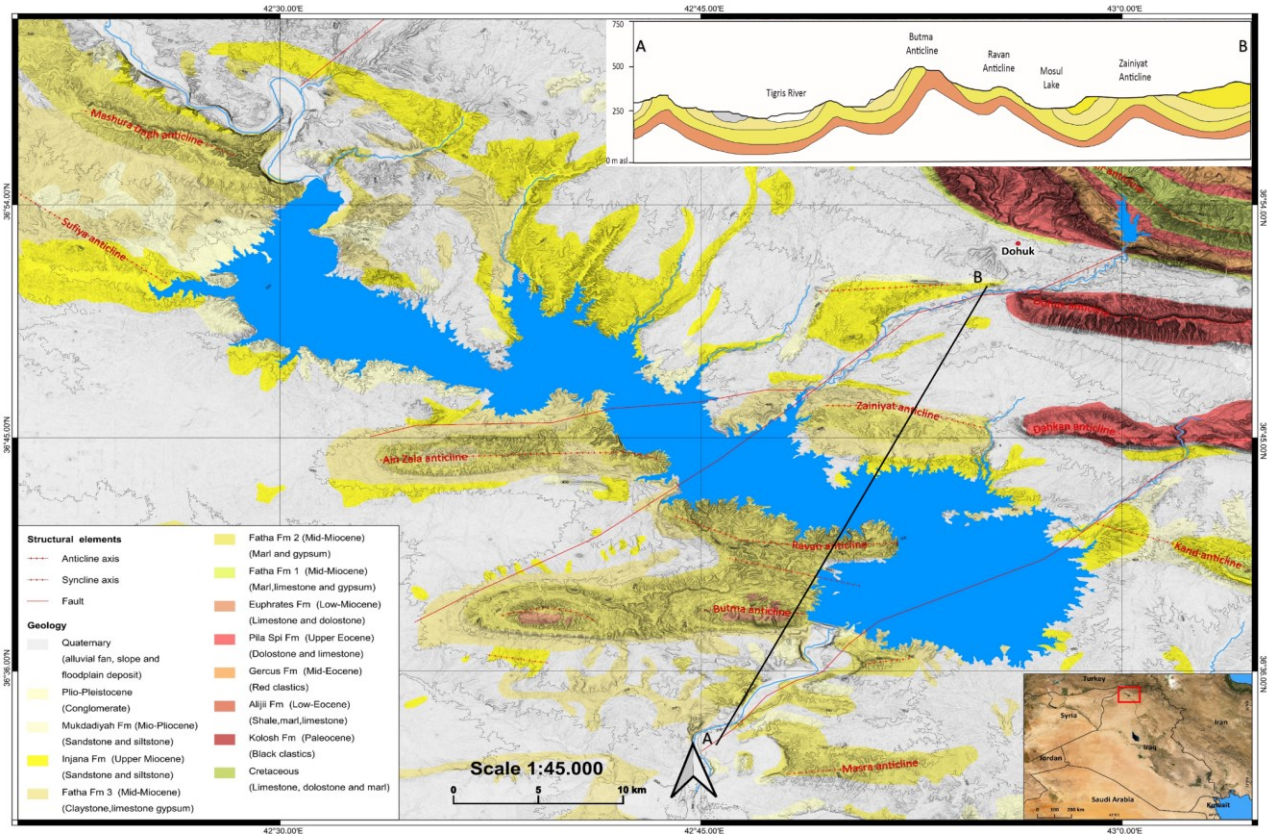


**Figure 1.** Simplified geological map and main structural elements of the study area (elaborated from Al-Mosul quadrangle geological map of the Ministry of Industry and Minerals, Iraq Geological Survey, 1995, 1997, 2014). The black line indicates the trace of the geological cross-section showing the local anticline and syncline systems.

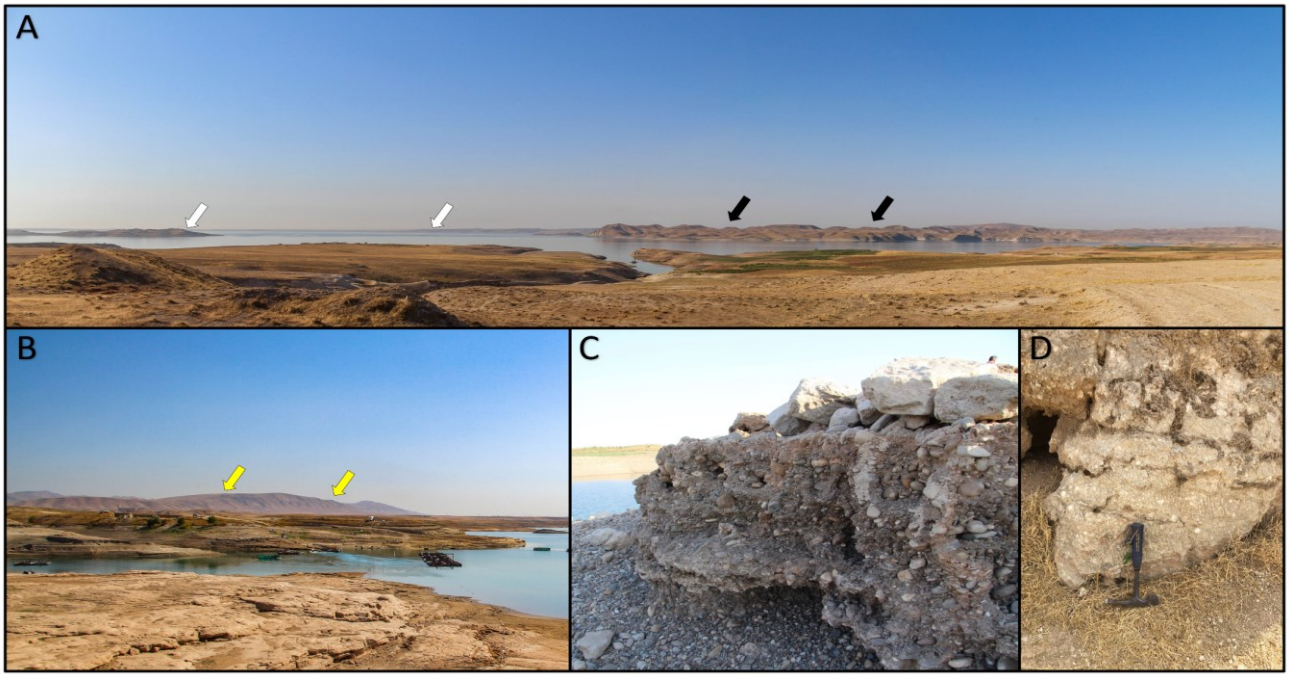


**Figure 2.** Field pictures from the MDL area. (A) Panoramic view from the left bank of MDL at a high stand in 2015; on the background the ridge of the Ravan anticline (black arrows) and the area of the dam (white arrows). (B) Panoramic view from the left bank of MDL towards the east; on the background the ridge of the Dakhan anticline (yellow arrows). (C) An outcrop of the Plio- Pleistocene conglomerates close to the left bank of MDL. (D) An outcrop of the gypsum-rich layers of Fathma Formation.

### 5.2.2. Hydrological setting of the Tigris River and the Mosul Lake Dam

The Tigris River originates in Turkey along the southern slope of the Taurus mountains (Altinbilek, 2007). The river flows through Turkey, Syria, and Iraq. After 1800 km the Tigris River merges with the Euphrates River in the South of Mesopotamia, forming the Shatt-Al-Arab River that flows into the Gulf, 220 km downstream (Figure 3A). The main tributaries from Iraq and Syria are the Feysh Khabur, Great Zab, Lesser Zab, Adhaim, and Diyala Rivers. The Feysh Khabur River joins the Tigris River west of the municipality of Zacko, while the Great Zab and Lesser Zab Rivers respectively to the SE of the cities of Mosul and Fatha. The Adhaim and Diyala River merge into the Tigris River south of Fatha and in the proximity of Baghdad; afterwards, no major tributary rivers are recognized except for a few agricultural canals draining from the Zagros piedmont in the internal floodplain of the Tigris River. The Tigris River drainage basin occupies a total area of ~221,000 km2, for the 60% in Iraq territory; its mean discharge at Mosul city was 700 m3/s in 1984 and dropped to 596 m3/s after the construction of the dam. The overall amount of the Iraqi catchment area is ~124,000 km2; the annual mean discharge changes according to the Tigris setting and the minor tributary basins to the South (Figure. 3 B, C) (Saleh, 2010; Al-Ansari & Knutsson, 2011; Al-Ansari, 2013; ESCWA, 2013). The MLD is the largest dam in Iraq and one of the biggest of the Near East with a storage capacity of 11.11 km3 of water (Al-Ansari et al., 2015). It is 3650 m in length and 113 m high with an embankment core composed by clays. It was built to provide water for irrigation, control floods, and hydropower generation (Figure 4). During the preparation of the site for construction operations, problems related to grouting work on the foundations of the dam were recognized. In fact, the geological bedrock of the dam consists of gypsum, marl, and limestone layers interbedded with breccias which are intensely fractured by the Dohuk Fault System, allowing seepage and karst processes to act on the stability of the dam (Al-Dabbagh & Al-Naqib, 2009; Al-Saigh, 2008, 2012; Sissakian et al., 2014). Construction works started in January 1981, and the dam became operational in July 1986.

## 5.3. Materials and methods

To investigate the recent evolution of the Tigris River and its riverscape in the area submerged by the MLD, including the major factors controlling its development, we performed a detailed geomorphological mapping of the area and an analysis of its seasonal changes.

Geomorphological mapping of the area was performed on data interpreted from both declassified Corona, Landsat, Sentinel 2A/2B, Esri World Imagery, Bing Virtual Earth and GoogleEarthTM satellite images (Bing Maps, 2021; Esri, 2021) (Figure 5). Declassified Corona satellite image dataset was downloaded from CAST Atlas of the University of Arkansas

(https://cast.uark.edu/research/corona.php) (USGS, 1968); in particular, we considered December 1967 (1102-1025) and August 1968 (1104-2138) images. Landsat and Sentinel 2 were selected from the Earth Explorer platform of the USGS (https://earthexplorer.usgs.gov) and cover a period from June 1984 to August 1986 and March and July 2016-2020. We used 11 declassified Corona, 15 Landsat and 11 Sentinel-2 images (Table 1). Landsat and Sentinel-2 imagery was observed in false colours (red = band 4, green = band 3, blue = band 2). Corona imagery was observed in single band grayscale. Corona images helped in mapping landforms to understand their seasonal geomorphic shift (Gilvear and Bryant, 2016; Gurnell et al., 2016). The mapping considered different geomorphic units, illustrating the effect of fluvial, slope, and anthropogenic processes. Fluvial geomorphic units are the most important for our study and were described to highlight seasonal changes in the fluvial pattern; we adopted the classification proposed by Brierley & Fryirs (2013). Landsat images taken from 1984 to 1986 were used to emphasize the time and steps of the infilling of the MLD. Moreover, true colour GoogleEarth™, Bing Virtual Earth and Esri World Imagery images were used to investigate the influence of the ancient river planform of the Tigris River on the present setting of the Mosul Lake. The choice of specific dates for Sentinel-2A/2B imagery is based on known operations and discharge variations for 2016, 2019, and 2020, as they were used for detecting seasonal fluctuations of lake shorelines controlled by variations in the discharge of the Tigris and seasonal dam operations. We reconstructed the discharge for the Tigris River ca. 20 years before the start of the construction of the dam, namely for the period between December 1967 and August 1968 (declassified Corona satellite imagery). The same was done for the period between 1984 and 1986 during the filling steps of the basin (Landsat imagery). Remote sensed images were projected in the UTM Zone 38 reference system and used as the background for remote observations in QGIS 3.16 software. Also, Digital Elevation Model (DEM) MERIT with 3 arcsec horizontal resolution (~90 m at the equator) was projected in the UTM Zone 38 and used to extrapolate the Tigris and tributaries watershed (Yamazaki et al., 2017). The geological bedrock and main linear structural features were extracted from the of Al-Mosul Quadrangle geological map (1:250,000) of the Series of the Geological Map of Iraq (Ministry of Industry and Minerals, Iraq Geological Survey, 1995; 1997; 2014) and from the Tectonic Map of Iraq (Fouad, 2012); additional structural data come from Al-Saigh (2008), Al-Dabbagh & Al-Naqib (2009), and Sissakian et al. (2018).

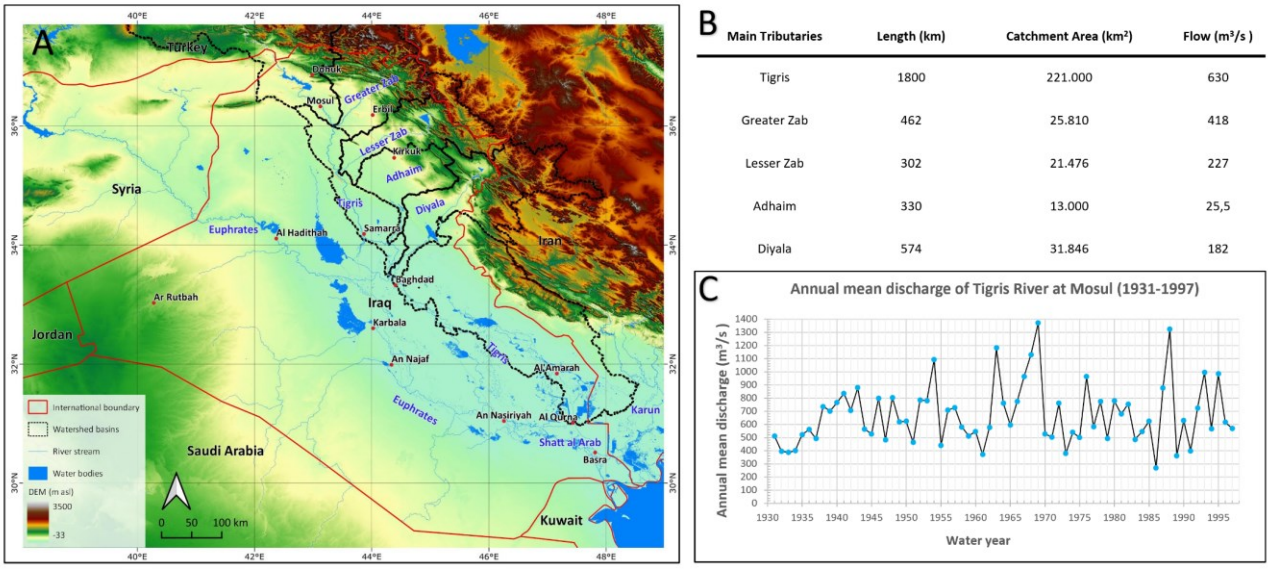


**Figure 3.** (A) Iraqi watershed basin of the Tigris River and its main tributaries extrapolated and superimposed on a MERIT DEM. (B) Information about length, catchment area and mean flow of the Tigris River and its major tributaries (Al-Ansari, 2013; Al-Ansari & Knutsson, 2011; ESCWA, 2013). (C) Annual mean discharge of the Tigris River at the Mosul stream gauge derived from the USGS database (Saleh, 2010)


**Figure 4.** Bing Virtual Earth imagery of Mosul Dam site; notice the dam operation and the huge anthropogenic impact on the surrounding landscape.

| Dataset | Name | Period | Ground Resolution | Monthly mean Discharge(m3/s) (MOS) |
|---|---|---|---|---|
| Declassified Corona Image | ds1102-1025df006 | 11/12/1967 | 6 feet | 481,4 |
| Declassified Corona Image | ds1102-1025df007 | 11/12/1967 | 6 feet | |
| Declassified Corona Image | ds1102-1025df008 | 11/12/1967 | 6 feet | |
| Declassified Corona Image | ds1102-1025df010 | 11/12/1967 | 6 feet | |
| Declassified Corona Image | ds1102-1025df015 | 11/12/1967 | 6 feet | |
| Declassified Corona Image | ds1102-1025df016 | 11/12/1967 | 6 feet | |
| Declassified Corona Image | ds1104-2138da003 | 16/08/1968 | 6 feet | 211,6 |
| Declassified Corona Image | ds1104-2138da004 | 16/08/1968 | 6 feet | |
| Declassified Corona Image | ds1104-2138da005 | 16/08/1968 | 6 feet | |
| Declassified Corona Image | ds1104-2138da006 | 16/08/1968 | 6 feet | |
| Declassified Corona Image | ds1104-2138da007 | 16/08/1968 | 6 feet | |
| Landsat 4-5 Thematic Mapper | LT05_L1TP_170034_19840606 | 06/06/1984 | 30 m | 535,4 |
| Landsat 4-5 Thematic Mapper | LT05_L1TP_170035_19840606 | 06/06/1984 | 30m | |
| Landsat 4-5 Thematic Mapper | LT05_L1TP_170034_19840926 | 26/09/1984 | 30 m | 118 |
| Landsat 4-5 Thematic Mapper | LT05_L1TP_170035_19840926 | 26/09/1984 | 30 m | |
| Landsat 4-5 Thematic Mapper | LT05_L1TP_170034_19841012 | 12/10/1984 | 30 m | 191,1 |
| Landsat 4-5 Thematic Mapper | LT05_L1TP_170035_19841231 | 13/12/1984 | 30 m | 659,3 |
| Landsat 4-5 Thematic Mapper | LT05_L1TP_170034_19850116 | 16/01/1985 | 30m | 350,6 |
| Landsat 4-5 Thematic Mapper | LT05_L1TP_170035_19850116 | 16/01/1985 | 30m | |
| Landsat 4-5 Thematic Mapper | LT05_L1GS_170034_19860103 | 03/01/1986 | 30 m | 92,1 |
| Landsat 4-5 Thematic Mapper | LT05_L1GS_170035_19860103 | 03/01/1986 | 30m | |
| Landsat 4-5 Thematic Mapper | LT05_L1TP_170034_19860220 | 20/02/1986 | 30 m | 102,5 |
| Landsat 4-5 Thematic Mapper | LT05_L1TP_170035_19860220 | 20/02/1986 | 30 m | |
| Landsat 4-5 Thematic Mapper | LT05_L1TP_170034_19860815 | 15/05/1986 | 30 m | 553,5 |
| Landsat 4-5 Thematic Mapper | LT05_L1TP_170034_19860628 | 28/06/1986 | 30 m | 503,1 |
| Landsat 4-5 Thematic Mapper | LT05_L1TP_170035_19860628 | 28/06/1986 | 30 m | |
| Landsat 4-5 Thematic Mapper | LT05_L1TP_170035_19860815 | 15/08/1986 | 30 m | 296,5 |
| Sentinel-2 | S2A_OPER_MSI_L1C_TL_MTI__20160308T080055_20160308T115917_A003707_T38SKF_N02_01_01 | 08/03/2016 | 10 m | |
| Sentinel-2 | S2A_OPER_MSI_L1C_TL_MTI__20160308T080055_20160308T115917_A003707_T38SLF_N02_01_01 | 08/03/2016 | 10 m | |
| Sentinel-2 | L1C_T38SKF_A005709_20160726T075850 | 26/07/2016 | 10 m | |
| Sentinel-2 | L1C_T38SLF_A005709_20160726T075850 | 26/07/2016 | 10 m | |
| Sentinel-2 | S2B_MSIL2A_20191106T080029_N0213_R035_T38SKF | 11/08/2019 | 10 m | |
| Sentinel-2 | S2A_MSIL2A_20191108T075131_N0213_R135_T38SLF_ | 11/08/2019 | 10 m | |
| Sentinel-2 | L1C_T38SKF_A024628_20200310T080339 | 10/03/2020 | 10 m | |
| Sentinel-2 | L1C_T38SLF_A024628_20200310T080339 | 10/03/2020 | 10 m | |
| Sentinel-2 | L1C_T37SGA_A026344_20200708T080203 | 08/07/2020 | 10 m | |
| Sentinel-2 | L1C_T37SGA_A026344_20200708T080203 | 08/07/2020 | 10 m | |
| Sentinel-2 | L1C_T38SLF_A026301_20200705T075705 | 08/07/2020 | 10 m | |

**Table 1.** Database of satellite imagery used in this work; the monthly discharge of the Tigris River is reported when available.

## 5.4. Results

### 5.4.1. Geomorphological variability of the Tigris riverscape before the MDL

The comparison between declassified Corona imagery from December 1967 and 1968 revealed several changes in the river planform, including variations in the setting of mid-channel and bank-attached landforms. In response to the seasonal variation of discharge (meant as flow stage), the behaviour of the river, or at least of some of its parts, starts to adjust and re-equilibrate erosional and depositional processes (Figure 5). The relationship between discharge variations and river pattern are strongly connected with the lithological and structural setting in which the Tigris River flows. In the study area, the Tigris River changes between different structural settings, which are ultimately related to the effects of the evolution of the local anticline-syncline system and the Dohuk Fault System. In fact, the anticline-syncline system influenced the ability of the river to cut into the bedrock and thus the width of its valley. Consequently, the Tigris River below the MDL shifts from partly confined to unconfined and the river planform is not homogeneous. Also, these elements impact on the shape and width of the floodplain and its related geomorphic units.

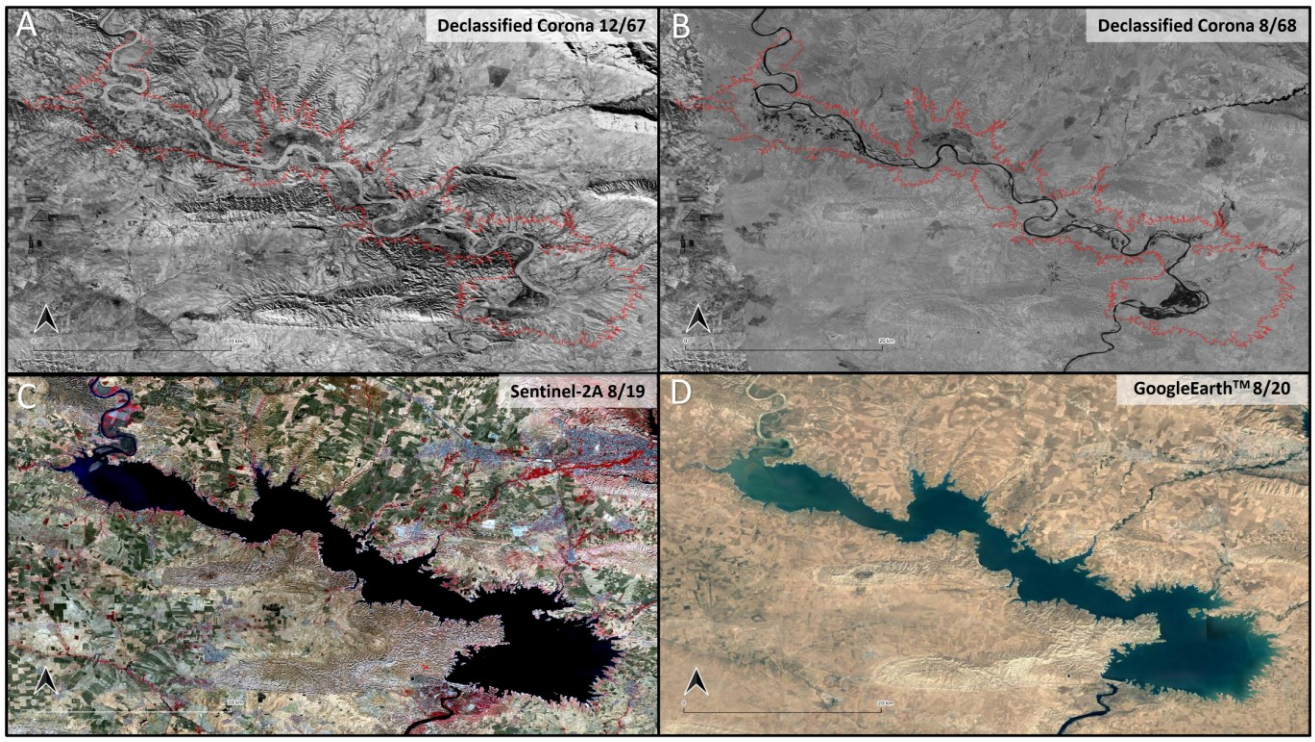


**Figure 5.** (A, B) Declassified Corona satellite images of the ancient Tigris riverscape below the MDL taken in two different phases of discharge. The red line is the current size of the MDL. (C, D) The current shape of the MDL elaborated from Sentinel-2A (false colours) and Google Earth™

### 5.4.2. Geomorphological mapping of the winter season

The declassified Corona imagery taken on 11 December 1967 recorded the Tigris River at its bank full stage. At that time, the monthly mean discharge at streamflow-gaging station of Mosul was 481.40 m3/s. The main recognizable features are fluvial landforms related to the active channel stream point and the mid-longitudinal bars. On the banks of the active channel a sequence of three levels of terraces is visible (T1, T2 and T3, oldest to youngest) (Figure 2C). Some reach banks of the Tigris River show an erosional scarp caused by undercutting and gravity collapse. Floodplains are in the proximity of the sinuous reach of the Tigris River; most of them display active chute channels and meander scars with traces of paleochannels. The latter were exploited for cultivation. Moreover, secondary tributaries are mainly distributed along the left bank of the Tigris; they flow along the erosional pediment that connects the anticline slope to the river (Figure 6). The lithological and structural setting of the bedrock affected the morphodynamics of the Tigris River, but also influenced the other geomorphological processes acting in its proximity. A homogeneous belt of flatirons is visible on anticline hills; minor streams also dissect the hillsides creating badlands upon marls, gypsum, and conglomerate outcrops.

South of the dam site, a landslide body and its denudation surface occur; the curved geometry of the foot of the deposit modifies the course of the Tigris River forcing the development of an irregular meander.

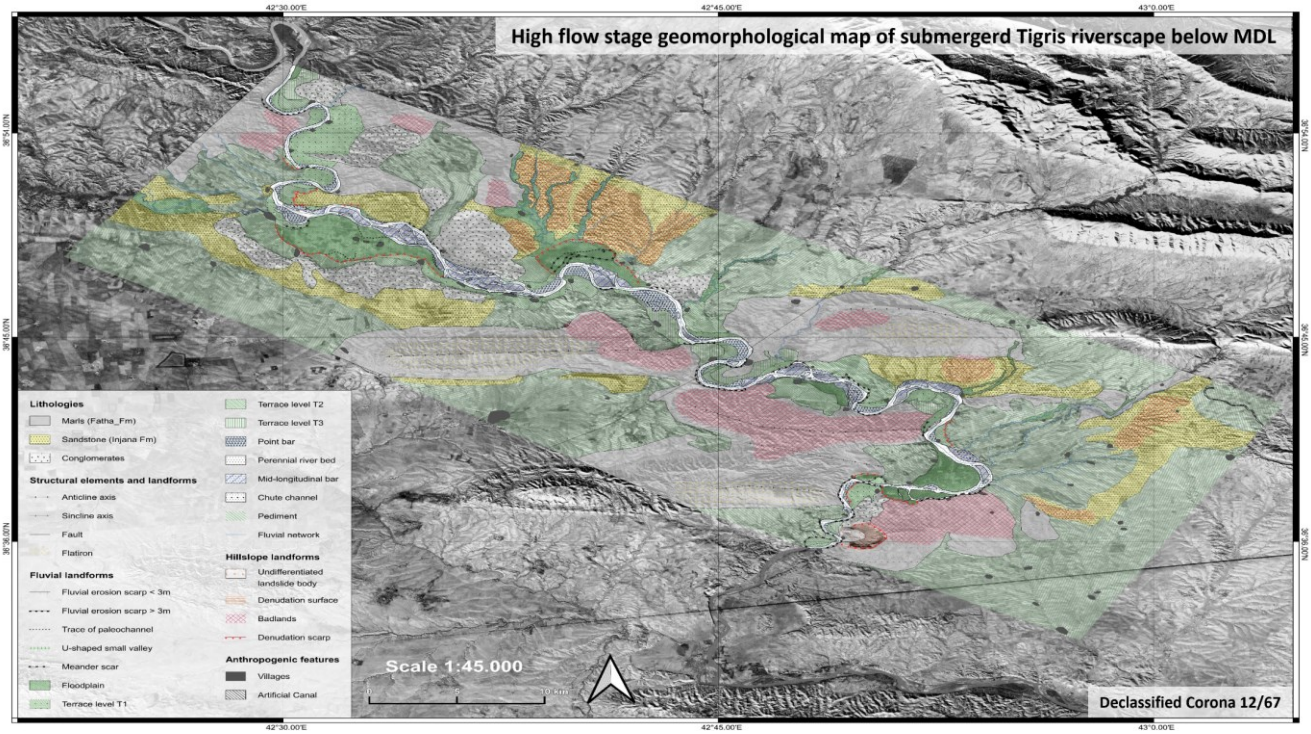


**Figure 6.** Geomorphological map of the ancient Tigris riverscape elaborated on the declassified Corona satellite image during its high-flow stage (December 1968).

### 5.4.3. Geomorphological mapping of the summer season

The declassified Corona images taken on 16 August 1968 capture the Tigris River during a phase of low flow stage. The monthly mean discharge recorded at the streamflow-gaging station of Mosul was 211.60 m3/s. Compared with the winter season, the general landscape of the area does not show evident changes. On the other hand, within and along the main course of the Tigris River visible variations appear. The low water level exposes several mid-channel and bank-attached geomorphic features, which reflect the variety of landforms – and related processes – that changed during the seasonal fluctuation of discharge (Figure 7). The main mid-channel geomorphic units recognized relate to the width of the channel and to the type and shape of the planform in which they developed. In the northern part of map, the river shows a decrease in the number of channels in which it flows. A single channel with low sinuosity and few meanders shifts to a course with multiple meanders and up to three channels. In general, compound and point bars occur on the convex banks of tortuous meander bends (Figure 8A). Bars are covered by ephemeral vegetation with slack water confined in chute channels and in the scours. Downstream, asymmetrical lateral bar, scroll bars, and mainly mid-channel bar units form along the low sinuosity reach (Figure 8B, C). The mid-channel units are

composed by raindrop shaped longitudinal bars, elongated along the direction of the flow, and by diagonal bars, oval to sigmoidal in shape and oriented perpendicularly to the channel banks (Brierley and Fryirs 2013) (Figure 8D, E). Vegetated mid-channel islands are strictly connected to the channel dynamics, reflecting the river storage capacity for sediments (Brierley & Fryirs 2013) (Figure 8E). This is, in turn, related to how processes reshaped the river course before and after flood events: in fact, during its low flow stage the Tigris River displays a multiple channels pattern only where mid-channel islands and compound bars occurred (Figure 8F).

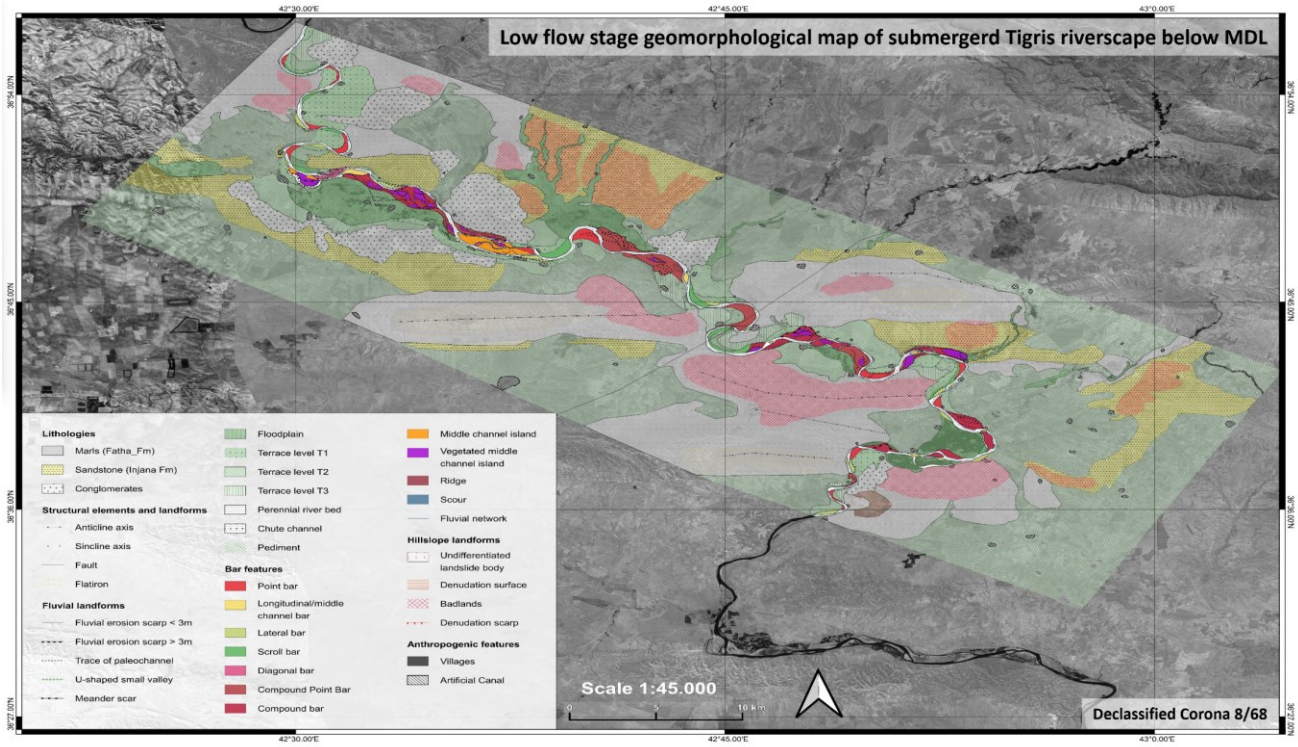


**Figure7.** Geomorphological map of the ancient Tigris riverscape elaborated on the declassified Corona satellite image during its low-flow stage (August 1967).

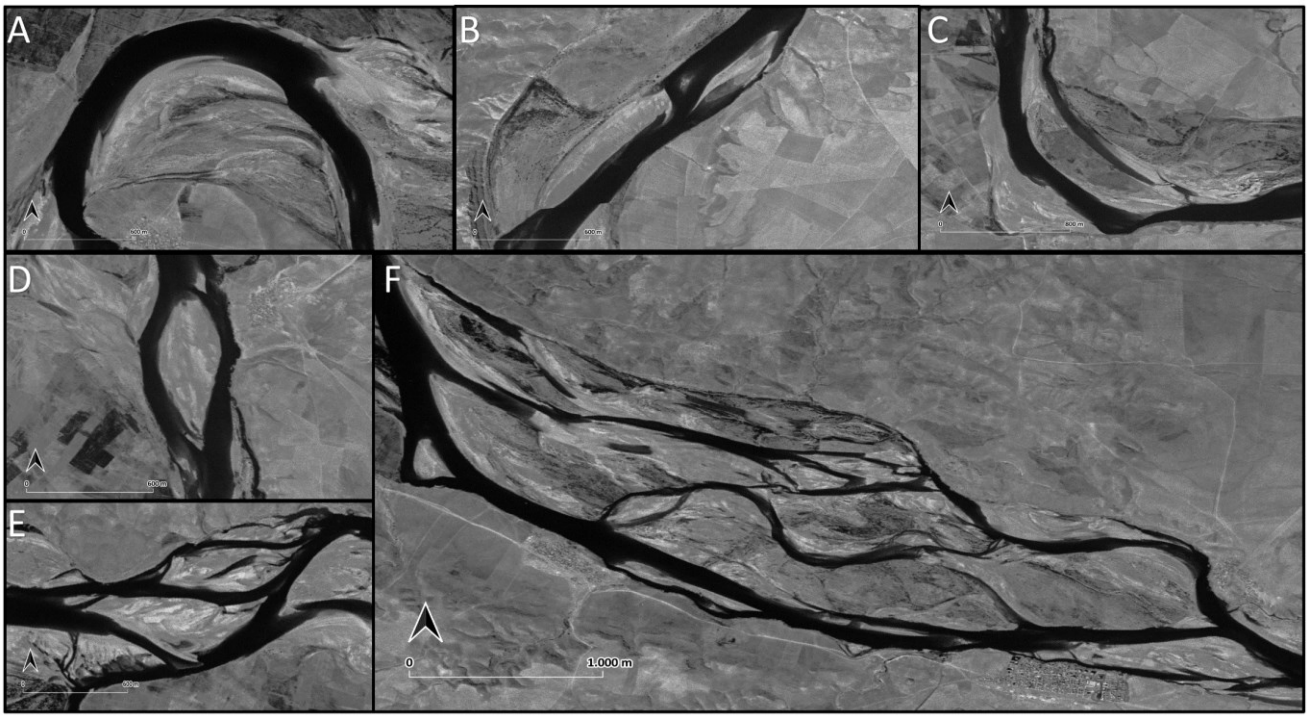


**Figure 8.** Examples of fluvial bars exposed during low-flow stage derived from declassified Corona acquired in August 1967: (A) point bar; (B, C) lateral and scroll bar; (D, E) longitudinal and diagonal bar; (F) plant-covered mid-channel islands.

## 5.5 Factors controlling the Tigris riverbed landscape

Reconstructing the landscape of the Tigris River before the filling of the Mosul Dam reservoir revealed the main factors that influenced the pattern and planform of channels over time. The different effects of lithology, geological structure and river behaviour allow to divide the area into three zones: upstream, middle-stream and downstream. These are treated separately to better expose the influence of each factor on the diversity of channel shapes.

### 5.5.1 Upstream lithological controls

The upstream river planform of the Tigris River is ca. 43 km long and different river planforms are visible during the bankfull (1967) and low flow stages (1968) (Figure 9A). From NW towards SE the Tigris River changes its sinuosity. The first portion of the stream is characterised by tortuous meanders with small point bars and two/three terrace levels; small floodplain pocket can also sometimes develop when the river course is partly confined inside a narrow valley. Afterwards, the number of channels increases, and the river setting shifts from a wandering to an anabranching gravel bed according to the flow stage (Figure 9B, C). A wide floodplain with meander scars, chute channels, paleochannels, and superimposed agricultural fields characterizes the right bank. On the 1967 Corona image, this part of the river shows a pathway of flood channels active during high discharge events. The shape of mid-channel and bank attached geomorphic units varies in both 1967 and 1968. In this

portion, the major constrain on the Tigris River dynamic is the lithological change of the bedrock from the marls and sandstones of the Injana and Fatha formations to the Plio-Pleistocene conglomerates (Figure 9D). The latter increases the size of the bed material with coarse grained sand and pebbles. These materials form river islands, flooded during high discharge flows and exposed and covered by vegetation in the low flow stage. The island plant cover ensures the stability of each bar: while the action of erosional and depositional processes can modify their shape with time, they never shift from their original location.

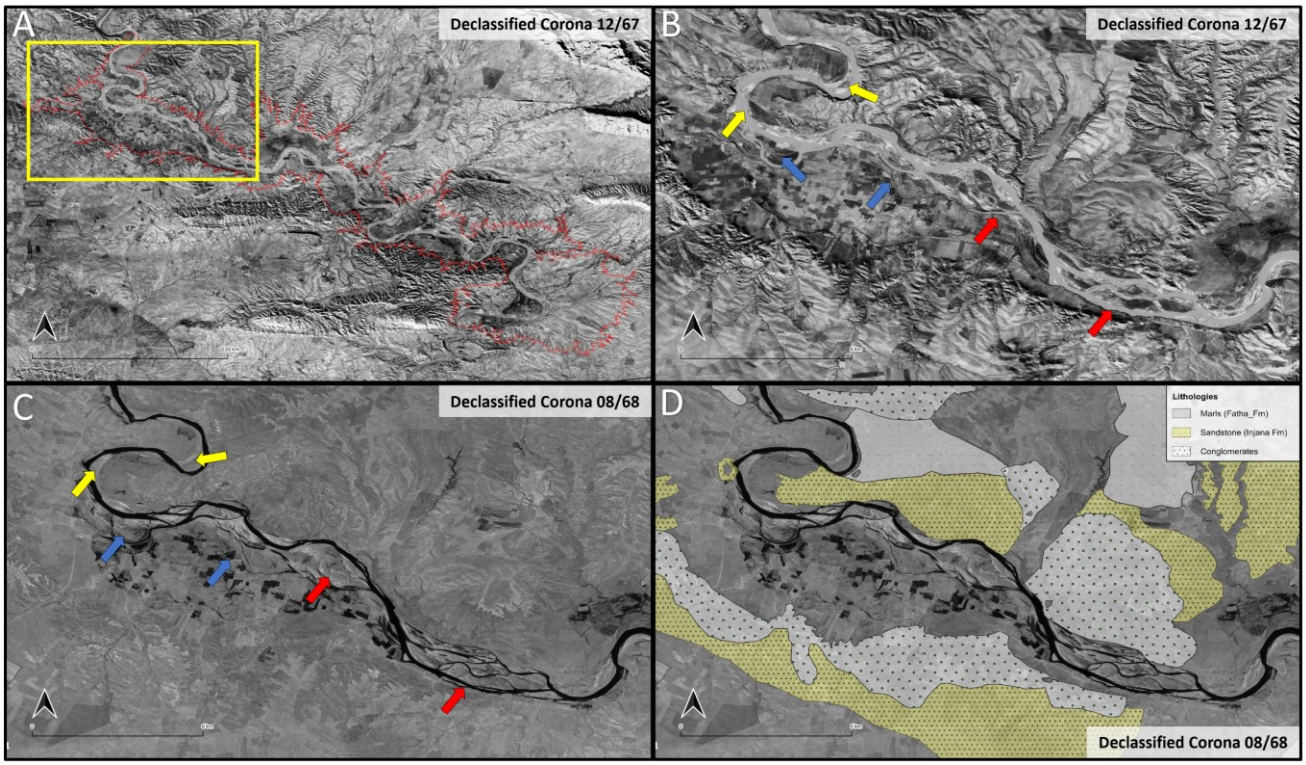


**Figure 9.** Details from the upstream sector of the river. (A) Position of the area along the Tigris River. Examples from the (B) winter and (C) summer season of the Tigris riverbed; along the northwestern part appear tortuous meanders with small point bars (yellow arrows); then, the number of channels increases, and according to flow stage this sector shifts from wandering to anabranching with gravel bed (red arrows). The right bank hosts a large floodplain with several small fluvial features (blue arrows). (D) Lithological map of this part of the Tigris River catchment highlighting the main rock formations.

### 5.5.2. Middle-stream channel shape change

The middle-stream is 45 km long and is characterized by a decrease of the braiding degree and a correspondent increase in sinuosity of the channel planform (Figure 10A). The uppermost part of this section follows a meandering pattern with point bars migrating northwards. More downstream, the low sinuosity reach hosts a small pocket floodplain with bank attached and mid-channel geomorphic features such as longitudinal, lateral, and compound bars. Afterwards, two tortuous meanders develop in a confined to partly confined valley; here are visible a compound point bar and an encased convex

bend with a scroll bar in the concave zone. In the lowest portion, the river planform changes into an irregular straight planform with lateral bars in the bankfull stage attached at the riverbanks during low flow stage (Figure 10B, C). The evolution of this part of the river was influenced by the structure of the anticline ridges of Ain Zala, Ravan, and Zainaiyat and by the effects of Dohuk Fault System driving the development of encased meanders into the marl bedrock of the Fatha Formation (Figure 10D).

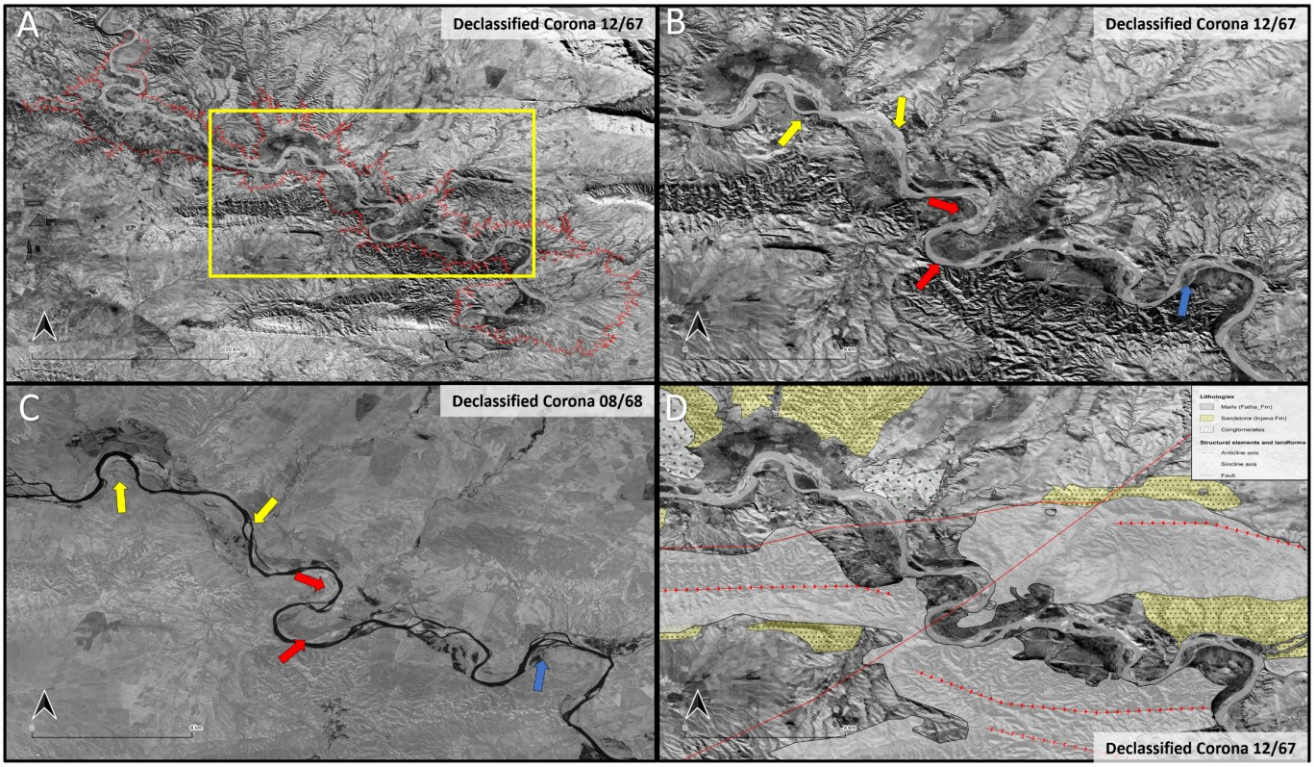


**Figure 10.** Details from the middle-stream sector of the river. (A) Position of the area along the Tigris River. Examples from the (B) winter and (C) summer season of the Tigris riverbed showing a low sinuosity with longitudinal, lateral and compound bars (yellow arrows). Afterwards, two tortuous meanders develop a point bar in the convex bend and a scroll bar in the concave zone (red arrows). In the lowest portion of the area, the river changes into an irregular straight planform with lateral bars (blue arrow). (D) Lithological and structural map of this part of the Tigris River catchment highlighting the litho-structural influence on the fluvial dynamic.

### 5.5.3. Downstream and Dam site diversity

The downstream portion of the Tigris River occupies the last 20 km before the dam site. The river follows a tortuous planform flowing in a partly confined valley setting; wide floodplains form in the inner bend of two meanders and along the left bank of the last straight part of river before the dam site (Figure 11A). At the low flow stage, lateral bars and compound bars with point bars occur. A series of floodchannels and a wide floodplain occupied by cultivations is visible in the inner part of the point bar, located in the last meander. The floodplain before the dam site is crossed by secondary little branches of the Tigris. During bankfull flow stage, such geomorphic features are submerged and

affected by erosional and depositional processes which change their shape and dimensions (Figure 11B, C).

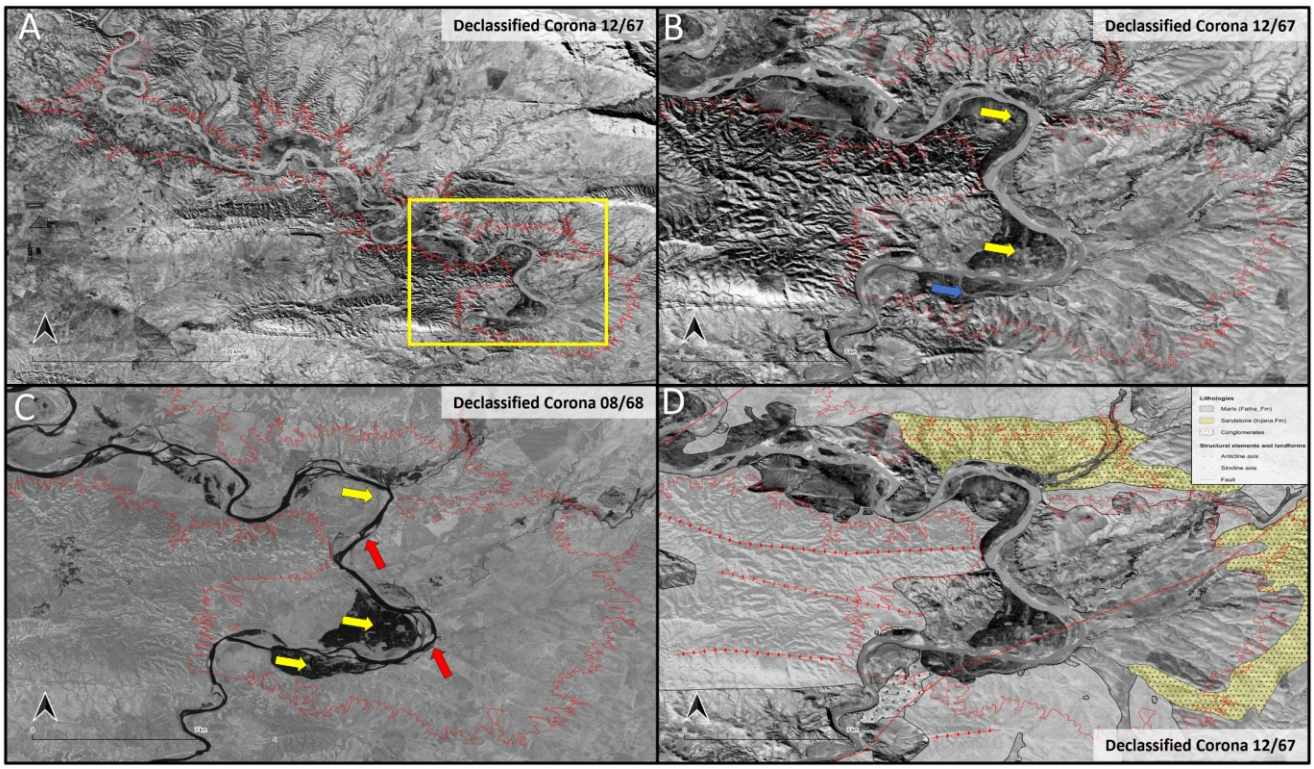


**Figure 11.** Details from the downstream sector of the river. (A) Position of the area along the Tigris River. Examples from the (B) winter and (C) summer season of the Tigris riverbed. In this portion the river shows a tortuous planform with wide floodplains in the inner bend (yellow arrows). At the low-flow stage, lateral bars and compound bars with point bars are exposed (red arrows). The floodplain located before the dam site is crossed by small secondary branches of the Tigris (blue arrow). Lithological and structural map of this part of the Tigris River catchment highlighting the influence of the anticline/syncline system and lithology on the fluvial dynamic.

### 5.5.4. Examples of variations of riverbed and mid-channel to bank-attached geomorphic features

The comparison between declassified Corona images reveals differences in the behaviour of the Tigris River planform and its related geomorphological features. Two examples from the upstream portion help in explaining how the Tigris channel belt adjusted to seasonal discharge fluctuations.

In the first example, the Tigris River flows in a partly confined valley forming a meandering planform; this area is characterized by floodplains and neck cut-offs. In the low flow stage, the meanders are partly interconnected and filled by water (Figure 12A). During the bankfull stage, a large meander is instead connected to the main Tigris River channel, with the formation of an island covered by vegetation and crossed by a flood channel network (Figure 12A).

The second example shows the effect of the switch in planform geometry caused by the transition from a fine- to a coarse-grained channel bedload. There, the seasonal change from bankfull to low flow stage triggered the shift of many channels from wandering to anabranching (Figure 12C, D).

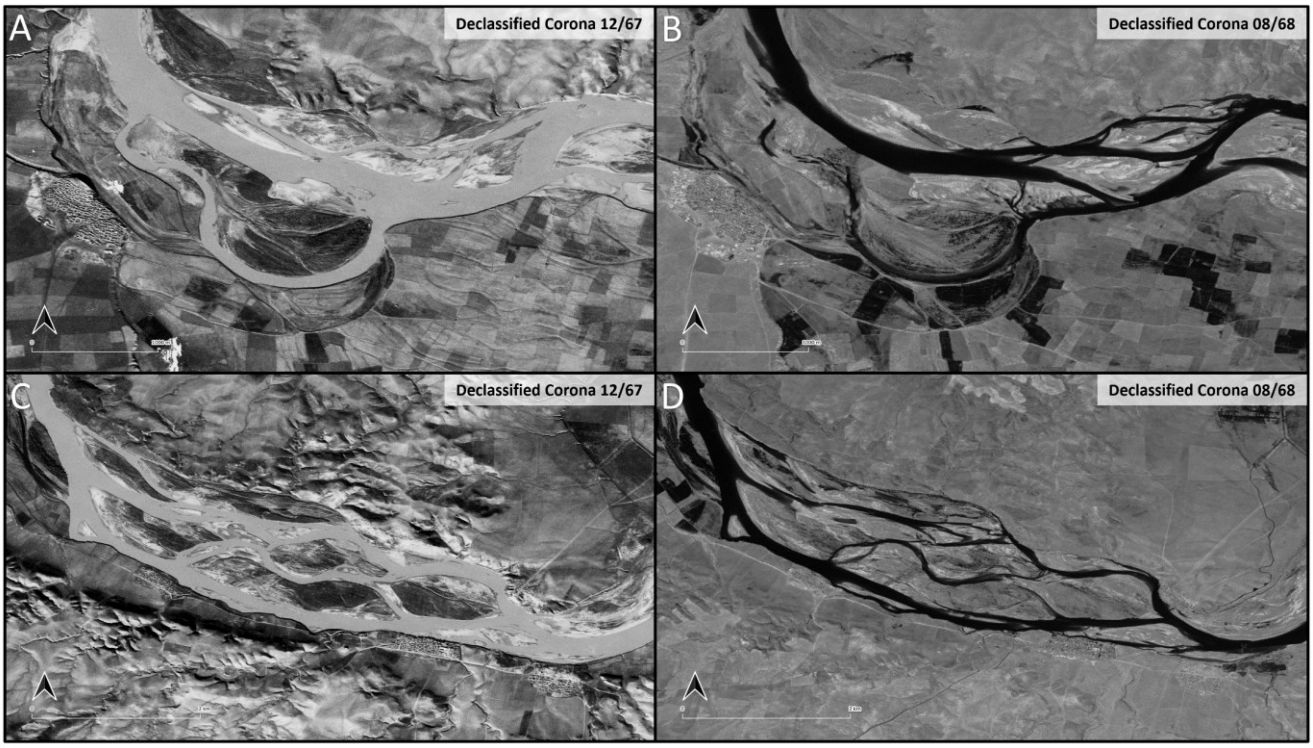


**Figure 12.** Comparison between the high and low stages of the Tigris River. (A) Large meander connected to main Tigris River channel during the bankfull stage with the formation of an island covered by vegetation and crossed by a flood-channel network. (B) In the same position as (A), meandering planform with floodplains and neck cutoff partly interconnected and filled by water during the low-flow stage. (C) Wandering to (D) anabranching seasonal shift of the fluvial planform from the bankfull to the low-flow stage.

## 5.6. The filling of the Mosul Dam reservoir (1984–1986)

The filling phases of the Mosul Dam reservoir are reconstructed through the comparison of a selection of Landsat images acquired from 1984 to 1986. Such reconstruction reveals the first impact of the barrage operations on the Tigris River. In 1984 and 1985, the Tigris River was progressively dammed with an embankment made by a core of silt and clay (Figure 13A–D). At this stage, the shape of the incipient lake in the first area subjected to inundation followed the inherited fluvial landform and valley setting of Tigris River. According to our analysis, the first inundated zones (inundation occurred between the end of 1985 and the beginning of 1986) were the lowlands and the floodplain located near the Mosul Dam site due to the laterally unconfined setting (Figure 13E). Subsequently, upstream migration flooding affected the middle and upstream area, in the meandering and floodplain locations towards NW in partly confined and unconfined valley settings (Figure 13F, G). The final filling of the reservoir took one year, between June 1985 and July 1986 (Figure. 13H, I). The impact on the 1986 annual discharge was important: it was estimated as only 269,88 m3/s, against 546.00 m3/s of 1984, 624,57 m3/s of 1985, and later 877,93 m3/s of 1987 (Saleh, 2010).

The impact of the extremely rapid filling phases of the MDL was not confined on the Tigris riverscape; this event also triggered several changes onto the local morpho-structural setting around

the dam site and the surrounding area. In fact, an increase in local seismic activity was recorded as a swarm of micro-earthquakes between 1986 and 1987; Al-Saigh (2008) suggests that micro-earthquakes were triggered by the large volume of water in the reservoir.

The construction of the dam also affected the aquifers hosted in the bedrock of the dam site increasing the circulation of groundwater in strata of gypsum with breccias (Fatha Fm.). As a result, the rate of karst dissolution of the bedrock increased dramatically. In fact, monitoring surveys of the area after 1985-1986 revealed the development of sinkholes and dolines in proximity of the dam, which also affected the stability of the dam itself (Kelley et al., 2007; Al-Saigh, 2008; Al-Dabbagh & Al-Naqib, 2009).

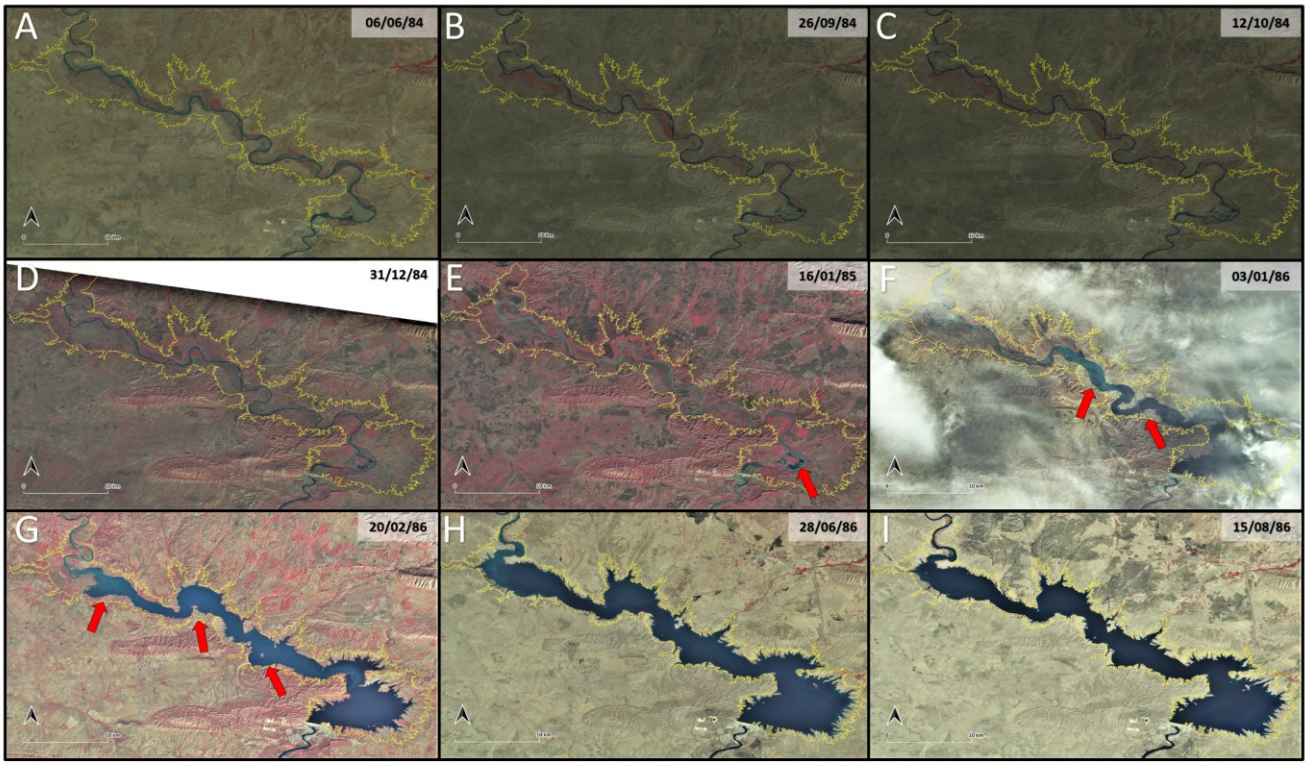


**Figure 13.** Landsat imagery (false colours) acquired during the filling phases of MDL; the yellow line is the present-day mean lake level. (A–D) Gradual embankment of the Tigris River from June to December 1984. (E) Initial inundation along the lateral unconfined setting near the dam site (red arrows). (F, G) Progressive upstream migration of the flooding, showing the inundation of the meandering area and the floodplain in the partly laterally confined valley (red arrows). (H, I) Final stages of filling of the MDL in the summer of 1986; the basin shape corresponds to the current one.

## 5.7. Discussion

### 5.7.1. Variations of the Tigris planform and litho-structural control

The mapping of the seasonal riverscape of the Tigris River obtained from the analysis of winter and summer Corona images allow to reconstruct the behaviour of a part of the river today submerged below the MDL. Our results highlight the litho-structural control over the fluvial pattern and the ability of the river to adjust its course during the low and high flow stages. Seasonal variations of the river discharge switched the processes of sedimentation and erosion, continuously reworking

geomorphological features such as middle and point bars. Our observations suggest that local lithology and tectonic settings are the major factors influencing fluvial dynamics, especially for valley setting, slope evolution, sedimentary budget, and the general flow direction of the Tigris River (Figure 14A). Upstream to downstream, it is possible to observe how the Tigris plan morphology changes according to the constrains imposed by these factors. The upstream area shows a meandering pattern with tortuous meanders switching from wandering (low flow stage) to anabranching (high flow stage) (Figure 12C, D); this pattern corresponds to areas with a bedrock composed mainly by marls and conglomerates (Figure 9D). The river behaviour influences the distribution and organization of bars downstream with the formation of small point and middle bars, and of a gravel bed with transversal bars and plant-covered islands. Further downstream, the shape and flow direction of the middle- and downstream portions are driven by the structure of anticline ridges and the activity of the Dohuk Fault System. Here, the direction and fluvial plan geometry of four distinct reaches clearly follow the strike direction of the anticlines and the Dohuk Fault System (Figure 14B). In the first portion, the Tigris River follows the general direction of the Ain Zala Anticline (Figure 14C); here the position of faults controls the downstream increase in sinuosity of the channel to the development of a tortuous meandering course with point bars (Figure 14D). Afterwards, the occurrence of the Ravan anticline triggers a river planform response, changing into an irregular straight planform with lateral bars; here the Tigris River generally flows parallel to the anticline ridge (Figure 14E). Before the dam, in the downstream portion of the river, the impact of the syncline and of the Dohuk Fault System on the shape, flow direction, and geomorphic dynamics of the Tigris is more evident. When the river reaches the subsidence area related to the syncline, the degree of sinuosity increases. Also, two meanders, a wide floodplain, and fluvial bars in different discharge settings appear (Figure 14F). In the area closest to the dam, the presence of the fault system drives a decrease in sinuosity and a change in the direction of the Tigris flow, that shifts from NW–SE to NE–SW.

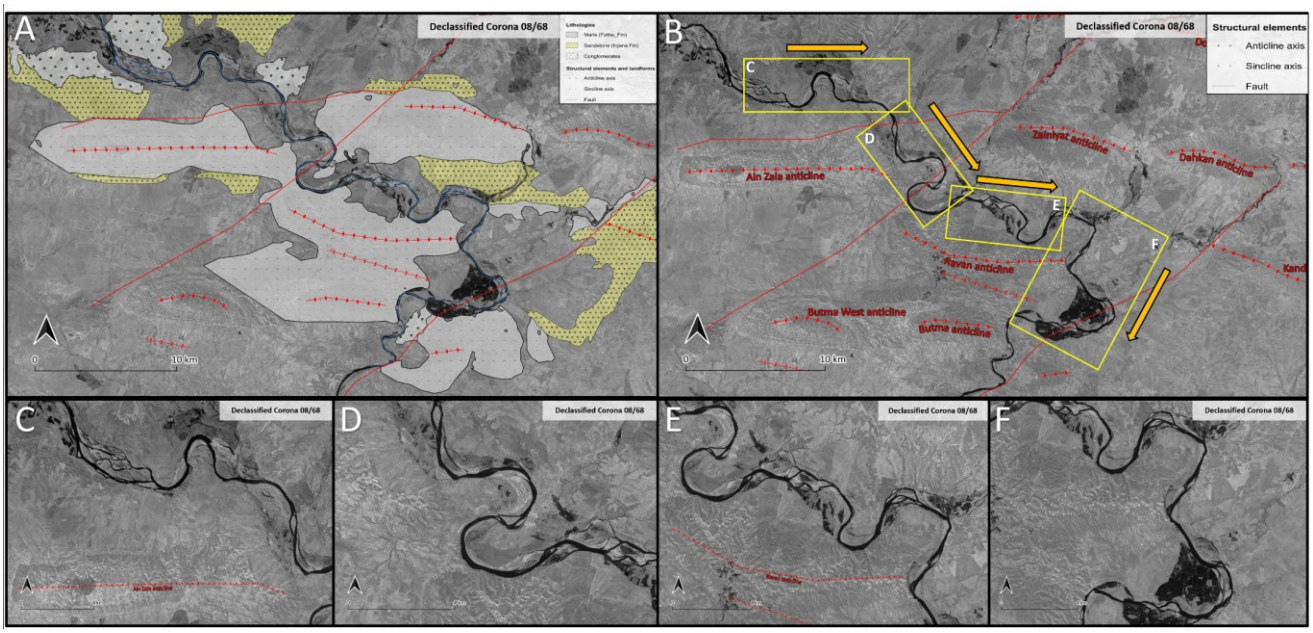


**Figure 14.** (A) Structural and lithological setting of the study area. (B) Division of the Tigris River into four sections corresponding to main planform and flow direction shifts. (C) Particular of the Tigris flowing W–E parallel to the strike direction of the Ain Zala anticline. (D) Tortuous meanders and NW–SE shifting of the Tigris River. (E) Subsequent changes towardsW–E following the growth of the Ravan anticline. (F) Irregular meandering pattern and direction shift towards NE–SW in the downstream portion of the river, due to the combined influence of the Dohuk Fault System and the syncline subsidence.

### 5.7.2 Control of the ancient Tigris riverscape over the shape of the MDL

The actual shape of the MDL reservoir is the result of the interplay between the ancient Tigris riverscape, the litho-structural setting of the area, and the dam post-filling operations (Figure 2A, B). During filling operations, the MDL shoreline varies especially between March and July (Ahmed et al.,2012; Khattab & Merkel, 2014; Khattab et al., 2017; Leabi et al., 2020). Sentinel-2 images in March and July 2016 and 2020 record these variations of lake shorelines, especially in the upstream and downstream portions of the newly formed lake (Figure 15). Shoreline variations are linked to the seasonal discharge of the Tigris as evidenced by data from the Ministry of Water Resources of Iraq (Leabi et al., 2020). Dam operations have a relevant impact on the variations of the lake level; for instance, shorelines periodical change in response to the seasonal drop of lake level permit to recognize some submerged archaeological sites that emerged during phases of seasonal drop of lake level (Titolo, 2021).

In this scenario, the morphology of the MDL appears to be strongly connected with the ancient geomorphological setting of the Tigris (Figure 16A). The morphology and shoreline of the northern area (upstream), relates to the development of the old meander planform with the formation of a huge floodplain with neck and chute cut-off processes in a partly unconfined setting. This framework influences the inlet processes of the Tigris, both during flood events and in low flow stages when a deltaic plain appears (Figure 16B). Afterwards, the narrowing of the lake is due to the same Plio-

Pleistocene conglomerate bedrock which turned the course of the Tigris River from a wandering to anabranching planform with the formation of plant-covered bars.

The central part of the MDL (middle Tigris River stream) is characterized by a partly straight, partly arcuate coastline profile on the right banks. The complex structural setting of this portion strongly influences the lake shape in the same way as it did with the ancient Tigris River, which displayed a semi regular meandering planform in a partly confined setting with the development of compound and middle-longitudinal bars. The connections between the ancient Tigris, the structural setting, and the present lake morphology are visible in the subangular shape of the right banks and in the left tributary derived from the Dohuk Lake and driven by the Dohuk Fault System (Figure 16C).

In the proximity of the dam, the reservoir reaches the maximum surface expansion due to the presence of a wide flat area formed by the interplay between the irregular growth of anticlines and the development of a syncline trough, in which the meandering ancient Tigris River created compound point bars and a floodplain (Figure 16D, Figure 2A).

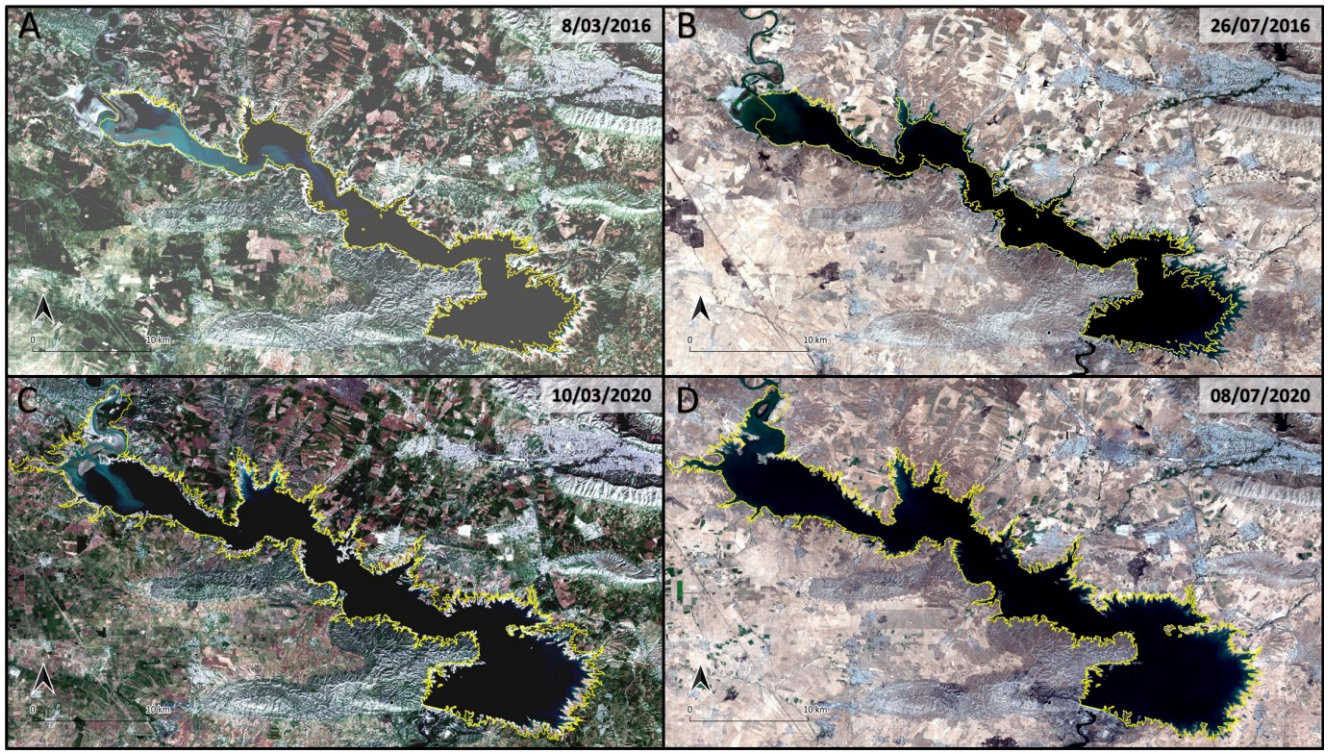


**Figure 15.** Recent dam operations triggering variations of the MDL water level and its shoreline captured by Sentinel-2 satellite imagery (false colours); lake level variations are also controlled by seasonal changes in fluvial discharge. (A, B) March–July 2016; (C, D) March–July 2020.

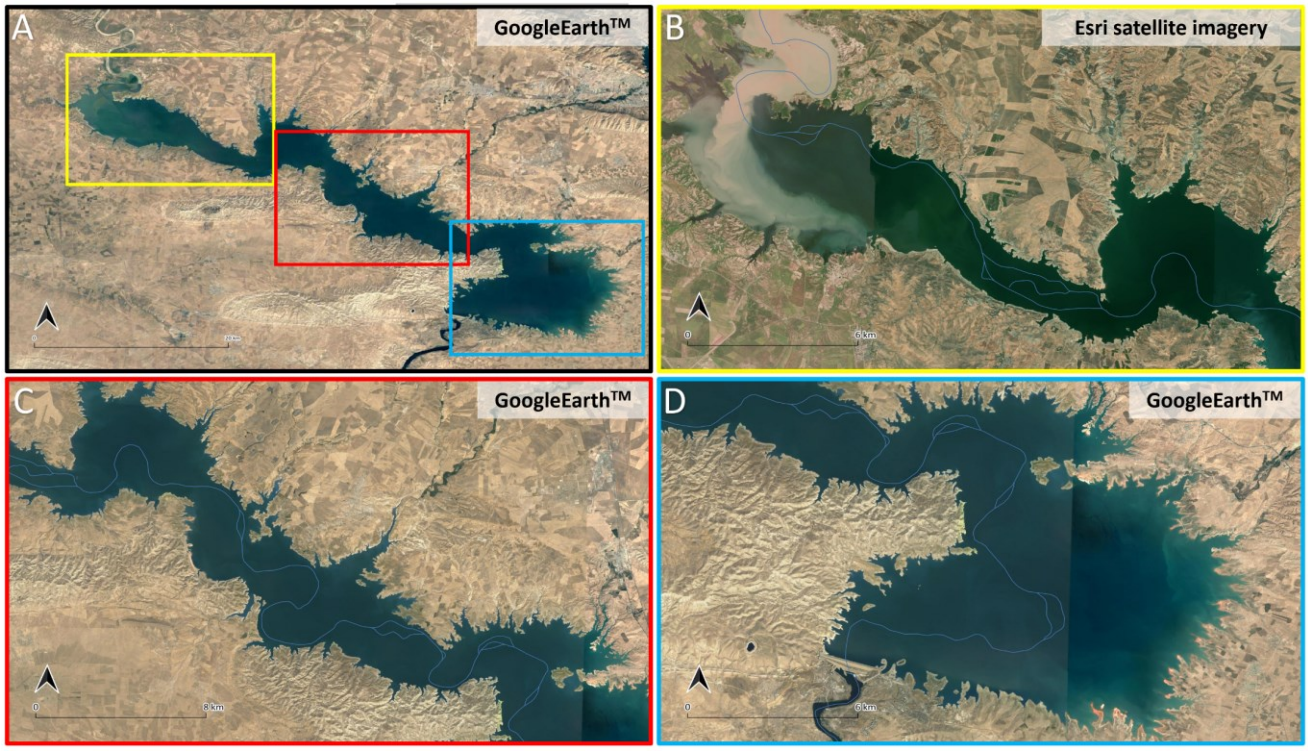


**Figure 16.** A) blue box); the submerged Tigris River stream is outlined in light blue. (B) The overprint of a submerged meander planform controls the aspect of the basin and shoreline in the upstream portion, also influencing the inlet of the Tigris River into the lake; this is highlighted by the curved shape of the deltaic plume. Afterwards, the narrowing of the lake is controlled by the presence of the confined Tigris River valley (canyon) cut into the Plio-Pleistocene conglomerates, indicating a strong lithological control. (C) The central part of the MDL (middle stream) is characterized by a partly straight, partly arcuate coastline profile on the right banks, influenced by the complex structural setting of the area that alternates faults and folds. (D) At the dam site, the reservoir reaches the maximum surface expansion by occupying the wide flat depression produced by the interplay between the syncline/anticline system and the Dohuk Fault System.

## 5.8 Conclusions

The geomorphological investigation of the submerged riverscape of the Tigris River along the MDL permitted to reconstruct the dynamic of the river where it is no longer visible, and to identify the main hydrological and geomorphological changes regulated by seasonal variations of the discharge. Moreover, we were also able to correlate the evolution the Tigris River in response to litho-structural forcing that controlled the size and direction of its course. In fact, variations in the competency of the geological bedrock and the growth of geological structures (faults and folds) resulted in a complex riverscape that – along a relatively short part of the river alternates confined and un-confined valleys, straight and meandering courses, anabranching to wandering settings. The same factors play an indirect control over the shape of the MDL; in fact, we identify an overprint of the submerged Tigris River riverscape on the present-day reservoir that is ultimately related to the major litho-structural forcing factors. In a more general perspective, our approach confirms the reliability of historical declassified intelligence aerial/satellite pictures in geomorphological studies. In fact, historical remote data, as the declassified Corona, have a quite high resolution and, especially, permit to

investigate regions in many cases not accessible and/or where intense urban expansion and human agency have disrupted the natural landforms and altered pristine surface processes, thus reconstructing the pre-anthropogenic geomorphic dynamic. The case study of the MDL is emblematic because the building of the dam and the infilling of the reservoir completely changed the dynamics of natural processes and shrouded pristine landforms. Such example could help in investigating other regions where less invasive events may have impacted the natural systems modifying surface processes and the dynamics of the Earth Critical Zone. The comparison of present geomorphic settings with historical aerial/satellite imagery, as much as the use of historical maps, may reveal in detail the impact of the onset of human agency on landscapes in the last few centuries, shedding light on the effect of the Anthropocene on geomorphic surface processes.

## 5.9 References

Abdulnaby, W. (2019). Structural geology and neotectonics of Iraq, Northwest Zagros. In *Developments in structural geology and tectonics* (Vol. 3, pp. 53-73). Elsevier.

Adamo, N., & Al-Ansari, N. (2016). Mosul dam full story: Safety evaluations of mosul dam. *Journal of Earth Sciences and Geotechnical Engineering*, *6*(3), 185-212.

Al-Ansari, N., Adamo, N., Issa, I., Sissakian, V., & Knutsson, S. (2015). Mystery of Mosul Dam the most dangerous dam in the world: karstification and sinkholes. *Journal of Earth Sciences and Geotechnical Engineering*, *5*(3), 33-45.

Adamo, N., Al-Ansari, N., Sissakian, V., Laue, J., & Knutsson, S. (2019). Mosul Dam: Geology and Safety Concerns. *Journal of Civil Engineering and Architecture*, *13*(3), 151-177.

Al-Ansari, N. (2021). Topography and climate of Iraq. *Journal of Earth Sciences and Geotechnical Engineering*, *11*(2), 1-13.

Al-Ansari, N.A. (2013). Management of Water Resources in Iraq. *Perspectives and Prognoses. Engineering*, 5, 667-668.

Al-Ansari, N., & Knutsson, S. (2011). Toward prudent management of water resources in Iraq. *Journal of Advanced Science and Engineering Research*, *2011*(1), 53-67.

Al-Dabbagh, T. H., & Al-Naqib, S. Q. (1991). Tigris River terrace mapping in northern Iraq and the geotechnical properties of the youngest stage near Dao Al-Qamar village. *Geological Society, London, Engineering Geology Special Publications*, *7*(1), 603-609.

Al-Dabbagh, T. H., & Al-Naqib, S. Q. (2009). The Impact of Some Geologic Structural Elements on Fuse Plug South-eastern Alignment of Mosul Dam. *Iraq Journal of Earth Science*, *9*(2), 27-38.

Al-Khafaji, M. S., & Al-Ameri, R. A. (2021, June). Evaluation of drought indices correlation for drought frequency analysis of the Mosul dam watershed. In *IOP Conference Series: Earth and Environmental Science* (Vol. 779, No. 1, p. 012077). IOP Publishing.

Al-Saigh, N. (2008). Seismicity of Mosul dam reservoir. *Iraqi National Journal of Earth Sciences*, *8*(2), 11-16.

Al-Saigh, N. (2012). Seismicity of Mosul Dam Reservoir for the Monitoring Year 1990. *Iraqi National Journal of Earth Sciences*, *12*(1), 17-22.

Altinbilek, D. (2004). Development and management of the Euphrates–Tigris basin. *International Journal of Water Resources Development*, *20*(1), 15-33.

Alwan, I. A., Karim, H. H., & Aziz, N. A. (2019, May). Agro-climatic zones (ACZ) using climate satellite data in Iraq Republic. In *IOP conference series: Materials Science and Engineering* (Vol. 518, No. 2, p. 022034). IOP Publishing.

Al-Zuhairi, M. F., Al-Jumaily, K. J., & Al-Salihi, A. M. (2016). Characteristics of precipitation systems over Iraq observed by TRMM radar. *American Journal of Engineering Research*, *5*(11), 76-81.

Awchi, T. A., & Kalyana, M. M. (2017). Meteorological drought analysis in northern Iraq using SPI and GIS. *Sustainable Water Resources Management*, *3*(4), 451-463.

Bing Maps. (2021). Bing Maps. [online] Available at: <https://www.bing.com/maps> [Accessed 5 November 2021].

Brierley, G. J., & Fryirs, K. A. (2013). *Geomorphology and river management: applications of the river styles framework*. John Wiley & Sons.

Brown, A. G., Tooth, S., Bullard, J. E., Thomas, D. S., Chiverrell, R. C., Plater, A. J., ... & Aalto, R. (2017). The geomorphology of the Anthropocene: emergence, status and implications. *Earth Surface Processes and Landforms*, *42*(1), 71-90.

Charlton, R. (2007). *Fundamentals of fluvial geomorphology*. Routledge.

Csontos, L., Sasvári, Á, Pocsai, T., Kósa, L., Salae, A. T. & Ali, A. (2012) Structural evolution of the northwestern Zagros, Kurdistan region, Iraq: Implications on oil migration. *GeoArabia*, 17, 81–116.

Dercourt, J., Zonenshain, L. P., Ricou, L. E., Kazmin, V. G., Le Pichon, X., Knipper, A. L., ... & Biju-Duval, B. (1986). Geological evolution of the Tethys belt from the Atlantic to the Pamirs since the Lias. *Tectonophysics*, *123*(1-4), 241-315.

Dollar, E. S. (2004). Fluvial geomorphology. *Progress in physical geography*, *28*(3), 405-450.

Eklund, L., & Seaquist, J. (2015). Meteorological, agricultural and socioeconomic drought in the Duhok Governorate, Iraqi Kurdistan. *Natural Hazards*, *76*(1), 421-441.

ESCWA (Economic and Social Commission for Western Asia),(2013). Inventory of Shared Water Resources in Western Asia. Salim Dabbous Printing Co., Beirut, 626 p

ESRI, (2021) "World Imagery [basemap]. "World Imagery". July 22, 2020. http://www.arcgis.com/home/item.html?id=10df2279f9684e4a9f6a7f08febac2a9 (accessed 11/11/2021).

Forti, L., Perego, A., Brandolini, F., Mariani, G. S., Zebari, M., Nicoll, K., ... & Zerboni, A. (2021). Geomorphology of the northwestern Kurdistan Region of Iraq: landscapes of the Zagros Mountains drained by the Tigris and Great Zab Rivers. *Journal of Maps*, *17*(2), 225-236.

Fouad, S.F. (2007). Tectonic and structural evolution. In: Geology of the western desert. I*raqi journal of geology and mining*, 1, 29–50

Fouad, S.F. (2012) Tectonic Map of Iraq, scale 1:1000000, 3rd edition. *Iraq Geological Survey Publication*s, Baghdad, Iraq.

Gilvear, D., & Bryant, R. (2016). Analysis of remotely sensed data for fluvial geomorphology and river science. *Tools in fluvial geomorphology*, 103-132.

Gurnell, A. M., Peiry, J. L., & Petts, G. E. (2003). Using historical data in fluvial geomorphology. *Tools in fluvial geomorphology*, 77-101.

Hasan, M., Moody, A., Benninger, L., & Hedlund, H. (2019). How war, drought, and dam management impact water supply in the Tigris and Euphrates Rivers. *Ambio*, *48*(3), 264-279.

Jassim, S. Z., & Goff, C. J. (2006). Geology of Iraq, Published by Dolin, Prague and Moravian. *Museum, Brno*.

Kelley, J. R., Wakeley, L. D., Broadfoot, S. W., Pearson, M. L., & McGill, T. E. (2007). Geologic setting of Mosul Dam and its engineering implications.

Khattab, M. F., & Merkel, B. J. (2014). Application of Landsat 5 and Landsat 7 images data for water quality mapping in Mosul Dam Lake, Northern Iraq. *Arabian Journal of Geosciences*, *7*(9), 3557-3573.

Khattab, M. F., Abo, R. K., Al-Muqdadi, S. W., & Merkel, B. J. (2017). Generate reservoir depths mapping by using digital elevation model: a case study of Mosul dam lake, Northern Iraq. *Advances in Remote Sensing*, *6*(3), 161-174.

Koppen, W. (1936). Das geographische system der klimat. *Handbuch der klimatologie*, 46.

Leabi, W. K., Wanas, A. H., Nussrat, T. H., Santiago, L. M., Shukri, Z. A., & AbdulKareem, W. S. (2020, June). Analysis of water flow during the drought and flood seasons case study: The Mosul dam, Iraq. In *IOP Conference Series: Materials Science and Engineering* (Vol. 870, No. 1, p. 012108). IOP Publishing.

Malinowski, J. C. (2002). Iraq: A Geography, Department of Geography & Environmental Engineering, West Point.

Ministry of Water Resources (2006). Board of Expert Report No.1, On Mosul Dam Project. Baghdad, Iraq.

Mouthereau, F., Lacombe, O., & Vergés, J. (2012). Building the Zagros collisional orogen: timing, strain distribution and the dynamics of Arabia/Eurasia plate convergence. *Tectonophysics*, *532*, 27-60.

Othman, A. A., & Gloaguen, R. (2013). River courses affected by landslides and implications for hazard assessment: A high resolution remote sensing case study in NE Iraq–W Iran. *Remote sensing*, *5*(3), 1024-1044.

Perego, A., Zerboni, A., & Cremaschi, M. (2011). Geomorphological Map of the messak settafet and mellet (central Sahara, SW Libya). *Journal of Maps*, *7*(1), 464-475.

Saleh, D. K. (2010). *Stream gage descriptions and streamflow statistics for sites in the Tigris River and Euphrates River basins, Iraq* (Vol. 540). Reston, VA, USA: US Department of the Interior, US Geological Survey.

Salman, S. A., Shahid, S., Ismail, T., Ahmed, K., Chung, E. S., & Wang, X. J. (2019). Characteristics of annual and seasonal trends of rainfall and temperature in Iraq. *Asia-Pacific Journal of Atmospheric Sciences*, *55*(3), 429-438.

Sconzo, P., & Simi, F. (2020). Settlement dynamics on the banks of the upper Tigris, Iraq: The Mosul dam reservoir survey (1980). *Journal of Open Archaeology Data*, *8*.

Sissakian, V. K., & Al-Jibouri, B. S. (2012). Stratigraphy of the low folded zone. *Iraqi Bulletin of Geology and Mining*, (5), 63-132.

Sissakian, V. K., Adamo, N., & Al-Ansari, N. (2020). The role of geological investigations for dam siting: Mosul Dam a Case Study. *Geotechnical and Geological Engineering*, *38*(2), 2085-2096.

Sissakian, V. K., Adamo, N., Al-Ansari, N., Knutsson, S., Laue, J., & Elagely, M. (2018). A comparative study of Mosul and Haditha Dams, Iraq: Geological conditions. *Journal of Earth Sciences and Geotechnical Engineering*, *8*(2), 35-52.

Sissakian, V., Al-Ansari, N., & Knutsson, S. (2014). Karstification effect on the stability of Mosul dam and its assessment, north Iraq. *Engineering*, *6*(2), 84-92.

Sissakian, V. K., & Fouad, S. F. (2012). Geological Map of Iraq, scale 1: 1000 000, 4th edit. *GEOSURV, Baghdad, Iraq*.

Sulaiman, A.H. (2016). Development of probability diagram for an observed annual rainfall in (Duhok and Sartang-Summel) Iraqi Kurdistan. In *The 2nd Scientific Agricultural Conference* (p. 640).

Tarolli, P., Cao, W., Sofia, G., Evans, D., & Ellis, E. C. (2019). From features to fingerprints: A general diagnostic framework for anthropogenic geomorphology. *Progress in Physical Geography: Earth and Environment*, *43*(1), 95-128.

Thorndycraft, V. R., Benito, G., & Gregory, K. J. (2008). Fluvial geomorphology: A perspective on current status and methods. *Geomorphology*, *98*(1-2), 2-12.

Titolo, A. (2021). Use of time-series NDWI to monitor emerging archaeological sites: Case studies from Iraqi artificial reservoirs. *Remote Sensing*, *13*(4), 786.

USGS (1968). Declassified Corona Imaging data. Retrieved from https://corona.cast.uark.edu (accessed 11/08/2020).

Yamazaki, D., Ikeshima, D., Tawatari, R., Yamaguchi, T., O'Loughlin, F., Neal, J. C., ... & Bates, P. D. (2017). A high-accuracy map of global terrain elevations. *Geophysical Research Letters*, *44*(11), 5844-5853.

Zerboni, A., Brandolini, F., Mariani, G. S., Perego, A., Salvatori, S., Usai, D., ... & Williams, M. A. (2021). The Khartoum-Omdurman conurbation: a growing megacity at the confluence of the Blue and White Nile Rivers. *Journal of Maps*, *17*(4), 227-240.

# Chapter 6
# Geomorphological assessment of the preservation of archaeological tell sites

## 6.1 Introduction

The formation, evolution, and preservation of archaeological landscapes and sites are ruled out by the interaction between natural surface processes of weathering, erosion and sedimentation, and human agency (Wilkinson, 2003). The latter include the ability of human groups of exploiting natural resources, coping with climate and environmental changes, and actively modifying natural landscapes, for instance modulating the intensity of surface processes, promoting the onset of anthropogenic geomorphological processes, building anthropogenic landforms (Wilkinson,2003). Looking at the Holocene, the evolution of cultural landscapes lasted for several millennia, and the result is a palimpsest of natural and human-related landforms and deposits that formed under different environmental settings and as a response to changes in settlement types, land use, and subsistence strategies (Goudie & Viles, 2006; Tarolli & Sofia, 2016; Biagetti et al., 2017; Nicoll & Zerboni, 2020) and deeply modified pristine environments.

Today, some of the processes – natural and artificial – in charge of the formation of archaeological landscapes and anthropogenic landforms may have been changed and new ones are involved in the dismantling or obscuring of the archaeological record (from site to landscape) due to erosion, over sedimentation, bioturbation (especially considering human as active agent), and intentional removal (Goudie & Viles, 2006; Tarolli et al., 2019). Such processes greatly threaten the preservation of archaeological sites (and in general of the cultural heritage) and hamper our ability in investigating past cultural dynamics. Geomorphology and geoarchaeology offer specific tools to explore archaeological sites and anthropogenic landforms and distinguish the origin of formative processes, evaluate the extant state of preservation of heritage, and thus plan scientific investigation. Moreover, such approach also allows to identify potential geomorphological risks and propose strategies for risk mitigation. Among others, soil erosion is one of the most significant environmental threats for the conservation of landforms as much as archaeological sites and monuments, especially in arid and semi-arid regions (Kirby & Kirby,1976; Davidson, 1986; Rosen, 1986; Agapiou, 2020; Costanzo et al.,2022). Recently, several models have been developed to estimate the rate of soil erosion, and among the others the Revised Universal Soil Loss Equation (RUSLE) has become the most adopted in a variety of environmental settings and at varying scales (Barton, Ullah & Mitasova, 2010; Howland et al., 2018; Agapiou, et al., 2020; Ames et al., 2020; Guiney et al., 2021; Papageorgiou &

Hadjimitsis, 2021). The same model can be applied to archaeological soils and human-made landforms. In this chapter, we propose a procedure for the geomorphological assessment of the potential risk for soil erosion on cultural heritage based on the investigation on two multiperiod tell-sites (tell means mound, sensu Rosen, 1986) in the Kurdistan Region of Iraq (KRI) – Tell Helawa and Tell Aliawa –, whose stratigraphy spans from the pre-Halaf phase (ca. 7th millennium BC) to the Early Islamic period (VII cent. AD) (Peyronel et al., 2019; Peyronel & Vacca, 2020). We carried out detailed archaeological and geomorphological survey coupled with the use of high-resolution UAV images and derived photogrammetric 3D models of each site to elaborate a digital surface model (DSM) employed to elaborate a RUSLE model for the two sites. This approach allows us to assess the rate of ongoing soil/sediment erosion affecting anthropogenic mounds, to reconstruct the evolution of the two tells, and identifying the major natural and human-driven ongoing processes threatening their preservation. We argue that the RUSLE model efficiently describes ongoing erosional processes along tell sites and offers a potential tool to identify geomorphological risks on archaeological sites. Moreover, this approach can be replicated at the regional scale, thus permitting to plan mitigation strategies to preserve endangered cultural heritage.

## 6.2 The study area and the two sites

The study area is in the Kurdistan Region of Iraq (KRI) within the Erbil Governorate (Figure 1A), along the Foothills Zone of the morphotectonic region related to the structuration of the Zagros orogen (Berberian, 1995; Fouad, 2015; Jassim & Goff, 2006; Zebari et al., 2019, Forti et al., 2021). Helawa and Aliawa are two multi-layered anthropogenic mounds located ca 28 km SW of Erbil, at the foothills of the Khormala Anticline (Figure 1). The tells arise along a wide flat flood plain, characterized by a reddish silty clay to clay deposit, corresponding to the Chai Kurdara (meaning Kurdara River) alluvial plain, which is a left tributary of the Great Zab River. The plain is dissected by two SE–NE-oriented tributaries of the Chai Kurdara and today exploited for agriculture and grazing purposes (Figure 1B-C). Climatic data from the computational models available for Erbil suggest a semi-arid to temperate warm climate with an average annual rainfall around 400 mm/y and temperatures ranging from -2 to 38 °C. Winters are wet and cold, concentrating the 90% of the annual rainfall between December and March; summers are dry and warm to extremely hot (Kramer et al., 1998; Harris et al., 2020). Few paleoclimatic data are available to reconstruct local Late Quaternary environmental changes. Most of data are derived from stable isotopes analysis on speleothems and lake deposits and recorded several climate fluctuations happened after the Last Glacial Maximum.

Hydroclimatic proxies from the Eastern Mediterranean recorded a shift from the cold and dried condition of the Younger Dryas (13-11,7 ka BP) towards warmer/wetter conditions in Early Holocene (11,7-8,5 ka BP), followed by a progressive increase of aridity in the Middle and Late Holocene (Stevens et al., 2006; Flohr et al., 2017; Marsh et al., 2018; Altaweel et al., 2019; Carolin et al., 2019; Roberts et al., 2019; Tudryn et al., 2021). Increased aridity potentially increased soil degradation and enhanced soil erosion (Prăvălie, 2021). In south-western Asia especially, tell-sites are one of the major anthropogenic features rising from the surrounding flat area and representing an example of Holocene anthropogenic landforms. Multi-period mounds are confined raised accumulations of multiple archaeological layers of building levels and wastes, which grew up through time due to stationary occupation of the site and subsequent phases of in-situ buildings decay (Butzer, 1982; Rosen, 1986; Wilkinson, 2003). The Erbil Plain is a densely settled and human-modified landscape with hundreds of archaeological sites, including tells, identified by means of extensive survey coverage carried out by the EPAS Expedition of the University of Harvard over the last decade (Ur, et al. 2013, 2021). Targeted ongoing excavations at different sites are also providing a reliable chronological scheme for the reconstruction of human occupation and landscape exploitation through time (Peyronel &Vacca, 2020; Ur, 2021; Palermo, 2022). Among the others, the multi-period mounds of Tell Helawa and Aliawa are noteworthy anthropogenic features, investigated since 2013 by the MAIPE Archaeological Project of the University of Milan. The two sites together allow to reconstruct a long occupational sequence spanning from the prehistoric period to the Islamic age (Peyronel et al., 2019). In fact, Helawa (Figure1B) shows a mainly pre- and proto-historic archaeological sequence dating from the pre-Halaf to the Late Chalcolithic 3 (7000–3600 BCE), followed by a period of abandonment and a short-term re-occupation during the early Late Bronze Age (1550-1400 BCE). The site of Aliawa (Figure 1C) is instead probably occupied during the Ubaid period (5300–4500 BCE) and extensively settled during the Early to Late Bronze Age (3000¬1200 BCE), as well as from the Iron Age (1200-550 BCE) until the Hellenistic/Seleucid and Parthian periods (late 4th-2nd century CE) with the latest settlement dated to the Late Islamic period.

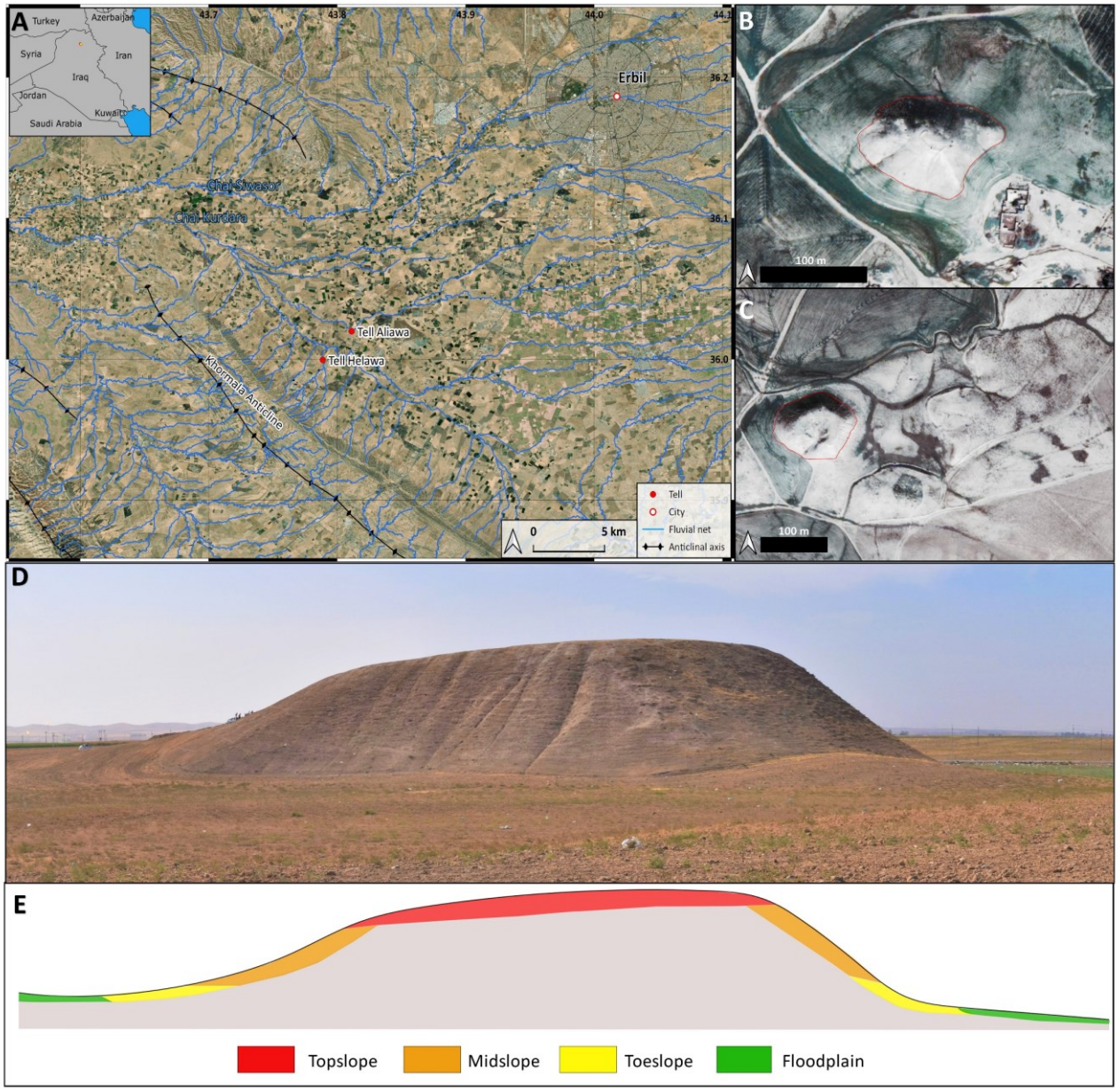


**Figure 1.** (A) GoogleEarth™ satellite imagery of the Erbil Plain crossed by a complex hydrographic network. (B) World View Imagery (12 March 2011) of Tell Helawa (red line indicates the mounds). (C) World View Imagery (12 March 2011) of Aliawa multiperiod mounds (red line indicates the main mound). (D-E) Theoretical model not to scale (based on the main mound of Tell Aliawa) illustrating the different topographic areas of a tell as discussed in the text.

## 6.3 Methods

### 6.3.1 Remote sensing and geomorphological mapping

High resolution geomorphological and archaeological mapping of Helawa and Aliawa has been performed both on the field and from remote sensing (Vacca et al., 2020; Peyronel & Vacca, 2020). In fall 2021, we acquired aerial pictures of the two areas performing a detailed UAV fly at 30 m above

the mounds; additionally, several nadiral photos of the sites and their surroundings were taken to obtain a detailed and updated topography of the two sites. High resolution 3D digital models of archaeological sites and features are commonly used in geo-archaeological research and elaborated starting from ground-acquired information (e.g., with laser scanner) and airborne data, as the LiDAR ones (Parcack, 2009; Sărășan et al., 2020; Altawell et al., 2022). Lacking such facilities, as in the study region, the application of photogrammetry based on the use of small and low-cost UAVs equipped with commercial cameras is becoming common practice (Brandolini et al., 2020); and the same methods are increasingly adopted in geomorphology (Cook, 2017). This approach permits to gather high-definition pictures useful to elaborate photogrammetric models of archaeological sites (Fernández-Hernandez et al., 2015; Abate et al., 2021). In archaeology, such reconstructions represent a tool to assess the shape and extension of sites and to measure the surface distribution of archaeological materials and features (Malinverni et al., 2016; Herrmann et al.,2018). Yet, only occasionally photogrammetric models have been applied to assess past and ongoing geomorphological processes affecting the archaeological record (Rinaudo et al., 2012; Stek, 2016 Jorayev et al., 2016; Lazzari, 2017;). In our case, the high-resolution mapping of the two tells was performed using an UAV DJI Phantom 4 with a flight at 30 m above the mounds and several nadiral photos taken to obtain a detailed and updated topography of the two sites. More than 149 photos were taken for the site of Helawa and 235 for Aliawa to achieve a 60% overlap, they were taken in regular parallel movements to reduce data loss. The images are at a 72-dpi resolution with 12000 pixels. Oblique aerial photos were imported and processed into Agisoft Metashape Professional (Version 1.5.5) with the standard workflow that includes photo alignment, built of dense cloud and mesh to produce a 3D model of the two sites with the extrapolation of Digital Surface Model (DSM). Afterwards, DSMs were imported in QGIS (QGIS Development Team 2021), and a hillshade model with contour lines at 1 and 0.5 m and a classification of streams were generated. High resolution geomorphological and archaeological mapping of Helawa and Aliawa has been performed both on the field and from remote sensing (Osellini et al., 2022), based on the observation of WorldView2 (acquired 12 March 2011) and Google Satellite Imagery for basemap visualized through "QuickMapServices" plugin on QGIS (NextGis 2021). For sake of clarity, a topographic theoretical model of tell topography is represented in Figure 2, reporting on the major parts of a tell and explaining the terminology here adopted: the uppermost part of a tell is the topslope, its middle part is the midslope, and the lowermost sector of the mound, connecting the tell with the surrounding floodplain, is the toeslope (Figure 1D-E).

### 6.3.2 Soil erosion modelling

To estimate long to term average annual soil loss and to map erosion hazard at Helawa and Aliawa a RUSLE empirical model was developed. RUSLE's elaboration requires five different factors describing the environmental settings of the region of interest and is based on the equation (1):

$$A = R \times K \times LS \times C \times P \qquad (1)$$

where R is the rainfall erosivity, K the soil erodibility, LS is the slope-length topographic factor, C and P represents the land cover and land management variables respectively, and A is the resulting average annual erosion rate measured in tonnes/hectare/year. Several methods have been developed in the last decades to calculate the five RUSLE factors ( Ghosal and Das Bhattacharya, 2020).

The R factor [MJ mm ha-1 h-1 year-1] represents the impact of rainfall that causes soil erosion (Wischmeier and Smith, 1978), and in this research, it was defined according to the formula (2) proposed by ( Arnoldus et al., 1980; Renard & Freimund, 1994):

$$R = 0{,}048380 * P\text{^}1.610 \qquad (2)$$

where P is the mean annual precipitation rate. This method has been demonstrated particularly effective in areas where P<850 mm/year ( Howland et al., 2018; Ames et al., 2020). According to CRU TS (Climatic Research Unit gridded Time Series) dataset elaborated Harris et al. (2020) in the study area, the average rainfall is 419.45 mm/year therefore the resulting R factor is 807.556536.

The definition of the Soil Erodibility Factor (K) is derived by the geomorphological processes behind the development of the two tells considered. As suggested by Menze & Ur (2012), tell sites consist of anthrosols, meaning soils that have been deeply modified by human activities (Scudder et al., 1996). In literature, the corresponding K factor value for anthrosols is 0,30 ( Hu et al., 2019). The topographic factor LS can be divided into two separated factors: the slope length L-factor and slope steepness S-factor. The DSM generated with a photogrammetric approach has been employed to calculate the LS factor in GRASS GIS ( GRASS Development Team, 2020) with the *r.uslek* module. The values for the land cover and crop management factor (C) were collected from the literature (see Table 1), while the support practice factor P is not considered (i.e., P = 1) because erosion control measures have never been established in the study area. The resulting RUSLE models were reclassified into five erosional risk categories: minimal (0–10 tonnes/hectare/year), very low (10-30), low (30-60), moderate (60-120), severe (120-150), and extreme (> 150).

| Land Cover Type | C Value | Reference |
|---|---|---|
| Fair Graziland | 0,16 | (Hussein, 1998) |
| Poor Graziland | 0,30 | (Hussein, 1998) |
| Continuos Cropland | 0,50 | (Hussein, 1998) |
| Natural Grassland | 0,0435 | (Panagos et al., 2015) |

**Table 1**. C Factor values considered in this study.

## 6.4 Results: Geomorphological assessment of ongoing processes at tell sites

### 6.4.1 Tell Helawa

The site of Helawa is located near a small village, on the right bank of a watercourse characterized by a low sinuosity that flows around the site and merges into one of the tributaries of Chai Kordara (Figure 1B). The site is a subrounded mound composed of two heights, the highest rising 22m above the floodplain level (top at 332,7 m a.s.l.), and the lowest, located to the north-east of the main one, rising 16 m above the floodplain (top at 326,7m. a.s.l.) (Figure 2A) (Peyronel et al., 2019). The Helawa mound lays along a bend of an ephemeral stream surrounding the tell at the foot of its western and south-western slopes. The geomorphological survey highlights that the N and NE sectors of Helawa are nowadays occupied by cultivated fields, whereas the effects of continuous livestock trampling (pathways) is evident on the western side of the tell (Figure 2B). Channels related to rill-interill and gully erosion are evident along the slopes. Gullies are natural, but occasionally their development is supported by human intervention; a further control over the formation of gullies is played by the topography of several areas of the mound, and specifically by lines of weakness related to the assessment of the mound after subsequent phases of human occupation. Therein, rill-interill and gullies as well as processes related to human and animal agency are the main factors mining the preservation of the archaeological record (Figure 2B). The topographic profile extracted from the DSM (Figure 3A) highlights how slopes have two different shapes based on the topographic gradient. Two sections, one oriented W-E (profile 1-2 in Figure 3) and the second oriented NW-SE (profile 3-4 in Figure 3), show that the southern and south-western sectors of the mound are steeper than the northern and eastern ones and the top of tell is almost flat. The uneven setting of the mound slopes

has consequences on the response to ongoing surface processes, thus differentiating the impact of erosion. In fact, along the S-SW edge of Helawa the rill-interill network carved 4 major gullies, that show an increasing rate of incision from upstream to downstream that is likely mitigated by the decreasing slope gradient (Figs. 3C- 4A-4B). Two major incised gullies, flowing from topslope northwards, are distributed along the gently northern slope. These gullies display a confinement setting with an increased rate of incision downstream that is highest at the toeslope, where the topographic gradient changes. Besides the obvious control of slope gradient, gullies' hydrodynamics along the tell slope is additionally driven by the different land use of each patch of ground: we notice that the shift from herding-related trampling to ploughing modify the rate of incision from the topslope to the toeslope (Figure 4C). The western toeslope is gently connected to the right bank of the low sinuosity stream and displays a sparse grass cover and domestic livestock trackways (Figure 4D). The evaluation of the erosional risk along the tell, based on the analysis of the DSM reveals that only 4 out of 6 identified stream classes (namely, class 3 to 6) are active after heavy rainfall; stream classes develop along the topslopes, toeslopes, and surrounding crop fields. The third and fourth stream classes encompass the shallow rill-interill network, while the fifth and sixth classes include the deep gullies and the uppermost reaches of the stream network (Figure 3C). The land cover (C), indeed, is categorized into 3 different classes: the first is grassland that is partly affected by the grazing of livestock, the second and third classes are the areas deeply affected by grazing and cropping activities (Figure 3D). The ratio between length and slope gradient (LS) displays that the maximum values are in the in southern and northern midslopes and in the proximity of gullies incision, while the minimum are in topslope, toeslope, and in the surrounding floodplain (Figure 3E). Along the northern and southern midslope, the maximum values of LS can be explained considering anthropogenic factors contributing to the shaping the mound, as for instance the substantial levelling, terracing, and building activities occurred during the Ubaid and Late Chalcolithic periods. In fact, archaeological excavations carried out along the southern slope of the mound in Step Trench B (over a N-S total length of 70 m and an E-W width of 4m) allowed documenting a packed sequence of monumental buildings and the generalised use of high, and in some cases relatively narrow, terraces during the Ubaid and Late Chalcolithic 1-3 (Vacca et al., 2020). Such terracing activities greatly contributed driving the actual shape of the tell and modulating the topographic control over erosion.

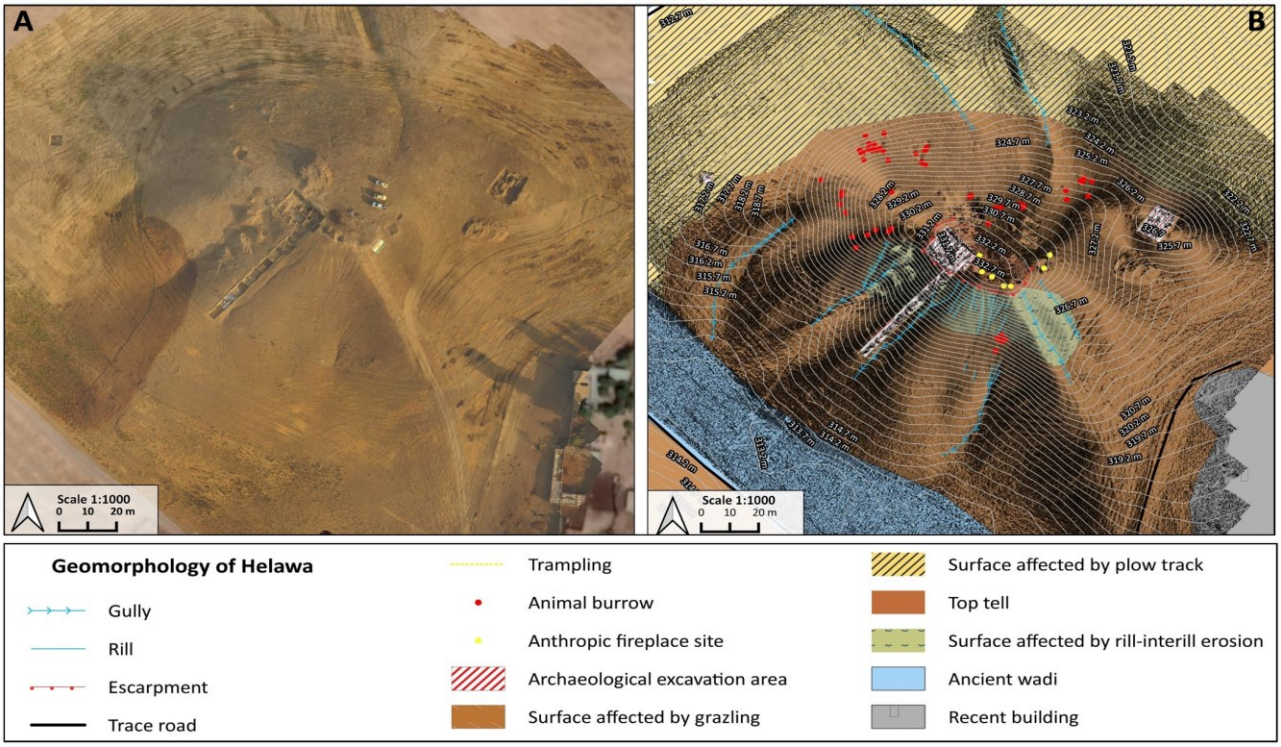


**Figure 2.** Geomorphological mapping of Tell Helawa. (A) Orthophoto of the tell elaborated from the UAV pictures. (B) Detailed geomorphological map of the tell illustrating the main landforms and active processes.

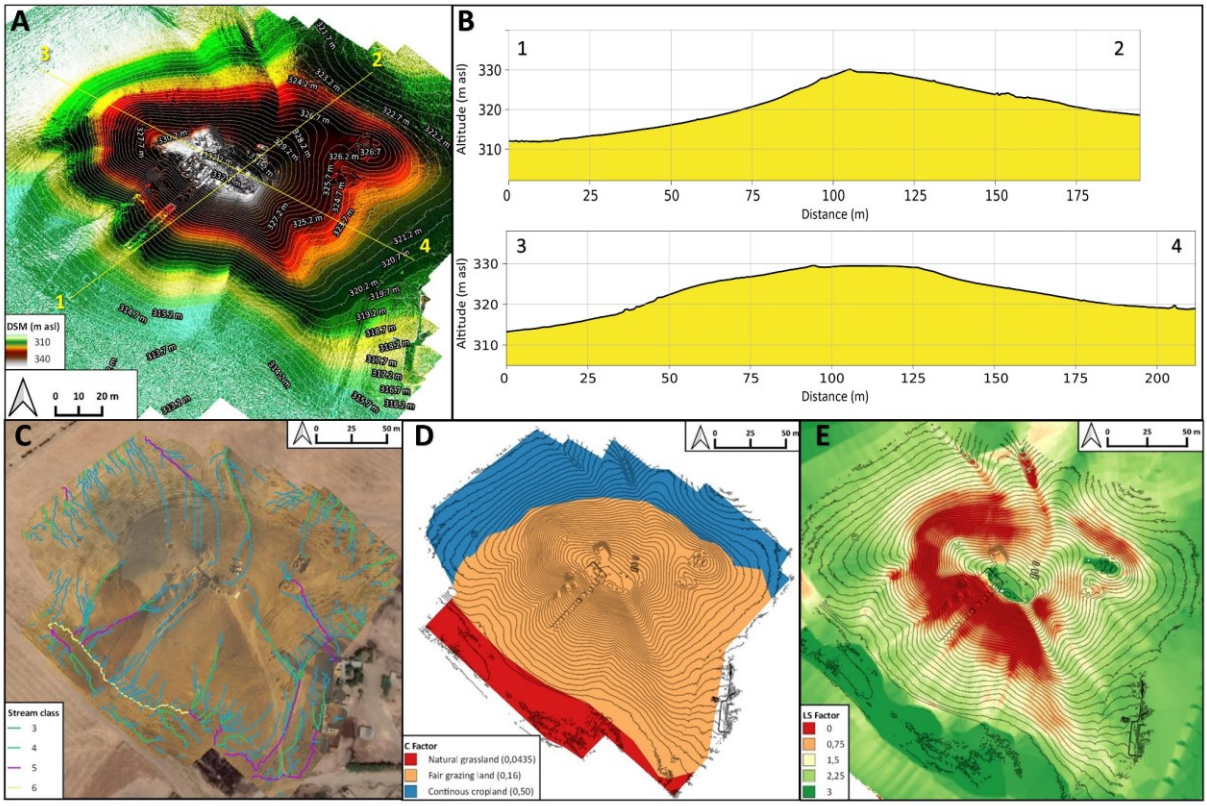


**Figure 3.** DSM and data required for the elaboration of the RUSLE model of soil erosion for Helawa. (A) DSM of the tell elaborated from the UAV pictures; the position of cross sections of (B) are reported. (C) The drainage network of Tell Helawa extrapolate from the DSM analysis. (D) C and (E) LS factors elaborated with QGIS software.

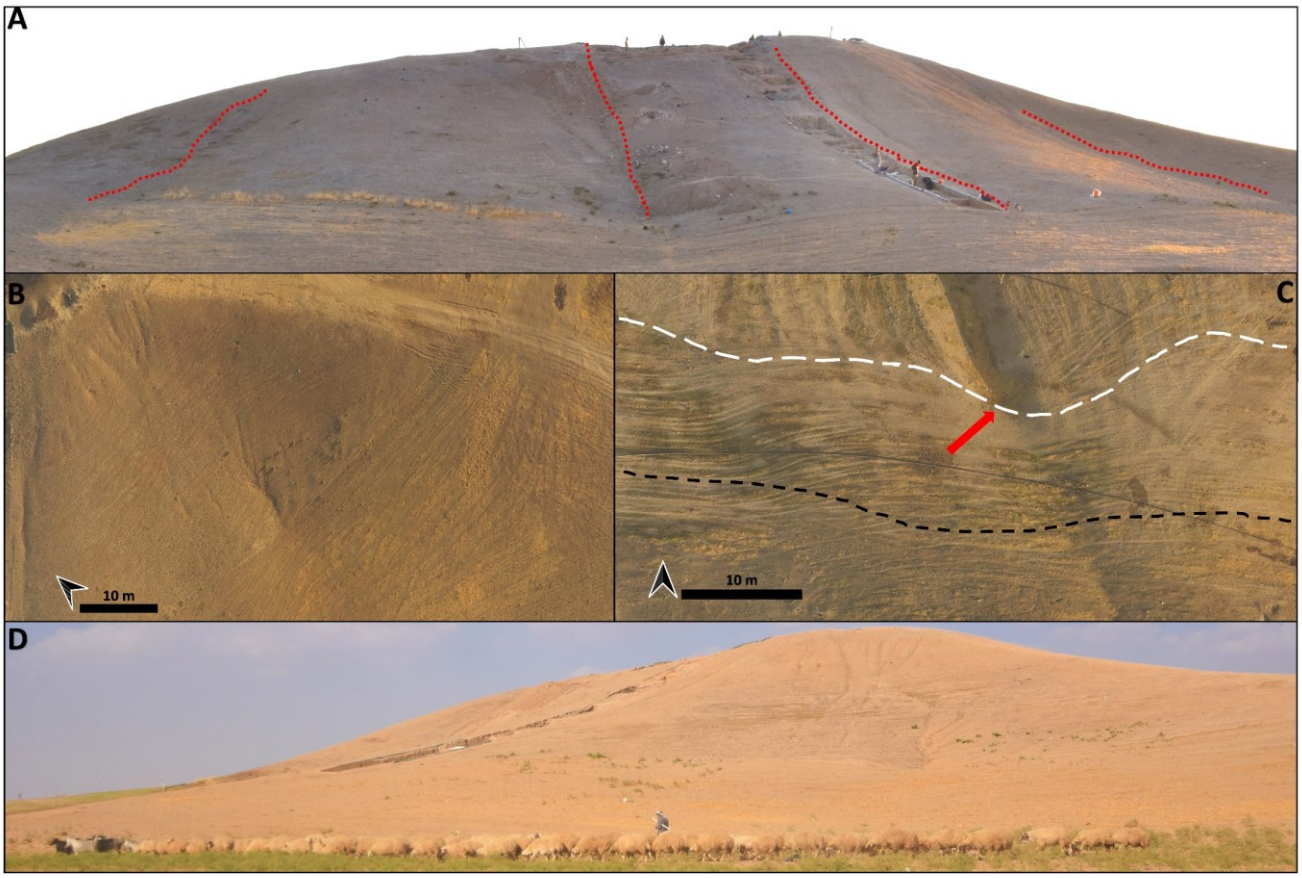


**Figure 4.** Field pictures of Tell Helawa. (A) Southern side of the tell, where main gullies (indicated by the red dashed lines) deeply cut the slope of the mound. (B) UAV imagery illustrating the southern side of Tell Helawa that is crossed by a rill-interill network. (C) UAV imagery of the northern toeslope highlighting the transition between the toeslope (white dashed line) and grazing and this latter with cropping belts (black dashed line); this transition is marked by the increased depth of gully in correspondence of the plough track furrows (indicated by the arrow). (D) Field picture (year 2021) of the southern toeslope that is daily exploited for sheep and goat grazing.

### 6.4.2 Aliawa

The general organization of Tell Aliawa is more complicate than that of Tell Helawa. The site of Aliawa extends over a surface of ~250.000m$^2$ and consists of a main mound rising 23m above the floodplain (top at 321m a.s.l.) and ~25.000m$^2$ large. The main mound is flat-topped and surrounded by several lower mounds (rising 3-5m above the floodplain), flanked by an ancient watercourse that runs along the northern edge of the site (Figure 1). In this work, we only consider the processes acting along the main mound, which therein is indicated as Aliawa (Figure 1).

The archaeological record suggests that the prehistoric and Bronze Age shape of Aliawa was modified by the construction of a high fortress bordered by brick embankments, probably dating to the Hellenistic/Seleucid periods. Such chronological attribution is preliminary and needs further excavation to be verified. In any case, a pentagonal perimetral wall was built over the mounds resulting after the prehistoric and Bronze Age occupation (3$^{rd}$ and 2$^{nd}$ millennia BC) (Peyronel &

Vacca, 2020). As a result, the extant steep slopes of the tell are the perimetral defences of the fortified settlement Hellenistic/Partian period, whilst the gently slope below the wall is part of a pristine Bronze Age settlement; the latter is especially visible in the southern sector of the mound, where it was not covered by the later fortress. Today, the top of Aliawa is flat, while its central part is a recessed area, interpreted as an inner space opened behind the fortress gate and then affected by intense natural and anthropic erosion (Figure 5A). Detailed geomorphological mapping (Figure 5B) shows that the Aliawa main mound suffered erosional processes, including the rill-interill network evident at the southern side and in the central part of the tell, a well-developed track sheep along its northern slope, and ploughing at its toeslope. Again, the slope gradient modulates the intensity of ongoing geomorphological processes; this is suggested by the analyses of two topographic profiles extracted from the DSM (Figure 6A). The SSW–NNE profile (section 1–2 in Figure 6A) displays a southern gentle slope with a progressive increase of the topographic gradient toward the S, up to the top of the tell. Yet, the northern slope shows a steep gradient with an abrupt transition to the surrounding flat area (Figure 6B). The E-W profile (section 3-4 in Figure 6) highlights the steepness of the eastern and western slopes of the mound (related to the fortress walls) and the central depression (Figure 7A). Topographic profiles underline the different slope gradient of the tell, with a gently slope in the southern part (Figure 7A) that becomes steeper toward the N (Figure 7B) and in the eastern and western sectors. Downstream the rill-interill network, the rate of incision increases and at the toeslope of the mound and the overland flow is drained into a gullies system developed along ploughing furrows (Figure 7C). Our survey suggests that the central part of the main mound is a sort of small badland-like basin, whose formation follows the excavation of the recessed area of the fortress. Therein, the original shape of the recessed area is deeply modified by the coalescence of several rills-gullies branches (Figure 7D), and several collapse scarps triggered by excavation of animal borrows (Figure 7D) and looting holes. The main features recorded along the northern mid-slope corresponding to the fort walls are several trails that runs parallels to the slopes according to contour lines of rows walls referred to domesticates trampling. Downslope, the boundary between the tell and the surrounding plain is marked by a shift in land use from animal grazing to cultivation; again, this results in a network of shallow and deep ploughing furrows (Figure 7F). The latter drain and redistribute the rainwater from the runoff of the downslope to the surrounding crop fields, as common in the contour farming practise (Thompson & Sudduth, 2020) Modern fire pits and trackways made by cars are further anthropogenic disturbances present on the top of Aliawa. Modelling on DSM of Aliawa detects 5 different stream classes (from 2 to 6). In details, the second and third classes are the shallowest drain network, while from the depth of incisions of the fourth, fifth, and sixth stream

classes increase along the inner part of the tell and along the toeslope (Figure 6C). The land cover (C) of Aliawa is characterized by sparse grassland vegetation, especially in the southern sector, while the northern slope is affected by livestock trampling and the surrounding area of the tell by cultivation (Figure 6D). The ratio between length and slope gradient (LS) highlights that the minimum values are in the flat area such as the top of the tell and the surrounding cropping fields, while the maximum are in the slopes and in the middle of the badland-like basin (Figure 6E).

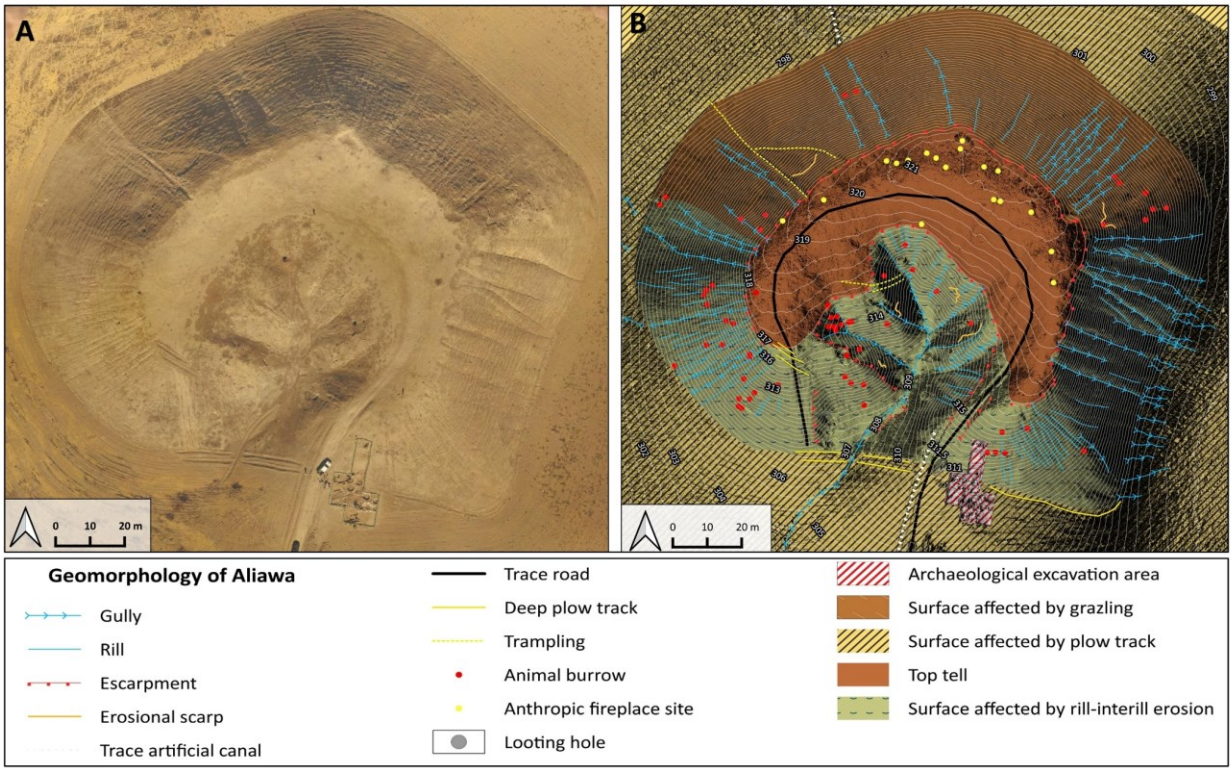


**Figure 5.** Geomorphological mapping of Tell Aliawa. (A) Orthophoto of the mound elaborated from the UAV pictures. (B) Detailed geomorphological map of the tell illustrating the main landforms and active.

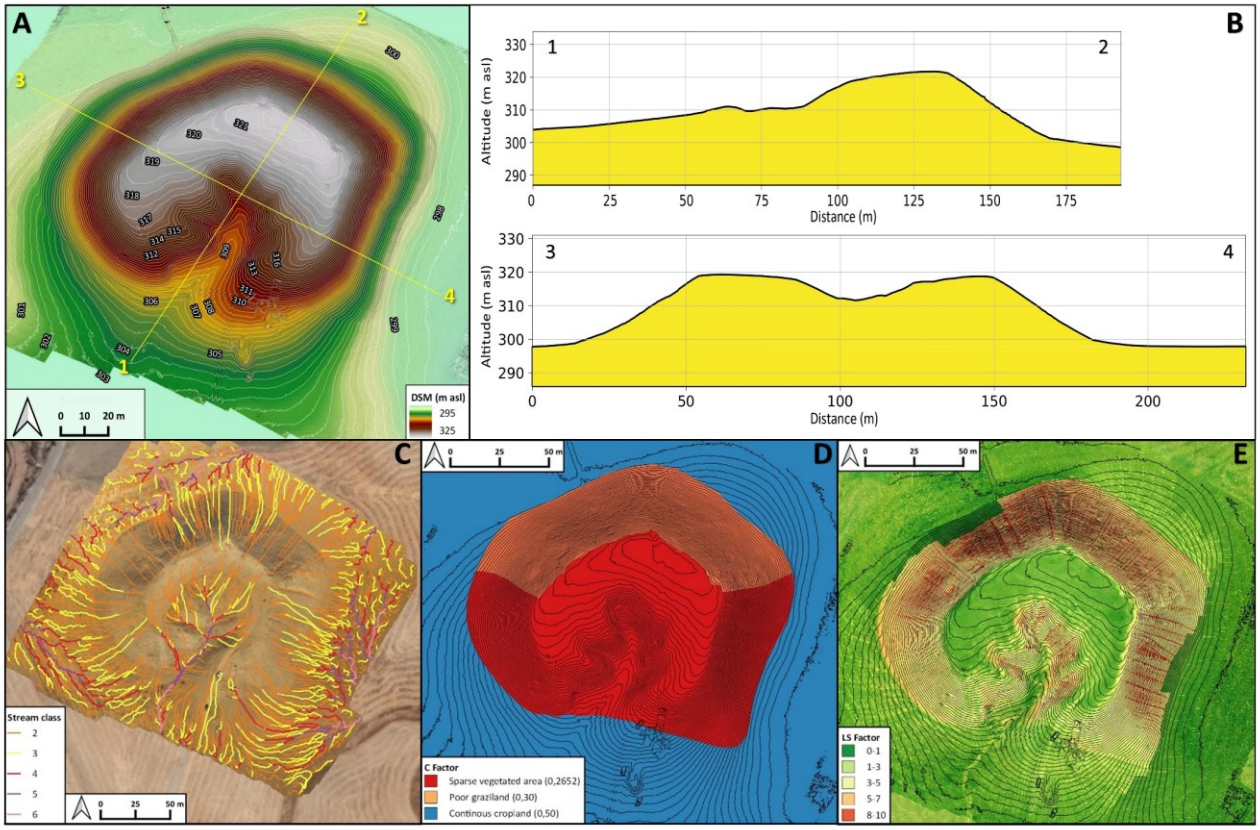


**Figure 6.** DSM and data required for the elaboration of the RUSLE model of soil erosion for Tell Aliawa. (A) DSM of Tell Aliawa elaborated from the UAV pictures indicating the position of cross sections of (B), that are illustrated in the text. (C) The drainage network of Tell Aliawa extrapolate from the DSM analysis. (D) C and (D) LS factors elaborated with QGIS software

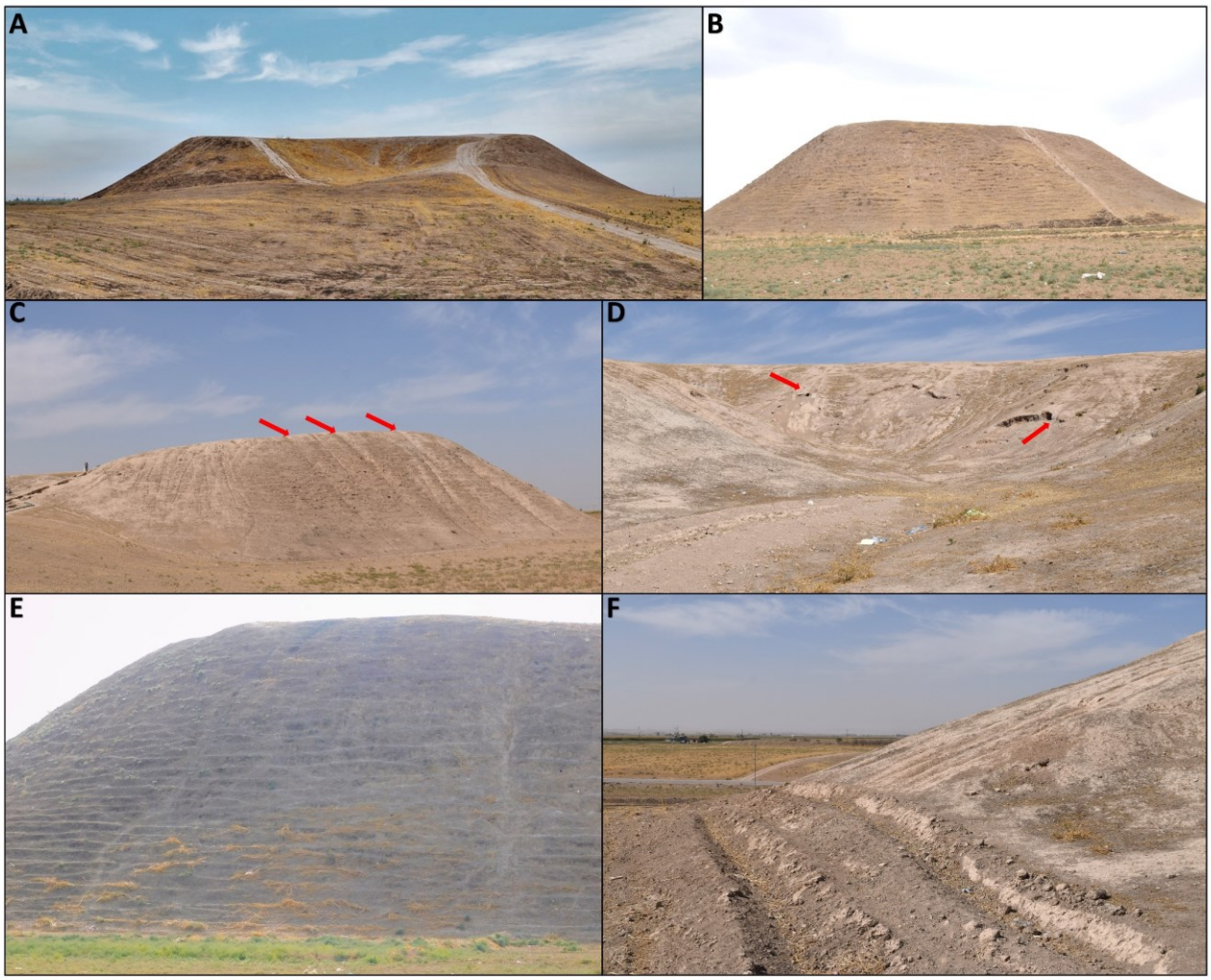


**Figure 7.** Field pictures on the main erosional features affecting the slopes of Tell Aliawa. (A) Southern side of the mound with a gently slope and showing the central main badland basin. (B) The steep northern slope of Tell Aliawa modelled by the contour track sheep and animal burrows. (C) Linear interill-rill network along the eastern slope of the tell (indicated by arrows). (D) The badland-like basin in the central part of the tell, developed in the internal aprt of the Seleucid fortress after the interplay between the rill-gullies erosion and the animal burrows (red arrows). (E) Sheep tracks following the direction of contour lines along the northern slope of the tell (sheep tracks follows the alignments of bricks of the Seleucid wall). (F) Deep plough furrows at the toeslope of the tell along the southern gentle slope.

## 6.5 Discussion on erosional processes affecting the preservation of the archaeological record.

Since its origin, the landscape surrounding Helawa and Aliawa – including the anthropogenic landforms represented by the two mounds – is deeply influenced by the interplay between natural and biogeomorphological (human and animal-controlled) surface processes. At multiple scales of resolution, such agencies oversee soil erosion and strongly impact on the conservation and preservation of the archaeological record. This is evident considering the nature of tells; in fact, they are entirely composed of superimposed (and decaying) clay buildings, archaeological materials and

architectonic structures thus representing landforms covered by anthrosols (Ur et al., 2011). The local climate promotes natural erosion processes leading to the formation of the rill-interill and gullies drainage network, which deeply carve the slopes of the tells. Human and animal agency further fuels erosion, enhancing the effect of linear erosion and increasing the rate of soil loss (Evans, 1991; Nielsen 1991; Zerboni & Nicoll, 2019). The geomorphological mapping shows that erosional processes are especially severe along the slopes of tells, where goats/sheep's trampling and the animals borrow trigger the mobilization, transport, dispersal, and secondary re-deposition of archaeological sediments and materials. The RUSLE models elaborated based on the interpolation between data derived from land cover, land management, type of soil, and the local amount of rainfall, show different degrees of geomorphological risk induced by erosion at different parts of each tell sites (Figure 8). The RUSLE models of Helawa and Aliawa also suggest that the tells' topography and the gradient of slopes are the main factors that promote erosion and trigger the loss of soil and/or archaeological sediments. The susceptibility to soil loss increases where the slopes switch from moderate to steeply; such change in topography is often related to the occurrence of specific archaeological structures (e.g., terraces). Moreover, potential erosion increases at the toeslope of each site in correspondence of ploughing furrows and drain canals. In the case of Helawa, the RUSLE model shows that the highest loss of soil and/or archaeological sediments occurs along the SW-NNW side of the mound (along the belt comprises between 325 and 330m a.s.l.), and along the N-NE side of the mound at the transition between the toeslope and the floodplain. These two different high values of estimated soil loss can be interpreted in two different ways. Along the SW-NNW part of tell, high values of soil loss are likely imputed to the interplay between the intense construction activities occurred in the Late Chalcolithic, which made the current slope very to moderate steep; this favoured the inset of gullying (Vacca et al., 2020). Instead, along the northern side at the transition with the floodplain extreme to severe values of soil loss estimation are related to a decrease in slope gradient coupled to intense ploughing operations, resulting into an intense soil erosion due to gully formation. A moderate to low geomorphological risk for soil and/or archaeological sediments loss is suggested for the southern and western sides of Helawa and along its northern toeslopes, where grassland covers the surface, and the LS ratio is low (Figure 8A). With respect to Aliawa, the RUSLE model highlights that the highest potential risk of soil and/or archaeological sediments loss is in the inner part of the tell and around the midslope. In such areas, erosion is fuelled by the rill-interill network, animal burrowing, and the contour tracks sheep. At the same site, moderate to low values of erosion risk were detected along the cropping area and at the top of the settlement, where the slope gradient is very low (Figure 8B). The distribution of soil loss estimation values at Aliawa is influenced by the

shape derived from the destruction and obliteration levels of the original prehistoric and Bronze Age settlement due to build activities of fortress. Hence, moderate to low values of erosion risk are recognized at the northern toeslope and in the southern side of the tell; such parts correspond to the slope of the original settlement. Yet, moderate to severe erosion risk is suggested for the parts of the mound corresponding to the walls of fortress, and in the central part of the mound (the artificial recession). In detail, the calculated potential soil loss elaborated from topographic parameters shows a lower susceptibility to erosion at Helawa than Aliawa. This is a snapshot of the current situation, resulting after centuries of erosion along the slope of tells and the building of fortification walls along the perimeter of Aliawa. If we consider field evidence, we notice that the toeslope of Helawa is composed of a large dispersion of archaeological sediment eroded from the Bronze and Late Chalcolithic layers of the tell and deposited in the area surrounding the site. This means that likely in the past, when the topography of the site was different, erosion rate was more intense than today. Yet, at Aliawa a few or clustered archaeological reworked sediments are dispersed along the toeslope of the tell, likely because the later budling of perimetral walls protected the pristine tell's stratigraphy from runoff and erosion. We suggest that different re-distribution of archaeological sediments at the toeslopes of each site was mostly controlled by erosional processes occurred in the last centuries (after the Seleucid occupation of the area), likely after the transformation of Aliawa into a fortress.

This hypothesis highlights that the amount of archaeological sediment loss at Helawa and Aliawa is triggered by the time of exposure to erosional processes. For that reason, today Aliawa displays higher values of potential soil loss than Helawa, but it is a consequence of the modification of the tell shape occurred during recent occupational phases; in fact, the fortified walls modified the topography of the site and increased the slope gradient. Finally, along Aliawa rills are more common and shallower compared to Helawa, where rills are concentrated at the southern edge of the mound with gullies that deeply cut the southern and northern sides of the tell (Figure 4A).

In conclusion, we noticed that the exposure to soil erosion values at each site is strongly influenced by the different shape of the settlements, depending on their evolution and human re-shaping. Helawa shows high values near the southern slope, where the different phases of the Chalcolithic construction have made the slope unstable and steep. This factor led to the consequent abandonment and later, Bronze Age, relocation of the settlement to the northern sector (Vacca et al., 2020). At Aliawa the pristine mound is preserved by the later fortifications, but the mound shows higher erosion risk values. This is due to the presence of the steam fortification walls and the opening of the inner recession, which exposed the archaeological stratigraphy to intense surface processes. Therefore, the different

nature and archaeological history of each tell shaped the current morphology of mounds and drive the intensity and efficiency of ongoing natural and human-controlled erosional processes.

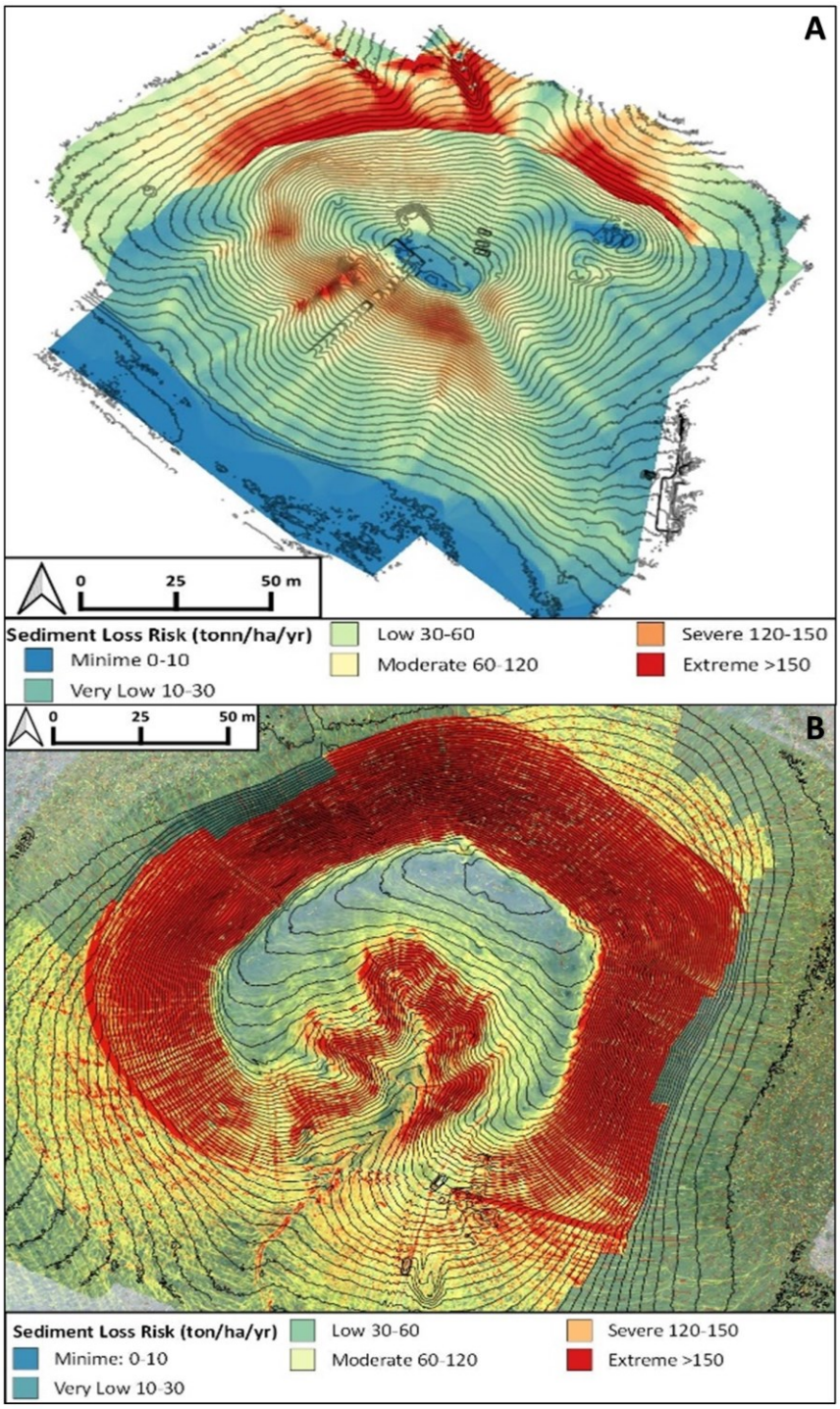


**Figure 8**. RUSLE models elaborated for (A) Tell Helawa and (B) Tell Aliawa. The colour scale (from blue to red) represents the increased risk for soil/sediment loss calculated in ton/ha/yr. The red areas are those where the archaeological record is mostly endangered by ongoing erosional processes.

## 6.6 Final highlight

In many regions of the planet, the preservation of anthropogenic landforms and their intrinsic archaeological record is today threatened by ongoing surface processes, and in some cases such processes area accelerated by human agency. In other words, humans built anthropogenic landforms and archaeological sites and today the same force is becoming a menace for the cultural landscape. This is especially true for the arid regions of Western Asia, where ongoing climate change and increase demographic pressure is dramatically increasing the severity of geomorphological processes (Zerboni et al., 2021). Our geomorphological analysis suggests that, besides natural surface processes, human, and animal agency on tell sites are resulting in rapid and negative effects. In fact, anthropogenic disturbances related to cultivation and animals' impact (burrowing and trampling) alter the stability of the original archaeological stratigraphy, leading to a progressive loss of archaeological heritage. Our innovative attempt to understand the rate of ongoing surface processes and impacts on tell sites using the RUSLE model is reliable. This automated geomorphological tool developed in the framework of soil loss appears to be efficient also in the context of archaeological tell sites. In fact, our investigation demonstrates the possibility to quantify the risk of losing archaeological soil and/or sediments due to slope erosion and to identify the areas more prone to destruction of anthropogenic landforms and their archaeological record. In this perspective, the procedure based on the RUSLE models tested at Tell Helawa and Tell Aliawa can be applied to a broader number of sites as a predictive geomorphological tool. In this respect, the RUSLE would support archaeologists and conservationists in planning specific archaeological operations aimed at investigating the most threatened parts of mounds' stratigraphy or to propose specific restoration/preservation strategies to mitigate the risk of loss of the archaeological record. Finally, this low-cost approach can be routinely applied to all the tell sites of the Near East to assess the susceptibility of archaeological heritage to the geomorphological risk promoted by ongoing climate change. In fact, the documentation of the preservation of archaeological monuments/sites and the assessment of the potential risk of destruction of cultural heritage at the scale of the single archaeological site are becoming urgent (Bewley, 2017) considering the increasing human pressure on archaeological areas and the acceleration of surface processes pushed by ongoing climate change.

## 6.7 References

Abate, N., Frisetti, A., Marazzi, F., Masini, N., & Lasaponara, R. (2021). Multitemporal–Multispectral UAS Surveys for Archaeological Research: The Case Study of San Vincenzo Al Volturno (Molise, Italy). *Remote Sensing*, *13*(14), 2719.

Agapiou, A., Lysandrou, V., & Hadjimitsis, D. G. (2020). A European-scale investigation of soil erosion threat to subsurface archaeological remains. *Remote Sensing*, *12*(4), 675.

Agisoft Metashape. (2022). Available online: http://www.agisoft.com/downloads/installer/ (accessed on 12 April 2022)

Altaweel, M., Khelifi, A., Li, Z., Squitieri, A., Basmaji, T., & Ghazal, M. (2022). Automated Archaeological Feature Detection Using Deep Learning on Optical UAV Imagery: Preliminary Results. *Remote Sensing*, *14*(3), 553.

Altaweel, M., Marsh, A., Jotheri, J., Hritz, C., Fleitmann, D., Rost, S., ... & Radeff, G. (2019). New insights on the role of environmental dynamics shaping Southern Mesopotamia: From the Pre-Ubaid to the early Islamic period. *Iraq*, *81*, 23-46.

Ames, C. J., Chambers, S., Shaw, M., Phillips, N., Jones, B. G., & Mackay, A. (2020). Evaluating erosional impacts on open-air archaeological sites along the Doring River, South Africa: methods and implications for research prioritization. *Archaeological and Anthropological Sciences*, *12*(5), 1-15.

Arnoldus, H. M. J. (1980). An approximation of the rainfall factor in the Universal Soil Loss Equation. *An approximation of the rainfall factor in the Universal Soil Loss Equation.*, 127-132.

Barton, C. M., Ullah, I., & Mitasova, H. (2010). Computational modeling and Neolithic socioecological dynamics: a case study from southwest Asia. *American Antiquity*, *75*(2), 364-386.

Berberian, M. (1995). Master "blind" thrust faults hidden under the Zagros folds: active basement tectonics and surface morphotectonics. *Tectonophysics*, *241*(3-4), 193-224.

Bewley, R. (2017). Endangered archaeology in the Middle East and North Africa (EAMENA): Approach and possible solutions. In *Post-conflict archaeology and cultural heritage* (pp. 123-137). Routledge.

Biagetti, S., Merlo, S., Adam, E., Lobo, A., Conesa, F. C., Knight, J., ... & Madella, M. (2017). High and medium resolution satellite imagery to evaluate late Holocene human–environment interactions in arid lands: A case study from the Central Sahara. *Remote Sensing*, *9*(4), 351.

Brandolini, F., Cremaschi, M., Zerboni, A., Degli Esposti, M., Mariani, G. S., & Lischi, S. (2020). SfM-photogrammetry for fast recording of archaeological features in remote areas.

Butzer, K. W. (1982). *Archaeology as human ecology: method and theory for a contextual approach*. Cambridge University Press.

Carolin, S. A., Walker, R. T., Day, C. C., Ersek, V., Sloan, R. A., Dee, M. W., ... & Henderson, G. M. (2019). Precise timing of abrupt increase in dust activity in the Middle East coincident with 4.2 ka social change. *Proceedings of the National Academy of Sciences*, *116*(1), 67-72.

Cook, K. L. (2017). An evaluation of the effectiveness of low-cost UAVs and structure from motion for geomorphic change detection. *Geomorphology*, *278*, 195-208.

Costanzo, S., Zerboni, A., & Manzo, A. (2022). Active surface processes at Mahal Teglinos (Kassala, Eastern Sudan): Archaeological implications for an endangered protohistoric site in Sahelian Africa. *Journal of Archaeological Science: Reports*, *43*, 103452.

Davidson, D. A., & Shackley, M. L. (1976). *Geoarchaeology: earth science and the past:(papers)/edited by DA Davidson and ML Shackley*.

Evans, R. (1998). The erosional impacts of grazing animals. *Progress in Physical Geography*, *22*(2), 251-268.

Fernández-Hernandez, J., González-Aguilera, D., Rodríguez-Gonzálvez, P., & Mancera-Taboada, J. (2015). Image-based modelling from unmanned aerial vehicle (UAV) photogrammetry: an effective, low-cost tool for archaeological applications. *Archaeometry*, *57*(1), 128-145.

Flohr, P., Fleitmann, D., Zorita, E., Sadekov, A., Cheng, H., Bosomworth, M., ... & Matthews, R. (2017). Late Holocene droughts in the Fertile Crescent recorded in a speleothem from northern Iraq. *Geophysical Research Letters*, *44*(3), 1528-1536.

Forti, L., Perego, A., Brandolini, F., Mariani, G. S., Zebari, M., Nicoll, K., ... & Zerboni, A. (2021). Geomorphology of the northwestern Kurdistan Region of Iraq: landscapes of the Zagros Mountains drained by the Tigris and Great Zab Rivers. *Journal of Maps*, *17*(2), 225-236.

Fouad, S. F. (2015). Tectonic map of Iraq, scale 1: 1000 000, 2012. *Iraqi Bulletin of Geology and Mining*, *11*(1), 1-7.

Ghosal, K., & Das Bhattacharya, S. (2020). A review of RUSLE model. *Journal of the Indian Society of Remote Sensing*, *48*(4), 689-707.

Goudie, A. S., & Viles, H. A. (2016). *Geomorphology in the Anthropocene*. Cambridge University Press.

GRASS Development Team(2020). Geographic Resources Analysis Support System (GRASS) Software, Version 7.8. Open-Source Geospatial Foundation, https://grass.osgeo.org.

Guiney, R., Santucci, E., Valman, S., Booth, A., Birley, A., Haynes, I., ... & Mills, J. (2021). Integration and analysis of multi-modal geospatial secondary data to inform management of at-risk archaeological sites. *ISPRS International Journal of Geo-Information*, *10*(9), 575.

Harris, I., Osborn, T. J., Jones, P., & Lister, D. (2020). Version 4 of the CRU TS monthly high-resolution gridded multivariate climate dataset. *Scientific data*, *7*(1), 1-18.

Herrmann, J. T., Glissmann, B., Sconzo, P., & Pfälzner, P. (2018). Unmanned aerial vehicle (UAV) survey with commercial-grade instruments: A case study from the Eastern Ḫabur Archaeological Survey, Iraq. *Journal of Field Archaeology*, *43*(4), 269-283.

Howland, M. D., Jones, I. W., Najjar, M., & Levy, T. E. (2018). Quantifying the effects of erosion on archaeological sites with low-altitude aerial photography, structure from motion, and GIS: A case study from southern Jordan. *Journal of Archaeological Science*, *90*, 62-70.

Hu, S., Li, L., Chen, L., Cheng, L., Yuan, L., Huang, X., & Zhang, T. (2019). Estimation of soil erosion in the Chaohu lake basin through modified soil erodibility combined with gravel content in the RUSLE model. *Water*, *11*(9), 1806.

Hussein, M. H. (1998). Water erosion assessment and control in Northern Iraq. *Soil and Tillage Research*, *45*(1-2), 161-173.

Jassim, S. Z., & Goff, J. C. (2006). *Geology of Iraq*. Eds by Geological Society of London.

Jorayev, G., Wehr, K., Benito-Calvo, A., Njau, J., & de la Torre, I. (2016). Imaging and photogrammetry models of Olduvai Gorge (Tanzania) by Unmanned Aerial Vehicles: A high-

resolution digital database for research and conservation of Early Stone Age sites. *Journal of Archaeological Science*, *75*, 40-56.

Kirkby, A., & Kirkby, M. J. (1976). Geomorphic processes and the surface survey of archaeological sites in semi-arid areas. *Geoarchaeology*, 229-253.

Kramer, C., Wilkinson, T. J., & Tucker, D. J. (1998). Settlement Development in the North Jazira, Iraq: A Study of the Archaeological Landscape. *Journal of the American Oriental Society*, *118*(4), 576.

Lazzari, M., & Gioia, D. (2017). UAV images and historical aerial-photos for geomorphological analysis and hillslope evolution of the Uggiano medieval archaeological site (Basilicata, southern Italy). *Geomatics, Natural Hazards and Risk*, *8*(1), 104-119.

Malinverni, E. S., Barbaro, C. C., Pierdicca, R., Bozzi, C. A., & Tassetti, A. N. (2016) UAV surveying for a complete mapping and documentation of archaeological findings. The early Neolithic site of Portonovo. *International Archives of the Photogrammetry, Remote Sensing & Spatial Information Sciences*, *41*

Marsh, A., Fleitmann, D., Al-Manmi, D. A. M., Altaweel, M., Wengrow, D., & Carter, R. (2018). Mid-to late-Holocene archaeology, environment and climate in the northeast Kurdistan region of Iraq. *The Holocene*, *28*(6), 955-967.

Menze, B. H., & Ur, J. A. (2012). Mapping patterns of long-term settlement in Northern Mesopotamia at a large scale. *Proceedings of the National Academy of Sciences*, *109*(14), E778-E787.

NextGIS (2021). QuickMapServices. https://nextgis.com/blog/quickmapservices/.

Nicoll, K., & Zerboni, A. (2020). Is the past key to the present? Observations of cultural continuity and resilience reconstructed from geoarchaeological records. *Quaternary International*, *545*, 119-127.

Nielsen, A. E. (1991). Trampling the archaeological record: an experimental study. *American Antiquity*, *56*(3), 483-503.

Oselini, V., Campeggi, M., Forti, L., Ginoli, E., Pezzotta, A., & Peyronel, L. (2021). From micro-regional to intra-site analysis: the GIS of the Italian Archaeological Expedition in the Erbil Plain (Kurdistan Region of Iraq) *Archeomatica*, *13*(3).

Palermo, R., De Jong, L., & Ur, J. A. (2022). Hellenistic Landscapes and Seleucid Control in Mesopotamia: The View from the Erbil Plain in Northern Iraq. *American Journal of Archaeology*, *126*(3), 425-442.

Panagos, P., Borrelli, P., Meusburger, K., Alewell, C., Lugato, E., & Montanarella, L. (2015). Estimating the soil erosion cover-management factor at the European scale. *Land use policy*, *48*, 38-50.

Papageorgiou, N., & Hadjimitsis, D. G. (2020, November). Evaluation of soil loss by water in archaeological landscapes by using the (R) USLE Model and GIS. The case study of Paphos district, Cyprus. In *Euro-Mediterranean Conference* (pp. 64-77). Springer, Cham.

Parcak, S. H. (2009). *Satellite remote sensing for archaeology*. Routledge.

Peyronel, L., & Vacca, A. (2020). The Italian Archaeological Project in the Erbil Plain (2013-2017). In *International Congress on the Archaeology of the Ancient Near East* (pp. 317-330). Harrassowitz.

Peyronel, L., Minniti, C., Moscone, D., Naime, Y., Oselini, V., Perego, R., & Vacca, A. (2019). The Italian Archaeological Expedition in the Erbil Plain, Kurdistan Region of Iraq: Preliminary Report on the 2016-2018 Excavations at Helawa.

Prăvălie, R. (2021). Exploring the multiple land degradation pathways across the planet. *Earth-Science Reviews*, *220*, 103689.

QGIS Development Team (2021). QGIS Geographic Information System. Open-Source Geospatial Foundation Project" Available: https://www.qgis.org/en/site/index.html

Renard, K. G., & Freimund, J. R. (1994). Using monthly precipitation data to estimate the R-factor in the revised USLE. *Journal of hydrology*, *157*(1-4), 287-306.

Rinaudo, F., Chiabrando, F., Lingua, A., & Spanò, A. (2012). Archaeological site monitoring: UAV photogrammetry can be an answer. *International Archives of the Photogrammetry, Remote Sensing and Spatial Information Sciences*, *39*(B5), 583-588.

Roberts, N., Woodbridge, J., Bevan, A., Palmisano, A., Shennan, S., & Asouti, E. (2018). Human responses and non-responses to climatic variations during the last Glacial-Interglacial transition in the eastern Mediterranean. *Quaternary Science Reviews*, *184*, 47-67.

Rosen, A. M. (1986). Cities of clay: the geoarcheology of tells. University of Chicago Press.

Sărășan, A., Ardelean, A. C., Bălărie, A., Wehrheim, R., Tabaldiev, K., & Akmatov, K. (2020). Mapping burial mounds based on UAV-derived data in the Suusamyr Plateau, Kyrgyzstan. *Journal of Archaeological Science*, *123*, 105251.

Scudder, S. J., Foss, J. E., & Collins, M. E. (1996). Soil science and archaeology. *Advances in agronomy*, *57*, 1-76.

Stek, T. D. (2016). Drones over Mediterranean landscapes. The potential of small UAV's (drones) for site detection and heritage management in archaeological survey projects: A case study from Le Pianelle in the Tappino Valley, Molise (Italy). *Journal of Cultural Heritage*, *22*, 1066-1071.

Stevens, L. R., Ito, E., Schwalb, A., & Wright, H. E. (2006). Timing of atmospheric precipitation in the Zagros Mountains inferred from a multi-proxy record from Lake Mirabad, Iran. *Quaternary research*, *66*(3), 494-500.

Tarolli, P., & Sofia, G. (2016). Human topographic signatures and derived geomorphic processes across landscapes. *Geomorphology*, *255*, 140-161.

Tarolli, P., Cao, W., Sofia, G., Evans, D., & Ellis, E. C. (2019). From features to fingerprints: A general diagnostic framework for anthropogenic geomorphology. *Progress in Physical Geography: Earth and Environment*, *43*(1), 95-128.

Thompson, A., & Sudduth, K. (2017). Terracing and contour farming. *Precision Conservation: Geospatial Techniques for Agricultural and Natural Resources Conservation*, *59*, 151-163.

Tudryn, A., Motavalli-Anbaran, S. H., Tucholka, P., Gibert-Brunet, E., Lankarani, M., Ahmady-Birgani, H., ... & Dufaure, O. (2021). Late Quaternary environmental changes of Lake Urmia basin (NW Iran) inferred from sedimentological and magnetic records. *Quaternary International*, *589*, 83-94.

Ur, J. (2005). Sennacherib's northern Assyrian canals: new insights from satellite imagery and aerial photography. *Iraq*, *67*(1), 317-345.

Ur, J., Babakr, N., Palermo, R., Creamer, P., Soroush, M., Ramand, S., & Nováček, K. (2021). The Erbil Plain Archaeological Survey: Preliminary Results, 2012–2020. *Iraq*, *83*, 205-243.

Vacca, A., Moscone, D., & Rosati, P. (2020). Managing survey data from Helawa, Erbil Plain (Kurdistan Region of Iraq). *West & East*.

Wilkinson, T. J. (2003). *Archaeological landscapes of the Near East*. University of Arizona Press.

Wischmeier, W. H., & Smith, D. D. (1978). *Predicting rainfall erosion losses: a guide to conservation planning* (No. 537). Department of Agriculture, Science and Education Administration.

Zebari, M., Grützner, C., Navabpour, P., & Ustaszewski, K. (2019). Relative timing of uplift along the Zagros Mountain Front Flexure (Kurdistan Region of Iraq): Constrained by geomorphic indices and landscape evolution modeling. *Solid Earth*, *10*(3), 663-682.

Zerboni, A., & Nicoll, K. (2019). Enhanced zoogeomorphological processes in North Africa in thehuman-impacted landscapes of the Anthropocene. *Geomorphology*, *331*, 22-35.

Zerboni, A., Brandolini, F., Mariani, G. S., Perego, A., Salvatori, S., Usai, D., ... & Williams, M. A. (2021). The Khartoum-Omdurman conurbation: a growing megacity at the confluence of the Blue and White Nile Rivers. *Journal of Maps*, *17*(4), 227-240.

# Chapter 7

# The geoarchaeological investigation on the defunctionalisation of an Assyrian canals system reveals late Holocene land use transitions in Northern Mesopotamia

## 7.1 Introduction

Along the Mesopotamian plains, some of the world's earliest civilizations flourished, bringing forth pioneering agricultural innovations for land use and water harvesting. In Lower Mesopotamia, agriculture was characterised by the development of complex irrigation systems draining the Euphrates and Tigris basins. Yet, in Upper Mesopotamia, 2nd and 1st millennium BCE communities developed innovative methods for dry farming (Bagg 2000; Ur 2005; Wilkinson et al., 2005; Tamburrino, 2010; Wilkinson et al., 2015; Morandi Bonacossi, 2018a). In both cases, the creation of complex canal systems facilitated the management of water resources, both for agriculture and economic stability and prosperity. In the case of Northern Mesopotamia – the heart of the Assyrian Empire –, archaeological and written records reveal that complex systems of canals were built from the 13th century BCE onwards by Assyrian kings. Such majestic features – also representing a monument to the power of the Assyrian Empire – contributed to modifying the regional natural drainage network with the introduction of regional-scale infrastructures (Oates, 1968; Reade, 1978; Bagg, 2000; Ur, 2005; Morandi Bonacossi, 2018a), thus representing a dramatic human modification of natural geomorphic systems. In the last heartbeats of the Assyrian rule over Northern Mesopotamia, King Sennacherib (705-681 BCE) ordered the realisation of the Khinis canal system, linking the Gomel River with the plains south of the modern city of Shaikhan (Reade, 1978, Bagg, 2000; Ur, 2005; Morandi Bonacossi, 2018a). The aim of building such a large-scale canal system, fed by perennial rivers and the numerous karst sources dotting the piedmont landscape along its course, was to establish a staple-crop economy in the hinterland of the capital city of Nineveh that could be substantially independent from intra- and interannual rainfall variability, and to establish a new engineering infrastructure that could simultaneously increase the cultivable land and represent a waterway for the movement of people and goods (Morandi Bonacossi, 2018a).

A sustainable population growth was a major consequence of such monumental operation; this implied the subsequent reorganisation of the regional settlement strategies and an improvement in the trade network and commodities throughout the Assyrian landscape (Oates, 1968; Morandi Bonacossi,

*Forti, L., Costanzo, S., Compostela, C., Garna, G., Morandi Bonacossi, D. & Zerboni A. (2023) The geoarchaeological investigation on the defunctionalisation of an Assyrian canals system reveals late Holocene land use transitions in Northern Mesopotamia. The Holocene.* https://doi.org/10.1177/09596836221145395

2018b). Nevertheless, shortly after their creation and following the downfall of the Neo-Assyrian Empire, the canals were rapidly dismissed, and their abandonment led to backfilling and partial obliteration (Morandi Bonacossi 2018a and in press). Field operations demonstrated that the post-abandonment infill of canals varies slightly depending on the location of the investigated portion and the local topography of the overlying anticline's slope. Generally, colluvial sediments interspersed with episodes of pastoral occupation and exploitation can be observed macroscopically by the exposed trenches, thus suggesting a marked acceleration of slope instability and a shift in local land use and land cover after the collapse of the Assyrian Empire and the social reorganisation of human groups. But more insightful analyses and tools offered by micromorphological investigation of archaeological and natural sediments offer a more nuanced reconstruction of surface processes and local land use shifts. Here, we present a geoarchaeological investigation on some branches of the Khinis canals and the Jerwan aqueduct with a multiscalar approach to elucidate processes that happened after the abandonment of the canal system and oversee their obliteration. Micromorphological and sedimentological analyses allow elucidating the formation process of natural and anthropogenic deposits infilling canals (e.g., Cremaschi et al., 2016; Charbonnier et al., 2017; Li et al., 2017; Cremaschi et al., 2018; Storozum et al., 2018; Mariani et al., 2020). In our case, the same methods disclose the characteristics of the post-abandonment backfill as well as some functional aspects of the canal's late phases of activity. We interpret the main natural and anthropogenic sedimentary processes that occurred during and after the abandonment of the canals, identifying different events of colluvial infilling, pedogenesis and subsequent late phases of reoccupation and repurposing, thus elucidating on late Holocene land-use changes in the region and its consequence on natural surface processes.

## 7.2. Geological, geomorphological, and climatic background

The study area is in the northwestern Kurdistan Region of Iraq (KRI), within the governorate of Dohuk. The investigated trenches are situated on the northern and southern foothills of the Shaikhan anticline, on the right bank of the Gomel River (Site 133 and Site 834) and in the proximity of Shaikhan village (Site 900) (Figure 1A). The regional geological setting is dominated by Cretaceous and Paleogene limestone, marl and dolostone, Mio-Pliocene sandstone, and Plio-Pleistocene conglomerate that compose the core of Gully Keer and Shaikhan anticlines. The region is part of the Zagros-Fold Thrust Belt (ZFTB), whose persistent alternation of W–E anticline ridges and synclines represents the main structural feature of the local and supra-regional landscape (Sissakian, 2014; Zebari et al., 2019; Forti et al., 2021). In the study area, lithological bodies were deformed during the continental collision between the Arabian and Eurasian plates, active since the Early Miocene (;

Dewey et al., 1973; Dercourt et al., 1986; Csontos et al., 2012; Mouthereau et al., 2012; Fouad, 2015). The interplay between tectonic uplift and surface/karst processes on the anticlinal ridges and syncline troughs controlled the formation and distribution of different physiographic units and resulted in the formation of a complex landscape (Forti et al., 2021). Indeed, the hillslopes of the anticline ridges of the study area are dissected by a complex network of narrow valleys and deep ravines that drain into the Gomel River, a tributary of the Tigris River (Figure 1A). In the study area, most of the streams - such as the Gomel River - are ephemeral and active only during the rainy season; only the Rubar el Atrush River (the uphill tract of the River Gomel), together with few of its tributaries, is perennial and drains into the Tigris River (Forti et al.,2021) (Figure 1A).

Middle to Late Holocene palaeoclimate data derived from speleothems sampled in the Gejkar, Shalaii and Kuna Ba caves detected strong climatic variability that occurred starting from ca. 4 ka (Flohr et al., 2017; Marsh et al.,2018; Sinha et al., 2019). From the end of the Middle Holocene to the onset of the Neo-Assyrian Empire (ca. 950 BCE), multi-decennial to centennial droughts and wet spells alternated. The period from ca. 950 to 740 BCE represented one of the wettest spells that occurred in the last 4000 years, with increased precipitation at the regional scale. This episode was shortly followed by a severe drought going from ca. 675 to 550 BCE.

Present-day regional climatic data collected by a meteorological station located in Dohuk, position the area within the Mediterranean or Dry Summer Subtropical (Csa) climatic zones of the climate classification proposed by Köppen & Geiger (1936) (Malinowski, 2002; Beck et al., 2018; Salman et al., 2019). The Csa climatic zone in this region is characterised by extremely to moderately cold and wet winters and moderately hot and arid summers. The rainy season is from November to April, with a mean rainfall of 570 mm/a, and temperature varies across the year from 10°C to 42°C (Malinowski, 2002; Awchi and Kalyana, 2017).

## 7.3. The Sennacherib canal system

The Khinis canal was commissioned by the Assyrian King Sennacherib around 690 BCE as part of his development plan for the northern outskirts of the upper Mesopotamian plains (Ur, 2005; Morandi Bonacossi, 2018a). The headwaters of the Khinis canal belong to the Rubar Atrush River, which is diverted at the outlet of its valley near the village of Khinis (Assyrian Khanusa), at the southern slope of the Gully Keer Anticline. At its upper initial stretch, the canal flows southwards and parallel to the right bank of the Gomel River, which represents the continuation of the Atrush River. When reaching the Shaikhan Anticline, the canal follows the slope bottom's contour with remarkable accuracy and diverges from the Gomel River after the ridge's eastern tip. As the Gomel River flows south, the canal

keeps following the foothill's contour with a constant gradient and an E-W trajectory, eventually reaching the Jerwan aqueduct (Figure 1A).

The great attention that King Sennacherib paid to the building of the northern system of canals (Maltai, Faida, Bandawai/Shiru Maliktha and Khinis) has been noted by scholars (Jacobsen and Lloyd, 1935; Reade, 1978) and recently investigated by a fieldwork project operating in the "Assyrian Triangle" (LoNAP - Land of Nineveh Archaeological Project, University of Udine; Morandi Bonacossi, 2018a). Different reaches of the canal system are commemorated by impressive monumental inscriptions (at Khinis and Jerwan) describing the canals' construction, and imposing rock reliefs (Khinis) depicting the king venerating the main Assyrian deities (Jacobsen and Lloyd 1935; Reade 1978), in a successful celebratory work of the generosity of the king who was able to provide exceptional commodities for his people and irrigation water for the capital Nineveh and its countryside.

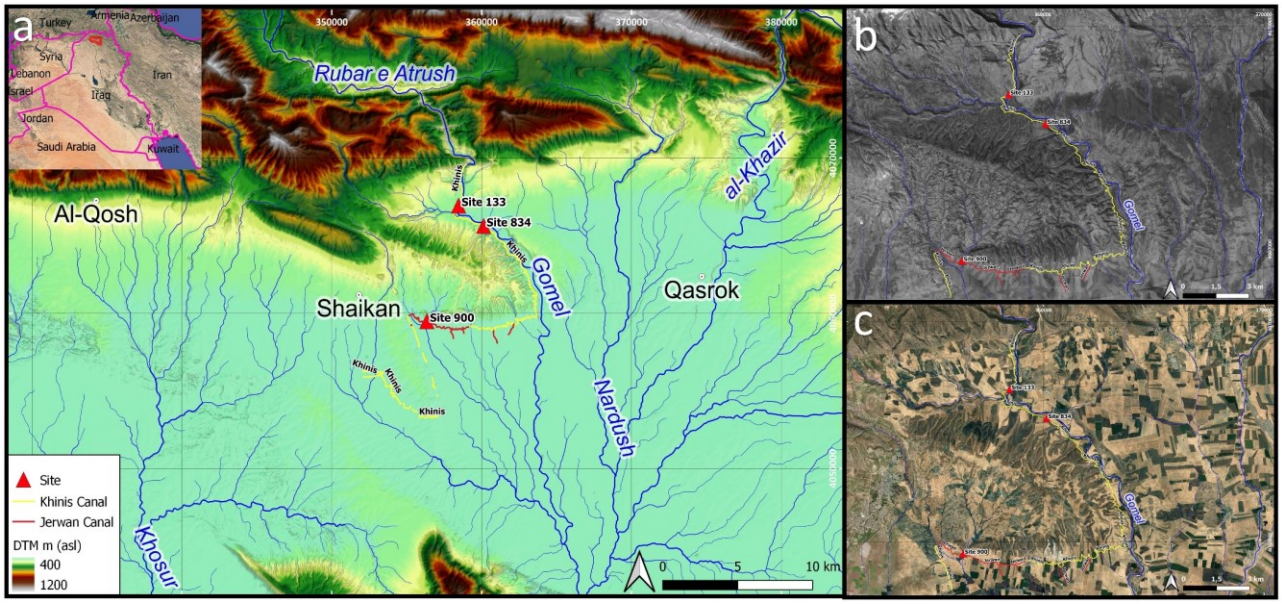


**Figure 1.** Distribution of the Khinis canals and Jerwan aqueduct in the study area on (A) a Digital Terrain Model, (B) Corona Declassified imagery (capt. 1968), and (C) from GoogleEarth™.

## 7.4. Materials and methods

The system for water management that includes the Khinis canal, the Jerwan aqueduct and the other four aqueducts discovered by LoNAP along its course was investigated and described in its general and functional terms in Morandi Bonacossi (2018a). In this work, we analyse, emphasise, and model the local landscape from different datasets through remote sensing analysis. Recent GoogleEarth™ high-resolution satellite imagery (2013-2021) was analysed and visualised through "QuickMapServices" plugin (NextGis, 2021) within QGIS 3.16 (QGIS Development Team, 2021) to locate and trace the trajectory of the archaeological features. Furthermore, declassified CORONA

intelligence satellite imagery (USGS, 1968) collected in 1968 was used to evaluate variations of landforms in recent historical times and rule out potential subrecent or active surface processes from the archaeological analysis (Forti et al. 2022). An AW3D30 Digital Terrain Model (DTM) with a horizontal resolution of 1 arcsecond (circa 30 m at the equator; JAXA, 2021) was used to produce a regional 3D graphic rendition, highlighting the landforms in the proximity of the sites Figure 1A. The natural hydrographic network was derived from DTM through GRASS software and processed to obtain a Strahler's hierarchical classification vector layer (Strahler, 1958). At each site, a section of the test trench was cleaned and described; for each stratigraphic section, colours were attributed according to the Munsell® colour chart. Preliminary chronologies were defined based on well-established pre-existent knowledge of the Assyrian canal systems, and fortuitous archaeological material found within the deposit. Samples for sedimentological analyses were collected, labelled, and processed with reference to the Stratigraphic Units (SU) identified during the archaeological excavation of the trenches. Physical sedimentological characterization of sediments was carried out at the Earth Sciences Department of the University of Milan. Characterization of sediments included the following analyses, whose results are graphically summarised in Supplementary Materials (File 1, S1.3): grain-size distributions were performed after removing organics by hydrogen peroxide (130 vol) pre-treatment; sediments were wet sieved (diameter 1.0–0.63 mm), then the fine fraction (<0.63 mm) was determined by hydrometer based on Stokes' law (Gale & Hoare, 1991). Undisturbed blocks for micromorphological investigations were collected from clean sections and thin sections were manufactured by Massimo Sbrana – Servizi per la Geologia laboratory (Piombino, Italy) following the procedure described by Murphy (1986). The finished thin section product is a 55x95mm slice mounted on a glass support. The thin sections were studied employing an optical petrographic microscope (Olympus BX41) mounting a digital camera (Olympus E420) for image acquisition. Observation was carried out at various magnifications (20x, 40x, 100x, 400x) under plane polarised light (PPL) and cross-polarized light (XPL). The description of the thin sections followed the terminology suggested by Stoops (2021), and their interpretation was aided by the coloured atlases and concepts summarised in Nicosia & Stoops (2017), Macphail & Goldberg (2018), and Stoops et al. (2018).

## 7.5. Results

### 7.5.1 Khinis canal site 133

Site 133 (36.737647°N, 43.414882°E) is a trench excavated along the trackway of the Khinis canal in the northern footslope of Shaikhan relief, on the right bank of Gomel River. Therein, the canal was

cut directly within the Plio-Pleistocene conglomerates of the Bai Hassan Formation (locally called Upper Bakhtiari Formation) reaching a depth varying from 5.6 m to 6.8 m and a width of 6.25 m, with a flat bottom and sub-vertical sides with an intentional overhang halfway up that might have been used as a walkway for maintenance. The right bank of the canal has a considerably higher altitude than its left bank, with a height difference of approximately 3 m providing a near-vertical rock shelter flanking long portions of the canal itself (Figure 2B-C). The freshly excavated archaeological trench of site Khinis 133 (W 6m; H 3.8m) revealed a well-defined and straightforward stratigraphy (Figure 3 and Supplementary Materials, File 1 S1.1). The lowest layer (SU 13) is a horizontal deposit of weakly laminated, matrix-supported silty clay with rare clasts and brittle aggregates. It is overlaid by a succession of subhorizontal layers of chaotic matrix-supported and gravel-rich colluvium (SU 9, 8, 7, 6, 5, 4), whose coarse rounded clasts derive from in-situ weathering of the conglomerate bedrock. The colluvial layers contain rare macroscopic traces of bioturbation, rare gastropod shell remains, and rare small charcoal flecks that were sampled for radiocarbon dating (SU 6, 2125±45 years BP, 230–39 cal BCE 78,7% 2σ sample #LTL21885 see S1.2 in Supplementary Materials, File 1). The stratigraphy is topped by weakly laminated occupational layers (SU 3, 10, 2) and sealed by more present-day colluvium (SU 1). The occupational layers contain ash and macroscopic interlaying of dark organic dung-rich strata and yielded some potsherds of the Islamic period. SU 1 too contains dung and traces of trampling, although to a lesser extent than the underlying layers. Moreover, large square stones are found arranged as probable barriers sectioning the canal's longitudinal axis to form sheltered corrals (Figure 3).

Sedimentological analyses are consistent with the field observations and show general poor sorting of the sediments throughout the stratigraphic succession. The amount of silt and clay (the matrix support) remains roughly unvaried throughout, but the central colluvial layers (SUs 8, 7, 6) display a slight enrichment in gravel, possibly due to their relative position within the shape of the cut in the progressively dismantling conglomeratic bedrock, which shows signs of unloading fragmentation along with the silhouette of the canal's cut. SUs 2, 3 and 10 too show gravel enrichment, but a lesser presence of very large clasts (Supplementary Materials, S4).

Micromorphological analysis (Table 1, Figure 4) adds further insights into the characterization of each SU and macro-phase. SU 13 shows diffuse hydromorphic features (i.e., related to Fe redistribution in water-logging conditions) such as Fe/Mn small nodules dispersed in a light brown silty clay matrix, micrite coating and infilling of voids, and solutional alteration with secondary clay formation of the few large clasts together with few traces of mild pedogenesis, sparse bioturbation (residual plant root tissue, worm channels) and small unaltered microfaunal faecal pellets. SUs 9, 6

and 4 show chaotic structures and poorly sorted clasts, widespread rounded and rolled Fe/Mn nodules - inherited from the soil overlying the higher-standing rocky slope -, and relatively limited traces of bioturbation with very rare organic constituents (shell, bone, charcoal, and residual plant fragments), consistent with subsequent colluvial events caused by soil destabilisation interspersed with occasional biostasy (i.e. periods of favourable climate that allows vegetation overgrowth with stabilization of soils and landforms, sensu Erhart, 1956). SUs 3 and 2, on the other hand, display great amounts of herbivore dung (suggested by notable concentrations of faecal spherulites, i.e., chemically stable spherical microscopic crystalline calcium carbonate features) and phytoliths mixed and welded with the underlying soil, together with abundant traces of bioturbation and residual organic matter (shell, bone, charcoal, and unburnt plant fragments). SU 1 shows intermediate characteristics between the colluvial and occupational phases, with sporadic inherited dung fragments, faecal spherulites, and organic remains mixed with pale unsorted colluvium to form a crumbly bioturbated deposit.

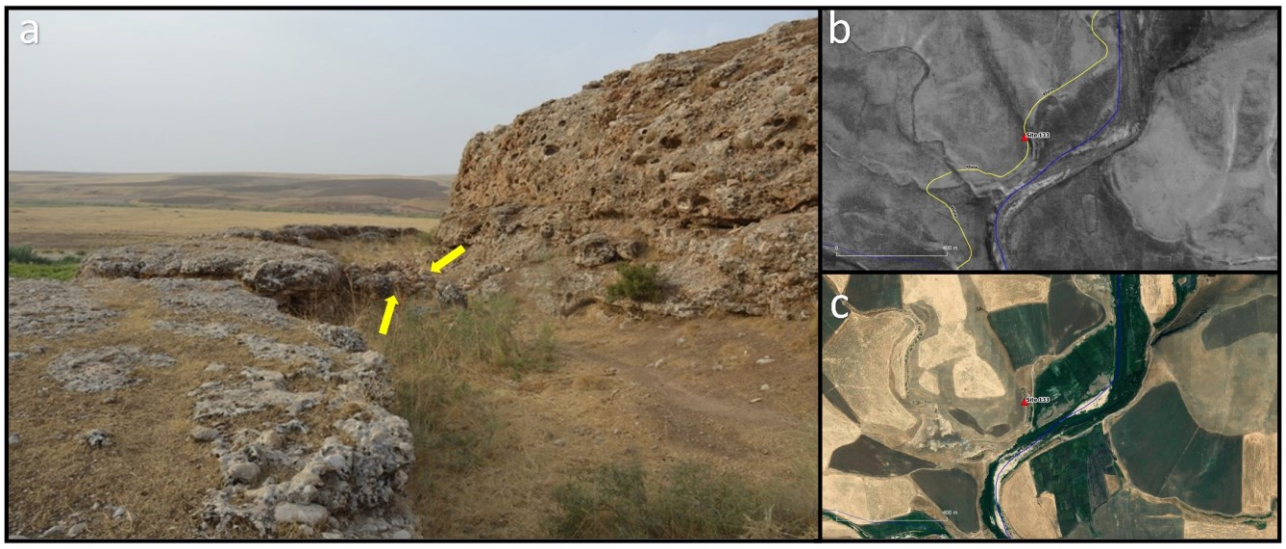


**Figure 2.** (A) Field picture of Site Khinis 133 in which the yellow arrows indicate the stones used for corrals and details of its position along the right bank of Gomel River shown on (B) Corona Declassified imagery (capt. 1968) and (C) Google Earth™ satellite image.

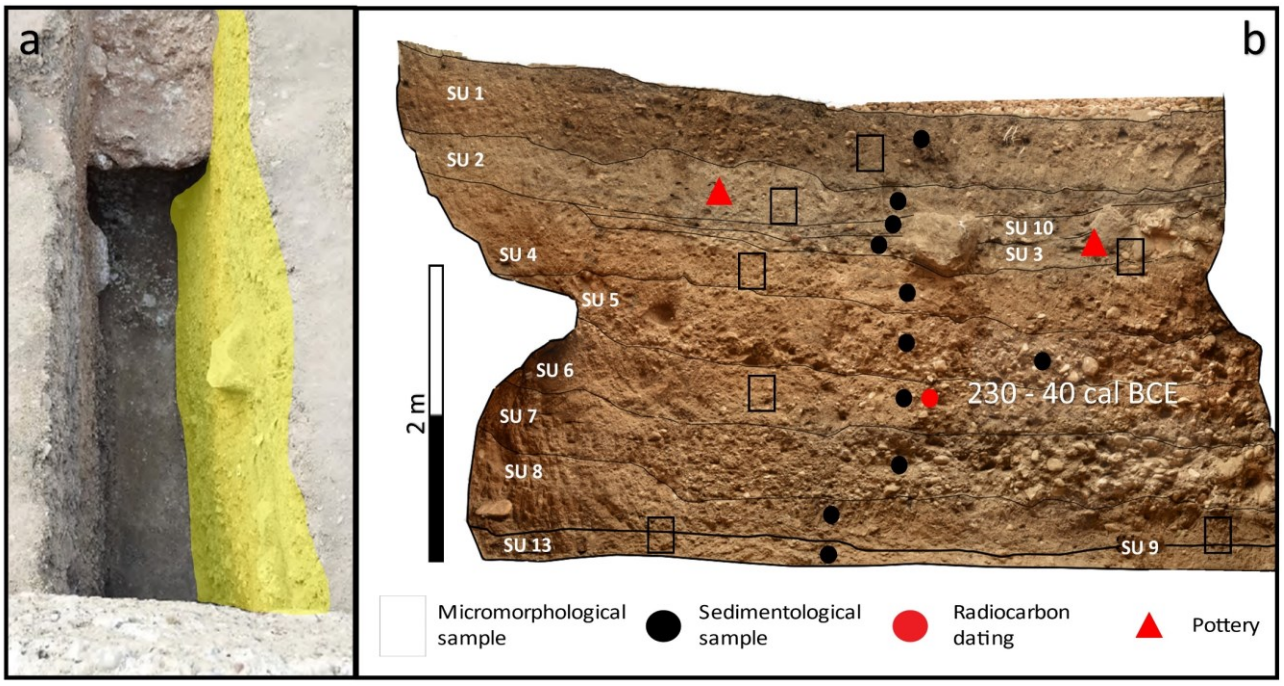


**Figure 3.** (A) Bird's eye view of the trench of Site Khinis 133. The yellow polygon identifies the analysed section. (B) The studied section at Site Khinis 133 reports SUs' numbers, sampling points (for dating, sedimentological analyses, and thin sections, and position of diagnostic archaeological findings.

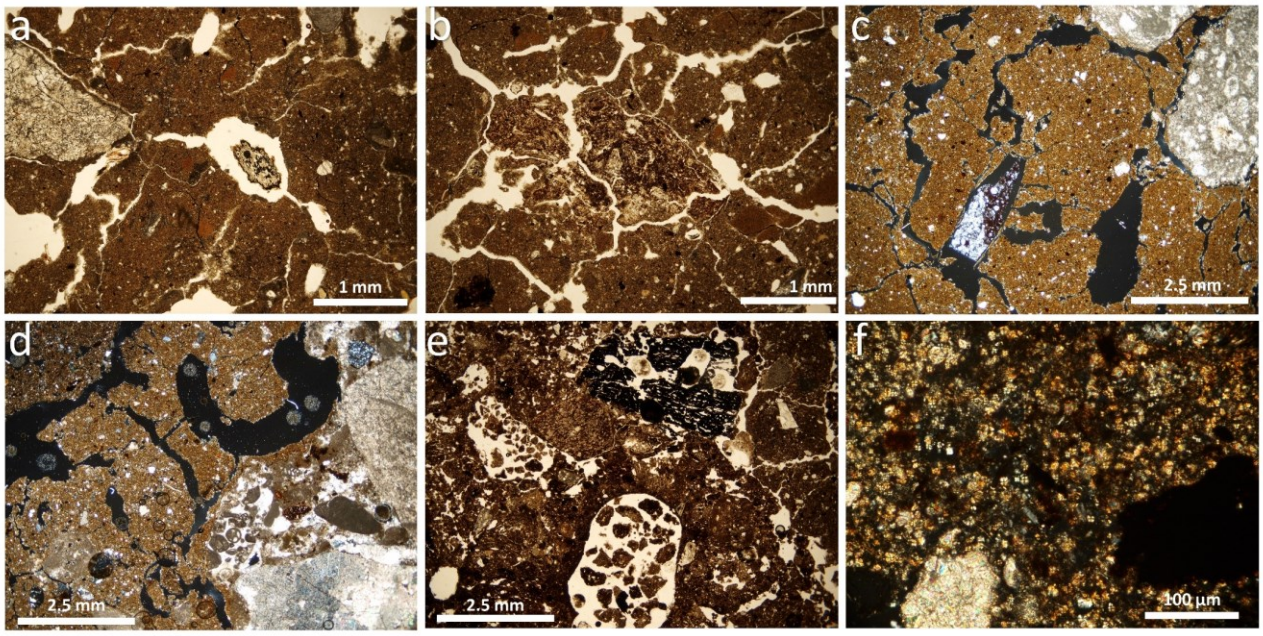


**Figure 4.** Thin section photomicrographs of notable features from Site Khinis 133. (A) and (B) respectively show PPL views of plant root tissue and a deformed small faecal pellet from SU13, both found within a mildly pedogenized silty clay matrix. (C) XPL view of unsorted clasts included within the chaotic crystallitic colluvial matrix of SU6. (D) XPL view of the upper unsorted colluvial deposit (SU4) showing bioturbation features. (E) PPL view of charcoal, bioturbation, and disrupted herbivore faecal remains from SU3, the lower pastoral occupation layer. (F) XPL view of faecal spherulites from SU2, the layer showing the most intense evidence of pastoral occupation within the pedostratigraphy of Site Khinis 133.

### 7.5.2 Khinis canal site 834 or Dar Basta

Site 834, or Dar Basta (36.726125°N, 43.433732°E), is a trench excavated approximately 3 km downstream of site 133, on the right bank of the Gomel River. Likewise, site 133, the canal was cut directly within the Plio-Pleistocene conglomerates of the Bai Hassan Formation, although the left bank partially sets within the heteromeric gravelly soil developed over the conglomerates (Figure 5A). The mean dimensions of the canal in this tract are 6 m deep and 18 m wide, but in the section here investigated the canal is narrower due to eastern bench sediments accumulation. The shape of the cut is different from Site 133, with a wider walkway indentation on the right bank and a very gently sloping left bank (Figure 1B-C). The excavated trench of site Khinis 834 (W 18.7m; H 3.4m), again, reveals a relatively simple stratigraphy (Figure 5B). The succession starts with a basal layer (SU 8) of weakly laminated clay-silt, showing macroscopic hydromorphic features such as iron-enriched oblate pseudo-laminations, whose original morphology is disrupted and altered by diffuse bioturbation caused by plants and fossorial animals (Figure 5C-D). The layer contains few organic remains (shell fragments, bone fragments, root tissue), and micromorphology (Table 1, Figure 6C-D and Supplementary Materials, File 2) reveals diffuse Fe/Mn nodules, solutional alteration of clasts and growth of acicular micrite (i.e., calcite mineralized as sub-millimetric needles) within voids, caused by slow progressive desiccation of the canal bottom. The overlying layers (SUs 6 and 5) are thick, poorly sorted colluvium. Micromorphology reveals the rare presence of organic remains (bone and shell fragments), although relatively common bioturbation, especially in SU 5, and slight pedogenesis are also present, along with acicular micrite within voids in the lower portion. The stratigraphy is sealed by a relatively dark topsoil (SU 1) developed, again, on a poorly sorted colluvial deposit. No micromorphology is available for this layer.

### 7.5.3 Jerwan aqueduct site 900

Site 900 (36.670245°N, 43.392145°E) is a trench excavated along the Jerwan aqueduct, a longitudinal E-W extension of the Khinis canal. The trench is placed approximately 5 km SE of Shaikhan village, but on the other side of the low-lying NW-SE anticline stemming just east of the village. The aqueduct was set on Quaternary fluvial and hillslope deposits and required a bottom plaster lining to hamper water permeability. The cut is shallow and very large, measuring approximately 1.7 m in depth and 26 m in width, with stone kerbs flanking the sides. The excavated trench of site Jerwan 900 (W 26.5m; H 1.7m) revealed a slightly different archaeological context compared to trenches Khinis 133 and 834 (Figure 6A-B). Herein, the original feature itself was, as introduced, an aqueduct built at ground level by lining a wide but relatively shallow cut with mortar and stones. The aqueduct was abandoned and filled with a depositional layer (SU 9) transitioning from water-lain pale hydromorphic clay-silt

to colluvial darker silty clay. Under the microscope (Table 1, Figure 6 C-D and Supplementary Materials, File 2), the lower portion shows abundant animal- and plant-caused bioturbation (plentiful canals, root tissue, worm calcite nodules) with minimal formation of peds, whereas moving upwards the deposit presents features of consistent threading such as the presence of faecal pellets and platy microstructure induced by unloading rebound of compressed clay. The canal was in fact later converted into a road, as further testified by added lateral stoneware kerbs and by macroscopic evidence of trodden and trampled dark layers (Sus 6, 10, 11, 8, unavailable for micromorphology). The road was later abandoned, and a thick, poorly sorted, and sparsely bioturbated colluvial deposit (Sus 4, 7, 2) took over again. In micromorphology, SU 2 presents an enhanced presence of phosphate nodules (i.e., sub-millimetric amorphous phosphate mineralization associated with abundant presence of degraded organic matter) compared to the neighbouring layers, testifying a possible increase in the presence of anthropic and/or animal transit. The sequence is sealed by a thin dark topsoil (SU1).

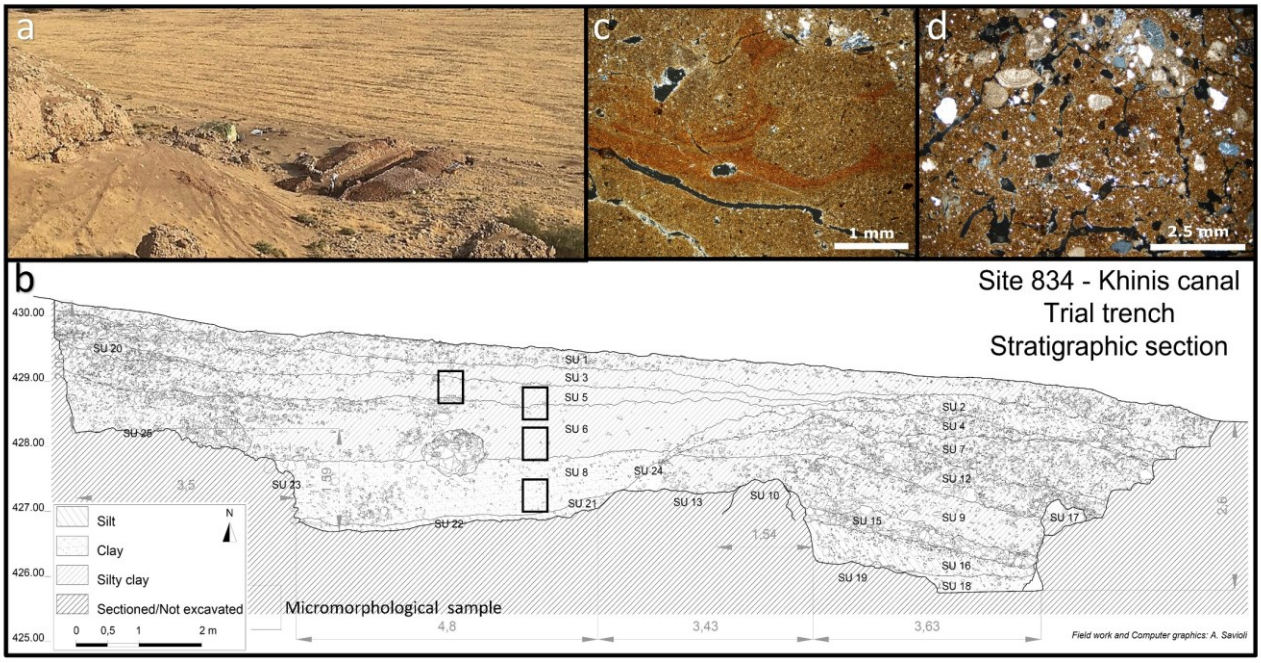


**Figure 5.** Site Khinis 834. (A) Field picture of Site Khinis 834 excavation view from West. (B) South-facing section drawing of the trench with the position of the collected micromorphological samples. Thin section photomicrographs in XPL of SU 8 and SU 5, showing (C) red hydromorphic pseudo-laminations within the basal water-lain clay-silt, and (D) unsorted colluvial material containing shell fragments and bioturbation features from the upper layers.

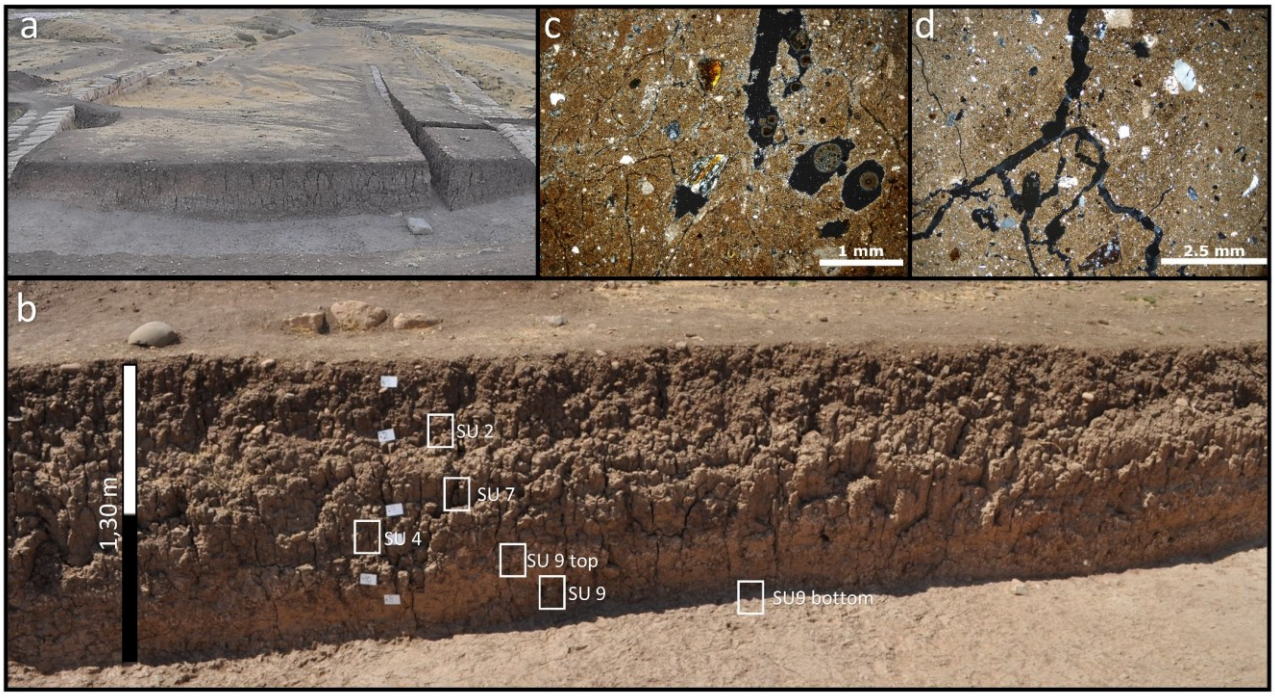


**Figure 6.** Site Jerwan 900. (A) Field picture of the Jerwan aqueduct operation with several trenches. (B) Orthomosaic picture of the northern section; rectangles indicate the position of micromorphological samples. (c) and (d) Thin section photomicrographs in XPL view of SU9 (bottom) and SU 2, showing (C) bioturbation, plant root tissue remains, and a phosphatic nodule included within mildly hydromorphic water-lain clay-silt and (D) unsorted colluvium with a silty crystalline matrix.

## 7.6 Discussion

The in-situ observations along the trenches excavated in two branches of the Khinis canal and the Jerwan aqueduct, and the micromorphological and sedimentological investigations on their natural and anthropogenic infillings, revealed consistent and substantially similar post-abandonment pedostratigraphic sequences in all sites. The sedimentary infilling of the Khinis canal, Site 133, represents the most continuous and informative among the studied ones, and its well preserved pedostratigraphic record provides higher stratigraphic resolution. The formation of the stratigraphic infilling at Site 133 can be subdivided into 5 main phases (Figure 7). The first phase refers to the period immediately after the construction and opening of the canal (post 688 ca. BCE, Neo-Assyrian Period). From the climatic point of view, it is not yet completely clear whether the activation of canals was sustained by a phase of generally high rainfall or a local decrease in precipitation stimulated its realization as a tool to harvest water in a phase of aridification (Flohr et al., 2019; Sinha et al., 2019) (Figure 8). Archaeological evidence suggests that since its excavation the canal was active and regularly managed, as testified by the absence of thick deposits of water-lain, hydromorphic sediments at its bottom. Such evidence suggests regular de-silting and maintenance. During the same period, the socio-economic structure of Northern Mesopotamia benefited from the effectiveness of

water-harvesting infrastructures, which allowed for successful emancipation from the rainfed agriculture economy (sensu Lancellotti et al., 2019) that was becoming increasingly unsustainable due to the slow but steady aridification of the climate and unreliability of the seasonal rains. While the canal was active, the hinterland of Nineveh experienced a feedbacking growth in settlement density – which reached its maximum –, societal layering, and intensification of the irrigation agricultural activity (; Morandi Bonacossi 2018a-b and references therein; Sinha et al.,2019). Nevertheless, shifting supra-regional economic and power balances, perhaps also coupled with the incipient deterioration and aridification of the climate (Sinha et al., 2019), led to the collapse of the core region of the Assyrian Empire at 612 BCE and the partial depopulation of the Assyrian hinterland settlements in favour of a southern relocation towards Lower Mesopotamia in the Neo-Babylonian Empire (Morandi Bonacossi 2008) (Figure 8). This event was probably not followed by any societal take-over in the management of the available infrastructures for water harvesting, thus resulting in the rapid desiccation and defunctionalisation of the canal system (Morandi Bonacossi in press). After the collapse of the Assyrian Empire large-scale urbanisation witnessed a severe crisis in northern Iraq. Over the course of the first millennium BCE, the region was transformed from an urbanised core area of Assyria to a rural hinterland of the Seleucid Empire, the capital of which – Seleucia on the Tigris – was located in central Iraq. However, some small-sized urban centres emerged in northern Iraq but cannot be associated with irrigation networks (Palermo et al., 2022). The lack of hydraulic infrastructures during the Seleucid period in Northern Mesopotamia indicates limited investment in the agriculture and urban life of the region during the Seleucid era. The radiocarbon determination LTL21885 from site 133 indicates that by the late Seleucid-Early Parthian period the canal had long been abandoned. The stratigraphic record for the canal's abandonment phase resides in a relatively thin layer of hydromorphic water-lain silty clay laying at the bottom of the canal (SU 13), which we interpret as the last remaining suspended load decanted from the rapidly drying up waters. Because the layer is not undisturbed, but rather shows signs of weak pedogenesis, evapotranspiration calcite nodules, diffuse bioturbation, and the presence of shell fragments and very small unaltered faecal pellets (possibly, rodent droppings), we speculate that for a short period the canal bottom was cyclically swamped by ephemeral ponds sustaining weed, reeds, invertebrate fauna, and small burrowing animals. The third phase of infilling of the canal (Figure 7) corresponds to profuse colluvial events that caused the build-up of more than 2m of heteromeric interlayered non-pedogenized deposit. Such sedimentary phase occurred under unstable climatic conditions (Sinha et al., 2019), and was likely triggered and promoted by trampling and grazing of flocks in the proximity of the steep overbank of the canal, which at the time was probably still considered a useful landmark

for optimal transit across the landscape. This is a common process found in semi-arid regions of the world (Henry et al.,2017; Zerboni & Nicoll, 2019), where pastoralism represented a recurrent subsistence strategy throughout historical and protohistoric times during spells of climatic unreliability. Therein, soil particles mobilization caused by herding is a major cause of destabilisation of fragile soils, which leads to widespread erosion and disruption of pristine deposits and subsequent mass displacement of mobilised material (Butler 1995; Evans 1998; Rosen 2016; Henry et al.,2017; Zerboni & Nicoll, 2019; Costanzo et al., 2022). With a chronological constraint bracketed between the late stages of phase 2 (supposed second half of the 6th century BCE) and the early second millennium CE – terminus determined on the basis of Middle Islamic period ceramic material found within the overlying layers (SU 10 and SU 3)–, and further anchoring provided by the above-mentioned radiocarbon date from SU6 (230–40 cal BCE), the colluvial build-up occurred for a long period encompassing the Neo-Babylonian, Achaemenid, Seleucid, Parthian, Sassanid and Early Islamic periods, without stratigraphically or pedogenetically noticeable discontinuities or stasis.

Phase 4 is posterior to the late 1st millennium CE, and more specifically can be ascribed to the Middle Islamic period (1200-1600 CE) based on ceramic finds included in the deposit. This phase is characterised by intensive stabulation and accumulation of herbivore dung, ash, and litter that were interlayered, compacted, and welded together with the underlying colluvium by trampling (SUs 2, 10, 3). The occupation was probably encouraged by the secluded setting of this specific trait of the canal, which is protected by a tall rock wall on its western side providing shade and shelter for animal-keeping, which was likely periodic and connected with strategic itinerant pasture. Paleoclimatic data for this period revealed a phase of moderate to intense climatic variability, with a marked trend towards dry conditions (Marsh et al., 2018).

The fifth and last identified phase of evolution of the pedostratigraphic sequence of the canal likely took place after 1600 CE and up to the present day, although the post-quem is only given by the lack of any dating material and relies on the presence of the Middle Islamic period's ceramics within the underlying level (Figure 7). During phase 5 SU 1 accumulated, which is again characterised by intense stabulation related to squattering pastoral occupation, with probable remains of shelters and corrals built with large square stones (Figure 2). Although to a lesser extent than in the older pastoral phases (SUs 2, 10, 3), accumulation of bone fragments, gastropod shells and abundant herbivore dung are compacted by continuous trampling and welded together with continuously amassing colluvial sediments, which kept building up because of hydrogeologic and biogeomorphological phenomena.

Over time, as the regional climate turned progressively drier, the water management system was abandoned, and we noted a general defunctionalisation of canals and aqueducts. Thin layers of

waterlain sediments are recurrent at the very bottom of canals, being the sole remains of sedimentation during the phases of activity of the system and testifying, like in other sites (Mariani et al., 2020), the regular maintenance of the canals. Moreover, microscopic traces of subaerial desiccation suggest the subsequent abandonment of the canal. At the same time, the sedimentary infilling of water-related implements suggests a shift in land use from agricultural to dominantly pastoral, also confirmed by the increased rate of denudation processes and activation of colluvial processes. The water lain sediments are overlain by a thick sequence of unsorted colluvial deposits that relate to an advanced abandonment stage characterised by slope instability caused by general neglect and probably exacerbated by deteriorating drying climate. Then, under relatively stable climatic conditions (Flohr et al., 2019) (Figure 8), the regional economy of what used to be the Assyrian Triangle balanced upon the establishment of "squatter" settled pastoralism (Curtis 2003). This is confirmed by the top layers of the sequences, that bear abundant evidence of trampling, stabulation and squattering, testifying intense pastoral occupation along the backfilled canals.

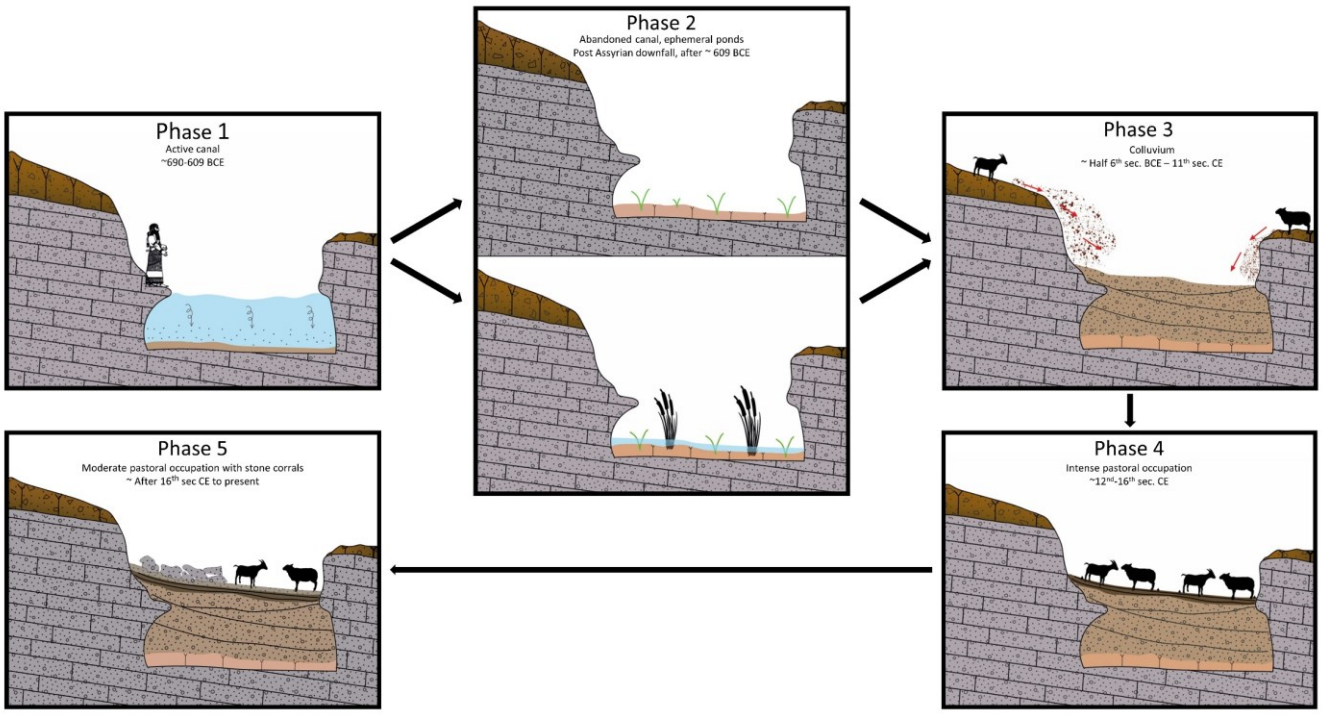


**Figure 7.** Graphic representation of the phases identified within the pedostratigraphic record of Site 133. Phase 1: the canal is active and regularly maintained, with only a thin layer of decanted fine-grained sediment coating the bottom. Phase 2: the canal is abandoned and alternating periods of desiccation and formation of small ponds and puddles take place. Phase 3: the climate dries up, the regional economy shifts towards pastoralism, and colluvial infilling is triggered by flocks trampling over unstable fragile soil surrounding the canal. Phase 4: the canal is partially backfilled and easily accessible for sheltering flocks on the move, which produce sizable dung layers trampled and welded with the underlying colluvium. Phase 5: the canal is established as a transhumance landmark, but stabulation is reduced compared to the previous period.

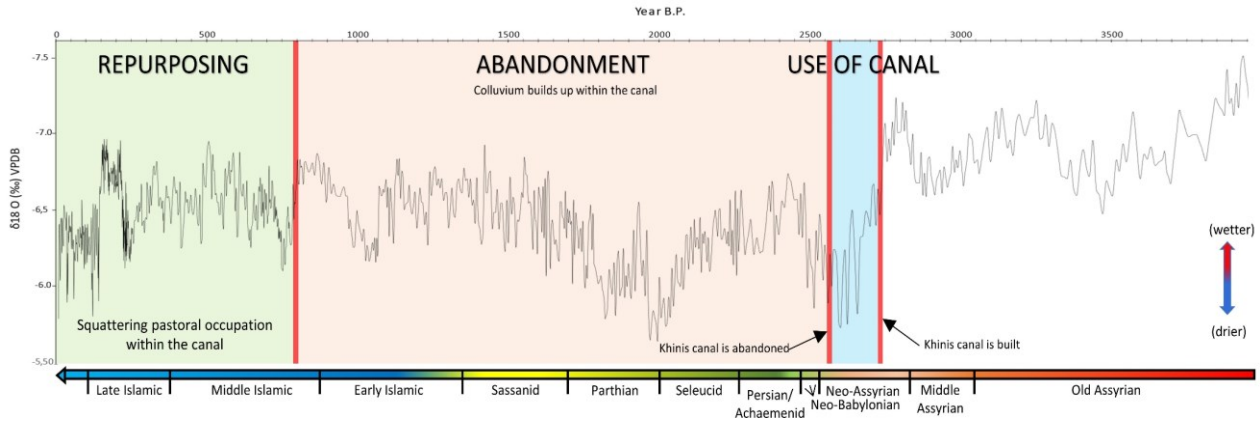


**Figure 8.** The main events of the canal's existence - construction, use, abandonment, repurposing -, are superimposed with a regional climatic (curve adapted from Sinha et al., 2019), providing context for the event.

## 7.7 Conclusion

In this study, we examined the post-abandonment formation processes of the natural and anthropogenic infilling of the Khinis canal system, commissioned by King Sennacherib and built during his reign between 705 and 681 BCE to provide water-management infrastructures to the northern outskirts of the Nineveh hinterland. The pedostratigraphic, sedimentological and micromorphological analyses of three excavated trenches highlighted consistency in the formation processes throughout the longitudinal extension of the canal, with a well-defined succession of processes and events that started in the second half of the 6th century BCE and protracted until the present day. The canal's infilling process can be subdivided into three separate main categories: (i) waterlain desiccated and pedogenized clay lies at the bottom, testifying the canal abandonment ad a subsequent short period of stasis; (ii) thick heterometric colluvium constitute the central and most prominent part of the pedostratigraphy, and testifies slope instability with episodes of mass displacement lasting for several centuries; (iii) anthropogenic layers, namely the Middle Islamic pastoral corral deposits such as ash and dung accumulation, sit atop the colluvium, testifying an opportunistic repurposing of the partially backfilled canal.

The investigation on the infilling of the Khinis canal also offers a further opportunity to investigate Late Holocene environmental changes and land use strategies from different perspectives (Stephens et al., 2020). From the paleoclimatic point of view, the geoarchaeological study of archaeological sediments contribute to reconstruct the influence of climate changes on surface processes, thus supporting paleoclimatic data from continental archives that in Northern Mesopotamia are scanty, in many cases discontinuous, and distributed far from the study area. Archaeological sediments are a complementary archive of environmental data useful to support regional to local reconstructions. On the other hand, our case study represents an exemplary case of the interconnection between human

dynamics, climatic unpredictability and shifts in subsistence strategies in times of societal changes (Zhang et al., 2018; Nicoll & Zerboni, 2020; Silva et al., 2022). In fact, all sedimentary deposits – thus the processes underlying their formation – are the result of interplay between moving human societies and the environmental conditions where they set in and suggest a transition from agricultural- to pastoral-dominated land use. Colluvial deposits are the outcome of slope instability of overhanging rock walls, conditioned by drying climate but triggered by the enhanced animal trampling and stripping of the fragile topsoil during a period of substantial transition in the regional economy from agriculture to pastoralism. Pastoral occupation layers are the outcome of opportunistic repurposing of the now backfilled canal, which became easily accessible by shepherds looking for sheltered stationing for their flocks in the culminating period of pastoralism, thus preserving evidence of land use changes and societal readjustments over centuries. This work further demonstrates that the post-abandonment infillings of negative archaeological structures efficiently support landscape archaeology studies in detecting evidence of past land use and exploitation of natural resources. Even though such deposits have a low chronological resolution (Mariani et al., 2020), their micromorphological investigation allows interpreting landscape evolution and land use changes occurred after the abandonment of an archaeological area supporting archaeological reconstruction. As in the case of Mesopotamian water harvesting systems, geoarchaeological investigation needs to focus on post-abandonment deposits that may disclose unexpected evidence describing the evolution of archaeological landscapes.

## 7.8 Supplementary material

### 7.8.1 S1 Stratigraphic Units description

***Site 133 Khinis Canal***

US 1: clay-silty with granular and blocky structure well expressed. Presence of subangular and rounded pebbles with evident bioturbation. Scarce and common centimetres CaCO3 concretions. Sharp lower boundary Colour 10YR 6/2

US 2: two black clay ashy layers with scarce charcoals with a middle massive layer similar to US 1 with bioturbation and mottling. Scarce centimetres CaCO3 concretions 2,5Y 4/1 (matrix) and 2,5Y 6/1 (mottling)

US 10: silty loam layer with common subrounded pebbles with scarce centimetres CaCO3 concretions Sharp lower boundary. Colour 10YR 5/3

US 3: two black clay ashy layers with scarce charcoals with a middle massive layer similar to US 1 with bioturbation and mottling. Scarce centimetres CaCO3 concretions Colour 2,5Y 4/1 (matrix) and 2,5Y 6/1 (mottling)

US 4: silty-clay colluvial matrix-support massive, with a very low porosity and scarce to common subrounded pebbles. Scarse centimetres CaCO3 concretions. Very sharp lower boundary. Colour 10YR 5/6 (matrix)

US 5: silty-clay matrix and locally clast support colluvial layer with abundant subrounded to angular pebbles. Scarce to rare charcoals, CaC03 concretions and Mn nodules Colour 7,5YR 5/6

US 6: silty-clay matrix and locally clast support colluvial layer with common small subrounded to angular pebbles. Scarce to rare charcoals and terrestrial shells Colour 7,5YR 5/6

US 7: silt, matrix and clast support colluvial layer with abundant small subrounded to angular pebbles. Scarce to rare charcoal fragments Colour 10 YR 4/2

US 8: silty-clay, matrix and locally clast support colluvial layer with abundant small subrounded to angular pebbles. Scarce to rare charcoals, CaC03 concretions and Mn nodules. Colour 7,5YR 4/4

US 9: clay layer with massive to blocky structure and scarce pebbles. Scarce to rare charcoals, CaC03 concretions. Colour 7,5YR 4/4

US 13: clay-silty layer with massive to platy structure and scarce pebbles. Scarce to rare charcoals, CaC03 concretions. Colour 7,5YR 4/4

***Site 834 Khinis Canal***

US 8: massive clay layer with CaCO3 concretions in the void. Low porosity and small CaCO3 nodules. 10YR8/2

US 6 and 5: compact and massive clay-slity layer with subangular blocky to prismatic structure. 10YR 5/4

***Site 900 Jerwan aqueduct***

US 1: silty clay layer with subangular blocky structure and heterometric pebbles. 2,5Y 4/2

US 2: clay layer with blocky to prismatic structure. Scarce to rare small Coarse fraction 2,5Y 5/2

US 7: clay layer with blocky to prismatic structure and CaCO3 concretions toward the bottom. 10YR 6/2

US 4: clay layer with blocky to prismatic structure, CaCO3 concretions with rare pebbles. 10YR 5/3

US 9: clay layer with angular blocky structure, CaCO3 concretions with hydromorphic traces 7,5 YR 5/3 mottles 2,5YR 6/6

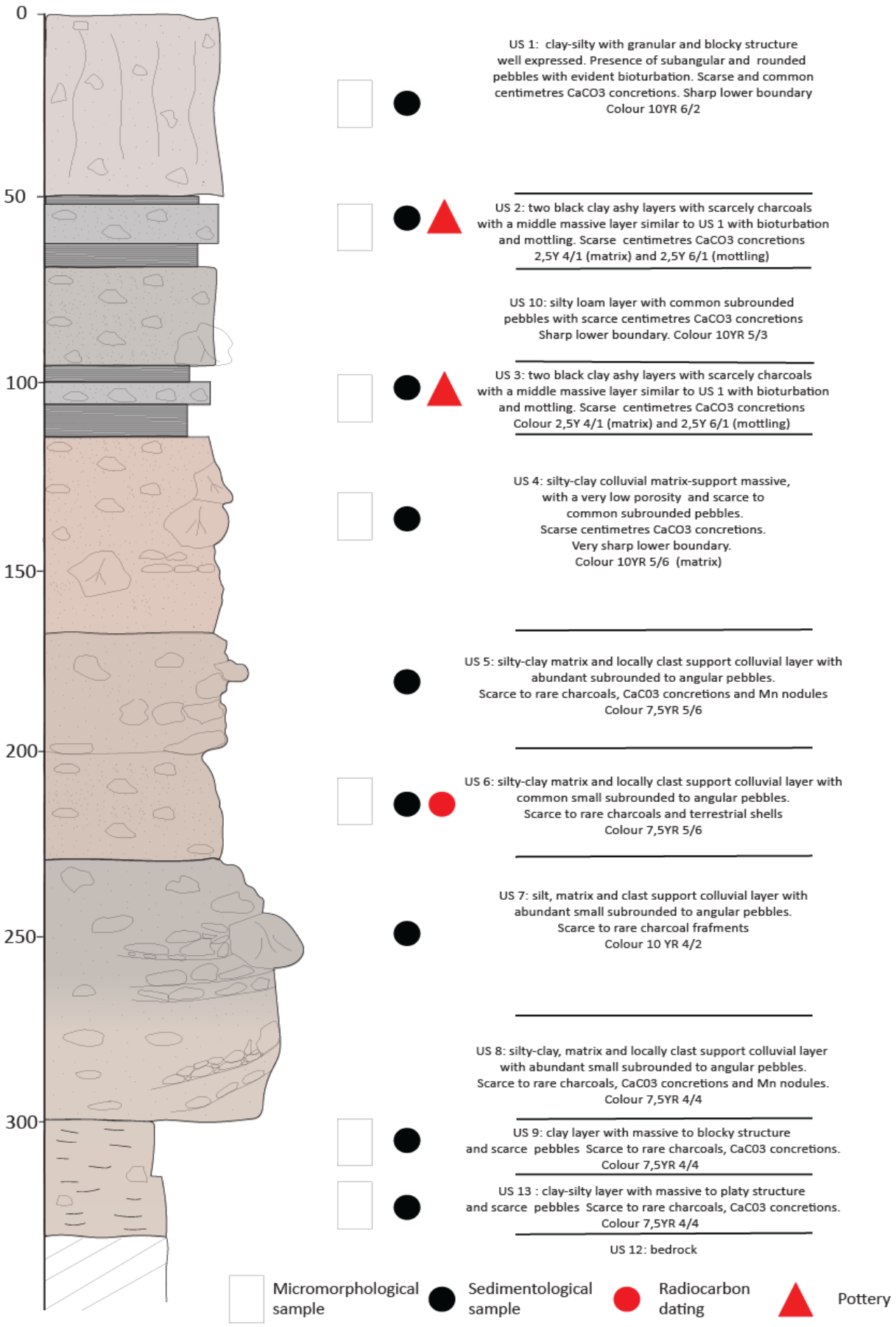


**Figure S1.** stratigraphic log of Khinis 133 and relative field descriptions and samples

### 8.8.2 S3 Radiocarbon dating

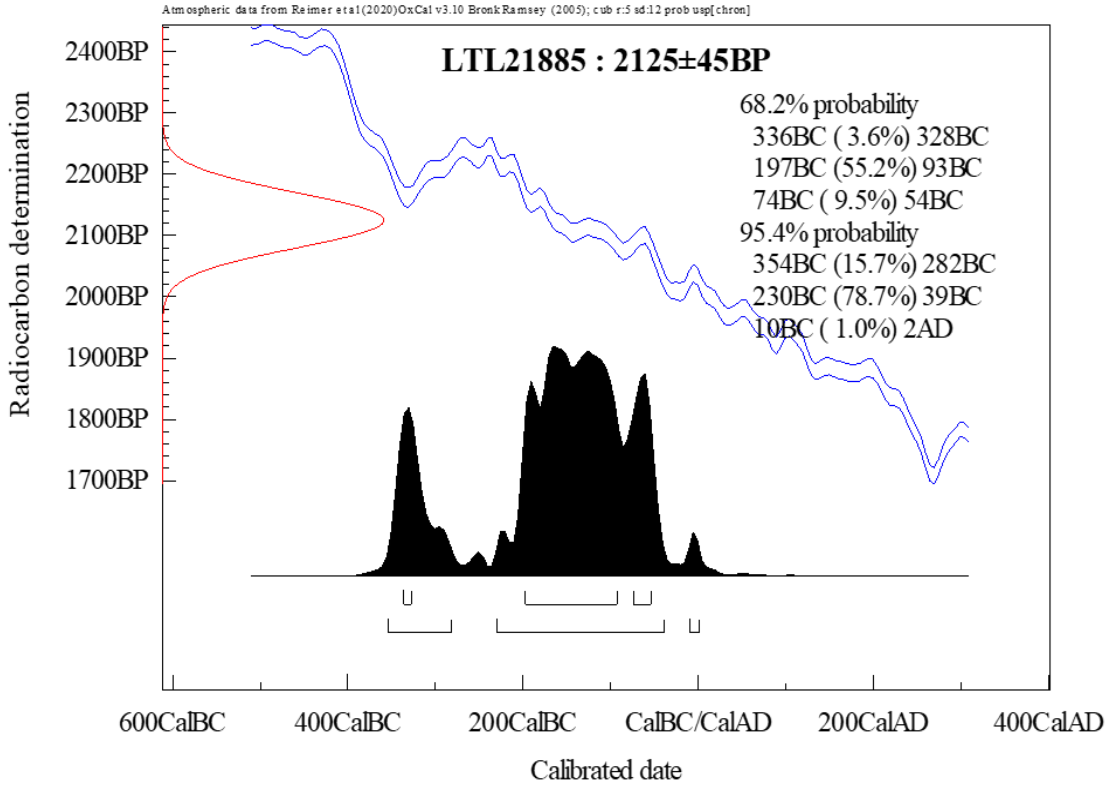


**Figure S3**. calibration curve of the LTL21885 with OxCal20

### 7.8.3 S4 Sedimentological analysis

Samples for sedimentological analyses were collected, labelled, and processed with reference to the Stratigraphic Units (SU) identified during the archaeological excavation of the trenches. Here we present a graphic representation of the relative grain size abundance.

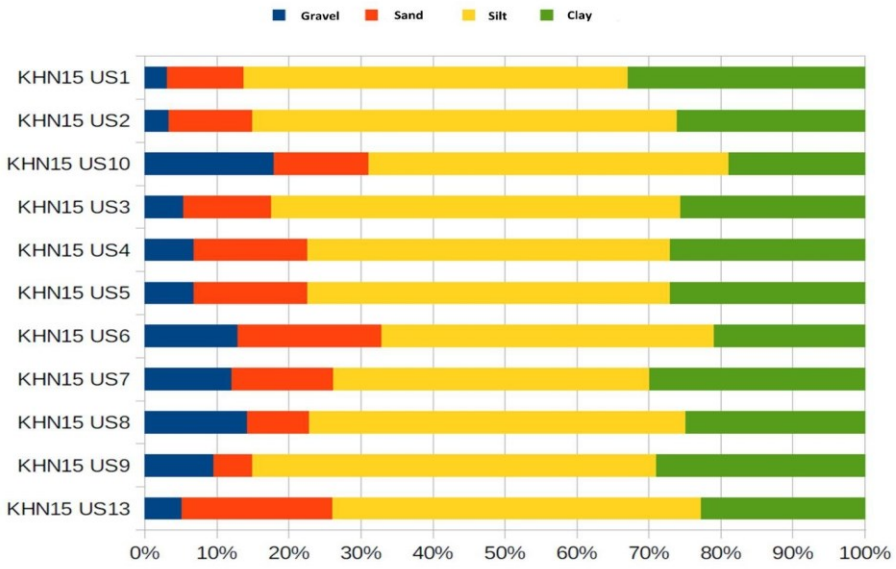


**Figure S4**. Graphic representation of the relative grain size abundance in the stratigraphic section of Khinis 133.

## 7.9 References

Awchi, T. A., & Kalyana, M. M. (2017). Meteorological drought analysis in northern Iraq using SPI and GIS. *Sustainable Water Resources Management*, *3*(4), 451-463.

Bagg, A. M. (2000). Irrigation in northern Mesopotamia: Water for the Assyrian capitals (12th–7th centuries BC). *Irrigation and Drainage Systems*, *14*(4), 301-324.

Beck, P. (2018). future Köppen-Geiger climate classification maps at 1-km resolution, Sci. *Data https://doi. org/10.1038/sdata*.

Butler, D. R. (1995). *Zoogeomorphology: animals as geomorphic agents*. Cambridge University Press.

Charbonnier, J., Purdue, L., & Benoist, A. (2017). Taming surface water in pre-Islamic southeast Arabia: archaeological, geoarchaeological, and chronological evidence of runoff water channeling in Masāfī (UAE). *Journal of Field Archaeology*, *42*(1), 13-28.

Costanzo, S., Zerboni, A., & Manzo, A. (2022). Active surface processes at Mahal Teglinos (Kassala, Eastern Sudan): Archaeological implications for an endangered protohistoric site in Sahelian Africa. *Journal of Archaeological Science: Reports*, *43*, 103452.

Cremaschi, M., Degli Esposti, M., Fleitmann, D., Perego, A., Sibilia, E., & Zerboni, A. (2018). Late Holocene onset of intensive cultivation and introduction of the falaj irrigation system in the Salut oasis (Sultanate of Oman). *Quaternary Science Reviews*, *200*, 123-140.

Cremaschi, M., Mercuri, A. M., Torri, P., Florenzano, A., Pizzi, C., Marchesini, M., & Zerboni, A. (2016). Climate change versus land management in the Po Plain (Northern Italy) during the Bronze Age: New insights from the VP/VG sequence of the Terramara Santa Rosa di Poviglio. *Quaternary Science Reviews*, *136*, 153-172.

László, C., Ágoston, S., Tamás, P., László, K., Salae, A. T., & Athar, A. (2012). Structural evolution of the northwestern Zagros, Kurdistan Region, Iraq: Implications on oil migration. *GeoArabia*, *17*(2), 81-116.

Curtis, J. E. (2003). The Assyrian heartland in the period 612-539 BC. *Continuity of Empire: Assyria, Media, Persia*, *5*, 157.

Dercourt, J., Zonenshain, L. P., Ricou, L. E., Kazmin, V. G., Le Pichon, X., Knipper, A. L., ... & Biju-Duval, B. (1986). Geological evolution of the Tethys belt from the Atlantic to the Pamirs since the Lias. *Tectonophysics*, *123*(1-4), 241-315.

Dewey, J. F., Pitman, W. C., Ryan, W. B., & Bonnin, J. (1973). Plate tectonics and the evolution of the Alpine system. *Geological society of America bulletin*, *84*(10), 3137-3180.

Erhart, H. (1956). *La genèse des sols en tant que phénomène géologique: esquisse d'une théorie géologique et géochimique, biostasie et rhexistasie* (Vol. 8). Paris: Masson.

Evans, R. (1998). The erosional impacts of grazing animals. *Progress in Physical Geography*, *22*(2), 251-268.

Flohr, P., Fleitmann, D., Zorita, E., Sadekov, A., Cheng, H., Bosomworth, M., ... & Matthews, R. (2017). Late Holocene droughts in the Fertile Crescent recorded in a speleothem from northern Iraq. *Geophysical Research Letters*, *44*(3), 1528-1536.

Forti, L., Mariani, G. S., Brandolini, F., Pezzotta, A., & Zerboni, A. (2022). Declassified intelligence satellite imagery as a tool to reconstruct past landforms and surface processes. The submerged riverscape of the Tigris River below the Mosul Dam Lake, Iraq. *Earth Surface Processes and Landforms*.

Forti, L., Perego, A., Brandolini, F., Mariani, G. S., Zebari, M., Nicoll, K., ... & Zerboni, A. (2021). Geomorphology of the northwestern Kurdistan Region of Iraq: landscapes of the Zagros Mountains drained by the Tigris and Great Zab Rivers. *Journal of Maps*, *17*(2), 225-236.

Fouad, S. F. (2014). Western Zagros fold–Thrust Belt, part II: The high folded zone. *Iraqi bulletin of geology and mining*, (6), 53-71.

Gale, S. J., & Hoare, P. G. (1991). *Quaternary sediments: petrographic methods for the study of unlithified rocks* (pp. 101-125). London: Belhaven Press.

Henry, D. O., Cordova, C. E., Portillo, M., Albert, R. M., DeWitt, R., & Emery-Barbier, A. (2017). Blame it on the goats? Desertification in the Near East during the Holocene. *The Holocene*, *27*(5), 625-637.

Jacobsen, T., & Lloyd, S. (1935). Sennacherib's aqueduct at Jerwan. *Oriental Institute publications*.

Jassim, S. Z., & Goff, J. C. (2006). *Geology of Iraq*. DOLIN, sro, distributed by Geological Society of London.

Koppen, W. & Geinger, G. (1936). Das geographische system der klimat. *Handbuch der klimatologie*, Gebr, Borntraeger, 1–44.

Lancelotti, C., Biagetti, S., Zerboni, A., Usai, D., & Madella, M. (2019). The archaeology and ethnoarchaeology of rain-fed cultivation in arid and hyper-arid North Africa. *antiquity*, *93*(370), 1026-1039.

Li, Y., Storozum, M. J., Wang, X., & Guo, W. (2017). Early irrigation and agropastoralism at Mohuchahangoukou (MGK), Xinjiang, China. *Archaeological Research in Asia*, *12*, 23-32.

Macphail, R. I., & Goldberg, P. (2018). *Applied soils and micromorphology in archaeology*. Cambridge University Press.

Malinowski, J. C. (2002). Iraq: A Geography. Department of Geography & Environmental Engineering, West Point

Mariani, G. S., Muntoni, I. M., & Zerboni, A. (2020). The Eneolithic/Bronze Age transition at Tegole di Bovino (Apulia): geoarchaeological evidence of climate change and land-use shift. *Quaternary*, *3*(2), 14.

Morandi Bonacossi, D. (2008). Betrachtungen zur Siedlungs-und Bevölkerungsstruktur des Unteren Habur-Gebietes in der neuassyrischen Zeit. *Umwelt und Subsistenz der neuassyrischen Stadt Dūr-Katlimmu am unteren Habur*, 189-214.

Morandi Bonacossi, D. (2018a). Water for Nineveh. The Nineveh Irrigation System in the regional context of the 'Assyrian Triangle': A first geoarchaeological assessment. *Water for Assyria*, 77-115.

Morandi Bonacossi, D. (2018b). The creation of the Assyrian Heartland: New data from the "Land behind Nineveh,". *The Archaeology of Imperial Landscapes. A Comparative Study of Empires in the Ancient Near East and Mediterranean World*, 48-85.

Morandi Bonacossi D (in press), The Assyrian Legacy in the Land behind Nineveh, in M. Blömer, M. Marciak, and T. Schreiber (eds.), *Trans-Regional Encounters. Kingdoms and Principalities of the Taurus, Zagros, and Caucasus Regions between 300 BCE and 200 CE*.

Mouthereau, F., Lacombe, O., & Vergés, J. (2012). Building the Zagros collisional orogen: timing, strain distribution and the dynamics of Arabia/Eurasia plate convergence. *Tectonophysics*, *532*, 27-60.

Murphy, C. P. (1986). *Thin section preparation of soils and sediments*. AB Academic Publishers, Berkhamsted.

NextGIS (2021). QuickMapServices. https://nextgis.com/blog/quickmapservices/.

Nicoll, K., & Zerboni, A. (2020). Is the past key to the present? Observations of cultural continuity and resilience reconstructed from geoarchaeological records. *Quaternary International*, *545*, 119-127.

Nicosia, C., & Stoops, G. (Eds.). (2017). *Archaeological soil and sediment micromorphology*. John Wiley & Sons.

Oates D (1968). Studies in the Ancient History of Northern Iraq. London: Oxford University Press for the British Academy.

Palermo, R., De Jong, L., & Ur, J. A. (2022). Hellenistic Landscapes and Seleucid Control in Mesopotamia: The View from the Erbil Plain in Northern Iraq. American Journal of Archaeology, 126(3), 425-442.

QGIS Development Team (2021) - QGIS Geographic Information System. Open-Source Geospatial Foundation Project

Reade, J. (1978). Studies In Assyrian Geography: Part I: Sennacherib and The Waters of Nineveh. *Revue d'Assyriologie et d'archéologie orientale*, *72*(1), 47-72.

Rosen, S. (2016). *Revolutions in the desert: the rise of mobile pastoralism in the Southern Levant*. Routledge.

Salman, S. A., Shahid, S., Ismail, T., Ahmed, K., Chung, E. S., & Wang, X. J. (2019). Characteristics of annual and seasonal trends of rainfall and temperature in Iraq. *Asia-Pacific Journal of Atmospheric Sciences*, *55*(3), 429-438.

Silva, F., Coward, F., Davies, K., Elliott, S., Jenkins, E., Newton, A. C., ... & Williams, A. (2022). Developing transdisciplinary approaches to sustainability challenges: the need to model socio-environmental systems in the longue durée. *Sustainability*, *14*(16), 10234.

Sinha, A., Kathayat, G., Weiss, H., Li, H., Cheng, H., Reuter, J., ... & Edwards, R. L. (2019). Role of climate in the rise and fall of the Neo-Assyrian Empire. *Science advances*, *5*(11), eaax6656.

Sissakian, V. K., & Fouad, S. F. (2014). Geological Map of Arbeel and Mahabad Quadrangles Sheets NJ-38-14 and NJ-38-15, Scale 1 V 250:000. *Iraq Geological Survey Publications, Baghdad, Iraq*.

Stephens, L., Fuller, D., Boivin, N., Rick, T., Gauthier, N., Kay, A., ... & Ellis, E. (2019). Archaeological assessment reveals Earth's early transformation through land use. *Science*, *365*(6456), 897-902.

Stoops, G. (2021). *Guidelines for analysis and description of soil and regolith thin sections* (Vol. 184). John Wiley & Sons.

Stoops, G., Marcelino, V., & Mees, F. (Eds.). (2018). *Interpretation of micromorphological features of soils and regoliths*. Elsevier.

Storozum, M., Liu, H., Qin, Z., Ming, K., Fu, K., Wang, H., & Kidder, T. (2018). Early evidence of irrigation technology in the North China Plain: geoarchaeological investigations at the Anshang site, Neihuang County, Henan Province, China. *Geoarchaeology*, *33*(2), 143-161.

Strahler, A. N. (1958). Dimensional analysis applied to fluvially eroded landforms. *Geological Society of America Bulletin*, *69*(3), 279-300.

Tamburrino, A. (2010). Water technology in ancient Mesopotamia. In *Ancient water technologies* (pp. 29-51). Springer, Dordrecht.

Ur, J. (2005). Sennacherib's northern Assyrian canals: new insights from satellite imagery and aerial photography. *Iraq*, *67*(1), 317-345.

USGS (1968). Declassified Corona Imaging data. Data retrvied on 16 august, 2020, from https://corona.cast.uark.edu.

Wilkinson, T. J., Rayne, L., & Jotheri, J. (2015). Hydraulic landscapes in Mesopotamia: The role of human niche construction. *Water History*, *7*(4), 397-418.

Wilkinson, T. J., Ur, J., Wilkinson, E. B., & Altaweel, M. (2005). Landscape and settlement in the Neo-Assyrian Empire. *Bulletin of the American Schools of Oriental Research*, *340*(1), 23-56.

Zebari, M., Grützner, C., Navabpour, P., & Ustaszewski, K. (2019). Relative timing of uplift along the Zagros Mountain Front Flexure (Kurdistan Region of Iraq): Constrained by geomorphic indices and landscape evolution modeling. *Solid Earth*, *10*(3), 663-682.

Zerboni, A., & Nicoll, K. (2019). Enhanced zoogeomorphological processes in North Africa in thehuman-impacted landscapes of the Anthropocene. *Geomorphology*, *331*, 22-35.

Zhang, J., Xia, Z., Zhang, X., Storozum, M. J., Huang, X., Han, J., ... & Dong, G. (2018). Early middle Holocene ecological change and its influence on human subsistence strategies in the Luoyang Basin, north-central China. *Quaternary Research*, *89*(2), 446-458.

# Chapter 8

# Reconstructing the buried riverscape of Erbil: long-term human overprint on landforms and present-day geomorphological hazard

## 8.1 Introduction

The geomorphological investigation on regions settled by humans since the prehistory revealed the long-term influence of the human actions on the Earth surface processes (Wilkinson 2003; Forti et al.,2021, 2022). In the contexts of urban areas, recent geomorphological mapping and analyses allowed the reconstruction of (i) human-impacted surface processes, (ii) the creation of anthropogenic landforms, (iii) the definition of urban geomorphosites, and the increased susceptibility of cities to geomorphological risks (Cremaschi, 2017; Brandolini et al., 2019; Faccini et al., 2021; Mandarino et al., 2021; Pelfini et al., 2021; Roccati et al., 2021; Vergari et al., 2021). In such contexts, the long-lasting stratification of urbanization makes difficult the observations of medium to small scale landform and the interpretation of surface processes. In fact, buildings, infrastructures, and recent anthropogenic landforms may hide pristine natural landforms (Faccini et al., 2021; Mandarino et al., 2021; Pelfini et al., 2021; Roccati et al., 2021; Vergari et al., 2021). To overcome this issue, a recent approach to reconstruct ancient riverscapes disturbed by human actions employed declassified intelligence satellite imageries (Forti et al., 2022). The geomorphological investigation on historical maps (Gurnell et al.,2003; Grabowski et al.,2014; Brandolini et al., 2019) and remote imagery (aerial and/or satellite) acquired before the great acceleration of urbanization started after WWII (Steffen et al.,2015; McNeill & Engelke, 2016) is an effective tool able to disclose the complex interaction between natural and anthropogenic geomorphic process. If we consider Western Asia, and especially the Kurdistan Region of Iraq (KRI) that was part of ancient Mesopotamia, the first human overprint on landscapes dates back to 8000 yr. BP, when at the emerge of the first urban centres settled along watercourses led to the building of anthropogenic mounds – the tells archaeological sites (Rosen, 1986) – and later to the modification of natural hydrography and a major shift in land use towards agriculture and herding tuned surface process (Zerboni & Nicoll, 2019). Moreover, the rapid and uncontrolled expansion of urban areas, soil overgrazing, the over exploitation of natural resources, and anthropogenic modification of the fluvial networks increased the susceptibility to geomorphological hazards of local urban areas (Mustafa et al., 2020).

In this contribution, we explore the geomorphological evolution of the city of Erbil in the KRI, whose fluvial landscape has been exploited and modified – especially in recent times – by the dramatic urban

expansion occurred in the last decades. Our investigation identified (i) ancient strategies to exploit local water resources by means of artificial landforms, (ii) the patterns of evolution of the city and how this process affected the natural hydrography, and (iii) the major consequences this had on the susceptibility to geomorphological hazard (e.g., floods) of Erbil. This case study highlights the importance of geomorphological mapping of urban areas using different data sources with a geoarchaeological perspective, to reconstruct the mode and tempo of urban expansion since the foundation of a city and the potential consequences of human overprint on geomorphic processes.

## 8.2 A geographic and historical perspective of Erbil

The city of Erbil or Arbil (in English) or Hawler (in Kurdish), located in a flat region at foothills of Zagros Mountain, is the capital and most populous city of the KRI (Figure 1A), being one of the four largest cities in Iraq. But the history of Erbil is very long; the city was established in the Sumerian period (912 to 609 BCE) with the name of Urbilum (from Sumerian Cuneiform Ur III) is likely one of the longest settled places in the world (Almukhtar, 2020). Today it includes the result of recent urban expansions (the modern city built since the 20th cent.) and the citadel (or Qalat) that is its historical centre of the city. Erbil is located 30 km south of Great Zab in in the alluvial plain composed by reddish clay, dissected by several streams that flowing from the Zagros foothills until to joint with the Great Zab (Forti et al., 2023). Before the middle 20th century urban expansion of Erbil, the Bastè and Tchekunem River were the main streams that crossed the city south and north respectively to the citadel (Figure 1B). The climate of Erbil is a semi-arid to Mediterranean climate with wet-cold winter and dry- hot to very hot summer and temperature ranging from 0 to 38°. The average annual rainfall is around 420 mm with 90% of the annual rainfall occurs in the winter months between December and March (Kramer et al., 1998; Hussien et al., 2019; Harris et al., 2020). The first traces of the long settlement history of Erbil date to the Ubaid and Chalcolithic period (6450-4950 BCE). Since the first settlements was established, the city progressively grew and its centrality in the socio-political scenario of Northern Mesopotamia increased during the third millennium BC (Nováček, Amin and Melčák 2008). Several written sources report that Erbil was conquered and incorporated into the empire of the Ur III dynasty (3931-3923 BCE) (Vacin, 2011). At the time of the Assyrian Empire, Erbil was an important economic and cultural centre for the heartland of Assyria as a crossroads between the cities of Babylon, Nineveh, and Assur. Under the Neo Assyrian control of the region, Erbil maintained the status of major economical centre, and achieved a great prosperity linked to the presence of a temple dedicated to the goddess Ishtar. Immediately after the fall of the Neo-Assyrian Empire (609 BCE), the city was besieged by the Medes, who turned it into an administrative centre. In the Parthian period, Erbil became one of the most important centres of Christianity in the Middle

East and experienced a great economic growth (Nováček et al., 2013; Ur et al., 2013). With the conquest by the Muslims in 642 CE, Erbil initially lost its centrality that was gained again later with the rebuilding of the fortress and the expansion of the lower agglomerations of the city during a period of strong conflicts and occupation by the Mongols between the 13th and 12th century CE. Under the Ottoman Empire, from 1534 CE onwards, the city lost importance, and in 1743 CE it was damaged during a siege of the Persians. After this event the citadel was repaired and turned into a military stronghold. Erbil remained part of the Ottoman territories until the end of World War I. Some travellers of the late 1800s reported the state of decay of building in the lower city and citadel (Rich 1836; Sarre & Herzfeld 1920; Doxiadis 1959; Al-Hashimi 2016). New improvements for the city came at the end of World War I, when the city passed under the British control with a population growth from 3,260 in 1892 to about 12,000 in 1920 (Hay,1921). This is evidenced by urban expansion occurring in the south and southwestern sectors of the citadel, along the main artery of communication towards Kirkurk (Doxidadis, 1959). The city from 1920 began a real social and economic growth coming to be established in 1971 as the capital of the Autonomous Region of Iraqi Kurdistan. In the late 20th century, the city took advantage of its administrative separation from the Republic of Iraqi and continued to grow despite several conflicts hit the region: in the last 30 years, the population increased to 1.5 million. Finally, in 2014 the citadel was addicted to the UNESCO list of World Heritage Sites thanks to its archaeological and historical value (Figure 1C-D).

## 8.3 Methods

The geomorphological mapping of the Erbil urban areas was performed through the comparison of different historical aerial imagery ranging from 1919 to 2022 derived from different datasets. The oldest images of Erbil derived from aerial flights carried out in February 1919 by the British Royal Air Force (RAF), when the urban agglomerations were concentrated within the citadel and the lower city only occupied the southern flank of the acropolis. These imageries belong to the Archaeological Institute of the University College of London and were used to map the pristine fluvial landscape before the middle 20$^{th}$ sec. urban expansion. Other aerial images used to compare the beginning of the urbanization in the citadel and northern sectors of the city were acquired by a RAF mission in January 1951 and collected by John Bradford; they are archived in the repository of the Pitt River Museum, University of Oxford (John Bradford Photographic Collection 1998.296.68). Declassified Corona satellite image dataset was derived from CAST Atlas of the University of Arkansas (https://cast.uark.edu/research/corona.php) (USGS, 1968); taken in August 1968 (1104-2138) were analysed to map the changes in land use and the rapid urbanization occurred at the end of 60ies. Furthermore, declassified HEXAGON intelligence satellite imagery of 1972 was downloaded from

Earth Explorer of USGS (https://earthexplorer.usgs.gov/) and compared with the Corona declassified imagery to highlight the fast expansion of urban areas. Historical satellite imagery has been compared to the more recent high-resolution (0.5–1 m) natural colour satellite images provided by Google Satellite imagery and Bing Virtual Earth visualized through the "QuickMapServices" plugin (NextGis, 2022) in QGIS 3.16 (Figure 1A). Digital Surface Model (DSM) AW3D30 with horizontal resolution of 1 arcsecond (circa 30 m at the equator) and hillshade model were used for highlighting the detailed scale landforms in the alluvial plain (Forti et al., 2023). The 37 imagery of the 1919 RAF acquisition were imported and processed into Agisoft Metashape Professional (Version 1.5.5) (Agisoft Metashape, 2022) with the standard workflow that includes photo alignment, built of dense cloud and mesh to produce a 3D model from which an orthophoto was extracted. The whole imagery dataset was projected to WGS84-UTM Zone 38N reference system in QGIS 3.16. Remote images were desk-analysed to detect natural landforms, especially those related to the hydrography, anthropogenic landforms, and evidence of land use before the urban expansion of Erbil (Figure 1B).

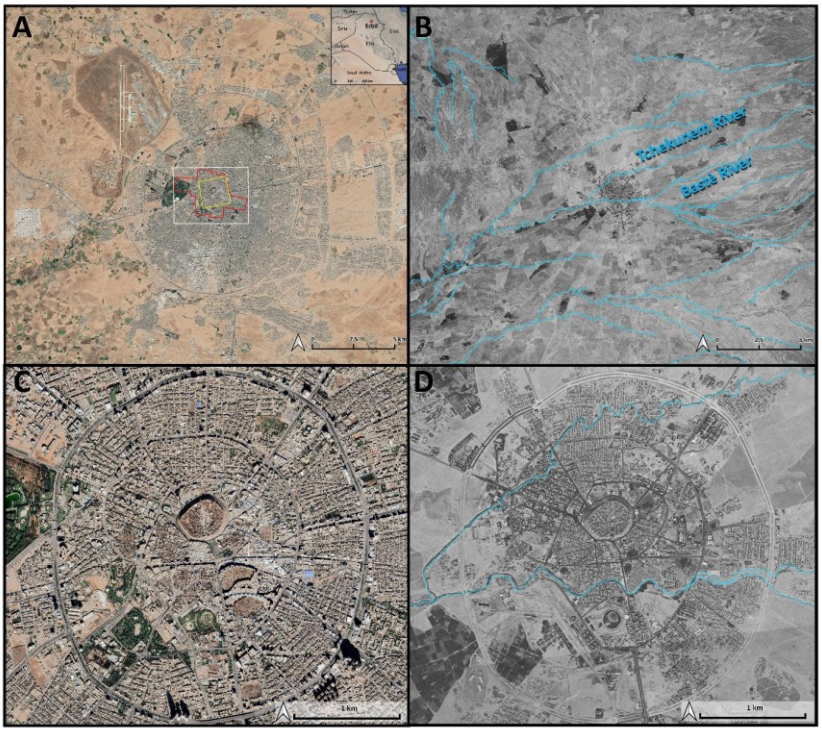


**Figure 1.** A) Recent (year 2022) high resolution satellite imagery of Erbil urban area derived from GoogleEarthTM. The red polygon indicates the area covered by RAF 1919 dataset, the yellow polygon the RAF 1951 dataset, and the white polygon is the area covered by declassified satellite imagery from 1968 to 1972. The latter is also the area covered by the detailed mapping of Figure 5. B-C) The Corona declassified imagery of the urban area of Erbil in 1968 highlights the local landscape and the pristine hydrographic network at the onset of intense urbanization. C) Recent (year2022) high resolution satellite imagery of centre of Erbil with the citadel. D) The Corona declassified imagery of the centre of Erbil in 1968.

## 8.4. Results

### 8.4.1 The 1919 RAF dataset: the riverscape, urban features and anthropogenic landforms

The aerial imagery captured in February 1919 defines the urban setting of Erbil before its major expansion occurred since the 1950s (Figure 2A). The main features of the landscape are related to the interplay between the fluvial network, in particular the streams flowing North and South of the citadel, and the human excavation accomplished to exploit natural resources. The latter includes the qanat shafts and several artificial ditches; moreover, the intense land use due to agricultural and herding activities is also evident. Geomorphological mapping was performed on the 1919 RAF dataset to detect natural fluvial features and early human control on the behaviour and shape of the streams. Here, we consider the floodplain portion stretched from the eastern termination of the alluvial fans from the Zagros foothills and the eastern side of the Daamer Dagh hills. The floodplain mainly consists of reddish silty-clay deposits interbedded with coarser layers while the alluvial fans are mainly conglomerates and the eastern slope of Daamer Dagh hills are characterized by badland landscape. Before the extensive urban expansions, this area was crossed by a hydrographic network that joined toward West into the Great Zab River (Forti et al., 2023). The main rivers that flowing surrounding Erbil were Bastè River (or Chai Erbil) in the southernmost and Tchekunem River (or Shaik Qazi) in the North that joined with the Bastè River 7 km after Erbil centre. In the area covered by 1919 RAF imagery, the Bastè River, located 600 m South of the Qalat, flowing from E to W for ca. 4 km and display a meandering planform with a regular to irregular meanders (Figure 3A). In the southeaster sector, the river initially flows in a semi-confined valley setting with a channel width of 50 m that reduces to ca. 10 m in correspondence of the urban centre. At this location, an imposed confined valley setting occurred (Figure 3B). The 1919 RAF imagery was captured during the low flow stage of the rivers (February), when different geomorphic units are exposed. Along the low sinuosity reaches, lateral, diagonal, and middle longitudinal bars are evident; while point, compound and scroll bars occurred in the inner bend of high to low sinuosity segments. Vegetated bars and compound bars are crossed by chute channel, likely active during seasonal high discharge. The seasonal discharge oversees the progressive erosion of the stream banks, where escarpment occurred sometimes marking the instream boundaries of fluvial terraces. Surrounding the Bastè River, paleochannels and ephemeral streams are evident (Figure 2B). Different from the Bastè River, the Tchekunem River, 900 m NE to Qalat, is less wide and deep with a low to sinuous/meandering planform and some straight reaches; already in the 1919 its banks seem to be reworked by human activity. In the RAF 1919 dataset, the Tchekunem River flows for ca 3 km from NNE to SSW with an upstream portion characterized by irregular meanders and steep banks that downstream display a

reduction of the degree of sinuosity and the development of small point and lateral bars (Figure 3C). The Tchekunem River suffered a wide operation of artificial rectification in the proximity of the northern fortification walls occurred during the construction of Assyrian Fortification (Novacek et al.,2013) (Figure 3D). Erbil, being one of the longest-settled places in the world, underwent numerous human modifications of the surrounding territory, but particularly of the citadel. In fact, the latter has been a fundamental point for human aggregation, which over the centuries also began to settle the territories to the south with the creation of the lower urban agglomerates and several settlement mounds surrounding the area of Erbil. The long settlement history of Erbil and the evolution of the Qalat is addressed by numerous authors in the literature (Novacek et al., 2013; Al-Hashimi 2016 and reference therein). In this context, the geomorphological map based on the RAF 1919 dataset highlights the extension of the urban setting at the end of the Ottomans dominance. The city is subdivided into two portions; the first one is the Qalat while the second is the lower city. The Qalat settlement is on the ancient artificial mound – the tell – that started growing since the Chalcolithic and arise 25-32 m above the surrounding plain (Nováček et al., 2013). Traces of ancient Assyrian to Medieval city walls and settlement mounds were mapped in the northern and southwestern sector of the area (Novaceck 2013, Al-Hashimi 2016). The urban setting is characterized by palace, public, administrative, and residential buildings with a fan-like alleyways and roads that that converge toward the southern gate destroyed in the 1940s and rebuilt several times until today (Nováček et al.2013; Al-Hashimi 2016). The toe of the Qalat is characterized by a circular moat, partially filled by rubbish, became a pathway that running along the entire perimeter of the mound Novacek et al., 2013; Al-Hashimi, 2016). The core of the lower city consists of bazaars, public areas, trading centres, mosques and an old minaret located to the SW of the citadel along the right bank of the Bastè River. The lower city is crossed by several roads and alleyways. Other urban elements mapped are the Islamic and pre-Islamic cemeteries used until the early 2000s (Novacek et al., 2013; Al-Hashimi 2016 and reference therein); the largest of them are located south of the citadel of Erbil along the banks of the Basté River and to the southwest (Figure 3B). The main anthropogenic feature identified in the area are the qanat ('Kahariz' in Kurdish) shafts, which drained groundwater from the alluvial fan located at the foothills of Zagros Mts to lowland (Shoroush et al., 2020). They consist of underground gravity-driven filtration galleries constructed for irrigation (Lightfoot, 2000; Wilkinson, 2003; Cremaschi et al., 2018); the underground galleries were connected to the surface through a series of shafts spaced 50, 100 and 200 metres where the groundwater infiltrating and transported by gravity through a gently sloping tunnel to a main canal and basin. From the geomorphological point of view, the qanat system for water management represents an anthropogenic landform of excavation (the shafts) and

accumulation (the soil heaps). At the termination of the underground system, the water was diverged by artificial ditches to fed farms, crop fields and villages. In the case of Erbil, the water supply for the qanat system come from the alluvial fans located at foothills of Zagros Mts. (Shoroush et al., 2020) and provided water to the city and the countryside from the 12th century CE until the mid-20th century (Al-Hashimi 2016 and reference therein) (Figure 4A). The 1919 RAF imagery highlight that around the citadel, excluding the urban portions, there are numerous cultivated fields, many of which are cultivated, while others have been ploughed. In some cases, due to the somewhat nadiral aerial image acquisition, it was not possible to recognise the land use of each field that were destined for agricultural and pastoral use. A wide water basin located 500 m SE the citadel with an area of approximately 6200 m2 (Figure 4B) and a large clay quarry located ca. 1 km south of the citadel on the left of the Bastè River (Figure 4C) are two further anthropogenic landforms recognized in the 1919 RAF imagery.

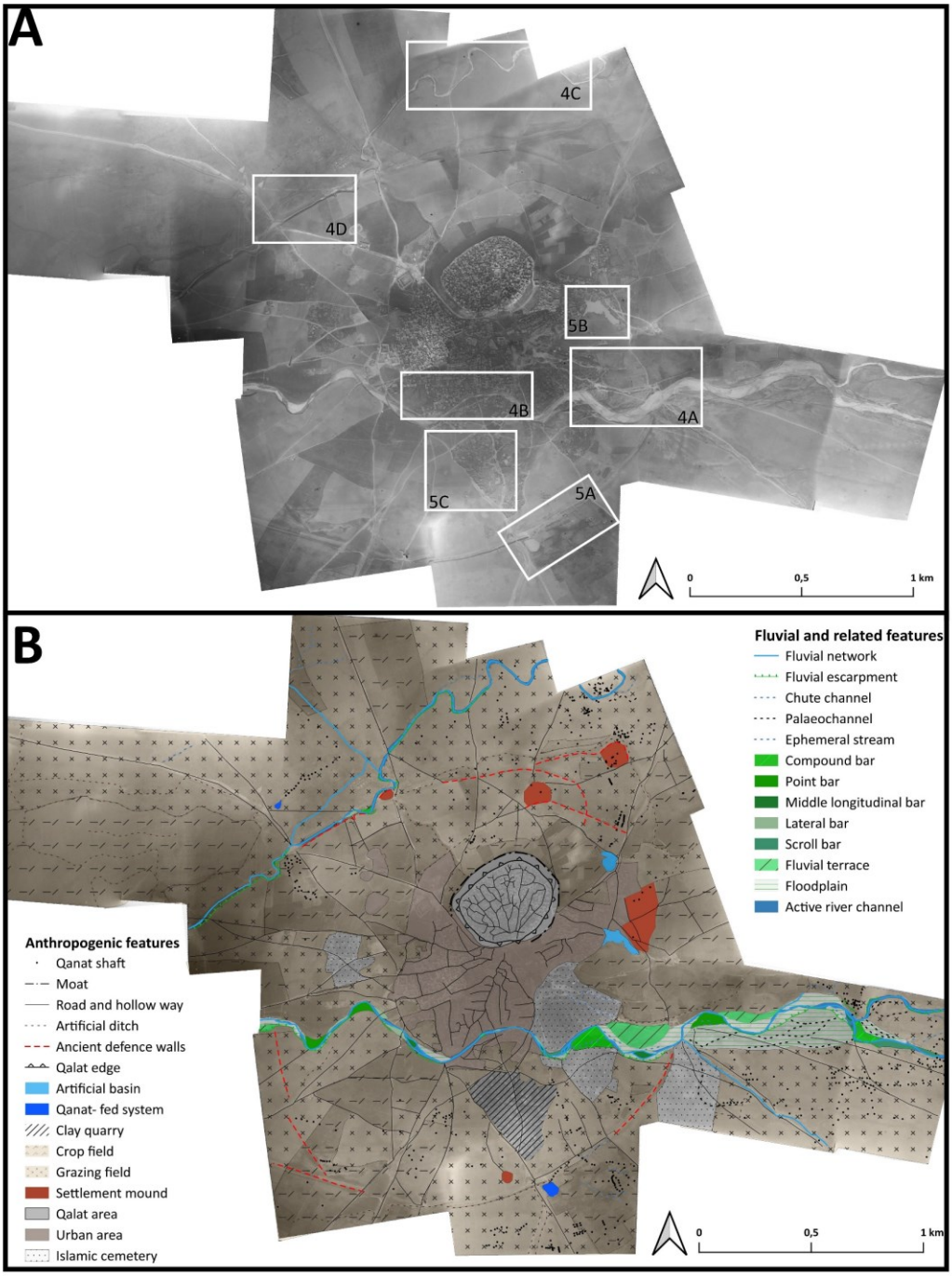


**Figure 2.** A) Erbil orthomosaic derived from RAF imagery acquired in February 1919 in which with the white polygon are reported some details of Figure 3 and 4. B) Geomorphological mapping performed on the RAF 1919 where the fluvial and anthropogenic features were mapped

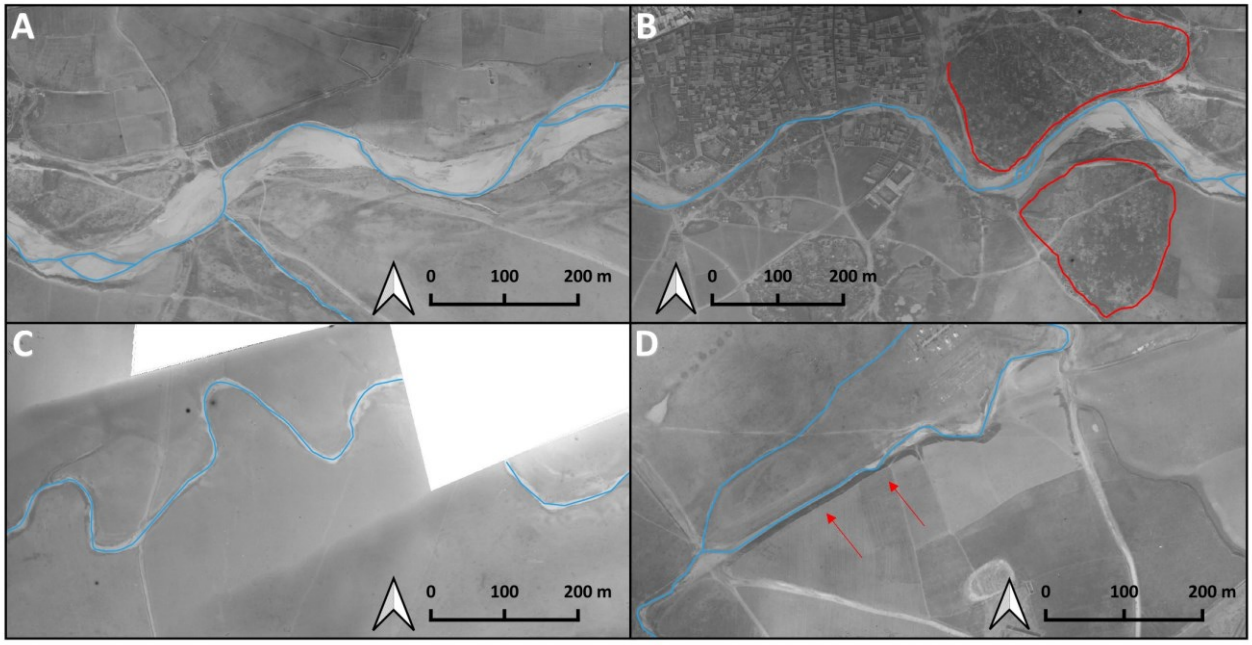


**Figure 3.** A) Detail of the upstream Bastè River where a meandering to anabranching river planform occurred in a semi-confined valley setting. B) Downstream of Bastè River characterized by a reduction in a cross section with a progressive passage toward confined valley setting in the proximity of the urban area. The red line envelopes the Islamic cemeteries C) Detail on the upstream portion of Tchekunem River where regular to irregular meander occurred. D) The downstream rectified reach of Tchekunem River (red arrows)

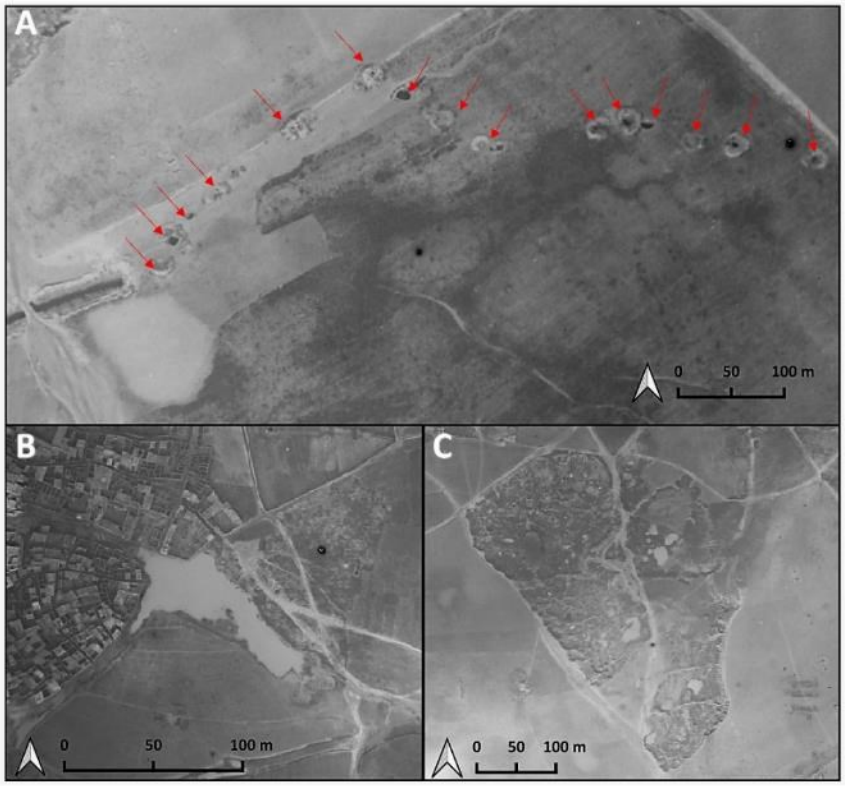


**Figure 4.** A) Qanat system with alignment of shafts (red arrows) with a basin water storage and ditch at the outlet of the Qanat system. B) The artificial basin in the SE of Qalat. C) The impressive clay quarry located in the southern sector respectively to the Qalat and the Bastè River.

### 8.4.2 The 1968 Corona dataset: the acceleration of the urbanization and the modification of the riverscape

The geomorphological mapping performed on the declassified Corona imagery taken in the August 1968 (Figure 5A) displays the intense urban expansion that overshadowed the natural elements of the landscape. In this process, the development of buildings and residential districts was organized following the urban master plan approved in the 1951 (Doxiadis, 1959) and eroded the extension of cultivated patch of land. The main plan was to expand the urban area in the western and north-western sectors and organised the city according to a grid pattern with ring road enveloping a series of residential and industrial districts (Al-Hashimi, 2016) for a radium of 1.5 km from the city centre. Almost all field surfaces appear to have been remodelled by human action, with the construction of buildings, parks, roads, and several ground movements operations (Figure 5B). The patch of land devoted to cultivation and pastoral activities occurring in the vicinity of the citadel were moved outside the ring road. Within the ring road, archaeological and historical features such as cemeteries and settlement mounds successfully escape from the intense growth of the city while most of the Assyrian-Medieval fortifications were demolished. A qanat systems, were recognized in the western sectors where a series of shaft are aligned along a road that connects directly to the city centre (Figure 6B) (Al-Hashimi,2016). If we consider the hydrography in the surrounding of the city, the Corona images illustrate that the fluvial geomorphic units of the Bastè and Tchekunem Rivers identified in the 1919 RAF pictures were drastically modified by the human action. The riverbeds of the watercourses were disrupted by bulldozing for buildings while others are cemented or culvert to build roads. The complete upheaval of the in-city hydrographic network has led to a strong reorganisation of river courses with paleochannels, and ephemeral streams activated during heavy rainfall (Figure 6A).

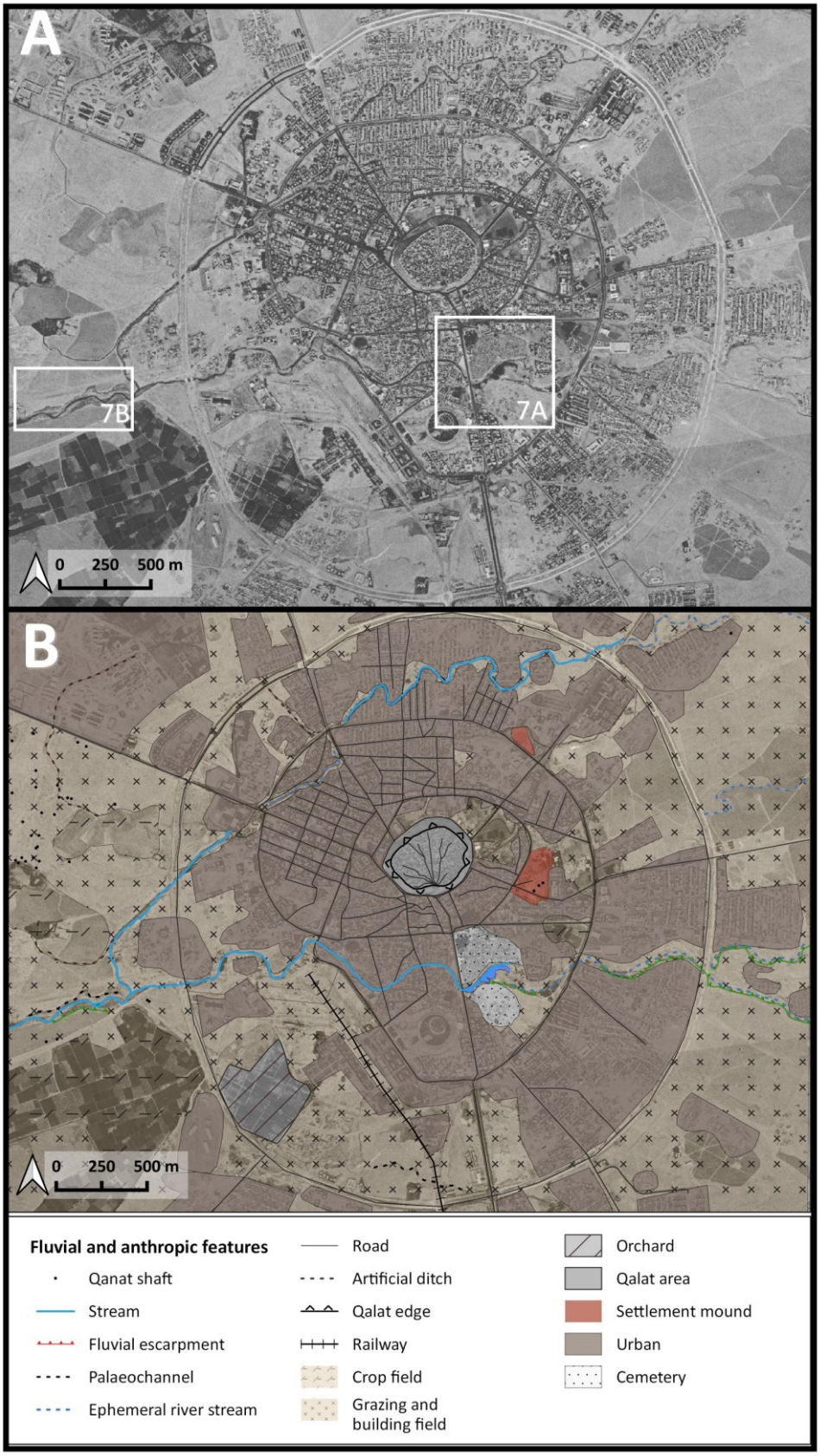


**Figure 5.** A) The 1968 Corona declassified Imagery of the Erbil urban area. B) Geomorphological mapping performed on the 1968 Corona declassified and reporting major fluvial and anthropogenic features.

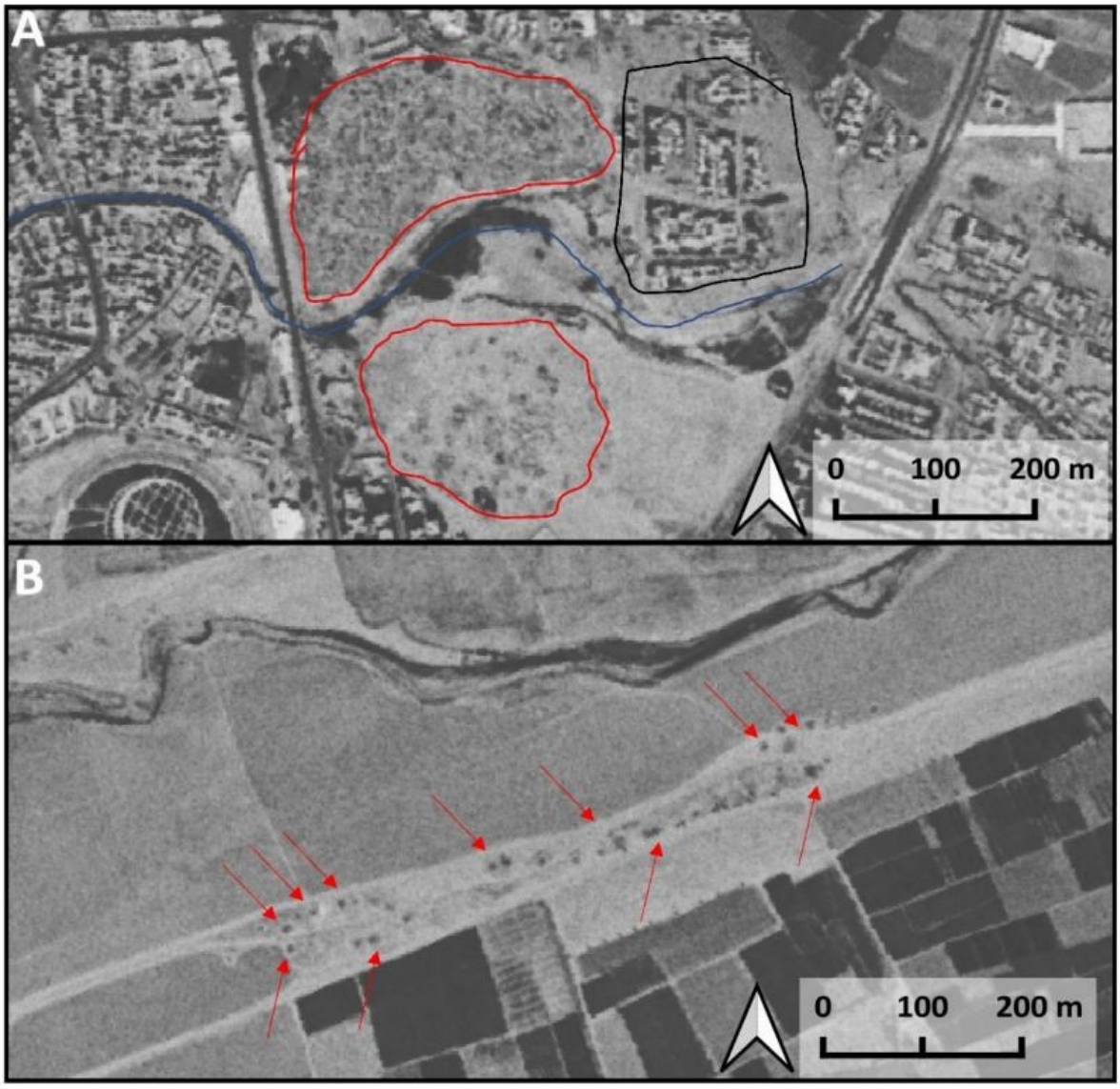


**Figure 6.** A) Detail of Bastè River in the proximity of the cemeteries (red polygon) where the residential district (black polygon) started to build on the bank and within the riverbed. B) Qanat system (red arrows are the shafts alignment) in the western sector of the mapping area.

### 8.4.3 Modern high-resolution satellite imagery: Erbil today

Current satellite imagery of the city of Erbil shows the rapid urban expansion of the city. The city was embedded within two circular roads where the first, built in the mid-1960s, has a radius of about 1.5 km, while the second has a radius of 5 km. A third circular road, currently in the construction, encompass the airport with a radius of 10 km. This continuous urban growth and expansion leads to a profound modification of the city's drainage network; today it is completely covered by road and buildings. The natural watercourses within the city were over time straightened by the human action with modification and management of the former fluvial planform that contribute an increase in flood hazard. The current literature, reports on the susceptibility of Erbil to flood risk; in fact, after intense heavy rainfall different districts of the city, in the north and south of the citadel, was inundated for

several hours. The increase in flood risk was recorded with three floods events occurred in Erbil between 2021 and 2022. Mustafa et al., (2021) argued that the increase in the flood risk in Erbil is related to overbuilding, culvert, and reduction in channel cross-section of the natural streams with a poor maintenance of riverbeds and an inadequate stormwater system drainage. Also, the expansion of the city reduces the capacity of infiltration of the water towards an increase in runoff.

## 8.5 Discussion: the progressive obliteration of the pristine riverscape

Through geomorphological reconstruction derived from historical images, it was possible to reconstruct the urban landscape immediately after the Ottoman dominance and mapped the changes in land use underwent during the intense urban growth started at the beginning of 1920s and exploded since the 1950s. Since the Chalcolithic period, Erbil was established in a fertile floodplain, in a landscape characterised by numerous watercourses which provide supply water for irrigation and raw clay material for the construction of the buildings. Throughout the millennia, the growth of Erbil is marked by the presence of the citadel, which is an elevated feature in the surrounding plain. This topographical element was possibly built on the summit of an existing natural feature, such as a fluvial bar or above the levee of an old river course and was hence a favourable place to protect against floods. The geomorphological mapping and reconstruction of Erbil's hydrographic setting prior to middle 20th century urban expansion has yielded a wealth of information regarding the management of water resources within the city. The two main watercourses, which in 1919 showed an almost entirely natural evolution, were over the years, modified, remodelled, and finally obliterated to make way for intensive urbanisation with the construction of residential neighbourhoods, parks and numerous new roads that totally altered the urban layout of Erbil. From the Assyrian period until the Middle Ages and later Ottoman rule, the city was totally concentrated in the vicinity of the Qalat. Only a few structures, such as cemeteries, public and trade buildings, two lines of fortifications and old settlements represented the only human-made elements that colonised the plain. Towards the end of Ottoman rule, in 1919, the major urban centre was concentrated in the citadel and the lower town, and their organisation was based on an organic pattern designed to support the main activities of commerce and daily life to sustain a population of about 8,000 people. During this phase, many fields were exploited for pastoralism and agriculture and fed through a system of qanats and artificial ditches. During the mid-20th century, Erbil began to expand according to an organised plan through the construction of a road network within the Qalat and the lower city that connected with a ring road built 1.5 km radius from the centre of the Qalat. There was a parcelling of lands for different uses, in particular the construction of grid shape residential districts and industrial areas related to agricultural activities in the south-western. Since the end of the Gulf War and the administrative detachment from

Iraq, Erbil became the most important centre in the Kurdistan Region of Iraq and encountered a large population growth due largely to migratory flows from Iraq and neighbouring countries, the city began a major expansion through the construction of a several lots of residential and industrial districts enclosed within a 5 and 10 km diameter ring road. Until the early 1900s, the use of natural resources around Erbil seems to be respectful of the natural setting of the territory; in fact, in this phase the use of water resources relies to traditional systems for water management, such as artificial basins and the use of the qanat technology, which is the most common strategy for water collection adopted in arid and semi-arid regions. Up to the Ottoman period, the city developed in accordance with the natural fluvial landscape that show only limited reworking (rectification), but afterwards the Ottoman dominance the city changed its shape due to an urban expansion and growing project that completely hidden the pristine fluvial landscape. Such a strong human impact was detected along the Tchekunem River, North of Qalat, through a comparison of declassified Corona and Hexagon images from 1968 and 1972 with current high-resolution satellite images. The declassified Corona satellite imagery captured in the 1968 revealed the construction of residential districts in the proximity of the Tchekunem River banks (Figure 7A). During this period the fluvial planform shape of the is still evident, but a comparison with the Hexagon satellite image acquired four years later (1972) showed the speed of expansion and construction of new houses within the riverbed (Figure 7B). In this case, the general shape of the river course is obliterated and reshaped by intense urbanisation. 50 years later, the river course has been completely obliterated by human-made structures. The analysis of current satellite images of the area revealed that traits of secondary roads are superimposed over the old course of the Tchekunem River (Figure 7C). The erosive processes are also present along the course and banks of the Basté River. In this case, historical RAF images from 1919 and 1951 compared with the 1972 Hexagon and the more recent satellite imagery revealed a profound modification of the river course caused by human operations. The geomorphological mapping recognized that in this portion the river displayed a meandering planform with regular to irregular meanders with a transition from semi confined to confined valley setting in the proximity of the Islamic cemeteries (Figure 2B and 3A). There, a fluvial escarpment developed in the upstream outer portion of the regular meander (Figure 8A). A comparison with 1951 and 1972 historical imagery highlights the retreat of this escarpment related to the interplay between fluvial and human processes with an intense exploitation along the banks and within the riverbed. Moreover, a shift in land use was recognized easternmost of the cemeteries, in correspondence of a fluvial terrace mapped on the RAF 1919 dataset, from cultivated fields in 1951, they transformed into a grid pattern residential district in 1972 (Figure 2B-8B-8C). Also, high resolution imagery highlights the intense urban

expansion along the pristine natural fluvial landscape visible from the big shopping galleries built along the left bank that displays an arcuate shape in according to a meander of the Basté River. Westernmost the former riverbed was turned into a road (Figure 8D). The continuous expansion over the past decades caused a complete obliteration of the hydrographic network, with increased sensibility to geomorphological hazard. The management of the Erbil hydrographic network consisted in channelization, cemented and culvert lead to an increased hydrogeological and flood risk (Mustafa et al., 2022). The increase in floods hitting the city in 2021 and 2022 after intense heavy rainfall had a major impact on different districts of the city, in the north and south of the citadel, that were completely inundated. Such districts are those in direct connection with parts of the natural hydrography buried under the urban expansion of the city, demonstrating that the urbanization plan did not take into account the potential geomorphological risk related to flooding. Sensitivity land use changes in Erbil associated with an increase in anthropic operations led to an increase in soil erosion, a reduction in infiltration coefficients, enhancing storm runoff and increasing the magnitude of flood peaks provided a disequilibrium in the response time of the fluvial system. city.

## 8.6 Conclusion

In this contribution, we explore the geomorphological evolution of the city of Erbil in the KRI, whose fluvial landscape has been exploited and modified – especially in recent times – by the dramatic urban expansion occurred in the last decades. Our investigation identified (i) ancient strategies to exploit local water resources by means of artificial landforms (e.g., using the qanat system), (ii) the patterns of evolution of the city and how this process affected the natural hydrography, and (iii) the major consequences this had on the susceptibility to geomorphological hazard (e.g., floods) of Erbil. This case study highlights the importance of geomorphological mapping of urban areas using different data sources with a geoarchaeological perspective, to reconstruct the mode and tempo of urban expansion since the foundation of a city and the potential consequences of human overprint on geomorphic processes.

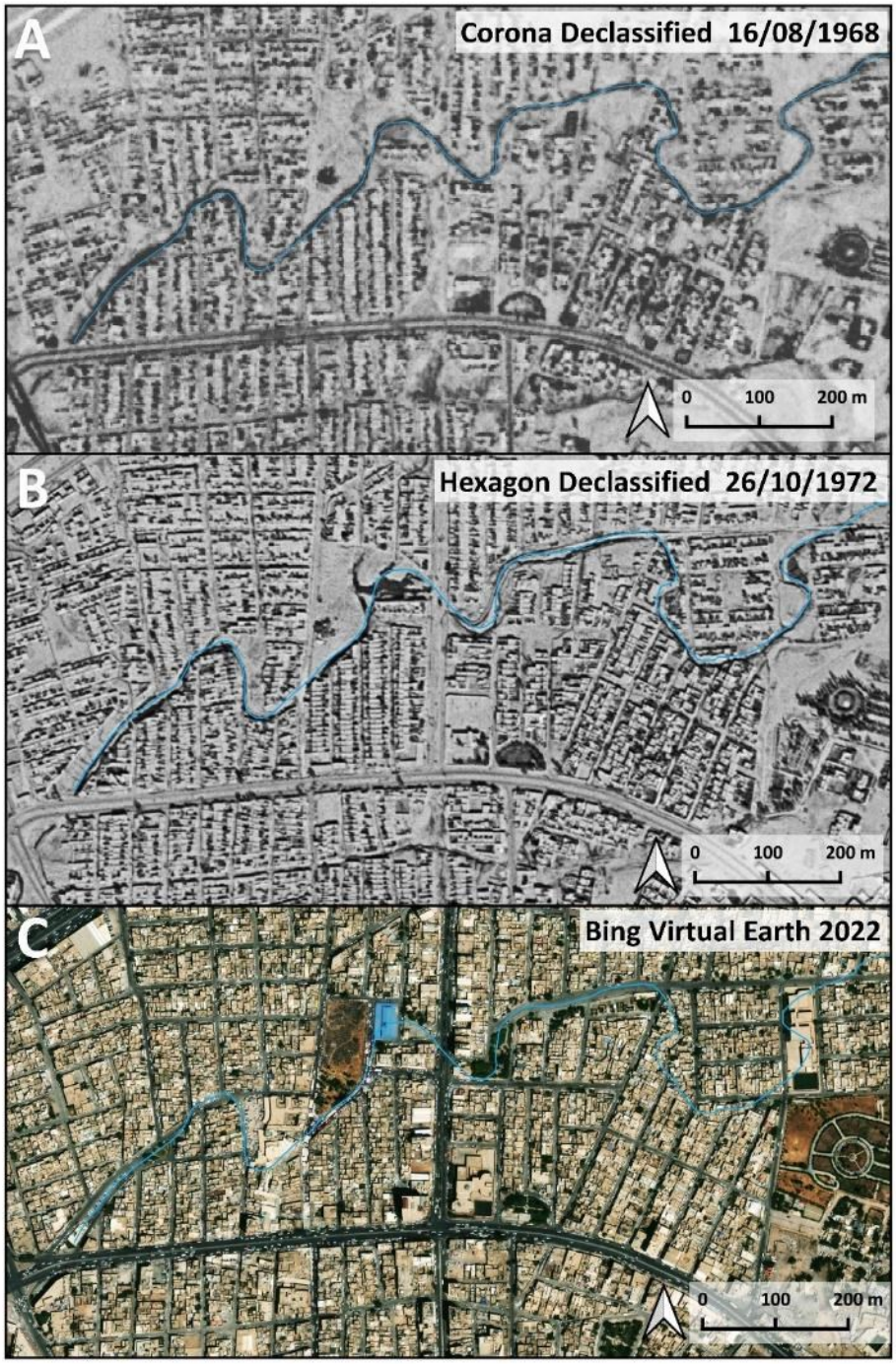


**Figure 7.** A) 1968 Corona Declassified satellite imagery of Tchekunem River where the urban expansion spread out. B) 1972 hexagon Declassified satellite imagery taken in 1972 revelated the speed of urban expansion that in just four years had almost obliterated the river course. D) Actual high resolution satellite imagery displays the influence of the pristine fluvial setting on the secondary roads.

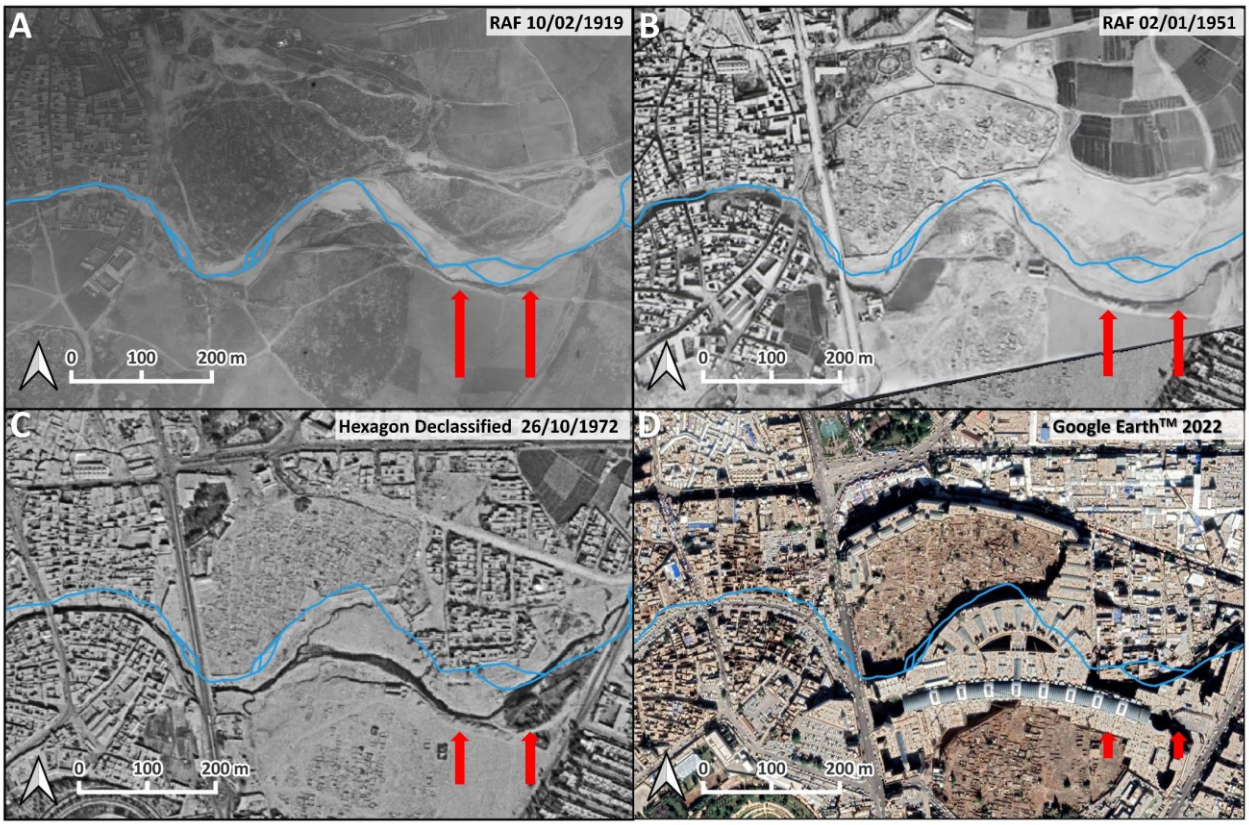


**Figure 8.** A) 1919 RAF imagery of the Bastè River in the proximity of the Islamic cemeteries. The red arrows indicate the fluvial escarpment. B-C) RAF 1951 and Hexagon Declassified satellite imagery display the intense exploitation of the area with a retreat of the fluvial escarpment (red arrows). D) Google Earth™ urban expansion spread out. B) 1972 hexagon Declassified satellite imagery taken in 1972 revelated the speed of urban expansion that in just four years had almost obliterated the river course. D) Actual high resolution satellite imagery displays the influence of the pristine fluvial setting on the secondary roads.

## 8.7 References

Agisoft Metashape. (2022). Available online: http://www.agisoft.com/downloads/installer/ (accessed on 12 April 2022)

Al-Hashimi, F. W. (2016). The hidden face of Erbil: change and persistence in the urban core. Nottingham Trent University (United Kingdom).

Almukhtar, A. (2020). Place-identity in historic cities; The case of post-war urban reconstruction in Erbil, Iraq. In Urban Heritage Along the Silk Roads (pp. 121-136). Springer, Cham. Almukhtar, A. (2020). Place-identity in historic cities; The case of post-war urban reconstruction in Erbil, Iraq. In Urban Heritage Along the Silk Roads (pp. 121-136). Springer, Cham.

Brandolini, P., Cappadonia, C., Luberti, G. M., Donadio, C., Stamatopoulos, L., Di Maggio, C., ... & Del Monte, M. (2020). Geomorphology of the Anthropocene in Mediterranean urban areas. Progress in Physical Geography: Earth and Environment, 44(4), 461-494.

Brandolini., F, Cremaschi, M., & Pelfini, M. (2019). Estimating the potential of archaeo-historical data in the definition of geomorphosites and geo-educational itineraries in the central Po plain (N Italy). Geoheritage, 11(4), 1371-1396.

Cremaschi, M., Storchi, P., & Perego, A. (2018). Geoarchaeology in an urban context: the town of Reggio Emilia and river dynamics during the last two millennia in Northern Italy. Geoarchaeology, 33(1), 52-66.

Doxiadis A. (1959). Ekistic Analysis of the Town of Arbil - DA Projects: Iraq V.144- Reports Dox-QA 92, Dox-QB (January-August 1959). Archive files 24018, Constantinos A. Doxiadis Archives, hosted at the Benaki Museum, Athens.

Faccini, F., Giardino, M., Paliaga, G., Perotti, L., & Brandolini, P. (2021). Urban geomorphology of Genoa old city (Italy). Journal of Maps, 17(4), 51-64.

Forti L., Pezzotta A., Zebari, M., & Zerboni, A. (2023) Geomorphology of the Central Kurdistan Region of Iraq: landscapes of the Erbil Plain between the Great Zab and Little Zab Rivers. Journal of Maps

Forti, L., Mariani, G. S., Brandolini, F., Pezzotta, A., & Zerboni, A. (2022). Declassified intelligence satellite imagery as a tool to reconstruct past landforms and surface processes. The submerged riverscape of the Tigris River below the Mosul Dam Lake, Iraq. Earth Surface Processes and Landforms.

Forti, L., Perego, A., Brandolini, F., Mariani, G. S., Zebari, M., Nicoll, K., ... & Zerboni, A. (2021). Geomorphology of the northwestern Kurdistan Region of Iraq: landscapes of the Zagros Mountains drained by the Tigris and Great Zab Rivers. Journal of Maps, 17(2), 225-236.

Grabowski, R. C., Surian, N., & Gurnell, A. M. (2014). Characterizing geomorphological change to support sustainable river restoration and management. Wiley Interdisciplinary Reviews: Water, 1(5), 483-512.

Great Britain. Naval intelligence Division, 1944. Iraq and the Persian Gulf. London: Naval intelligence Division.

Gurnell, A. M., Peiry, J. L., & Petts, G. E. (2003). Using historical data in fluvial geomorphology. Tools in fluvial geomorphology, 77-101.

Harris, I., Osborn, T. J., Jones, P., & Lister, D. (2020). Version 4 of the CRU TS monthly high-resolution gridded multivariate climate dataset. Scientific data, 7(1), 1-18.

Hay, R., & Hay, W. R. (1921). Two Years in Kurdistan: experiences of a political officer, 1918-1920. Sidgwick & Jackson.

Hussein, M. H. (1998). Water erosion assessment and control in Northern Iraq. Soil and Tillage Research, 45(1-2), 161-173

Kramer, C., Wilkinson, T. J., & Tucker, D. J. (1998). Settlement Development in the North Jazira, Iraq: A Study of the Archaeological Landscape. Journal of the American Oriental Society, 118(4), 576.

Lawrence, D., Palmisano, A., & de Gruchy, M. W. (2021). Collapse and continuity: A multi-proxy reconstruction of settlement organization and population trajectories in the Northern Fertile Crescent during the 4.2 kya Rapid Climate Change event. PloS one, 16(1), e0244871.

Lightfoot, D. R. (2000). The origin and diffusion of qanats in Arabia: new evidence from the northern and southern peninsula. Geographical Journal, 166(3), 215-226.

Mandarino, A., Luino, F., Turconi, L., & Faccini, F. (2021). Urban geomorphology of a historical city straddling the Tanaro River (Alessandria, NW Italy). Journal of Maps, 17(4), 29-41.

McNeill, J. R., & Engelke, P. (2016). The great acceleration: An environmental history of the Anthropocene since 1945. Harvard University Press.

Mustafa, A., & Szydłowski, M. (2020). The impact of spatiotemporal changes in land development (1984–2019) on the increase in the runoff coefficient in Erbil, Kurdistan Region of Iraq. Remote Sensing, 12(8), 1302.

Mustafa, A., Szydłowski, M., Veysipanah, M., & Hameed, H (2022). Challenges in Flood Risk Identification, Assessment and Modeling in Data Scarcity Regions; Erbil, Kurdistan Region of Iraq as a Case Study. Assessment and Modeling in Data Scarcity Regions.

NextGIS (2021). QuickMapServices. https://nextgis.com/blog/quickmapservices/.

Nováček, K., Amin, N. A. M., & Melčák, M. (2013). A medieval city within Assyrian walls: the continuity of the town of Arbīl in Northern Mesopotamia. Iraq, 75, 1-42.

Nováček, K., Amin, N. A. M., & Melčák, M. (2013). A medieval city within Assyrian walls: the continuity of the town of Arbīl in Northern Mesopotamia. Iraq, 75, 1-42.

Pelfini, M., Brandolini, F., D'Archi, S., Pellegrini, L., & Bollati, I. (2021). Papia civitas gloriosa: urban geomorphology for a thematic itinerary on geocultural heritage in Pavia (Central Po Plain, N Italy). Journal of Maps, 17(4), 42-50.

Rich, C. J. (1836). Narrative of a Residence in Koordistan, and on the Site of Ancient Nineveh: With Journal of a Voyage Down the Tigris to Bagdad and an Account of a Visit to Shirauz and Persepolis. J. Duncan.

Roccati, A., Mandarino, A., Perasso, L., Robbiano, A., Luino, F., & Faccini, F. (2021). Large-scale geomorphology of the Entella River floodplain (Italy) for coastal urban areas management. Journal of Maps, 17(4), 98-112.

Rosen, A. M. (1986). Cities of clay: the geoarcheology of tells. University of Chicago Press.

Sarre, F. P. T., & Herzfeld, E. (1920). Archäologische Reise im Euphrat-und Tigris-Gebiet (Vol. 2). D. Reimer.

Soroush, M., Mehrtash, A., Khazraee, E., & Ur, J. A. (2020). Deep learning in archaeological remote sensing: Automated qanat detection in the kurdistan region of Iraq. Remote Sensing, 12(3), 500.

Steffen, W., Broadgate, W., Deutsch, L., Gaffney, O., & Ludwig, C. (2015). The trajectory of the Anthropocene: the great acceleration. The Anthropocene Review, 2(1), 81-98.

Ur, J., De Jong, L., Giraud, J., Osborne, J. F., & MacGinnis, J. (2013). Ancient Cities and Landscapes in the Kurdistan Region of Iraq: The Erbil Plain Archaeological Survey 2012 Season1. Iraq, 75, 89-117.

USGS (1968). Declassified Corona Imaging data. Retrieved from https://corona.cast.uark.edu (accessed 11/08/2020).

Vacin, L. (2011). Šulgi of Ur: Life, Deeds, Ideology and Legacy of a Mesopotamian Ruler as Reflected Primarily in Literary Texts. Declaration for PhD Thesis, University of London.

Vergari, F., Marco Luberti, G., Pica, A., & Del Monte, M. (2021). Geomorphology of the historic centre of the Urbs (Rome, Italy). Journal of Maps, 17(4), 6-17.

Wilkinson, T. J. (2003). Archaeological landscapes of the Near East. University of Arizona Press.

Zerboni, A., & Nicoll, K. (2019). Enhanced zoogeomorphological processes in North Africa in the human-impacted landscapes of the Anthropocene. Geomorphology, 331, 22-35.-

# Chapter 9

## Conclusion and future perspective

The geoarchaeological, multiscale approach performed in this research provides several new perspectives for the Holocene paleoclimatic and paleoenvironment reconstruction in the KRI Moreover, it enhances our understanding of the human responses and adaptation to climate, landscape, ecosystem, and natural resources availability changes across the last millennia.

The geomorphological analysis and mapping of the Northwestern and Central Kurdistan Region of Iraq offers important insights on the interplay between active tectonic and climatic-driven processes that affected landforms and fluvial development during the Neogene and the Quaternary. The different physiographic units of such complex landscape reflect the uplift and exhumation rate of the anticlinal ridges and syncline troughs. In this scenario, overlapping of endogenous and exogenous factors has determined the formation of a palimpsest landscape, in which active and fossil stratified elements and processes can be recognized. Moreover, a detail geomorphological investigation performed on the historical imagery permits to reconstruct the dynamic of local rivers and the submerged riverscape of the Tigris River along the Mosul Dam Lake and identify the main hydrological, geomorphological changes regulated by seasonal variations of the discharge and the litho-structural control on the size and direction. This methodological approach demonstrated the reliability of historical declassified intelligence aerial/satellite pictures in geomorphological studies. Moreover, our protocol permits to investigate regions in many cases not accessible and/or where intense urban expansion and human agency have disrupted natural landforms and altered pristine surface processes, thus reconstructing the geomorphic dynamic predating human overprint.

The research focus on the beginning of the Holocene when the study region suffered intense and widespread modification of the landscape contemporaneous to a major change in humans subsistence strategies and land use. At that time, the Early Holocene archaeological record preserves evidence for the progressive transition from mobile hunter-gathering groups to the emergence of with sedentary farmers and herders' societies with permanent settlements, in the framework of the so-called "Neolithic Revolution".

Paleoclimatic data retrieved from a flowstone ranging from 11 to 7.3 ka recorded wetter conditions between 9.7 and 9.0 ka, followed by an abrupt reduction of precipitation between 9.0 and 8.5 ka, and by a wetter interval between 8.5 and 8.0 ka. Comparison with the archaeological data revealed the influence on the socio-economic, technological transformations, variations of the availability of natural resources (water) and settlement dynamics on the widespread of complex

societies. The exploitation of natural resources has determined the transformation and continuous shaping of the territory, which have increased in parallel with the development of complex societies. Our record does not support a direct influence of Early Holocene RCCs on the process of Neolithization and its cultural dispersal. Although it is still debated whether Neolithic cultural changes were forced directly by climatic variability, we show robust chronological agreement between changes in precipitation pattern and the alternation of local cultural phases, suggesting that hydroclimate variability supported the way in which Neolithic population exploited the surrounding environment.

The geomorphological mapping of long-time settled landscapes offers important tools for urban planning as much as a plethora of information to reconstruct past human adaptations, subsistence strategies, and early human overprints on pristine geomorphic systems. In the Kurdistan Region of Iraq, the preservation of anthropogenic landforms and their intrinsic archaeological record is today threatened by ongoing surface processes, and in some cases such processes are accelerated by human agency. For instance, we proposed an empirical model usually applied to describe soil loss (RUSLE) and derived from UAV imagery to estimate the rate of erosion along slopes of archaeological sites. In such contexts, the loss of archaeological soils and sediments is tuned by natural and human-driven factors that mining the preservation of archaeological record. The proposed approach is an effective contribution to the preservation of archaeological sites because offers fresh tools to archaeologists and conservationists. Finally, this low-cost approach can be routinely applied to archaeological sites of the Near East to assess the susceptibility of archaeological heritage to the geomorphological risk promoted by ongoing climate change. In fact, the documentation of the preservation of archaeological monuments/sites and the assessment of the potential risk of destruction of cultural heritage at the scale of the single archaeological site are becoming urgent considering the increasing human pressure on archaeological areas and the acceleration of surface processes pushed by ongoing climate change. In the region, Late Quaternary human activities became progressively more impacting on the natural landscape especially in the Meghalayan stage of the Holocene: from other hand, humans built monumental canals systems that are still evident from remote and in the field, whose main effect was to alter the local hydrography building anthropogenic landforms. The application of micromorphological and sedimentological analysis on the filling sediments of Assyrian canals, examined the different phases of use, abandonment a repurposing disclosed that the formation of their infilling was triggered by a shift in land use related to climate and human dynamics changes. This work further demonstrates that the post-abandonment infillings of negative archaeological structures efficiently support landscape archaeology studies in detecting evidence of past land use and exploitation of natural resources. Even though such deposits have a low chronological resolution

their micromorphological investigation allows interpreting landscape evolution and land use changes occurred after the abandonment of an archaeological area supporting archaeological reconstruction. As in the case of Mesopotamian water harvesting systems, geoarchaeological investigation needs to focus on post-abandonment deposits that may disclose unexpected evidence describing the evolution of archaeological landscapes.

In the Kurdistan Region of Iraq, as much as in many other parts of the world, the great urban expansion started in the 1950s has completely disrupted the pristine landscape that was the result of a long-lasting and balanced interaction between natural and anthropogenic geomorphic processes. A detailed analysis of the landscape before the intense urbanisation carried out on the town of Erbil, through a collection of historical aerial and satellite images from 1919 to the present day, has documented the large-scale urban expansion that has completely obscured the old rural and fluvial landscape. In such context, the obliteration of natural stream increased the geomorphological risk of floods in the city, but the geomorphological mapping based on historical aerial pictures and the identification of the areas more prone to the geomorphological risk offer a tool for future urban planning. More in general, the comparison of present geomorphic settings with historical aerial/satellite imagery, as much as the use of historical maps, reveal in detail the impact of the onset of human agency on landscapes in the last few centuries, shedding light on the effects of anthropogenic modifications on geomorphic surface processes.

From a more general point of view, most of the case studies of this thesis highlight examples of human impacts on the landscape, in some cases occurring hundreds to thousands of years ago, thus suggesting early and permanent human overprint on pristine environments and localized early emergence of the Anthropocene, meaning a phase when humans started to modify actively and permanently natural processes, landscapes and ecosystems.

The work carried out in this thesis is the first attempt to accomplish a holistic geoarchaeological investigation in this region, critical for human dynamic. The use of a multi-scalar and geoarchaeological approach has enabled the reconstruction of Late Quaternary landscape and climates within the KRI. However, this region offers still many opportunities to investigate the settlement dynamics and subsistence strategies adopted by ancient Mesopotamian societies in reaction to climate change. This approach will allow the investigation of further areas in the KRI, which are extremely interesting in terms of archaeological complexity, and to correlate with paleoenvironmental and paleoclimatic data. New investigations should be performed on the relationship between the archaeological landscape and the exploitation of natural resources to produce raw materials, such as clay for the manufacture of pottery and bricks. Furthermore, an extensive study could be carried out on the pastoral landscape investigating the ancient sheep-tracks and the large

number of shelters used by shepherds. Other data may be obtained from the investigation of archaeological sites in mountainous areas, e.g., caves, to understand the relationship between the social dynamics of mountains and lowlands. New field activities may provide data on the paleoclimate with the individuation of both lacustrine and cave sequences to investigate precise archaeological periods more accurately to better understand the relationships between climatic changes and subsistence strategies during the formation and emergence of new empires (e.g., Assyrian periods). Our experience confirms that the fresh methods of geoarchaeological investigation can be used to understand the formation and evolution of specific archaeological sites in response to political and social events, but particularly with changes in climate and landscape. Specifically, reconstituting the settlement processes of archaeological centers placed on the banks of rivers in response to changes in fluvial dynamics according to climate setting.

# Appendix I

High resolution map available at: https://doi.org/10.1080/17445647.2021.1906339

# Geomorphology of the northwestern Kurdistan Region of Iraq: landscapes of the Zagros Mountains drained by the Tigris and Great Zab Rivers

Luca Forti(1,2*), Alessandro Perego(1), Filippo Brandolini(1), Guido S. Mariani(3), Mjahid M. Zebari(4), Kathleen Nicoll(5), Eleonora Regattieri(2), Cecilia Conati Barbaro(6), Daniele Morandi Bonacossi(7), Hasan Ahmed Qasim(8), Mauro Cremaschi(1), Andrea Zerboni(1)

1) Dipartimento di Scienze della Terra "A. Desio", Università degli Studi di Milano, Italy. 2) Istituto di Geoscienze e Georisorse, CNR, Pisa, Italy. 3) Dipartimento di Scienze Chimiche e Geologiche, Università degli Studi di Cagliari, Italy. 4) Institute of Geological Sciences, Friedrich-Schiller University Jena, Germany. 5) Department of Geography, The University of Utah, Salt Lake City, USA. 6) Dipartimento di Scienze dell'Antichità, Sapienza Università di Roma, Italy. 7) Dipartimento di Studi Umanistici e del Patrimonio Culturale, Università degli Studi di Udine, Italy. 8) Director of Antiquities of Duhok, Iraq.
* Corresponding authors e-mail: luca.forti@unimi.it

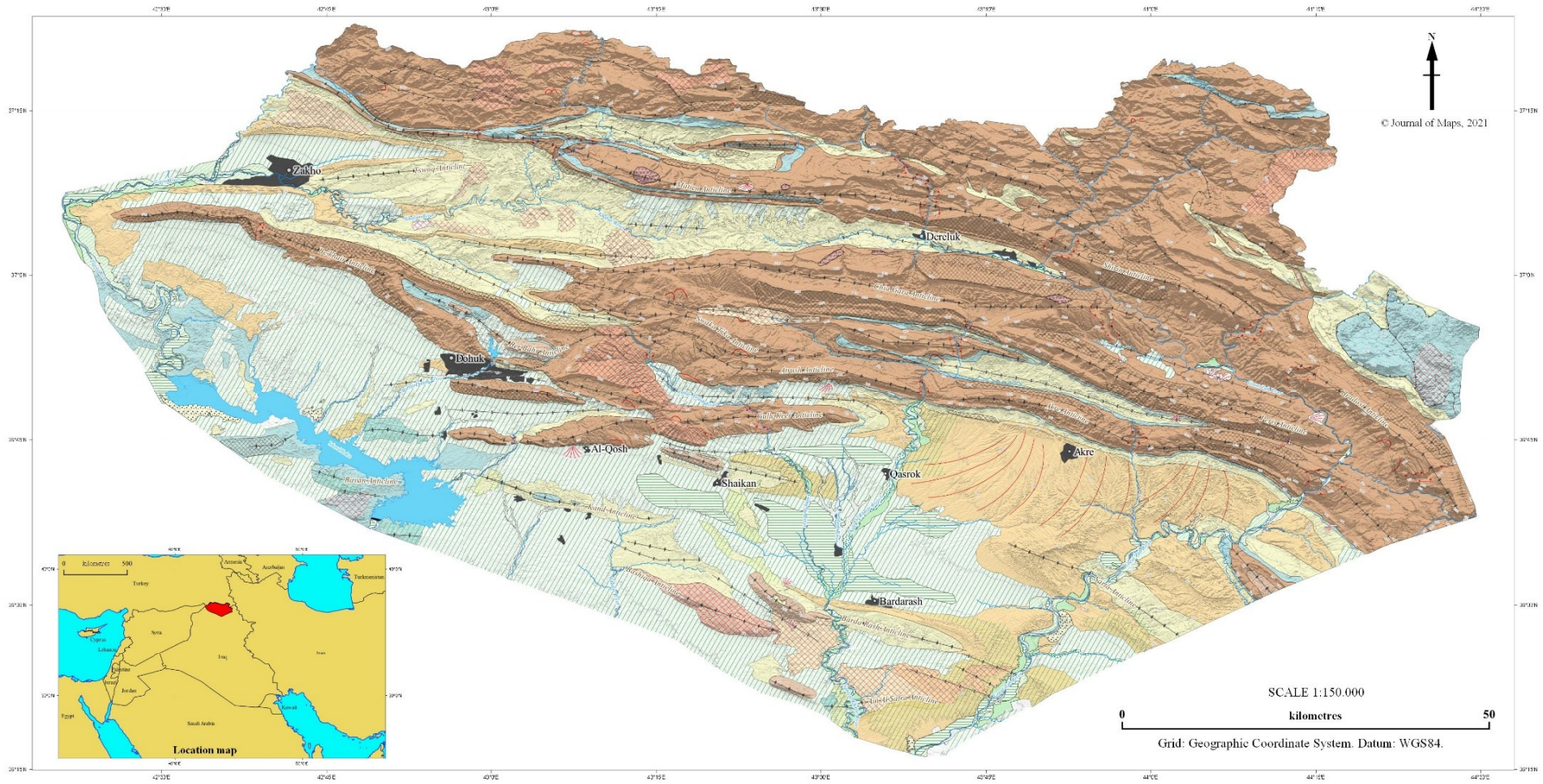


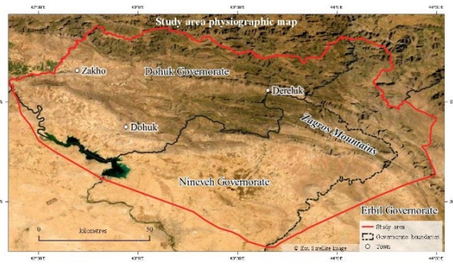


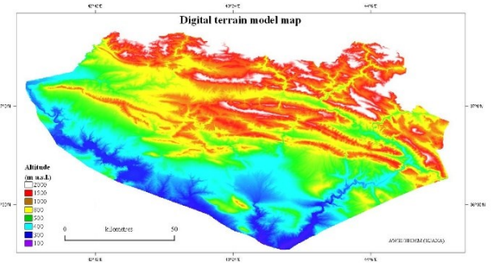


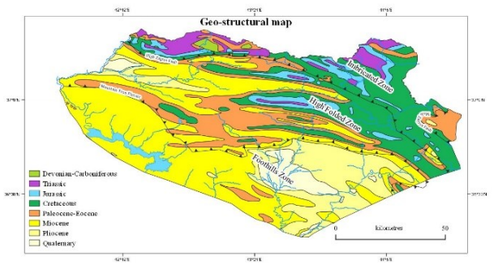


**Lithologies**
- Limestone
- Marls
- Sandstone
- Conglomerates

**Structural elements and landforms**
- Anticline axis
- Syncline axis
- Normal fault
- Thrust fault
- Flatiron
- Water gap escarpment

**Hillslope landforms**
- Deep-seated gravitational slope deformation
- Badlands

**Karst landforms**
- Limestone pavement

**Fluvial landforms**
- Floodplain
- Terrace level T1
- Terrace level T2
- Terrace level T3
- Terrace level T4
- Perennial river bed
- Ephemeral river bed
- Pediment
- Alluvial fan
- Fluvial network

**Anthropogenic features**
- Urban areas
- Dam

## Appendix II

High resolution map available at: https://doi.org/10.1080/17445647.2022.2164527

# Geomorphology of Central Kurdistan Region of Iraq: landscapes of the Erbil Plain between the Great Zab and Little Zab Rivers

Luca Forti[1] [2]*, Andrea Pezzotta[1]*, Mjahid Zebari[3], Andrea Zerboni[1]

[1] Dipartimento di Scienze della Terra "A. Desio", Università degli Studi di Milano, Milano, Italy; [2] Istituto di Geoscienze e Georisorse, CNR, Pisa, Italy; [3] Department of Earth and Environmental Sciences, Ludwig Maximilian University of Munich Luisenstr, Munich, Germany.
Corresponding authors e-mails: *luca.forti@unimi.it, andrea.pezzotta@unimi.it*